Aspects of extra dimensional supersymmetric unified theories

Sylvain Fichet

UNIVERSITÉ DE GRENOBLE

THÈSE

Pour obtenir le grade de

DOCTEUR DE L'UNIVERSITÉ DE GRENOBLE

Spécialité : **Physique des Particules**

Arrêté ministérial : 24 Août 2006

Présentée par

Sylvain Fichet

Thèse dirigée par **Sabine Kraml**

préparée au sein **Laboratoire de Physique Subatomique et Cosmologie** et de **Ecole doctorale de Physique**

Aspects de théories unifiées supersymmétriques en dimensions supplémentaires

Thèse soutenue publiquement le **23 Septembre 2011**, devant le jury composé de :

Pr. Jean Orloff
LPC, Université Blaise Pascal and CNRS, Président
Pr. Emilian Dudas
CPhT, Ecole Polytechnique and CNRS, Rapporteur
Pr. Benjamin Allanach
DAMTP, Centre for Mathematical Sciences, Cambridge, Rapporteur
Pr. Laura Covi
Institute for theoretical Physics, Georg-August University, Examinatrice
Dr. Jean-Loïc Kneur
LPTA, Université Montpellier II and CNRS, Examinateur
Pr. Aurélien Barrau
LPSC, Université de Grenoble and CNRS, Examinateur
Dr. Sabine Kraml
LPSC, Université de Grenoble and CNRS, Directeur de thèse

A ma famille.

Life is growth.
If we stop growing,
technically and spiritually,
we are as good as dead.

Morihei Ueshiba

Remerciements

Avant toute chose, je dois exprimer toute ma gratitude envers ma directrice de thèse Sabine Kraml, pour la confiance qu'elle m'a accordée et la qualité de son encadrement. Au-delà des articles et des connaissances scientifiques, son engagement, sa curiosité, son ouverture d'esprit, ainsi que son sens pratique, font d'elle une chercheuse exemplaire à mon sens. Merci donc, pour ces trois années grâce auxquelles, je l'espère, je deviendrait moi aussi un chercheur digne de ce nom.

Je remercie Emilian Dudas et Ben Allanach de m'avoir fait l'honneur d'accepter d'être mes rapporteurs. Je remercie bien sûr aussi les autres membres du jury, Jean Orloff, Jean-Loïc Kneur, Laura Covi, et Aurélien Barrau.

Une part de ma reconnaissance va à toutes les personnes qui ont bien voulu répondre à mes questions au cours de ces trois années. Comme une liste exhaustive serait très longue, je citerai simplement mes collaborateurs Arthur Hebecker, Ritesh Singh, et tout particulièrement Felix Brümmer pour les très très nombreux emails que nous avons échangé, ainsi que quelques autres personnes choisies presque au hasard : Gero Von Gersdorff, Thorsten Ohl, Tim Jones, Kin-Ya Oda , Kiwoon Choi, Geneviève Bélanger, Laura Covi, Harrison Prosper, ...

Alors qu'il est facile de remercier les gens du travail, les mots me manquent pour exprimer la reconnaissance envers mes parents en quelques lignes. En restant un peu formel, je dirai simplement qu'ils m'ont toujours apporté tout les deux un soutien (quasiment) sans failles quelques fussent mes choix, y compris quand je me suis engagé dans la voie de la recherche.

J'en profite pour passer le bonjour à mon frère, avec qui entre autre, nous fîmes trembler l'institution QPUC sur ses bases durant ces années de thèse, à un point tel que les hautes instances décidèrent de tout arrêter.

Cette thèse s'est déroulée en parallèle avec celles de mes collocataires du 52, Docteur Poual et Docteur Zouave. Les mots là-aussi me manquent pour évoquer ces moments intenses, partagés dans le meilleur et dans le pire. Messieurs, que félicité, stupre et opulence vous accompagne. Une pensée également pour les autres anciens habitants, Furby et Mini-Jenna, tout deux brillants dans leur spécialité. Je tient aussi à remercier Régis-Robert, qui

a exploré à sa manière tout un pan de l'expression orale et corporelle, ouvrant des routes jusque-là insoupçonnées pour l'évolution du genre humain.

Je remercie aussi Anaïs pour tout les bons moments que nous avons partagé les trois années précédentes. Une autre chercheuse exemplaire soit dit en passant, bien que ce ne soit qu'un aspect de ses nombreux talents.

Les autres amis et copains mériteraient certainement tous d'être cités. Cependant, pour éviter tout oubli malencontreux, je n'en ferait rien, ils se reconnaîtront d'eux même. Je remercie aussi tout les collègues de travail avec qui j'ai passé de bons moments au cours de ces trois années. Là encore, pour éviter tout oubli tragique, je préfère ne citer personne.

Pour que cette page de remerciement ne sombre pas dans l'hypocrisie, je me doit aussi de ne *pas* remercier certaines personnes, sans désigner quiconque explicitement. Comme la liste, là encore, pourrait devenir très longue, je me concentrerai sur une une seule catégorie. Tout mon mépris va aux personnes qui forcent leur collaborateurs à consacrer tout leur temps au travail, et qui considèrent que le repos est une perte de temps. C'est, bien sûr, en suivant son rythme naturel et en ayant une vie équilibré que les idées neuves et les solutions à tout les problèmes, des plus abstraits aux plus terre-à-terre, peuvent apparaître. Par un juste retour des choses, les personnes de ce type n'ont elles-même pas d'idées intéressantes, et produisent des articles particulièrement ennuyeux.

Enfin, pour conclure ces remerciements, je doit inévitablement parler de Wikipédia, qui est un accélérateur incroyable pour la recherche. Le site a participé à créer ma vocation, m'a accompagné tout au long de ma thèse, et a même été crucial pour le démarrage et le développement du projet sur l'approche Bayesienne de la naturalité (à paraître d'ici peu). Etant donné qu'aujourd'hui le prix d'une revue avoisine le dollar US par page, il paraîtrait raisonnable que les organismes de recherche puissent donnent un petit peu à ce site.

Mais trêve de balivernes, sortez vos stylo-plumes et rangez vos calculettes, l'heure est venue de passer aux choses sérieuses !

Contents

Foreword

During the $XVII^{\text{th}}$ century, Sir Isaac Newton applied differential and integral calculus to the real world to describe the behavior of objects under forces and motions. Since this time, often considered as the advent of modern physics, mathematics have found more and more roots into the real world. For example, developments in quantum mechanics lead to the development of distribution theory, while Einstein's General Theory of Relativity is based on what is now known as differential geometry. This fascinating link between mathematics and the real world culminates today in the domain of particle physics.

In particular, the notion of symmetry plays a central role in particle physics, where the objects are defined by their transformations under symmetry groups. For example, the spin of elementary particles characterizes their transformation laws under the spacetime symmetry group (the Poincaré group). Even better, quantum field theories with local continuous symmetries are at the origin of the description of particle interactions. Indeed, a local symmetry group is a fiber bundle over spacetime, whose the curvature form describes the vector fields, mediating particle interactions [1]. Such fields are called gauge fields, and are associated to the generators of the continuous symmetry group.

It appeared that strong interaction, confining quarks into nucleons, is described by the gauge group $\mathrm{SU}(3)_c$, while the electroweak interaction can be described by the gauge group $\mathrm{SU}(2)_L \times \mathrm{U}(1)_Y$. These descriptions have been tested at the level of three-particle interactions with an impressive success at LEP, for instance in the process $e^{\pm}e^{\mp} \to W^{\pm}W^{\mp}$. However, at the level of two-particle interactions (i.e. the masses), the gauge structure is strongly broken in the electroweak sector, calling for a mechanism of symmetry breaking. While the preferred candidate for this role is the Brout-Englert-Higgs mechanism, there is for the moment no direct proof of the existence of the scalar particle it predicts, the Higgs boson.

There are many pieces of evidence that this Standard Model is not the ultimate theory. In particular, neutrino oscillations prove that they are massive, which is not possible within the Standard Model. And in any case, a theory of quantum gravity, necessary at the Planck scale, remains to be found. However, at less small distances, there are also clues, deeply linked to electroweak symmetry breaking, that new extended symmetries should be restored at the TeV-scale. This could be new gauge symmetries, or even new spacetime symmetries.

Since 2000, the Large Hadron Collider has been built at CERN, in order to discover the mechanism of electroweak breaking as well as these new TeV-scale symmetries. This construction is presently finished, and we are at the dawn of an era of discovery. Since March 2010, the LHC hunting for the Higgs boson and TeV particles has begun. The LHC is presently running in a first stage of 3.5 TeV by beam, and has already accumulated more than 1 fb^{-1} of data. However, even if all eyes are upon the LHC, other experiments (Tevatron, low-energy precision experiments, as well dark matter detection, and astrophysics and cosmology observations) are also promising, such that one cannot predict in which domain the first discovery will appear.

Among the different TeV-scale symmetries postulated, a particularly attractive proposition is supersymmetry. In particular, simple supersymmetric realizations lead naturally to the unification of the three gauge interactions into a single gauge group at very small distances. Among realistic versions of these so-called Grand Unified Theories (GUTs), the ones realized in an extra-dimensional framework are particularly simple and attractive.

The purpose of this work is to investigate such models and to make the link with passed and upcoming experiments. The structure of this thesis is as follows.

- In the first chapter, we will briefly review the sequence of arguments leading to the Higgs mechanism, then to the different concepts underlying physics beyond the Standard Model, and to the paradigm of extra dimensional supersymmetric grand unified theories. At each level of the argumentation, we will mention the different solutions available.

- The second chapter introduces more formally supersymmetry and extra dimensions, focusing in particular on the aspects of symmetry breaking.

- Then, in the third chapter, we present in details the two frameworks of extra dimensional theories in which we worked, called supersymmetric gauge-Higgs unification (GHU) and holographic grand unification (HGU) as well as the developments and modifications we brought to them.

- The fourth chapter is devoted to the low energy viability of the GHU framework, as well as its phenomenologic implications.

- The fifth chapter presents a more generic study of the property of GUT-scale degenerate Higgs mass matrix, common to both frameworks.

- Finally, the sixth chapter is devoted to the viability and phenomenologic implications of the HGU framework, with special emphasis on lepton flavour violation. This quantitative study takes properly into account effects of matrix anarchy, as well as exact flavour observables. The results obtained should generalize, at least qualitatively, to any other model with similar localization and supersymmetry breaking features.

- The Appendix contains a brief review on Bayesian statistics, a comment on a Bayesian approach to the fine-tuning concept, and an analytic study of Yukawa textures in the HGU framework.

Chapter 1

From electroweak breaking to extra dimensional supersymmetric models

After a comment on renormalization, we will shortly review the motivation leading to extra dimensional supersymmetric grand-unified theories. Indeed, it is important to be aware of the sequence of arguments leading to such ideas, as well as the other solutions available at each level of the puzzle.

1.1 On renormalization

One of the most fascinating aspects of interacting quantum field theories (QFT) is renormalization [2–4]. Since the first loop calculations by Bethe in 1947, its conceptual understanding has strongly evolved. Indeed, historically, the procedure of canceling divergences appearing in closed loops of virtual particles by redefining the Lagrangian constants was considered like an ugly trick, for example by Dirac and Feynman. Moreover, theories with non renormalizable couplings were considered as totally inconsistent. Today, we know that the redefinition of parameters is natural and unavoidable, and the criteria of renormalizability has been replaced by the paradigm of effective theory.

To better understand renormalization, an important conceptual step is to be aware of a degree of freedom in the description itself: the unit scale μ with respect to which all dimensionful parameters are expressed. Clearly, this is not a physical degree of freedom. In fact, by definition, observables have to remain invariant under any change of this scale. This even defines how the Lagrangian parameters should vary under a change of μ: the renormalization flow, formalized by the renormalization group equations. This unit scale μ is usually called renormalization scale, and really can be seen as the scale at which we observe the theory, just like a magnification scale.

It is instructive to consider the simplest example: a free massive scalar field of mass

m. The Lagrangian describing such a field is

$$\mathcal{L} = \int d^d x \left(|\partial\phi|^2 - m^2 |\phi|^2 \right) \ . \tag{1.1}$$

The propagator of ϕ is

$$\langle \phi(k)\phi(-k) \rangle = \frac{i}{k^2 - m^2} \ . \tag{1.2}$$

At small distances $|x - y| \ll m^{-1}$, the mass term becomes negligible and the scalar field behave as a massless field. In contrast, at large distances $|x - y| \gg m^{-1}$, the field becomes static. The renormalization group will precisely highlight this scaling property. If one defines $\hat{m} = m/\mu$, the variation with μ, of $\hat{m}$ is:

$$\mu \frac{d\hat{m}}{d\mu} = -\hat{m} \ . \tag{1.3}$$

This is the renormalization group equation of $\hat{m}$. At high scale, $\hat{m}$ flows to zero, while at low scale, $\hat{m}$ flows to infinity. One thus finds again that ϕ becomes massless at high scale and static at low scale. On other words, by magnifying the theory, the field appears less ans less massive. The -1 coefficient corresponds to the scaling dimension of $\hat{m}$. This is here an integer, as we consider a pure classical scaling.

In comparison to this simple example, the quantum dynamics of an interacting QFT will simply induce a non-integer, anomalous scaling of the parameters in addition to the classical scaling. However the conceptual situation will be in fact more subtle, with the raise of a second energy scale.

Before going to this point, we first recall the idea of effective field theory, which has replaced the idea of renormalizable theory. An effective field theory is a theory permitting to describe phenomena occurring below a cutoff scale Λ. It contains a renormalizable part, and a non-renormalizable part made of an infinity of operators suppressed by negative powers of Λ. Due to the classical renormalization flow, this non-renormalizable part decreases with the renormalization scale, and becomes quickly negligible. For example, one should add to the Standard Model operators suppressed by powers of the Planck mass, but their effects are absolutely undetectable at our scale of energy. More precisely, one can see that integrating out an heavy field of mass M has two effects: it gives a finite shift to the Lagrangian parameters, and provides infinite series of operators suppressed by M. The cutoff of such an effective theory is then typically M.

We can now speak about the modern, Wilsonian approach to the renormalization flow in QFT. It is closely related to the concept of effective quantum field theory. Indeed, one defines a cutoff scale Λ above which all physics is hidden, absorbed in the fundamental parameters. All quantum effects involving an impulsion larger than Λ are thus not taken into account. Changing infinitesimally this cutoff will then induce an infinitesimal change in the fundamental parameters: the renormalization group flow appears again.

This cutoff scale Λ is conceptually rather different from the renormalization scale μ, which we interpreted as the scale at which we look at the theory. Instead, this cutoff could be compared to a length of resolution, below which we don't see the details of the theory. We have thus two different approaches to understand the renormalization flow, involving two conceptually different energy scales. One could be surprised by such a situation. This property is in fact a manifestation of the self-similarity of the quantum dynamics: the picture remains invariant if one increases the resolution $\Lambda \to \alpha\Lambda$ and magnify by the same coefficient $\mu \to \alpha\mu$.

1.2 The $W_L W_L$ scattering

The theoretical pillar for the description of particle interactions is gauge theory. That is, quantum field theory with a Lagrangian invariant under some continuous local transformation. Indeed, the gauge fields arising in such a theory describe the interaction fields. They are equivalent, in a more mathematical view, to the curvature form associated to the connexion on a fiber bundle, in which the base space is spacetime and the fiber is the continuous symmetry group [1]. It turns out experimentally that the gauge fields associated to the $\mathrm{SU}(2)_L$ group of the Standard Model, describing weak interaction, are massive. It is possible to include these masses in an effective, non-renormalizable model. However we should wonder what is the value of this cutoff, and which inconsistencies are concretely appearing beyond it.

The masses of $\mathrm{SU}(2)_L$ gauge bosons give them a longitudinal polarization. It is thus not surprising that inconsistencies come from this sector. It turns out that the interaction cross-section for the scattering of longitudinal component of W bosons in this effective theory grows with the energy [5–8]:

$$\frac{d\sigma}{dE} \sim g^4 \frac{E^4}{M_W^4} \quad . \tag{1.4}$$

However a cross-section computed with perturbation theory is necessarily bounded. To be more precise, the optical theorem, based on conservation of probability (i.e. unitarity of the S matrix), provides a bound on the scattering amplitudes composing the cross-section. This bound in the above case translates as a bound on the center of mass energy:

$$\sqrt{s} = 2E \leq 1.2 \quad \text{TeV} \quad , \tag{1.5}$$

above which there is "violation of pertubative unitarity" (see for example [9] and references therein).

1.3 Beyond 1.2 TeV

What can we expect above this cutoff? Either new degrees of freedom have to appear to cure or postpone unitarity violation, or the framework of perturbation theory is no longer valid. We will now shortly discuss these different possibilities. The frameworks presented addresses in fact two, different but closely related, questions: what is the origin of degrees of freedom providing a mass to electroweak gauge bosons, and what happens beyond 1.2 TeV ?

1.3.1 Higgs framework

A first solution is to consider that a scalar particle h, called Higgs boson, with an appropriate charge under $\mathrm{SU}(2)_L \times U(1)_Y$, and mass smaller or close from the energy limit, is present in the theory. It can cancel the E^4 contributions, providing a finite cross-section [5–8]:

$$\frac{d\sigma}{dE} \sim g^4 \frac{m_h^4}{16 M_W^4} \quad . \tag{1.6}$$

This is what happens in a spontaneously broken gauge theory. In such a theory, a scalar field gets a non-zero vacuum expectation value (vev), due to an appropriate shape of potential. The fundamental state is symmetric only under a subgroup $\mathcal{H}$ of the original group $\mathcal{G}$. The Goldstone bosons associated to the coset $\mathcal{G}/\mathcal{H}$ are absorbed in the longitudinal degrees of freedom of gauge bosons, making them massive. This is the Brout-Englert-Guralnik-Hagen-Higgs-Kibble mechanism [10–13], another pillar of the Standard Model. Fermion masses can also be generated through couplings to this scalar field. Note that if the Higgs boson is elementary, like in the standard mechanism, the cancellation is exact. In a more general framework where the Higgs is a composite state arising from a stronger interaction, cancellations are not exact anymore, and the cutoff scale is postponed to higher values.

1.3.2 Higgsless models

Another solution, more recent than the well-know Higgs mechanism, is to make use of an extra dimension [14, 15]. In so-called Higgsless models, the electroweak gauge bosons are identified as part of a field confined in a compact extra-dimension. From the 4-dimensional point of view, this extra-dimensional field decomposes as a serie of fields with different masses, called Kaluza-Klein modes. The lightest, fundamental mode, is identified as an electroweak gauge boson. In such models, the heavier kaluza-Klein modes will enter in the game to postpone unitarity violation to a higher energy scale. This higher scale will in fact be the cutoff scale of the 5D theory.

1.3.3 Strong dynamics

One can also assume that perturbative unitarity is violated because perturbation theory does not apply anymore. This would happen if the degrees of freedom giving mass to the electroweak gauge bosons were Goldstone bosons coming from a spontaneously broken global symmetry, induced by the dynamic of a new, stronger interaction. These Goldstone bosons would then be composite, made of new fermions confined by this interaction. This is the basic idea of "technicolor" theories (see for example [16] and references therein). An analogy with the light spectrum of QCD can be done. Indeed, the pions are Goldstone bosons associated to chiral symmetry breaking. Their scattering can be described by a weakly coupled effective theory, which violates unitarity at some energy scale because resonances like the ρ meson are not included. Following this analogy, manifestations of the new strong dynamics should appear beyond 1.2 TeV.

1.4 More on the Higgs framework

The different frameworks described above all lead to new phenomena at the TeV-scale: scalar particle, heavy replicas of vector bosons, resonances, etc. It seems that whatever unitarizes the $W_L W_L$ scattering, the LHC will have the potential to observe it.

However, these frameworks are constrained by observation, because then can potentially generate large effects in flavour changing neutral currents or CP violation. They are also tightly constrained by electroweak precision measurements, performed at LEP between 1989 and 2000 [17–19]. A lot of work has been done within the Higgsless and technicolor frameworks to make them comply with experiments, but we will not go further in these directions in this thesis. Instead, we will keep the widely known Higgs mechanism as paradigm.

Let us focus on the scalar potential used to break electroweak symmetry in the Higgs mechanism. To give a non zero vev to the scalar field H, one defines a quartic potential:

$$V(H) = -\frac{1}{2}\mu^2|H|^2 + \frac{1}{4}\lambda|H|^4 \quad . \tag{1.7}$$

This potential can be seen as a local expansion of any more evolved potential around the minimum. At the fundamental state, the Higgs vev is

$$\langle H \rangle = v = \mu/\sqrt{\lambda} \tag{1.8}$$

and the mass of the physical particle, the Higgs boson h, responsible of $W_L W_L$ unitarization, is

$$m_h^2 = 2\mu^2 \ . \tag{1.9}$$

The Higgs vev is fixed by the measurements of the electroweak gauge bosons masses, while the physical Higgs mass remains a free parameter. LEP set a bound of [20]

$$m_h > 114.4 \text{ GeV} \quad (CL = 95\%) \ , \tag{1.10}$$

while LHC excludes presently (see [21, 22] for last public results)

$$145 - 216, \ 226 - 288, \text{ and } 310 - 400 \text{ GeV} \quad (CL = 95\%) \ . \tag{1.11}$$

More theoretical constraints also apply to the Higgs mass. For example, unitarity requires a sufficiently light mass: $m_h < 780$ GeV. There are also constraints coming from the quantum behaviour of the quartic coupling (see for example [23] and references therein). Indeed, if the quartic coupling is large, it reaches a Landau pole, signaling the need of new physics. On the other hand, if the quartic coupling is sufficiently small, the Higgs potential can have a deeper minimum, far from the origin such that one can assess stability or metastability bounds requiring that the tunneling time be longer than the age of the universe.

1.5 Gauge hierarchy problem an its solutions

Can the Standard Model be valid up to very high energy scales, like the Planck mass? The study of the quantum contributions to the potential (1.7) shows that the answer is very probably no. The quantum behaviour of the quartic coupling λ leads to interesting constraints on m_h^2, but we will here focus on the quantum behaviour of m_h^2 itself [24].

1.5.1 Gauge hierarchy problem

Let's consider a Lagrangian describing a single free particle with mass $m_{phys} = m$. Then add a heavier particle with mass $M \gg m$, which is interacting with the first one through some interaction with strength α. Due to quantum effects, the mass of the light particle m_{phys} will get threshold corrections. In case of fermions [resp. vectors], these corrections will be proportional to m:

$$m_{phys} = m(1 + \frac{\alpha}{4\pi} \log(M/m)) + ... \tag{1.12}$$

This is due to the presence of the chiral [resp. gauge] symmetry, which protects the light particle from getting large quantum corrections. This is an illustration of the "t'Hooft naturalness principle", stating that a parameter can be naturally small if the symmetry of the system increases in the limit where this parameter goes to zero. Contrary to the fermions and vectors, a scalar is not protect by any symmetry. Its mass receive quadratic corrections, instead of logarithmic ones:

$$m_{phys}^2 = m^2 + \frac{\alpha}{4\pi} M^2 + ... \ . \tag{1.13}$$

This property holds up to additional loop factors if the elementary scalar is not interacting directly with the heavy state. Note that we only comment on the threshold correction here, without precising the running of the coupling α.

Given that new physics must arise at the Planck scale $M_{Pl} \approx 10^{18}$ GeV, where a theory of quantum gravity is needed, M is at least $\mathcal{O}(M_{Pl})$. Thus, unless a tuning of order 10^{-30} of the Standard Model parameters occurs, the mass of the Higgs boson should be $\mathcal{O}(M_{Pl})$. This is the so-called gauge hierarchy problem, and we will now discuss different approaches to solve it.

1.5.2 Anthropic coincidence

An interesting hypothesis is that we live in a multiverse like the superstring landscape. In such a configuration, fundamental constants could be varying from different locations in spacetime. The existence of such a distribution for the Higgs vev permits to apply a robust anthropic reasoning.

Indeed, it is observed that if the Higgs vev was slightly different from the measured value, life as we know could not exist [25]. More precisely, if $\frac{v}{v_{phys}} < 0.39$, hydrogen would decay through $p + e \to n + \nu$, while if $\frac{v}{v_{phys}} > 1.64$, complex nuclei could not be formed anymore. In the light of such argument, we are simply in a location of the multiverse where the Higgs vev is within the appropriate range to let us exist and measure it. This is an anthropic answer to the gauge hierarchy problem.

1.5.3 Apparent Planck scale

Another hypothesis is that the Planck mass, estimated through dimensional analysis of the gravity strength, is not so high. If for any reason, the Planck mass was much lower, the gauge hierarchy problem would be alleviated. However, one has to assume that the new theory of the quantum gravity beyond should not contribute to the scalar mass. This idea is realized in the original Randall-Sundrum scenario [26]. In such a scenario, the Standard Model is confined on a 3-brane, while gravity is propagating in an extra dimension with negative curvature, and is mostly confined on a different 3-brane. A consequence of this geometry is that the apparent gravity strength observed is much smaller than the actual one. The scale where quantum gravity appears is then much lower than the usual Planck mass.

1.5.4 TeV-scale symmetries

Another type of hypothesis is that at some cutoff scale, a new symmetry is restored to protect the Higgs mass from quadratic corrections. As no manifestation of such symmetry has been detected up to now, this scale of spontaneous breaking is constrained to be at least one order of magnitude above the weak scale. The tension between these two scales leaves some degree of fine-tuning, which is however far from the initial gauge hierarchy problem.

The interpretation of a degree of fine-tuning is something subjective, which leads some people to irrational believes and endless debates. To offer a consistent framework to this important concept, as well as a better control on the subjectivity associated, Bayesian statistics seems very appropriate. This idea is developed in Appendix A.

Higgs as pseudo Nambu-Goldstone boson

Another possibility is to consider the Higgs as a Goldstone boson arising from a spontaneously broken gauge symmetry. Its mass is then protected by a non-linear symmetry at any loop order. To make it massive, this gauge symmetry should also be explicitly broken. The Higgs mass can then be generated at the one-loop level. Once again, this is the analogy with pions, the pseudo Nambu-Goldstone bosons (pNGBs) arising from the quark chiral symmetry breaking, triggered both spontaneously by QCD dynamics and explicitly by quark masses. The idea of a pNGB Higgs [27] is for example exploited in the Little Higgs framework [28], where a collective breaking of gauge groups is used to push the new physics scale sufficiently high. It is also used in the holographic Higgs framework [29], where the Higgs arise as a composite state of a strongly coupled conformal field theory.

Higgs protected by gauge symmetry

Another possibility is to consider the Higgs as a part of a gauge field (see [30–32], or [33] for a recent review). This idea is used in the gauge-Higgs unification framework, where one lets some gauge field propagate in a compact extra dimension. Due to compactification, the fifth component of such a gauge field is a scalar which can be identified as the Higgs. This Higgs inherits the good quantum behaviour of gauge fields: it is protected by gauge symmetry.

Higgs protected by chiral symmetry

Yet another possibility is to make the Higgs inherit the quantum behaviour of fermions. This idea is realized by supersymmetry, where scalar and fermions are merged in more global entities.

Concretely, for each of these proposed symmetries, new particles will appear at the breaking scale, to cancel the loops providing quadratic contributions to the Higgs mass. One of the purpose of the LHC is to discover these new particles.

In the following, we will focus on the last proposition. Supersymmetry indeed possesses other interesting virtues. Replicants of the other ideas evocated will re-appear in the context of high energy frameworks described in Chapter 3, but for other purposes than solving the gauge hierarchy problem.

1.6 MSSM and grand unification

1.6.1 Minimal Supersymmetric Standard Model

We now present the simplest supersymmetric version of the Standard Model (see for example [24] or [34]). In the so-called Minimal Supersymmetric Standard Model (MSSM), all SM fields are embedded in different supermultiplets [1] . It was shown that embedding the Higgs and a lepton in a single chiral multiplet is not phenomenologically viable. However this attempt can reappear in more evolved models.

The MSSM field content is summarized in Table 1.6.1. In this notation, all spin 1/2 fields are left-handed two components Weyl fermions. Due to holomorphy of the superpotential, one needs to couple two different Higgs doublets to up and down quark families. Moreover, with only one of these Higgses, one would get gauge anomalies due to hypercharges. The most general superpotential is

$$W = W_{MSSM} + W_{\not R}, \tag{1.14}$$

$$W_{MSSM} = y^e_{ij} L_i H_1 E_j + y^d_{ij} Q_i H_1 D_j + y^u_{ij} Q_i H_2 U_j + \mu H_1 H_2. \tag{1.15}$$

$$W_{\not R} = \frac{1}{2}\lambda_{ijk} L_i L_j E_k + \lambda'_{ijk} L_i Q_j D_k + \frac{1}{2}\lambda''_{ijk} U_i D_j D_k + \kappa_i L_i H \tag{1.16}$$

In the MSSM, the $U(1)_R$ symmetry associated to $\mathcal{N} = 1$ SUSY is explicitly broken by gaugino masses, but a residual R-parity can remain. If it is present, then $W_{\not R}$ is forbidden. It then ensures stability of the lightest supersymmetric particle. On the opposite, if all couplings of $W_{\not R}$ can exist, it then induces proton decay. But other discrete symmetries allowing one or two of the R-parity violating coupling can also be viable.

The μ parameter is the only dimensionful supersymmetric parameter. Special mechanisms are needed to give it $\mathcal{O}$(TeV) values. This is one of the motivation for the NMSSM, where it is dynamically generated by the vev of an additional scalar singlet. Another solution, realized in the models we will present, is to generate it only through supersymmetry breaking.

[1] Some notions used in this section will be defined in Chapter 2.

Superfield	Name		spin 0	spin 1/2	spin 1
Chiral	(s-)quarks	Q	$(\tilde{u}_L\, \tilde{d}_L)$	$(u_L\, d_L)$	
	(3 generations)	U	$\tilde{u}^*_R$	$u^\dagger_R$	
		D	$\tilde{d}^*_R$	$d^\dagger_R$	
	(s-)leptons	L	$(\tilde{\nu}\, \tilde{e}_L)$	$(\nu\, e_L)$	
	(3 generations)	E	$\tilde{e}^*_R$	$e^\dagger_R$	
	Higgs(-inos)	H_1	$(H_1^+\, H_1^0)$	$(\widetilde{H}_1^+\, \widetilde{H}_1^0)$	
		H_2	$(H_2^0\, H_2^-)$	$(\widetilde{H}_2^0\, \widetilde{H}_2^-)$	
Vector	gluon(gluino)			$\tilde{g}$	g
	boson W (wino)			$\widetilde{W}^\pm \widetilde{W}^0$	$W^\pm W^0$
	boson B (bino)			$\widetilde{B}^0$	B^0

Table 1.1: The MSSM supermultiplet content. Q,L,H_1 and H_2 are $\mathrm{SU}(2)_L$ doublets.

As we will explain in more details in Subsection 2.1.6, supersymmetry needs to be broken, if not we would have already discovered it. The soft-breaking parameters of the MSSM are:

- the gaugino masses $M_a\lambda_a\lambda_a$, associated to each vector multiplet, with $a = 1, 2, 3$ corresponding to the gauge groups $U(1)$, $SU(2)$ et $SU(3)$,
- the scalar masses $m^2_{ij}\phi_i\bar{\phi}_j$, which are 3×3 hermitian matrices, associated to each chiral superfield Q, U, D, L, E, $H_{1(d)}$, $H_{2(u)}$
- the trilinear couplings between scalars $a_{ijk}\phi_i\phi_j\phi_k$ (or $A_{ijk}y_{ijk}\phi_i\phi_j\phi_k$) , which are 3×3 complex matrices, in correspondence with each Yukawa coupling,
- and the bilinear coupling for the Higgs masses $B_\mu H_1 H_2$.

These parameters enter in the canonically normalized Lagrangian as

$$\mathcal{L}_{soft} = (M_a\lambda_a\lambda_a - a_{ijk}\phi_i\phi_j\phi_k - B_\mu H_1 H_2) + \text{h.c.} - m^2_{ij}\phi_i\bar{\phi}_j \tag{1.17}$$

This sets the convention for the soft terms which will be derived in Sections 3.1 and 3.2. Note there are around 100 parameters in these soft terms. Such a large number strongly suggests to look for an underlying principle of SUSY breaking. This is the approach we adopted in our work.

The renormalization group equations for the MSSM soft terms can be found in [24] (1-loop) or in [35] (2-loop and flavours). An appealing feature is that the $m^2_{H_u}$ soft mass

is driven toward negative values in the RGEs, by top quark loops. This produces at low energy the appropriate potential to trigger electroweak breaking. The scalar potential of the electroweak sector is

$$\mathcal{V} = m_1^2|H_{1(d)}| + m_2^2|H_{2(u)}| + (m_3^2 H_1 H_2 + \text{h.c}) + \frac{1}{8}(g_1^2 + g_2^2)||H_1|^2 - |H_2|^2|^2 \ , \qquad (1.18)$$

with $m_1^2 = m_{H_d}^2 + |\mu|^2$, $m_2^2 = m_{H_u}^2 + |\mu|^2$ and $m_3^2 = B_\mu$. Two conditions have to be fulfilled to trigger electroweak breaking. Having a non-trivial minimum recquires

$$m_3^2 > m_1^2 + m_2^2 \ . \qquad (1.19)$$

On the other hand, the condition

$$m_3^4 < m_1^2 m_2^2 \qquad (1.20)$$

is necessary to avoid the presence along the D-flat direction of a deeper radiatively stabilized minimum, far from the origin.

1.6.2 Grand Unification

A striking feature of the MSSM field content is that, contrary to the SM, it gives to the three gauge couplings exactly the good anomalous scaling to make them unify, at a scale $\sim 2 \times 10^{16}$ GeV. This is precisely what would happen if the SM gauge groups where arising from a larger, unifying gauge group, broken at the unification scale [36–38]. Moreover, at this scale the massive gauge bosons of this broken Grand Unified Theory(GUT) would be sufficiently heavy to not induce fast proton decay, bounded by the SuperKamiokande experiment (see the excellent review [39] for everything about proton decay). However it is also possible to imagine special mechanisms to avoid fast proton decay.

The simplest group could be SU(5) or SO(10). Strikingly, the matter fields Q, U, D, L and E can be embedded in the complete representations 10 and $\bar{5}$ of SU(5), or even better in the 16 of SO(10), by adding the right-handed neutrino necessary for a see-saw mechanism. This would explain, in particular, why electrons and protons have exactly the opposite charge.

However, the two Higgses should also arise from representations of the GUT group. They should then necessarily be accompanied by colored particles coming from the same multiplets. But such states would trigger fast proton decay and spoil couplings unification if they were too light. Making them heavy is a challenge, generally called "doublet-triplet splitting problem". Another challenge is to trigger the spontaneous GUT breaking into $\mathcal{G}_{SM}$.

Mechanisms solving these two problem in 4D GUTs are either very fine-tuned, or rather convoluted ([40] contains an example). Curing the doublet-triplet splitting problem is a strong motivation for building extra-dimensional Grand-Unified Theories. Indeed, gauge

breaking by orbifolding (see Subsection 2.2.1) will permit to suppress light triplets rather easily. This will be realized in the two frameworks described in Section 3. Independently from this "bottom-up" approach, orbifold SUSY GUTs are also well motivated as low-energy limits of string theory (see [40] for a review).

1.7 Flavours in the Standard Model

To close this introductive chapter, we discuss the so-called Standard Model flavour puzzle and its solutions.

The observed quark and lepton masses and mixing angles exhibit a fascinating structure and regularity [20]. The masses of up quarks, down quarks and charged leptons are spanning more than five orders of magnitude, each of these types of particles following a hierarchical structure. The CKM matrix (i.e. up/down quark mixing matrix, see Sect. D.1) also has a hierarchical structure, with small mixing angles between the different generations, and with the largest mixing between adjacent generations. These properties are not explained by the Standard Model, and therefore calls for an explanation coming from new physics. Interestingly, these properties are sensibly conserved by the RGE running, so that they are also valid at the GUT scale. Flavour physics can therefore be a direct probe of GUT theories.

Several classes of mechanisms have been proposed to explain these hierarchical structures. We will briefly describe them below, referring to the literature for details.

Froggatt-Nielsen mechanism In this widely known mechanism, one assumes that SM fermions of different generations have different charges under a so-called "horizontal symmetry" $\mathcal{H}$. Assuming that this symmetry is broken at a typical scale Λ by one or several SM singlets vevs $\langle\phi\rangle$ charged under $\mathcal{H}$, the effective theory below the Λ scale can contain higher-dimensional operators coupling the Higgs to the fermions. Due to the $\mathcal{H}$ breaking, these higher-dimensional operators reduce to effective Yukawa couplings, suppressed by powers of $\langle\phi\rangle/\Lambda$ fixed by the charges. With an appropriate choice of charges, this permits to produce effective Yukawa matrices which are hierarchical, and which can reproduce the realistic structure of masses and mixings. To avoid Goldstone bosons, one usually assumes that $\mathcal{H}$ is gauged. There are many versions of this mechanism involving abelian or non-abelian horizontal gauge symmetries, and a huge amount of corresponding literature (see for example [41] and references therein). A geometrical realization of this mechanism has been recently proposed in the context of F-theory (see [42] and subsequent papers).

Hierarchy from power-law running Another mechanism, involving again a broken horizontal symmetry $\mathcal{H}$, was proposed in [43]. This time one considers that the SM gauge

singlet ϕ breaking $\mathcal{H}$ propagates along a compact extra dimension of radius R. Its vev does not need to be tuned to a specific, small value, as in the Froggatt-Nielsen mechanism. Above the KK scale $1/R$, the higher-dimensional couplings involving two fermions, the Higgs and powers of ϕ experiences a power-law running, induced by the ϕ KK states. With an appropriate choice of charges, this power-law running can generate the hierarchical, effective Yukawa matrices wanted. In this mechanism, even if one uses an horizontal symmetry, hierarchies are generated by a purely extra dimensional effect.

Nelson-Strassler mechanism In that mechanism [44], one considers that MSSM fields are coupled through superpotential terms to a strongly coupled sector $\mathcal{G}$, becoming a CFT in the infrared. MSSM fields are assumed to be neutral under $\mathcal{G}$, and it can be shown that operators involving only such neutral fields have a positive anomalous dimension. The Yukawa couplings will thus rapidly flow to small values in the IR, scaling as power laws depending on the anomalous dimensions $\gamma_{1,2,H}$ associated to the three fields:

$$y(\mu_{IR}) = y(\mu_{UV}) \left(\frac{\mu_{IR}}{\mu_{UV}}\right)^{\frac{1}{2}(\gamma_1+\gamma_2+\gamma_H)} . \tag{1.21}$$

Assuming appropriate values for the anomalous dimensions of different generations, one can once again obtain hierarchical Yukawa matrices in the infrared.

Wave-function localization Flavour hierarchies can also be generated by localizing differently each generations of matter fields in the bulk of a compact extra dimension. This can be done by using the bulk mass term defined in Eq. (2.52), inducing the exponential zero mode profiles of Eq. (2.53). Effective Yukawa couplings are given by the overlap of the matter fields and the Higgs field. In particular, if the Higgs is localized on a brane, the suppression of these Yukawa couplings depends exponentially on bulk masses. If the background is AdS_5, this mechanism is in fact related to the previous one through the gauge-gravity correspondence (see Subsection 2.2.2). The bulk mass c of a bulk field is in fact related to the anomalous dimension of the corresponding CFT operator $\mathcal{O}$. For example, for a chiral [antichiral] superfield, one has $\dim\mathcal{O} = 3/2 + |c + 1/2|$ [$\dim\mathcal{O} = 3/2 + |c - 1/2|$] (see the review [45] for a derivation).

Fermions on a vortex All the mechanisms described above contain independent (continuous or discrete) parameters for each generation, which permits to differentiate the different generations. In contrast, in the framework presented in [46, 47], it is proposed that our 4D world resides in the core of a higher-dimensional topological defect. It turns out that, starting from one extradimensional generation, the number of 4D zero modes is fixed by the topological number of the defect. A 6D model is developed, where the background is a 2D vortex made of a scalar field and a U(1) gauge field. Fixing the winding

number of the vortex at three produces therefore three generations. The elegant feature is that these fermion zero modes have automatically different profiles inside the vortex, leading to different overlap with the Higgs field. A flavour hierarchy is therefore naturally generated, without the need of differentiating by hand the different generations.

In extra-dimensional GUT building, the flavour mechanisms based on extra dimensions are of course particularly natural. For the framework of holographic GUT, described in Section 3.2, this is the mechanism of wave-function localization which will be exploited. In the 4D, dual description of this model, flavour hierarchy will thus be generated by the Nelson-Strassler mechanism. The low energy consequences of this setup will be investigated in Chapter 6.

Résumé de la section

Nous avons, dans cette Section, présenté la séquence de motivations qui mènent de la brisure électrofaible au Modèle Standard, puis aux théories de Grande Unification supersymmétriques en dimension supplémentaires. A chaque étape de l'argumentation, nous avons pris soin de parler des différentes solutions disponibles. En effet, toutes les idées, même si elles ne sont pas forcément retenues dans cette séquence, peuvent être réexploitées plus tard pour la construction de modèles.

Chapter 2

Introduction to supersymmetry and extra dimensions

We now present more formally two unavoidable ingredients of physics beyond the Standard Model: supersymmetry and extra dimensions. This chapter is supposed to be short and synthetic. For various reviews on global and local supersymmetry, see for example [3, 24, 34, 48–50]. For various reviews on extra space dimensions, possibly associated with supersymmetry, see for example [45, 51–53]. We also refers to the books [54, 55].

2.1 Supersymmetry and Supergravity

2.1.1 Supersymmetric algebra

The symmetries of the $3+1$ dimensional spacetime we observe is described by the Poincaré group. This group is composed of the four spacetime translations and the six Lorentz transformations. The Lie algebra of the Poincaré group, encoding commutations between the different generators, is:

$$[P_\mu, P_\nu] = 0, \tag{2.1}$$

$$[M_{\mu\nu}, P_\rho] = \eta_{\mu\rho} P_\nu - \eta_{\nu\rho} P_\mu, \tag{2.2}$$

$$[M_{\mu\nu}, P_{\rho\sigma}] = \eta_{\mu\rho} M_{\nu\sigma} - \eta_{\mu\sigma} M_{\nu\rho} - \eta_{\nu\rho} M_{\mu\sigma} + \eta_{\nu\sigma} M_{\mu\rho}. \tag{2.3}$$

where P contains the generators of translations and M contains the generators of rotations and boosts. The work of Haag-Lopuszanski-Sohnius shows that the only way to extend this algebra within an interacting quantum field theory is to add anticommuting generators of spin $1/2$ in addition to the Poincaré algebra generators. These fermionic generators can be written as:

$$Q = \begin{pmatrix} Q_\alpha \\ Q^{\dagger\dot{\alpha}} \end{pmatrix}, \quad \bar{Q} = \begin{pmatrix} Q^\alpha & Q^\dagger_{\dot{\alpha}} \end{pmatrix}, \tag{2.4}$$

where Q_α and $Q^{\dagger\dot{\alpha}}$ transforms like the representations 2 and $\bar{2}$ of SU(2). Commuting relations between fermionic and Poincaré generators are

$$\begin{aligned} [Q_\alpha, P_\mu] &= 0, \quad [Q_\alpha, M_{\mu\nu}] = i(\sigma_{\mu\nu})_\alpha{}^\beta Q_\beta, \\ \left[\bar{Q}_{\dot{\alpha}}, P_\mu\right] &= 0, \quad [Q_{\dot{\alpha}}, M_{\mu\nu}] = i(\sigma_{\mu\nu})^{\dot{\beta}}{}_{\dot{\alpha}} Q_{\dot{\beta}}, \end{aligned} \tag{2.5}$$

and anticommuting relations between fermionic generators are

$$\left\{Q_\alpha, \bar{Q}_{\dot{\beta}}\right\} = 2(\sigma^\mu)_{\alpha\dot{\beta}} P_\mu, \quad \{Q_\alpha, Q_\beta\} = 0. \tag{2.6}$$

This extended Poincaré algebra is called superalgebra. It is possible to construct such superalgebras with $\mathcal{N}$ pairs of Q_α, $Q^{\dagger\dot{\alpha}}$.

The Poincaré algebra is in fact embedded in a larger algebra: the conformal algebra. It contains for example the scale transformations evocated when presenting the renormalization flow. Similarly, the superalgebra can be embedded in a larger algebra: the superconformal algebra. The superconformal algebra with $\mathcal{N}$ pairs of generators contains a global so-called R-symmetry $\mathrm{SU}(\mathcal{N})_R$. The particularity of this R-symmetry is that it commutes with bosonic generators, but not with fermionic generators. Equivalently, in the superspace, the θ are charged under the R-symmetry, while the x^μ are not.

2.1.2 Supermultiplets in $3+1$ and $4+1$ dimensions

Having extended the symmetry group, we can now discuss what happens to the irreducible representations. It turns out they are made of particles with same mass and gauge quantum numbers, and different spin, called supermultiplets. Supermultiplets contains the same number of bosonic and fermionic degrees of freedom. In $3+1$ dimensions, only $\mathcal{N}=1$ supersymmetry is phenomenologically viable, because it is the only one providing chiral fermions.

The two $\mathcal{N}=1$ supermultiplets sufficient to build an extension of the Standard Model fields are called chiral multiplet and vector multiplet. They will contain static, unphysical fields called auxiliary fields, to let the supersymmetric algebra close off-shell.

The off-shell chiral multiplet is made of a complex scalar field, a Weyl fermion (with 4 degrees of freedom), and a complex auxiliary field. Going on-shell, the auxiliary field is integrated out and the Weyl fermion looses two degrees of freedom. The off-shell vector multiplet contains a Majorana fermion (with 4 degrees of freedom), a vector field with three degrees of freedom and a real auxiliary field. Going on-shell, the auxiliary field is integrated out, the vector field looses one degree of freedom and the Majorana fermion two.

In $4+1$ dimensions, the smallest spinor is a Dirac spinor with eight components. It implies that $\mathcal{N}=1$ $5D$ supersymmetry can be described as a $\mathcal{N}=2$ $4D$ supersymmetry. This property is used later to formulate 5D supersymmetry using 4D superfields.

Supermultiplets of $\mathcal{N}=2$ supersymmetry are called hypermultiplet and $\mathcal{N}=2$ vector multiplet. The hypermultiplet contains the same degrees of freedom as two conjugated $\mathcal{N}=1$ chiral multiplets. The $\mathcal{N}=2$ vector multiplet contains the same degrees of freedom as a $\mathcal{N}=1$ vector multiplet and a $\mathcal{N}=1$ chiral multiplet.

2.1.3 Superfield formalism

After extending the Poincaré algebra, one needs to extend spacetime in the same spirit, to provide coordinates on which the Q_α generators will act. One introduces two fermionic supercoordinates with two anticommuting components: $(\theta^\alpha, \bar{\theta}_{\dot{\alpha}})$. These Grassmann numbers have interesting properties, leading to a simple and compact formalism. In particular, any product of three θ or more is zero.

While in any rigorous introduction to supersymmetry, supersymmetric transformations have to been written and commented, we will here skip this part and refer to lectures and reviews cited.

Fields are now functions defined on the superspace: $\phi(x^\mu, \theta, \bar{\theta})$. Thanks to Grassmann numbers properties, the exact Taylor expansion with respect to θ, $\bar{\theta}$ is:

$$\phi(x^\mu, \theta, \bar{\theta}) = A + \theta\psi + \bar{\theta}\bar{\chi} + \theta^2 F + \bar{\theta}^2 G + \theta\sigma^\mu\bar{\theta}A_\mu + \theta^2\bar{\theta}\bar{\lambda} + \bar{\theta}^2\theta\xi + \theta^2\bar{\theta}^2 D \ , \tag{2.7}$$

where x^μ A, F, G and D are complex scalars, A_μ a complex vector, and ψ, χ, λ and ξ are fermionics. There are thus 16 scalar degrees of freedom and 16 fermionic degrees of freedom. This is twice more than the off-shell supermultiplets described previously.

By applying supersymmetric transformations to this general superfield, it turns out that two subsets are stable under transformations. These two subsets will in fact contain the degrees of freedom corresponding to the two off-shell supermultiplets.

The chiral superfield

The components A, ψ and F are stable under supersymmetric transformations, and correspond to the chiral supermultiplet. It can be written in a simple form:

$$\phi(x^\mu, \theta, \bar{\theta}) = A(y^\mu) + \sqrt{2}\theta\psi(y^\mu) - \theta^2 F(y^\mu) \tag{2.8}$$

where $y^\mu = x^\mu + \theta\sigma^\mu\bar{\theta}$. Expanding with respect to the θ makes appear spatial derivatives, which will make up kinetic terms in Lagrangians.

The vector superfield and field strength

The situation of the vector superfield is somewhat less straightforward. Indeed, one needs to assume a reality condition $\phi = \bar{\phi}$ on the general superfield, to make appear a Majorana

fermion and a real vector field:

$$V(x^\mu,\theta,\bar\theta) = C+i\theta\chi-i\bar\theta\bar\chi+\frac{1}{2}\theta^2(M+iN)-\frac{1}{2}\bar\theta^2(M-iN)+\theta\sigma^\mu\bar\theta(A_\mu)+i\theta^2\bar\theta\bar\lambda-i\bar\theta^2\theta\lambda+\frac{1}{2}\theta^2\bar\theta^2 G. \tag{2.9}$$

The first terms, which looks like a sum of chiral and antichiral superfield, are in fact unphysical components, and can be canceled within a particular gauge choice (the Wess-Zumino gauge). The remaining components correspond to the content of the vector supermultiplet.

From this field, one can build a chiral superfield, the field strength which is the supersymmetric equivalent of the $F_{\mu\nu}$ tensor:

$$W_\alpha = -i\lambda_\alpha + \theta_\alpha G - \frac{i}{2}(\sigma^\mu\bar\sigma^\nu\theta)F_{\mu\nu} - \theta^2(\sigma^\mu\partial_\mu\bar\lambda)_\alpha \ . \tag{2.10}$$

This will make up the gauge kinetic term in the Lagrangians. It is in fact possible to keep only the components appearing in the field strength, by an appropriate gauge choice(the Wess-Zumino gauge).

2.1.4 Lagrangians

Once again, we will only present a short summary of supersymmetric Lagrangians. The interested reader should look into the lectures and reviews cited. We thus start directly with the most general renormalizable Lagrangian, which can be written as:

$$\mathcal{L} \ = \ \left(\frac{1}{4g^2}\int d\theta^2 \mathrm{tr}(\mathcal{W}_a\mathcal{W}^a) + \mathrm{h.c.}\right) + \sum\int d\theta^2\bar\theta^2\bar\phi e^{2gV}\phi + \left(\int d\theta^2 W(\phi) + h.c.\right) \tag{2.11}$$

The last term is called superpotential, and contains chiral superfields:

$$W = a_i\phi_i + b_{ij}\phi_i\phi_j + c_{ijk}\phi_i\phi_j\phi_k \ . \tag{2.12}$$

The b_{ij} are mass terms. The a_i can exist only for a gauge singlet. By construction, the superpotential is an holomorphic function: it does not contains antichiral superfields.

To better see what this Lagrangian is describing, we integrate the auxiliary fields F and D, using their equations of motion:

$$F_i = -\frac{\partial W}{\phi_i} \ , \tag{2.13}$$

$$D^a = -g\bar\phi_i T^a_{ij}\phi_j \ . \tag{2.14}$$

The Lagrangian then becomes:

$$\begin{aligned}\mathcal{L} = \quad & -\frac{1}{4}F^a_{\mu\nu}F^{a\,\mu\nu} - i\lambda^a\sigma_\mu D^\mu\bar\lambda^a - i\psi^i\sigma_\mu D^\mu\bar\psi^i - |D^\mu\phi^i|^2 \\ & +\frac{1}{2}\left(\frac{\partial^2 W}{\partial\phi^i\partial\phi^j}\psi^i\psi^j + \mathrm{h.c.}\right) + i\sqrt{2}g^a T^a_{ij}(\bar\phi^i\lambda^a\psi^j - \phi^i\bar\lambda^a\bar\psi^j) \\ & -\mathcal{V}(\phi^i,\bar\phi^j)\end{aligned} \tag{2.15}$$

First line corresponds to kinetic terms for components of the vector and chiral superfields. Second line corresponds to Yukawa-type interactions, between two fermions and one scalar. Finally, third line is the scalar potential:

$$\mathcal{V} = \sum_i |F^i|^2 + \frac{1}{2}\sum_a (D^a)^2 \tag{2.16}$$

$$= \sum_i \left|\frac{\partial W}{\partial \phi^i}\right|^2 + \frac{1}{2}\sum_a g_a^2 \left(\bar{\phi}^i T^a_{ij} \phi^j\right)^2 \ , \tag{2.17}$$

which contains interactions between scalars and will have a crucial role in supersymmetry breaking.

The same work can be carried out in 5D. In practice, we used a formulation of 5D supersymmetry in terms of the previous 4D $\mathcal{N} = 1$ superfields ([56, 57]). In such a formulation, only half of the supersymmetry is explicit, but the other half disappear below the compactification scale.

2.1.5 Renormalization properties

Renormalization of supersymmetric quantum field theories is particularly simple. Indeed, in $\mathcal{N} = 1$ supersymmetry, there is only wave-function renormalization. The superpotential couplings are not renormalized at any order: all renormalization effects take place in the kinetic function. While this appears through the usual renormalization procedure, it can be elegantly shown by promoting all constants to superfields. In particular, the kinetic function and even the cutoff of the regulator are considered has superfields in such arguments. The superpotential can however be renormalized by nonperturbative effects.

In $\mathcal{N} = 2$ supersymmetry, hypermultiplets are not renormalized, and vector multiplets are renormalized at one-loop only. Supersymmetric Yang mills theory with $\mathcal{N} = 4$ and beyond are not renormalized at all. They are thus conformal: the gauge coupling are invariant under changes of scale.

2.1.6 Supersymmetry breaking

Coming back to the superalgebra, one can see that the Hamiltonian can be written as

$$H = P^0 = \frac{1}{4}\left(Q_1 Q_1^\dagger + Q_1^\dagger Q_1 + Q_2 Q_2^\dagger + Q_2^\dagger Q_2\right) \ . \tag{2.18}$$

This implies that $\langle a| H |a\rangle \geq 0$, whatever the state $|a\rangle$ is. It implies that energy has to be positive in supersymmetric theories! This will be different with explicit breaking or local supersymmetry. Moreover, considering a ground state $|0\rangle$, $\langle 0| H |0\rangle = 0$ implies that supersymmetry is unbroken, while $\langle 0| H |0\rangle > 0$ implies that supersymmetry is broken.

At least in 4D, fermions and vectors should not get any vacuum expectation value to not break 4D Lorentz invariance. Supersymmetry breaking has to come from the scalar potential. If either the F-part or the D-part are non zero at the ground state, then supersymmetry is broken. We will not go further into models of spontaneous breaking. Note that such minimum can be eventually metastable, and there is an interplay with the $U(1)_R$-symmetry breaking [58]. A lot of work has been done on dynamical supersymmetry breaking, and dualities relating theories with different color and flavour numbers (see for example the original ISS paper [59]).

If supersymmetry is broken within a supersymmetric Standard Model, some of the sparticles should be sufficiently light to be already observed. This is due to unavoidable sum rules like $m^2_{\tilde{e}_1} + m^2_{\tilde{e}_2} = 2m^2_e$ (more generally $\mathrm{Str}(\mathcal{M}) = 0$), which can however be modified through loop effects, but not sufficiently. This situation suggests that supersymmetry should be broken by some dynamics in a hidden sector, then transmitted to the supersymmetric Standard Model. Supersymmetry breaking coming from the unknown, hidden sector is generically modeled by couplings to a "spurion", static field, such that $\phi_{hidden} = \theta^2 F_{hidden}$ with $\langle F_{hidden} \rangle \neq 0$.

In any case, if the breaking is spontaneous, a Nambu-Goldstone particle associated to the broken generator appear in the spectrum. This will be a fermion, called Goldstino. As it is unobserved, one needs to make it heavy by doing an explicit breaking, or make absorb it by gauging supersymmetry.

An explicit supersymmetry breaking has to be well controlled, to not reintroduce quadratic divergences to the Higgs mass. It turns out that only few terms are allowed: fermion masses in the vector multiplet and scalar interactions with positive mass dimension in the chiral multiplet. These operators are designed as "soft". The MSSM soft terms are described in Subsection 1.6.1 and Eq. (1.17). If they are induced by mediation from a hidden sector, they will be proportional to $\langle F_{hidden} \rangle$.

Let us now introduce local supersymmetry, the other approach to make the goldstino massive.

2.1.7 Local supersymmetry

Local supersymmetry, called supergravity, is a wide subject. In this subsection, we will only introduce the few aspects directly related to our work. Even if one's interest is to suppress the Goldstino from the spectrum, it has been studied for a long time for many theoretical and phenomenological features.

By letting the supersymmetric transformation be local, one has to introduce a corresponding gauge field to let the Lagrangian invariant under the supersymmetry transformation. This is the usual procedure to gauge a continuous symmetry. It turns out the

gauge field has to be of spin 3/2. By supersymmetry, a spin 2 and a spin 1 field also needs to be introduced. These new terms in the Lagrangian are irrelevant operators: they are multiplied by a dimension -1 constant, sometimes called κ. Such a Lagrangian describes thus a non-renormalizable, effective theory, valid below the cutoff scale κ.

2.1.8 Gravity multiplet

Of course this spin 2 field describes gravity, and κ^{-1} can be identified to the Planck mass. The spin 3/2 field is called gravitino, describing the supergravity interaction. The spin 1 field is the graviphoton. Together, they form the gravity supermultiplet. The off-shell supergravity multiplet also contains auxiliary fields, depending on the formulation adopted. These auxiliary fields are in fact the gauge fields of the local R-symmetry $\mathrm{SU}(\mathcal{N})_R$.

When one considers 5D supersymmetry with a compactified dimension of radius R, with 4D $\mathcal{N} = 1$ formulation, the gravity supermultiplet contains a chiral superfield:

$$T = R + iB_5 + \theta\Psi_R^5 + \theta^2 F_T \ . \tag{2.19}$$

The scalar component of this field is made up of the radius and the fifth component of the graviphoton. The fermionic component is a piece of the gravitino, and F_T is the auxiliary field. The whole superfield is called radion superfield. Only R and F_T will be relevant for our study. Indeed, at a given point one will assume some radius stabilization mechanism, giving a non zero vev to the radion field $\langle T \rangle = R \neq 0$. This mechanism can eventually break supersymmetry, which can be parametrized by the vev of the auxiliary field $\langle F_T \rangle \neq 0$.

The Goldstino, the massless particle arising from spontaneous breaking of global supersymmetry, should disappear once supersymmetry is gauged. It turns out the Goldstino is absorbed by the gravitino, making it massive and providing a $\pm 1/2$-helicity longitudinal polarization. As far as interactions with other particles are concerned, it is in fact possible to neglect the $\pm 3/2$ helicity, which interact only with gravity strength. Depending on its mass, the gravitino can play a crucial role in collider physics or in cosmology.

2.1.9 Scalar potential

There are several, equivalent formulations of supergravity, related by field redefinitions. To study how supergravity participate in supersymmetry breaking, an appropriate formulation is the one making use of superconformal invariance. Just like Einstein gravity, which can be reformulated in a scale invariant way by introducing an additional auxiliary scalar field, supergravity can be reformulated in a scale invariant way by introducing an additional auxiliary chiral superfield. This chiral superfield is called chiral compensator and can be written as:

$$\varphi = 1 + F_\varphi \ . \tag{2.20}$$

The most general effective Lagrangian of chiral superfields Φ and vector superfields V (up to higher order derivatives) is:

$$\mathcal{L} = \sqrt{-g}\left\{\int d\theta^2\bar{\theta}^2\varphi\bar{\varphi}f(\bar{\Phi},e^{-V}\Phi)+\int d\theta^2\left(\tau(\Phi)\mathrm{tr}(\mathcal{W}_a\mathcal{W}^a)+\varphi^3W(\Phi)\right)+\mathrm{h.c.}\right\} \quad (2.21)$$

One defines the Kähler potential K such that:

$$f=-3M_{Pl}^2e^{-K/3M_{Pl}^2}\ , \quad (2.22)$$

and the Kähler metric such that

$$K_{i\bar{j}}=\frac{\partial}{\partial\phi_i}\frac{\partial}{\partial\bar{\phi}_j}K\ . \quad (2.23)$$

The general scalar potential of supergravity is then:

$$\mathcal{V}=e^{K/M_{Pl}^2}\left\{\left(W_i+\frac{W}{M_{Pl}^2}K_i\right)K^{i\bar{j}}\left(W_{\bar{j}}+\frac{W}{M_{Pl}^2}K_{\bar{j}}\right)-3\frac{|W|^2}{M_{Pl}^2}\right\}+\frac{1}{2}g^2\left(K_{\bar{i}}T^a_{ij}\phi_j\right)^2\ . \quad (2.24)$$

This potential is invariant under the so-called Kähler-Weyl transformations

$$K(\Phi,\bar{\Phi})\to K+f(\Phi)+f(\bar{\Phi})\ ,\qquad W(\Phi)\to e^{-f(\Phi/M_{Pl}^2)}W(\Phi)\ , \quad (2.25)$$

where $f(\Phi)$ is a holomorphic function of superfields. To make the supergravity lagrangian (2.21) manifestly invariant, one has to add the transformation of the chiral compensator

$$\varphi\to\varphi e^{\frac{1}{3}f(\Phi)/M_{Pl}^2}\ . \quad (2.26)$$

In the limit without gravity $M_{Pl}\to\infty$, and one comes back to the potential of global supersymmetry (2.16). The gravitino mass is

$$m_{3/2}=e^{K/2M_{Pl}^2}\frac{|W|}{M_{Pl}^2}\ . \quad (2.27)$$

A crucial property of Eq. (2.24) is that it is not a sum of positive terms anymore. This means that the cosmological constant $\langle\mathcal{V}\rangle$ can be zero. Assuming that an unknown mechanism forces it to zero, the gravitino mass then becomes

$$m_{3/2}^2=\frac{K_{i\bar{j}}F_i\overline{F}_j}{3M_{Pl}^2}\ . \quad (2.28)$$

2.1.10 Anomaly-mediated supersymmetry breaking

If supersymmetry is broken in some sector, it induces $\langle F_\varphi\rangle\neq 0$. This produces tree-level soft terms for supersymmetric dimensionful parameters (like the μ-term). However more importantly, this also induces contributions to all soft terms at one-loop. This mechanism is a consequence of the fact that super-Weyl transformations are anomalous at the quantum level [60]. This mechanism is thus called anomaly-mediated supersymmety breaking [61]: supersymmetry can be broken in a hidden sector, then transmitted to chiral and vector superfields of the supersymmetric Standard Model through gauge and Yukawa couplings, which now feel the anomaly of super-Weyl invariance in addition to the usual scaling anomaly.

2.2 Extra dimensions

We now introduce extra dimensions. Since the pioneer attempt made by Kaluza and Klein [62,63], and their natural apparition in superstring theories and M-theory [55], they have been used to solve different problems in a plethora of interesting mechanisms. We already evocated electroweak symmetry breaking, and solving the gauge hierarchy problem either by warped geometry or gauge-Higgs unification. Extra dimensions provide in fact a general mechanism to break symmetries, which will be described here. They also provide mechanisms to generate realistic flavor hierarchy [43,64,65], get chiral fermions from vector-like theories, build hidden sectors, modify the running of gauge couplings [43], supress proton decay, and so on and so forth. Ultimately, they could even permit to model strongly interacting gauge theories like QCD through the gauge-gravity correspondence [66–68]. There is a huge amount of model-building literature on these subjects. We will simply present some aspects relevant for the models we are treating in this manuscript.

2.2.1 Compactifications and symmetry breakings

Torus, orbifold and Scherk-Schwarz breaking

As we do not observe other dimensions than our familiar 3+1, either extra dimensions are compactified, or we are confined on a particular 3+1 hypersurface living in a higher-dimensional space.

Most generically, we consider a D-dimensional theory ($D = 4 + d$) with d extra dimensions and an action defined as

$$\mathcal{S}_{\mathcal{D}} = \int d^D z \mathcal{L}_D[\Phi(z^M)] \tag{2.29}$$

The theory is compactified on $\mathcal{M}_4 \times C$, where $\mathcal{M}_4$ is the Minkowski spacetime and C a compact space if the coordinates of the D-dimensional space can be split as $z^M = (x^\mu, y^m)$ with $m = (1, ..., d)$, the coordinates y^m describing the compact space C. The four dimensional Lagrangian is obtained by integration of the compact coordinates y^m as

$$\mathcal{L}_4 = \int d^d y \mathcal{L}_D[\Phi(x^\mu, y^m)] \tag{2.30}$$

In general we can write $C = M/G$, where M is a (non-compact) manifold and G is a discrete group acting on M by operators $\tau_g : M \to M$ with $g \in G$, which are representations of G. C is then defined by the orbit associated to each point y^m. One can thus write

$$\mathcal{L}_D[\Phi(x^\mu, y^m)] = \mathcal{L}_D[\Phi(x^\mu, \tau_g(y^m)] \ . \tag{2.31}$$

While a sufficient condition to fulfill the previous equality is

$$\Phi(x^\mu, \tau_g(y^m)) = \Phi(x^\mu, y^m) \ , \tag{2.32}$$

known as ordinary compactification, the necessary and sufficient condition is

$$\Phi(x^\mu, \tau_g(y^m)) = T_g \Phi(x^\mu, y^m) \tag{2.33}$$

where T_g has to be a global or local symmetry of the Lagrangian by construction, and is also a representation of G in the field space. This is known as Scherk-Schwarz compactification [69, 70], and T_g is intuitively called a twist.

If the Scherk-Shwarz twist belongs to a local symmetry of the Lagrangian, then Scherk-Schwarz breaking can be equivalent to Wilson/Hosotani breaking (see [53]). In Wilson/Hosotani breaking, an extra dimensional component of the gauge field of this local symmetry gets a non-zero vev (like A_5). It is possible to show that this vev can be related to the parameter of the twist. This works in flat space, however, as soon as one considers another metric, this equivalence does not hold necessarily. In particular, this does not hold in warped space [71].

G can act on C freely, i.e.with no fixed points except the one given by the neutral operator. In that case, C is a smooth manifold on which extra dimensional Lorentz invariance is broken. In particular, if G is a group of translations, C is a torus. But G can also act on C non-freely, i.e.with non trivial fixed points. C is then a non-smooth manifold with singularities, called orbifold. In that case, extra dimensional Poincaré invariance is broken, because fixed points break invariance under translations. We start again with a smooth compact manifold $C = M/G$, with τ_g being representation of $g \in G$ on M, and add now another discrete group H acting non-freely on C, with γ_h being representation of $h \in H$ on M. Similarly to what we saw for the Scherk-Schwarz mechanism, the Lagrangian depends only on orbits

$$\mathcal{L}_D[\Phi(x^\mu, y^m)] = \mathcal{L}_D[\Phi(x^\mu, \gamma_h(y^m)] \ . \tag{2.34}$$

and the necessary and sufficient condition is

$$\Phi(x^\mu, \gamma_h(y^m)) = Z_h \Phi(x^\mu, y^m) \tag{2.35}$$

where Z_h has to be a global or local symmetry of the Lagrangian by construction, and is also a representation of H in the field space. It is also possible to write particular Lagrangians on these fixed points, which will describe particular hypersurfaces of C, called branes, where fields can eventually be confined.

Scherk-Schwarz compactification and orbifolds are two different mechanisms to break symmetries. In the more general situation, one can make use of both simultaneously. Generally, $g \cdot h \neq h \cdot g$ thus $\tau_g \cdot \gamma_h(y) \neq \gamma_h \cdot \tau_g(y)$. Moreover some necessary conditions on T_g and Z_h have to be fulfilled. This leads to interesting model-building perspectives, see for example [72].

While interesting models are built in 6D or more, we will be much more specific. We consider only the 5D case, with the orbifold $C = S_1/\mathbb{Z}_2 = (\mathbb{R}/\mathcal{T})/\mathbb{Z}_2$, where $\mathcal{T}$ is the action

of translation by $2\pi R$. A lot of models are built on this simple structure. Keeping the same notations, we have now one generator of translation $\tau(y) = y + 2\pi R$, and one generator of reflexion $\gamma(y) = -y$. The transformations on the fields are then

$$\Phi(x^\mu, \tau(y^m)) = T\Phi(x^\mu, y^m) \ , \tag{2.36}$$

$$\Phi(x^\mu, \gamma(y^m)) = Z\Phi(x^\mu, y^m) \ . \tag{2.37}$$

T being the Scherk-Schwarz twist and the Z the orbifold reflexion on field space. Provided that one can identify

$$\tau \cdot \gamma = \gamma \cdot \tau^{-1} \ , \tag{2.38}$$

the consistency condition on field space is

$$TZ = ZT^{-1} \ . \tag{2.39}$$

One see that for any non trivial T, a new reflexion $Z' = TZ$ appears, $(Z')^2 = 1$ being enforced by the previous necessary condition. On C, this new reflexion is located at the fixed point of $\tau \cdot \gamma(y) = y - 2\pi R$, which is πR. It thus appears that a generic $S_1/\mathbb{Z}_2$ orbifold with Scherk-Schwarz twist is finally equivalent to an interval $\mathbb{R}/(\mathbb{Z}_2, \mathbb{Z}_2')$, with two independent reflexions at the boundaries Z an Z'. Generally Z and Z' do not commute. If they do, $T^2 = 1$, all fields can then be classified with respect to their parity under the reflexions: $(\pm, \pm)$. On this orbifold, a general 5D action will be

$$\mathcal{L}_5 = \int_0^{\pi R} d^y d^4x \left(\mathcal{L}_5 + \delta(y)\mathcal{L}_0 + \delta(y - \pi R)\mathcal{L}_{\pi R}\right) \tag{2.40}$$

Kaluza-Klein decomposition

In such compact spaces, impulsion along the fifth dimension is quantized. This is the same phenomenon as light confinement in an optic fiber. One can decompose any field on an orthogonal basis of eigenvectors f_n:

$$\Phi(x^\mu, y) = \sum_n f_n(y)\phi(x^\mu) \ . \tag{2.41}$$

Plugging this decomposition in the Lagrangian and integrating along the fifth dimension gives a 4D Lagrangian containing an infinite number of particles with different masses, collectively called Kaluza-Klein tower. The 4D Lagrangian for a scalar field is then

$$\mathcal{L}_4 = \sum_n \partial^\mu \bar{\phi} \partial_\mu \phi - m_n^2 \bar{\phi}\phi \ . \tag{2.42}$$

The profiles f_n do not appear in this part of the Lagrangian, but can play a crucial role for interactions between different fields. The massless particles, called zero modes, always

remain in the spectrum, while the other modes are heavy and can eventually be integrated out below some cutoff scale.

The reflexions of the orbifold play a crucial role. Indeed, by looking at the 5D equation of motion and boundary conditions, one can see that only the fields with $(+,+)$ parity, i.e with vanishing $\partial_5\phi$ on both boundaries, can have a zero mode. This is a crucial property to get chiral theories like the Standard Model. Indeed, it turns out that on a torus all fermion modes are of Dirac type. In contrast, on the orbifold, fermions zero modes are Weyl spinors, while KK excitations are still of Dirac type. The effective theory of zero modes is thus chiral.

We will now study supersymmetry breaking and gauge symmetry breaking on this orbifold.

Supersymmetry breaking

Orbifold effect As we said in the previous section, $\mathcal{N}=1$ supersymmetry in 5D non compactified is equivalent to $\mathcal{N}=2$ supersymmetry in 4D. Compactifying on a torus, we will get a theory with $\mathcal{N}=2$ supersymmetry. In contrast, compactifying on an orbifold will leave only a $\mathcal{N}=1$ supersymmetry for the zero modes. This is a consequence of the orbifold reflexion Z. Indeed, in 4D superfield formulation, the reflexions on each brane for the hypermultiplet made of a chiral multiplet H and an antichiral multiplet H^c are constrained to be:

$$ZH(0) = -ZH^c(0)\ ,\ Z'H(\pi R) = -Z'H^c(\pi R)\ , \tag{2.43}$$

Z having the eigenvalues ± 1. In other words, the chiral and antichiral multiplets have opposite parities. This condition can be derived from the kinetic Lagrangian. In particular, it implies that only one of these fields can have a $(+,+)$ parity, and the theory is thus chiral at the level of zero modes.

The reflexions on each brane for the 5D vector multiplet, containing a 4D vector multiplet $V=(\lambda_1, V_\mu)$ and a chiral multiplet $\chi = (\Sigma + iA_5, \lambda_2)$, are constrained to be:

$$ZV(0) = -Z\chi(0)\ ,\ Z'V(\pi R) = -Z'\chi({}_piR)\ , \tag{2.44}$$

In particular, V_μ and V_5 have opposite parities. This properties will permit to make appear the Higgses from the 5D vector superfield, in gauge-Higgs unified models.

In addition, the brane Lagrangians are also $\mathcal{N}=1$ supersymmetric. We have thus the following picture: on the orbifold, $\mathcal{N}=2$ supersymmetry is broken to $\mathcal{N}=1$ at the level of zero modes and on branes.

Scherk-Schwarz effect Breaking the remaining supersymmetry can be done as described in previous section by turning on the F-term of a spurion field on a brane or in the

bulk of the extra dimension. But it is also possible to break it using the 5D mechanisms described above. To do so, one identifies the Scherk-Schwarz twist as a generator of the $SU(2)_R$ global symmetry of $\mathcal{N}=2$ supersymmetry. It is interesting to look at the different possibilities. They can be summarized as

$$\left(Z=\sigma^3, T=e^{i2\pi\omega\sigma^2}\right) \text{ or } (Z=\pm 1, T=\pm 1) \tag{2.45}$$

In the first case, the $\mathcal{N}=2$ supersymmetry transformation rotates along the fifth dimension by the twist of angle ω. This implies that the $\mathcal{N}=1$ supersymmetries on each brane are not colinear anymore. In that case, the supersymmetry breaking parameters are then proportional to the amplitude of the angle ω/R. An interesting property of this kind of models is that, while supersymmetry is globally broken, there is still a local supersymmetry remaining everywhere, protecting the Higgs from quadratic divergences. For the particular case $\omega=1/2$, supersymmetries on each branes are orthogonal. In that case $[Z,T]=0$.

For the second case, Z and Z' commutes and are in fact associated to the usual $\mathcal{N}=1$ R-parity. Bosons and fermions inside a same supermultiplet can be given different parities on the branes, thus breaking supersymmetry.

If one considers local supersymmetry, the $\mathrm{SU}(2)_R$ has to be gauged. The Hosotani breaking, equivalent to the Scherk-Schwarz breaking in flat space, corresponds to give a non-zero vev to the extra dimensional components of the $SU(2)_R$ gauge fields. In the off-shell supergravity multiplet, these components enter in fact in the radion superfield F-term. Thus, local supersymmetry Scherk-Schwarz breaking in flat space is in fact equivalent to radion mediation. In the models we will discuss, we will use radion mediation [73, 74].

Gauge symmetry breaking

One can break gauge symmetry either by orbifold reflexions [75] or by Scherk-Schwarz twist. We will here present only the former possibility, we refer to [53] for discussion of the later.

The idea is simply to break the gauge symmetry $\mathcal{G}$ to the group $\mathcal{H}$ at the level of zero modes, using appropriate parity operators acting in gauge space. The gauge group has $(\dim\mathcal{G})^2-1$ generators T^A. One can also express them in the Cartan-Weyl basis, with H_i ($i=1..\mathrm{rank}(\mathcal{G})$) diagonal generators and $E_{\pm\alpha}$ ($\alpha=1..(\mathcal{G}-\mathrm{rank}(\mathcal{G}))/2$) pairs of generators, such that

$$[H_i, E_{\pm\alpha}] = \pm\alpha_i E_{\pm\alpha} \ , \tag{2.46}$$

where $\overrightarrow{\alpha}$ is the root vector associated to $E_{\pm\alpha}$. One can distinguish rank preserving or rank-lowering breaking [76]. We will here consider only rank-preserving operators. In that case, the diagonal generators H_i are unbroken.

In gauge space, the orbifold reflexion on a gauge field $F_{MN} = F^A_{MN} T^A$ can then be written as

$$F_{MN} \to G F_{MN} G^{-1} \text{ with } G = e^{i2\pi \overrightarrow{w}\overrightarrow{H}} \ , \tag{2.47}$$

where $\overrightarrow{w}$ is the reflexion vector, containing all information on the parities. In the Cartan-Weyl basis, this condition becomes

$$H_i \to G H_i G^{-1} = H_i \ , \tag{2.48}$$

$$E_{\pm\alpha} \to G E_{\pm\alpha} G^{-1} = e^{i2\pi \overrightarrow{w}\overrightarrow{\alpha}} E_{\pm\alpha} \ . \tag{2.49}$$

The H_i are as expected not sensitive to the reflexion. The pairs of generators $E_{\pm\alpha}$ are broken by the reflexion if $\overrightarrow{w}.\overrightarrow{\alpha} \neq 0$.

For example, one gets the breaking $\mathrm{SU}(3) \to \mathrm{SU}(2) \otimes \mathrm{U}(1)$ if one pair of $H_{\pm\alpha}$ is broken by the reflexion, and $\mathrm{SU}(3) \to \mathrm{U}(1) \otimes \mathrm{U}(1)$ if both pairs of $H_{\pm\alpha}$ are broken.

Concerning hypermultiplets, whatever the breaking is, one can show that the reflexion acting on an hypermultiplet charged under $\mathcal{G}$ has to commute with the unbroken T^A and to anticommute with the broken T^A.

However, these restriction on parities can be modified by coupling the bulk fields to brane-localized fields with mass terms. In fact, letting this brane-localized mass term go to infinity exchange the initial parities, offering more freedom for the model-building.

2.2.2 Warped orbifold

We now present more precisely the properties of a warped metric [45, 51]. Some properties discussed are the same as in flat metric, which corresponds to the limit case $k \to 0$. Such warped metric is used for various purposes in model-building (see for example [45, 51] and references therein).

Gravity background

We consider the previous $S^1/\mathbb{Z}_2$ orbifold, with a Scherk-Schwarz twist $T^2 = 1$ such there are two independent reflexions on each fixed point. Equivalently, this is the interval $\mathbb{R}/(\mathbb{Z}_2, \mathbb{Z}_2')$. Said again differently, we are considering an extra dimension $y \in [0, \pi R]$, where we can give Neumann or Dirichlet boundary conditions to the fields propagating in the bulk of the extra dimension.

The 5D gravity action is

$$\mathcal{S} = \int d^4x \int_0^{\pi R} dy \sqrt{-g} \left(\frac{1}{2} M_5^3 \mathcal{R} + \Lambda + \delta(y) \left(\mathcal{L}_0 + \Lambda_0 \right) + \delta(y - \pi R) \left(\mathcal{L}_{IR} + \Lambda_\pi \right) \right) \ , \tag{2.50}$$

where $\mathcal{R}$ is the 5D Ricci scalar, Λ is the bulk cosmological constant and Λ_0, Λ_π the brane tensions. One assumes that this structure is stabilized by some mechanism, such that the brane tensions are equal and opposite and the the 4D effective cosmological constant is zero. This in fact recquires that $\Lambda < 0$, so that the 5D space is anti-de Sitter (AdS_5). The metric of this structure can be written as

$$ds^2 = e^{-2ky}\eta_{\mu\nu}dx^\nu dx^\mu + dy^2 = g_{MN}dx^M dx^N \ , \tag{2.51}$$

where $\eta_{\mu\nu} = (-1,+1,+1,+1)$ is the Minkowski spacetime metric. The parameter k ($\dim(k) = 1$) induces a warping effect. The two branes are not symmetric anymore. One usually calls the brane in $y = 0$ the UV brane and the brane in $y = \pi R$ the IR brane. In particular, all operators of $\mathcal{L}_\pi$, localized on the IR brane, will be redshifted by the so-called warp factor $e^{-\pi kR}$. This property is exploited in the RS1 model to explain gauge hierarchy: the Standard Model is localized on the IR brane, the Higgs mass is naturally of the order of the cutoff scale of the 5D theory M_5, but it is multiplied by $e^{-\pi kR}$, which can be naturally very small. By choosing πkR 34.5, the Higgs mass is naturally $\mathcal{O}(0.1$ TeV).

The action for scalars, fermions and gauge fields propagating on this background is:

$$\mathcal{S} = \int d^4x \int_0^{\pi R} dy \left\{ \frac{1}{4g_5^2} F^{MN}F_{MN} + i\bar{\Psi}\gamma^M D_M \Psi + im_\Psi \bar{\Psi}\Psi \right\} \ . \tag{2.52}$$

The fermion bulk mass m_Ψ is parametrized as $m_\Psi = ck$. We will focus directly on the supersymmetric case. In an hypermultiplet, m_ϕ is related to m_Ψ, so that both components have the same profile. Note that the situation changes if supersymmetry is broken. The scalar component then gets an additional supersymmetry-breaking mass term, which modifies his profile. If this mass term goes to infinity, the boundary condition is exchanged. If there was a zero mode, it is removed. This is equivalent to the Scherk-Schwarz breaking involving R-parity mentioned previously in 2.2.1.

Spectrum and profiles

Massless modes By solving the 5D equation of motion, it turns out the profile along the fifth dimension for the zero mode $H^{(0)}$ of an hypermultiplet (H, H^c) is

$$H^{(0)}(y) \propto \frac{1}{\sqrt{\pi R}} e^{(c-1/2)ky} \ . \tag{2.53}$$

For $c > 1/2$, the zero mode is localized toward the UV brane and exponentially suppressed on the IR brane. This is the opposite for $c > 1/2$. For $c = 1/2$, the zero mode is the same as with a flat metric:

$$H^{(0)}(y) = \frac{1}{\sqrt{\pi R}} \ , \tag{2.54}$$

one then says that the profile is conformaly flat. If the zero mode is $H^{c\ (0)}$, one takes $c \to -c$. The zero mode of the vector supermultiplet is always conformally flat:

$$V^{(0)}(y) = \frac{1}{\sqrt{\pi R}} \ , \tag{2.55}$$

One can also derive the graviton zero mode by considering fluctuations of the metric:

$$h_{\mu\nu}^{(0)}(y) \propto e^{(-1/2)ky} \ , \tag{2.56}$$

which is localized toward the UV brane.

Massive modes The profiles of massive modes for all the fields $f^{(n)}$ above are combinations of Bessel functions:

$$f^{(n)}(y) \propto J_\alpha(\frac{m_n}{ke^{-ky}}) + b_n Y_\alpha(\frac{m_n}{ke^{-ky}}) \ , \tag{2.57}$$

where b_n and m_n are fixed by the two boundary conditions. Contrary to the zero modes , all these fields are localized toward the IR brane.

The masses of almost all KK excitations are roughly $nke^{-\pi kR}$, with $n > 0$. So the warping is also redshifting the spectrum. For example in the RS1 model, the first KK excitation is $\mathcal{O}$(TeV). An interesting exception is for hypermultiplets with twisted boundary conditions $(+,-)$. In that case the mass of the first KK excitation will be exponentially suppressed for $c < -1/2$: $m_1^{(+,-)} \propto ke^{(c+1/2)\pi kR}$.

Brane-localized operators

The brane Lagrangians can also contain additional mass terms or kinetic terms, which affects the bulk fields and can be used for several model-building purposes. These terms can be seen as modifications of Neumann or Dirichlet conditions on the boundaries. They will modify the solution of the 5D equation of motion and modify the overall normalization.

Brane-localized kinetic terms Brane kinetic terms do not modify the equation of motion of zero modes. But they modify their canonical normalization. Considering the example of the vector field:

$$\mathcal{L} = \frac{1}{4g_5^2}\left\{F^{MN}F_{MN} + r_{UV}\delta(y)F^{\mu\nu}F_{\mu\nu} + r_{IR}\delta(y-\pi R)F^{\mu\nu}F_{\mu\nu}\right\} \ . \tag{2.58}$$

The effective 4D gauge coupling

$$g^4 = \frac{g^5}{\sqrt{\pi R}} \ , \tag{2.59}$$

is modified to be

$$g^4 = \frac{g^5}{\sqrt{\pi R + r_{UV} + r_{IR}}} \ . \tag{2.60}$$

Brane kinetic terms affect the spectrum and the profiles of massive modes. The spectrum is shifted toward lighter values and a light, "collective" mode appear, with mass

$$m_1 \propto \sqrt{\frac{k}{r_{IR}}}e^{-\pi kR} \tag{2.61}$$

in case of a IR kinetic term. In addition, the fields are repulsed from the brane where the kinetic term resides.

Brane-localized mass terms Continuing with the vector field, an IR brane mass term, looks like:

$$\mathcal{L} = \left\{ M^2 \delta(y - \pi R) \eta^{\mu\nu} A_\mu A_\nu \right\} \ . \tag{2.62}$$

If the brane mass term is small compared to the KK scale, it is just a small perturbation which shifts the whole spectrum including the zero mode. But if the mass term becomes sizeable, it repulses the fields from the brane. In the limit where it becomes infinitely large, the field is completely expulsed from the brane and the boundary conditions are inverted. For example the 5D vector $(A_\mu^{(+,+)}, A_5^{c\ (-,-)})$ where the superscript $(\pm, \pm)$ are the UV and IR brane parities, will be turned into $(A_\mu^{(+,-)}, A_5^{c\ (-,+)})$ if it feels the IR brane mass term above, in the limit $M \gg k$.

Gauge-gravity correspondence

An exact duality between a type-IIB string theory on $AdS_5 \times S^5$ and the 4D $\mathcal{N} = 4$ supersymmetric Yang-Mills (conformal) theory was conjectured in [66]. This duality has been shown to apply, in a less rigorous sense, to the warped orbifold structure described above [67, 68]. It is then called gauge-gravity correspondence or holography. It relates the AdS_5 orbifold to a nearly conformal field theory (CFT), coupled to an external elementary sector. While there are no rigorous proofs, these dualities passed many non trivial checks.

For our purposes, we summarize the elements of the dictionary relevant for the model of Section 3.2. One has to assume that the CFT has a large number of colors N_c and a large t'Hooft coupling $g^2 N_c / 16\pi^2 \gg 1$.

- The fifth dimension of AdS_5 has to be taken has the renormalization scale of the CFT.
- A bulk gauge symmetry $\mathcal{G}$ corresponds to a global symmetry $\mathcal{G}$ of the CFT.
- The UV brane represents a cutoff scale Λ_{UV} explicitely breaking the CFT. Fields localized on the UV brane are external elementary fields, coupling to CFT operators through operators involving powers of Λ_{UV}. $\mathcal{G}$ broken to $\mathcal{H}$ on the UV brane corresponds to global $\mathcal{G}$ with a subgroup $\mathcal{H}$ weakly gauged, in the CFT.
- The IR brane represents a spontaneous breaking of the CFT at the scale $\Lambda_{IR} = \Lambda_{UV} e^{-\pi k R}$. Fields localized on the IR brane are pure composite state arising through the CFT spontaneous breaking. $\mathcal{G}$ broken on the IR brane corresponds to $\mathcal{G}$ spontaneously broken by the CFT dynamics.
- Bulk fields correspond to a mix of composite and elementary states in the CFT. Their localization in the bulk indicates which component dominates. In particular, KK excitations are often pure composite states of the CFT.

Résumé de la section

Dans cette Section, il a été présenté de façon plus formelle deux piliers de la physique au delà du Modèle Standard, que sont la supersymmétrie et les dimensions supplémentaires. Nous avons d'abord introduit la supersymmétrie et la supergravité $\mathcal{N} = 1$ en quatre dimensions. Puis, nous avons introduit les dimensions supplémentaires, en se focalisant sur les méchanismes de brisure de symmétries qu'elles permettent. Nous avons ensuite décrit les propriétés d'un orbifold à courbure négative, construction classique qui permet entre autre d'appliquer le principe holographique.

Chapter 3

Realizations of 5D supersymmetric grand-unified theories

We have introduced the sequence of motivations leading to the construction of 5D supersymmetric grand-unified theories. We now present two concrete realizations. The spacetime geometry for these two models is the one described in the previous Chapter. This is a $S_1/\mathbb{Z}_2$ orbifold with a Scherk-Schwarz twist $T^2 = 1$, or equivalently the interval $[0, 2\pi R]$ with independent reflexions Z and Z' at each boundary. We will use the $\mathcal{N} = 1$ formulation of 5D supersymmetry, based on [56], and [57] for radion mediation. We refer to these works for complete Lagrangians. This 5D structure is assumed to be stabilized by some unspecified mechanism.

In these two realizations, the first KK modes have a mass $\mathcal{O}(M_{GUT})$, and the 4D effective theory remaining below is the MSSM. Extra dimensions will therefore not directly manifest at low-energy. The studies done in Chapters 4, 5, 6 will thus come within SUSY phenomenology, not KK phenomenology.

Concerning supersymmetry breaking, we will consider that it is spontaneously triggered in some hidden sector, possibly simultaneously with radius stabilization, and transmitted to the MSSM through three different F-terms : the radion superfield F^T, the supergravity compensator F^φ, and a brane superfield F^Z. F^T and F^φ parametrizes the SUSY breaking effects of supergravity background. The brane Z superfield can be seen as a Goldstino superfield, parameterizing the SUSY breaking effect of the brane localized hidden sector. Z will in general be composite, but we can treat it as a single, elementary, canonically normalized field for our purposes, absorbing any compositeness factors of 4π or warp factors in the definition of F^Z.

For each of these class of models, we will first present the original idea, then the developments or modifications we made.

3.1 Gauge-Higgs unification framework

The basic idea of gauge-Higgs unification (GHU) is to make arise Higgs fields from extra dimensional gauge fields. GHU is for instance realized in many grand-unified models derived from heterotic string theory, where one or both of the MSSM Higgs doublets can come from the untwisted sector (see e.g. [77]; for a recent review see [78]). At a simpler level, GHU can be realized in purely field-theoretic 5D or 6D orbifold GUT models [75]. These can be viewed as effective unified field theories, valid directly below the heterotic string scale. Such constructions receive independent support from the string-scale/GUT-scale problem [79] as follows: one of the possibilities for overcoming this problem is the compactification on anisotropic orbifolds [80–83], where one or two of the compactification radii are much larger than the string length scale. This naturally allows for an intermediate effective description in terms of a 5D or 6D orbifold GUT.

We will largely follow the 5D SU(6) model of Burdman and Nomura [84]. However, we expect that the phenomenological results of 4 will carry over to similar models, including more elaborate string-derived constructions. Related models include, e.g., the 5D SU(6) model with warped extra dimensions of [85] and the 6d models of [86–88]. For more work on SUSY GHU in orbifold GUTs, see for instance [89] and references therein.

3.1.1 Geometry and field content

In the GHU framework, the SM gauge groups as well as the MSSM Higgses arise from the 5D ($\mathcal{N} = 2$) vector multiplet. $\mathcal{N} = 2$ supersymmetry is broken to $\mathcal{N} = 1$ supersymmetry by orbifolding, and the gauge symmetry at the level of zero modes is broken by appropriate boundary conditions. The compactification scale is taken to be the GUT scale $1/R = M_{GUT}$.

The GUT group is SU(6) for now. The gauge breaking is rank-conserving and is described by two reflexions G and G' introduced in the previous chapter. The (G, G') eigenvalues of the $\mathcal{N} = 1$ vector multiplet V and the chiral multiplet Σ making up the $\mathcal{N} = 2$ vector multiplet are :

$$(G,G')V = \begin{pmatrix} (+,+) & (+,+) & (+,+) & (+,-) & (+,-) & (-,+) \\ (+,+) & (+,+) & (+,+) & (+,-) & (+,-) & (-,+) \\ (+,+) & (+,+) & (+,+) & (+,-) & (+,-) & (-,+) \\ (+,-) & (+,-) & (+,-) & (+,+) & (+,+) & (-,-) \\ (+,-) & (+,-) & (+,-) & (+,+) & (+,+) & (-,-) \\ (-,+) & (-,+) & (-,+) & (-,-) & (-,-) & (+,+) \end{pmatrix} V \tag{3.1}$$

$$(G,G')\Sigma = \begin{pmatrix} (-,-) & (-,-) & (-,-) & (-,+) & (-,+) & (+,-) \\ (-,-) & (-,-) & (-,-) & (-,+) & (-,+) & (+,-) \\ (-,-) & (-,-) & (-,-) & (-,+) & (-,+) & (+,-) \\ (-,+) & (-,+) & (-,+) & (-,-) & (-,-) & (+,+) \\ (-,+) & (-,+) & (-,+) & (-,-) & (-,-) & (+,+) \\ (+,-) & (+,-) & (+,-) & (+,+) & (+,+) & (-,-) \end{pmatrix} \Sigma \tag{3.2}$$

The SU(6) gauge symmetry is broken to $\mathrm{SU}(3) \times \mathrm{SU}(2) \times \mathrm{U}(1)_Y \times \mathrm{U}(1)'$ in the bulk, where $\mathrm{U}(1)_Y$ is a generator contained in the SU(5) part, and thus identified as the SM U(1). The gauge symmetry is broken to $\mathrm{SU}(5) \times \mathrm{U}(1)'$ on the $y = 0$ brane and $\mathrm{SU}(4) \times \mathrm{SU}(2) \times \mathrm{U}(1)_Y$ on the $y = \pi$ brane. The $SU(5)$ symmetry being broken on the $y = \pi$ brane , the brane kinetic terms do not have to respect the GUT symmetry, and can spoil the observed coupling unification :

$$\frac{1}{g_U^2} = \frac{\pi R M^*}{g_5^2} + r_0 + r_\pi^i \ . \tag{3.3}$$

The 5D cutoff scale M^* is therefore assumed to be sufficiently large so that the volume factor $\pi R M^*$ enhances sufficiently the 5D contribution to make the dangerous brane kinetic terms negligible.

A crucial point is that the Higgs doublets transform non-linearly under the gauge symmetry, as they arise from the vector multiplet. Brane Yukawa couplings like $\delta(y)\bar{q}qA_5$ are therefore forbidden. The remaining possibility is to let the matter fields propagate in the bulk. The 4D Yukawa couplings are then generated through gauge interactions $\int d^4x\ dy \int d^2\theta\ Q^c \Sigma Q'$. To generate a realistic hierarchy, three different generations of matter fields are introduced, with different bulk masses $\int d^4x\ dy \int d^2\theta\ MQQ^c$, confining the matter fields toward the branes with exponential profiles $e^{-|M|y}$. The overlap with the Higgs gives a 4D effective Yukawa coupling

$$y = g \frac{\pi R M}{\sinh(\pi R M)} \ , \tag{3.4}$$

where g is the 4D effective gauge coupling.

To reproduce the MSSM matter field content, one introduces hypermultiplets transforming as the 15 and 20 of SU(6). However, some unwanted massless modes appear. To supress them from the massless spectrum, one has to marry them with new chiral multiplets localized on the $y = 0$ brane. These brane fields are charged under $\mathrm{SU}(5) \times \mathrm{U}(1)'$, and are also used to break spontaneously the extra $\mathrm{U}(1)'$. A consequence is that the massless quark and lepton doublets Q, L will then be a mix of bulk and brane fields, parametrized by two angles ϕ_Q and ϕ_L. The third generation Yukawa couplings in the realistic unified model will finally be :

$$y_t = \sin(\phi_Q) g_U \frac{\pi R M_Q}{\sinh(\pi R M_Q)} \ , \quad y_b = \sin(\phi_Q) g_U \frac{\pi R M_D}{\sinh(\pi R M_D)} \ , \tag{3.5}$$

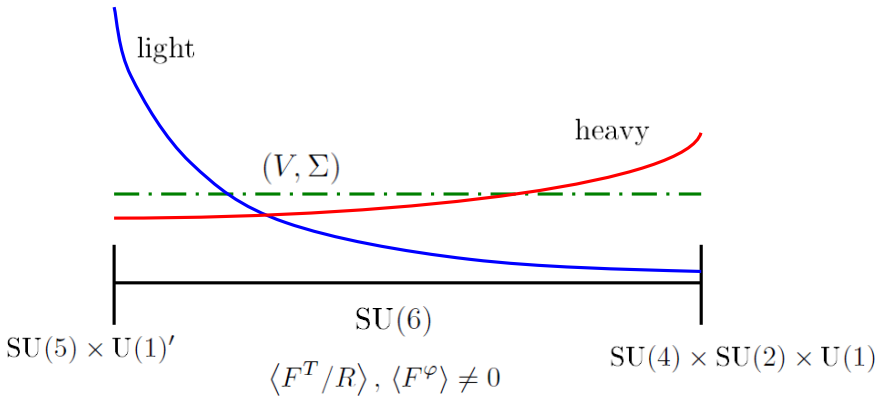

Figure 3.1: GHU framework in a nutshell. The fifth dimension is small ($R \sim M_{GUT}^{-1}$) and un-warped. The GUT group is broken by boundary conditions on both branes. Gauge and Higgs fields arise from the 5D vector multiplet (V, Σ). They have a flat profile along the fifth dimension. Matter fields can be localized towards one of the branes. First generation has to be more localized than the third, to reduce the overlap with the Higgs field, and thus generate flavour hierarchy. Supersymmetry breaking is transmitted to the MSSM through radion mediation.

$$y_\tau = \sin(\phi_L) g_U \frac{\pi R M_E}{\sinh(\pi R M_E)} \ , \quad y_\nu = \sin(\phi_L) g_U \frac{\pi R M_\nu}{\sinh(\pi R M_\nu)} \ . \tag{3.6}$$

Yukawa couplings of first and second generation are neglected here. The three generations case can be worked out similarly. However, three generations of brane fields need to be included, introducing more mixing angles. The basic setup is described in the original paper [84]. We restrict ourselves to the one generation case : Yukawa couplings of first two generations are neglected. Only the the $(3, 3)$ entries of Yukawa couplings and scalar soft terms are then non zero. A three generations study will be done in the HGU framework, which we consider as more predictive and more generic at the level of flavours.

3.1.2 Radion-mediated supersymmetry breaking and Chern-Simons term

Is brane-localized supersymmetry breaking acceptable in this model? Given that the 4D effective Yukawa couplings are given by the overlap of matter fields with the Higgs field in the bulk, the lightest modes have to be localized towards the branes. On the other hand, the source of supersymmetry breaking should not be on the brane where the lightest matter modes are localized, to avoid large flavour violation, induced by the soft terms. However, by construction, some of the matter field zero modes are chiral, while others are antichirals, which implies they are localized toward opposite branes. Given that situation, to avoid large flavour violation, one would have to tune the signs of bulk masses to localize

all matter fields toward the same brane, and put the source of supersymmetry breaking on the other brane. While this is possible, this solution is clearly convoluted and inelegant . We will thus favorize the two other sources of breaking: the radion F^T/R and the chiral compensator F^φ, such that

$$F^Z/M^* \ll F^T/R,\ F^\varphi\ . \tag{3.7}$$

In the framework described above, the gauge and Higgs soft terms are tightly constrained by their common origin :

$$M_a = \frac{F^T}{2R}\ , \tag{3.8}$$

$$\mu = -F^\varphi + \frac{F^T}{2R}\ , \tag{3.9}$$

$$m_{H_1}^2 + |\mu|^2 = m_{H_2}^2 + |\mu|^2 = B_\mu = -|M_a|^2 + |\mu|^2\ . \tag{3.10}$$

It is stated in [90] that in this setup, it is not possible to achieve radiative electroweak breaking : at least one of the conditions necessary for electroweak breaking (1.19), (1.20) cannot be fulfilled at the electroweak scale, due to the relation $|M_a|^2 = -m_{H_{1,2}^2}$. The μ term is generated by supersymmetry breaking effects, this is thus a realization of the Giudice-Masiero mechanism [91].

The starting point of our developments in this framework is the crucial remark made in [92]. Indeed, in odd number of dimensions, there is also a Chern-Simons term generically present in the theory. This Chern-Simons term concerns usually only the gauge sector. But, in the present setup, by construction, it will also act on the Higgs sector. A Chern-Simons term can be radiatively induced in 5D, and can ensure global anomaly cancellation if brane chiral multiplets induce localized gauge anomalies on each branes (see [93–96]). The relevant pieces of the Lagrangian showing the coupling of the gauge-Higgs sector to the radion superfield are

$$\mathcal{L} \supset \frac{1}{2g_5^2}\mathrm{tr}\left[\int d^2\theta\ T\,W^2 + \mathrm{h.c.} + 2R^2\int d^4\theta\,\frac{(\Sigma+\bar\Sigma)^2}{T+\bar T}\right] \tag{3.11}$$

for the normal part, and

$$\mathcal{L} \supset c\,\mathrm{tr}\left[R\int d^2\theta\ \Sigma\,W^2 + \mathrm{h.c.} + \frac{4R^3}{6}\int d^4\theta\,\frac{(\Sigma+\bar\Sigma)^3}{(T+\bar T)^2}\right]\ . \tag{3.12}$$

for the Chern-Simons contribution. The c coefficient is fixed by anomaly cancellation, and naturally $\mathcal{O}(1)$.

The effects of a Chern-Simons term are parametrically important if the scalar component Σ of the gauge chiral superfield gets a non zero vev. This vev can be induced by a brane superpotential, and can also be seen as the effect of a non-zero Wilson line from a higher dimensional theory. This situation is therefore well motivated from the string theory perspective.

The simplest way to include the effect of the Chern-Simons term in the previous model is to consider that the SU(6) GUT group is contained in a larger group containing at least U(6) $\equiv$ SU(6) $\times$ U(1). This extra U(1) is assumed to be broken on one of the branes, its scalar component getting a non-zero vev $\langle\Sigma\rangle = v1_6$. The effective contribution of the Chern-Simons term to the soft terms will be of order c' with

$$c' = c\,\langle\Sigma\rangle\,2g_5^2\ . \tag{3.13}$$

It can be argued [92], for example by taking the 5D limit of a $6D$ orbifold, that the effective coefficient c' is also naturally $\mathcal{O}(1)$. However, we will simply let this coefficient free, considering it as an additional parameter of the model.

Taking properly into account this term, the gauge-Higgs soft terms are modified to be [1]

$$M_a = \frac{F^T}{2R}\frac{1}{1+c'}\ , \tag{3.14}$$

$$\mu = -F^\varphi + \frac{F^T}{2R}\frac{1+2c'}{1+c'}\ , \tag{3.15}$$

$$m_{H_1}^2 + |\mu|^2 = m_{H_2}^2 + |\mu|^2 = B_\mu = |F^\varphi|^2 - \frac{F^\varphi\bar{F}^T + \text{h.c.}}{2R}\frac{1+2c'}{1+c'} + \left|\frac{F^T}{2R}\right|^2\frac{(2c')^2}{(1+c')^2}\ . \tag{3.16}$$

The 4D gauge coupling is modified to be

$$\frac{1}{g_4^2} = \frac{2\pi R}{g_5^2}(1+c')\,. \tag{3.17}$$

The anomaly-mediated $F^\varphi/8\pi^2$ contributions are not taken into account. This is justified if $F^T/2R \gg F^\varphi/8\pi^2$, which has to be checked a-posteriori. It appears in these modified formulas that the relation $|M_a|^2 = -m_{H_{1,2}^2}$ is alleviated, permitting eventually to trigger electroweak breaking.

$$M_{1/2} = \frac{\overline{F}^T}{2R}\frac{1}{1+c'} \tag{3.18}$$

as well as the 4d gauge coupling

$$\frac{1}{g_4^2} = \frac{2\pi R}{g_5^2}(1+c')\,. \tag{3.19}$$

The soft masses and trilinear terms for the matter multiplets are more model-dependent. Quite generally the relevant piece of the kinetic action can be written as

$$\begin{aligned} S \supset \int d^4x \int d^4\theta\,\overline{\varphi}\varphi\,\Big[&Y_U(T,\overline{T})\,|U|^2 + Y_Q(T,\overline{T})|Q|^2 + Y_D(T,\overline{T})|D|^2 \\ &+ Y_E(T,\overline{T})\,|E|^2 + Y_L(T,\overline{T})|L|^2 + Y_N(T,\overline{T})|N|^2\Big]. \end{aligned} \tag{3.20}$$

[1] Note that this agrees with [92] only after a substitution $c' \to c'/2$, which is due to our modified definition of c'. However, after this substitution, it becomes apparent that Eqns. (3.15) and (3.16) are truly different from [92]. This is the result of our SU(6)-preserving Σ-VEV, as opposed to the SU(6)-breaking Σ-VEV of [92].

The kinetic functions Y_X (with $X = U, D, Q, E, N, L$ standing for up-type and down-type right-handed quarks, quark doublets, charged and uncharged right-handed leptons and lepton doublets) determine the soft masses according to

$$m_X^2 = -|F^T|^2 \frac{\partial^2}{\partial T \partial \overline{T}} \log Y_X(T, \overline{T}) \,. \tag{3.21}$$

The trilinear couplings are given by

$$A_{U,D} = F^T \frac{\partial}{\partial T} \log \left(Y_H Y_Q Y_{U,D} \right) , \tag{3.22}$$

$$A_E = F^T \frac{\partial}{\partial T} \log \left(Y_H Y_L Y_E \right) . \tag{3.23}$$

Note that these soft terms are defined with conventions of Eq. (1.17).

The precise form of the matter kinetic functions depends on the model under consideration. We will assume throughout that the first two generations of MSSM matter are brane-localized and that their GUT-scale soft terms are negligible. This gives no-scale boundary conditions for the first and second generation. For the third generation, we will consider two cases: first the approximation that only the top quark receives a Yukawa coupling induced by the 5D gauge coupling, and second the case of the Burdman–Nomura model with realistic top, bottom and tau Yukawa couplings.

3.2 Holographic grand unification framework

We now present the model of holographic grand unification (HGU), which is the main model presented in the original paper [85]. In this model, the MSSM Higgses are realized as pseudo-Nambu Goldstone bosons, arising from the spontaneous breaking of an approximate global symmetry.

This model will admit two equivalent description thanks to the gauge-gravity correspondence. We will first present the 4D picture, then go into the more detailed description, on a slice of AdS_5 .

3.2.1 Basic strongly coupled picture

One considers that the SM gauge group $\mathcal{G}_{SM}$ is embedded in a SU(5) GUT group. This GUT group is assumed to be broken by the dynamics of another, strongly coupled gauge group G. By construction, the G sector is thus necessarily charged under SU(5). On the other hand, there can be fields which are singlets under G, called elementary fields. The theory contains also $n = 3$ generations of chiral matter fields, transforming in the 10 and $\bar{5}$ of SU(5). Note that $n_{10} = n_{\bar{5}}$ is ensured by gauge anomaly cancellation.

The crucial point is to consider that G possesses a global SU(6) symmetry, whose $\mathrm{SU}(5)\times\mathrm{U}(1)'$ is a gauged subgroup, and that its strong dynamics breaks this approximate global SU(6) to $\mathrm{SU}(4)\times\mathrm{SU}(2)\times\mathrm{U}(1)$, at a scale Λ.

The composite pseudo-Goldstone bosons parameterizing the coset $\mathrm{SU}(6)/\mathrm{SU}(4)\times\mathrm{SU}(2)\times\mathrm{U}(1)$ transform under $\mathcal{G}_{SM}$ as $(\mathbf{3},\mathbf{2})_{-\frac{5}{6}}+(\overline{\mathbf{3}},\mathbf{2})_{+\frac{5}{6}}+(\mathbf{1},\mathbf{2})_{\frac{1}{2}}+(\mathbf{1},\mathbf{2})_{-\frac{1}{2}}$. The colored components are absorbed by SU(5) gauge bosons, but not the $(\mathbf{1},\mathbf{2})_{\frac{1}{2}}+(\mathbf{1},\mathbf{2})_{-\frac{1}{2}}$ components, which by consequent remains in the massless spectrum.

Given the appropriate choice of groups, the Goldstone bosons quantum numbers corresponds exactly to the MSSM Higgses. Note that this kind of setup was first build without supersymmetry [29]. In the supersymmetric case, these Goldstone bosons are embedded in supermultiplets. By construction, all components of these supermultiplets are then massless at tree level. This will not be the case anymore once supersymmetry is broken.

In this model, all massless fields are present for an underlying symmetry reason. Gauge fields, matter fields, Higgses, are respectively protected from getting a $\mathcal{O}(\Lambda)$ mass by gauge symmetry, chiral symmetry, and the non-linear symmetry of Goldstone particles. Goldstone particles are prevented from getting a mass at any loop-order. In our case, given that the global symmetry is only approximate due to weak gauging, the protection holds only at tree-level.

The G dynamics can also produce composite states with the same quantum numbers as the elementary fields. These composite states couple to the composite Higgs bosons with $\mathcal{O}(4\pi)$ Yukawa couplings. On the other hand, they can mix to the elementary states. This is the strength of these mixings which will permit to reproduce the realistic Yukawa structure. The strength of these mixings is itself determined by the scaling dimension of G-invariant operators interpolating the states. This is a realization of the Nelson-Strassler mechanism, described in Section 1.7, where the Higgs arise from the G dynamics.

Assuming that G is an almost conformal gauge theory above its scale of spontaneous conformal breaking, with large number of colors N_c and large t'Hooft coupling $\tilde{g}^2N_c/16\pi^2\gg 1$, the gauge-gravity correspondence can be applied.

3.2.2 Scales and gauge-Higgs content

As briefly explained in Section 2.2.2, the 4D picture can be formulated on a slice of AdS_5, following the dictionary of gauge-gravity correspondence. It is assumed that couplings in the bulk and on the IR brane can be estimated making use of naive dimensional analysis (NDA), because they describe the strongly coupled G dynamics. In addition to the extra dimension radius πR and the curvature k, the 5D cutoff scale M^* is also important. A prime will denote quantities multiplied by the warp factor $e^{-\pi kR}$. There is some freedom in the choice of scales k, R, M^*. This will be detailed below.

As G has a global SU(6) in the 4D picture, there is now a SU(6) gauge symmetry in the bulk. This bulk gauge symmetry has to be broken to SU(5) $\times$ U(1)$'$ on the UV brane, and to SU(4) $\times$ SU(2) $\times$ U(1) on the IR brane. The simplest setup of symmetry breakings is to consider a breaking by boundary conditions on the UV brane, and by a Higgs mechanism on the IR brane. The boundary conditions of the SU(6) vector multiplet (V, Σ) are consequently chosen to be

$$(G, G')V = \begin{pmatrix} (+,+) & (+,+) & (+,+) & (+,+) & (+,+) & (-,+) \\ (+,+) & (+,+) & (+,+) & (+,+) & (+,+) & (-,+) \\ (+,+) & (+,+) & (+,+) & (+,+) & (+,+) & (-,+) \\ (+,+) & (+,+) & (+,+) & (+,+) & (+,+) & (-,+) \\ (+,+) & (+,+) & (+,+) & (+,+) & (+,+) & (-,+) \\ (-,+) & (-,+) & (-,+) & (-,+) & (-,+) & (+,+) \end{pmatrix} V \tag{3.24}$$

$$(G, G')\Sigma = \begin{pmatrix} (-,-) & (-,-) & (-,-) & (-,-) & (-,-) & (+,-) \\ (-,-) & (-,-) & (-,-) & (-,-) & (-,-) & (+,-) \\ (-,-) & (-,-) & (-,-) & (-,-) & (-,-) & (+,-) \\ (-,-) & (-,-) & (-,-) & (-,-) & (-,-) & (+,-) \\ (-,-) & (-,-) & (-,-) & (-,-) & (-,-) & (+,-) \\ (+,-) & (+,-) & (+,-) & (+,-) & (+,-) & (+,+) \end{pmatrix} \Sigma \ . \tag{3.25}$$

On the other hand, one introduces on the IR brane a chiral superfield Φ with superpotential

$$\mathcal{L}_\Phi = \delta(y - \pi R) \int d^2\theta \left(\frac{M^2}{2}\Phi^2 + \frac{\lambda}{3}\Phi^3 \right) \ , \tag{3.26}$$

whose couplings are estimated with NDA to be $M \sim M^{*'}$, $\lambda \sim 4\pi$. This potential can trigger the spontaneous breaking. Indeed, one of the possible vaccua is SU(4)$\times$SU(2)$\times$U(1)$'$ symmetric, the Φ vev being then

$$\langle \Phi \rangle = \mathrm{diag} \left(-\frac{2M}{\lambda}, -\frac{2M}{\lambda}, \frac{M}{\lambda}, \frac{M}{\lambda}, \frac{M}{\lambda}, \frac{M}{\lambda} \right) \ . \tag{3.27}$$

Note there are also higer-dimensional operators, which do not modify qualitatively the previous vacuum.

The gauge symmetry at the level of zero modes is the intersection of both breaking patterns SU(4) $\times$ SU(2) $\times$ U(1) and SU(5) $\times$ U(1)$'$, leaving SU(3) $\times$ SU(2) $\times$ U(1) $\times$ U(1)$'$, as in the 4D description. The extra U(1)$'$ has to be broken, by some superpotential or Fayet-Iliopoulos term on the UV brane.

Let us come back to the scales of the setup. In the 4D picture, the UV brane represents the Planck scale, while the IR brane represents roughly the GUT scale. The warp factor is supposed to be small, roughly $e^{-\pi kR} = \mathcal{O}(10^{-2})$, to explain the GUT/Planck hierarchy. More precisely, the GUT scale is set by the Φ vev, $M_{GUT} \equiv \langle \Phi \rangle$, which depends itself (again with a large uncertainty) on the 5D cutoff M^*. The 4D Planck is related to the

5D Planck mass by $M_{Pl}^2 \sim M_{5D}^3/k$, which is in turn roughly related to the 5D cutoff scale by $M_{5D} \sim M^*/10$ (this can be seen from NDA estimation, but also from more precise computations, see [51, 52] and references therein).

In this framework, different choices of scales are possible, constrained by the values of the Planck and GUT scales. One has also to verify that the first KK modes, with masses $\sim ke^{-\pi kR}$, are not lighter than the GUT scale. If it was the case, they would enter in the running and would modify this unification scale. This situation could be viable, but these KK towers do not respect the SU(5) which is broken on the IR brane , and could therefore spoil couplings unification.

The quantities relevant for the effective 4D theory remaining below the KK scale will be the warp factor (used to generate flavour hierarchy) and the volume factor πRM^*, which suppresses brane operators with respect to bulk operators.

3.2.3 Matter content

Let us now introduce the matter fields. As the MSSM Higgses are localized on a brane, matter fields have to propagate in the bulk. One can then make use of bulk masses to localize them in order to generate the realistic flavour patterns.

As they propagate in the bulk, matter fields come in SU(6) multiplets. It is convenient to show their decomposition under SU(5) $\times$ U(1)$'$, as well as boundary conditions. In the original paper, the SU(6) matter fields are hypermultiplets $(\mathcal{T}, \mathcal{T}^c)$, $(\mathcal{F}, \mathcal{F}^c)$, $(\mathcal{N}, \mathcal{N}^c)$, transforming under the representations **20**, **70**, **45** :

$$\begin{aligned}
\mathcal{T}(\mathbf{20}) &= \mathbf{10}_1^{(+,+)} + \mathbf{10}^{*(-,+)}_{-1} \\
\mathcal{T}^c(\mathbf{20}^*) &= \mathbf{10}^{*(-,-)}_{-1} + \mathbf{10}_1^{(+,-)} \\
\mathcal{F}(\mathbf{70}^*) &= \mathbf{5}^{*(+,+)}_{-3} + \mathbf{10}^{*(-,+)}_{-1} + \mathbf{15}^{*(-,+)}_{-1} + \mathbf{40}^{*(-,+)}_{1} \\
\mathcal{F}^c(\mathbf{70}) &= \mathbf{5}_3^{(-,-)} + \mathbf{10}_1^{(+,-)} + \mathbf{15}_1^{(+,-)} + \mathbf{40}_{-1}^{(+,-)} \\
\mathcal{N}(\mathbf{45}) &= \mathbf{1}_5^{(+,+)} + \mathbf{5}_3^{(-,+)} + \mathbf{15}_1^{(-,+)} + \mathbf{35}_{-1}^{(-,+)} \\
\mathcal{N}^c(\mathbf{45}^*) &= \mathbf{1}_{-5}^{(-,-)} + \mathbf{5}^{*(+,-)}_{-3} + \mathbf{15}^{*(+,-)}_{-1} + \mathbf{35}^{*(+,-)}_{1} \ ,
\end{aligned} \tag{3.28}$$

where the superscripts correspond to the parities under brane reflexions. The remaining massless modes are thus the chiral multiplets **10** and $\mathbf{5}^*$, containing respectively the MSSM fields Q, U, E and L, D, and the SU(5) singlet **1**, identified as the right-handed neutrino.

The 4D Yukawa couplings then arise from the IR brane superpotential

$$\mathcal{L}_{\text{Yukawa}} = \delta(y - \pi R) \left(\int d^2\theta h^{\mathcal{T}} \mathcal{T}\mathcal{T}\Phi + h^{\mathcal{F}} \mathcal{T}\mathcal{F}\Phi + h^{\mathcal{N}} \mathcal{F}\mathcal{N}\Phi + \text{h.c.} \right) \ . \tag{3.29}$$

To reproduce a realistic flavour pattern, one introduces three copies of the above fields, with identical bulk masses for the $\mathcal{F}$, $c_{\mathcal{F}_1} \sim c_{\mathcal{F}_2} \sim c_{\mathcal{F}_3}$, and hierarchical masses for the $\mathcal{T}$,

$c_{\mathcal{T}_1} > c_{\mathcal{T}_2} > c_{\mathcal{T}_3}$, such that the exponential localization of these different field reproduces the realistic SM flavour hierarchy. We define the profile factors f_i^x as the value of the profile functions (defined by Eqns. (2.41), (2.53)) on the IR brane:

$$f_i^x = \frac{1}{\sqrt{\pi R}} e^{(\frac{1}{2} - c_{x_i})\pi k R} . \tag{3.30}$$

If one assumes the typical structure $f_1^{\mathcal{T}} \approx \epsilon^2$, $f_2^{\mathcal{T}} \approx \epsilon$, $f_1^{\mathcal{T}} \approx 1$, $f_1^{\mathcal{F}} \approx f_2^{\mathcal{F}} \approx f_3^{\mathcal{F}} \approx \epsilon$, the 4D Yukawa matrices arising from Eq. (3.29) takes the form:

$$y^u_{ij} \sim h^{\mathcal{T}}_{ij} \begin{pmatrix} \epsilon^4 & \epsilon^3 & \epsilon^2 \\ \epsilon^3 & \epsilon^2 & \epsilon \\ \epsilon^2 & \epsilon & 1 \end{pmatrix} , \qquad y^d_{ij} = (y^e_{ij})^t \sim h^{\mathcal{F}}_{ij} \begin{pmatrix} \epsilon^3 & \epsilon^3 & \epsilon^3 \\ \epsilon^2 & \epsilon^2 & \epsilon^2 \\ \epsilon & \epsilon & \epsilon \end{pmatrix} \tag{3.31}$$

The h matrices are supposed to be anarchical. In fact, the holographic approach tells that these coefficients should be estimated from naive dimensional analysis (NDA), as the IR brane represents the scale where the G sector enters in strong regime. The NDA estimation is done later in this Section. The general form for such Yukawa matrices generated from wave-function localization will be written in Eq. (3.48). An analysis of such Yukawa textures is done in Section 6. In particular, the anarchical aspect of the h matrices will be taken into account properly.

The extra U(1)$'$ is broken on the UV brane by adding a superpotential

$$\mathcal{L} = \delta(y) \left(\int d^2\theta Y (X\bar{X} - \Lambda^2) + \text{h.c.} \right) , \tag{3.32}$$

which gives the vevs $\langle X \rangle = \langle \bar{X} \rangle = \Lambda$. The Majorana mass of the right-handed neutrino can be generated by coupling the bulk singlet to one of these X. Operators of the form $\mathcal{TTTF} \supset QQQL, UUDE$ can be present on the UV brane. They are especially dangerous for proton decay. Indeed, as all matter fields are localized toward this brane, there is no exponential, Yukawa-type suppression. In the original model, the additional ingredient of a $Z_{4,R}$ symmetry is introduced to forbid these dangerous UV-brane operators. This then recquires to add new spurions to break this discrete symmetry on the IR brane.

Another matter realization

While the $\mathcal{T}$ sector is very simple, one could find that the $\mathcal{F}$ and $\mathcal{N}$ sectors are a bit engineered, as zero modes have to arise from rather large representations. In addition, new brane fields need to be added to break the extra U(1)$'$, and a discrete symmetry has to be added to avoid fast proton decay, requiring also new brane fields. Taking principles of simplicity and economy as guideline, we propose here another realization of this matter

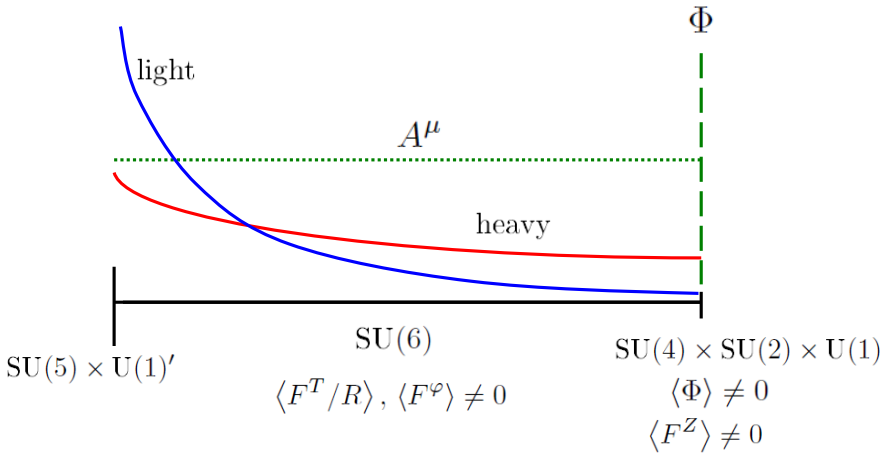

Figure 3.2: HGU framework in a nutshell. The warp factor is small ($\mathcal{O}(10^{-2})$) and KK modes are heavy ($\mathcal{O}(M_{GUT})$). The GUT group is broken by boundary condition on the UV brane ($y = 0$, left), and by the vacuum expectation value of Φ on the IR brane ($y = \pi R$, right). The Higgses arise from Φ, as pseudo-Goldstone fields. Matter fields have to be appropriately localized towards the UV brane to generate flavour hierarchy. First generations of matter fields have to be more localized than the third, to reduce the overlap with the Higgs field. Supersymmetry breaking is transmitted to the MSSM through radion mediation, and through a source F^Z on the IR brane.

sector. The field content we propose is made of three copies of

$$\begin{aligned}
\mathcal{T}(\mathbf{20}) &= \mathbf{10}_1^{(+,+)} + \mathbf{10}^{*(-,+)}_{-1} \\
\mathcal{T}^c(\mathbf{20}^*) &= \mathbf{10}^{*(-,-)}_{-1} + \mathbf{10}_1^{(+,-)} \\
\mathcal{F}(\mathbf{21}^*) &= \mathbf{1}_{10}^{(-,-)} + \mathbf{5}^{*(+,+)}_4 + \mathbf{15}^{*(-,+)}_{-2} \\
\mathcal{F}^c(\mathbf{21}) &= \mathbf{1}_{-10}^{(+,+)} + \mathbf{5}_{-4}^{(-,-)} + \mathbf{15}_2^{(+,-)} \ ,
\end{aligned} \tag{3.33}$$

and a new bulk field $\mathcal{S}$

$$\begin{aligned}
\mathcal{S}(\mathbf{6}^*) &= \mathbf{1}_5^{(+,+)} + \mathbf{5}^{*(-,+)}_{-1} \\
\mathcal{S}^c(\mathbf{6}) &= \mathbf{1}_{-5}^{(-,-)} + \mathbf{5}_1^{(+,-)} \ .
\end{aligned} \tag{3.34}$$

The zero modes of $\mathcal{T}$, $\mathcal{F}$ contains the MSSM fields, and the zero mode of $\mathcal{F}^c$ is identified as the right-handed neutrino.

At that point, the only Yukawa couplings possible are $W \supset y_\mathcal{T}\mathcal{T}\mathcal{T}\Phi + y_\mathcal{N}\mathcal{F}\mathcal{F}^c\Phi \supset y_u Q U H_u + y_n L N H_u$. Moreover, the right-handed neutrino is massless.

The matter sector are simpler, but how the missing Yukawa couplings can be generated? The crucial point is to break the extra U(1)′ using a (possibly effective) Fayet-Iliopoulos term $\delta(y)\xi$ or $\delta(y-\pi R)\xi$. As the $\mathbf{1}_5^{(+,+)}$ component of $\mathcal{S}$ has a positive charge under $U(1)'$, one assumes $\xi < 0$. Under this condition, this $\mathbf{1}_5^{(+,+)}$ component gets a non-zero vev $\langle \mathcal{S} \rangle$,

together with the scalar component of the corresponding $U(1)'$ $\mathcal{N}=2$ vector multiplet. This is imposed by the D-part of the scalar potential, and detailed in [97] or [98].

The $\mathcal{S}$ vev will be involved in higher dimensional operators on the branes, the leading one being

$$W \supset \frac{1}{M^*}\mathcal{T}\mathcal{F}\mathcal{S}\Phi \ . \tag{3.35}$$

Once $\langle\mathcal{S}\rangle$ gets a non zero value, this operator generates the effective Yukawa couplings $W \supset y_{\mathcal{F}}\mathcal{T}\mathcal{F}\Phi \supset y_d QDH_d + y_e LEH_d$. Note that the size of the largest of these Yukawa couplings, y_b, constrains $\langle\mathcal{S}\rangle/M^*$ to not be too small.

Assuming $c_{\mathcal{S}} = 1/2$ for simplicity, one has

$$\langle\mathcal{S}\rangle(y) = \sqrt{\frac{\xi}{2\pi R g_U q}} f_{\mathcal{S}}(y) \ , \tag{3.36}$$

where g_U is the GUT gauge coupling, $q=5$ is the charge of $\langle\mathcal{S}\rangle$, and $f_{\mathcal{S}}(y)$ the profile along the fifth dimension. This profile is no longer flat due to the vev of the scalar component of the $U(1)'$ vector multiplet, which acts like a bulk mass. One defines the conformaly flat vev $\widetilde{\langle\mathcal{S}\rangle}$ such that $\langle\mathcal{S}\rangle = \widetilde{\langle\mathcal{S}\rangle} f_{\mathcal{S}}(y)$.

In addition, we also assume that the three generations of $\mathcal{F}$ are conformaly flat. The bottom Yukawa coupling is then roughly given by

$$y_b \sim \frac{6\pi^2}{M^*\pi R}\frac{\widetilde{\langle\mathcal{S}\rangle}}{M^*} f_{\mathcal{S}}(\pi R) \ . \tag{3.37}$$

The $\mathcal{S}$ vev also gives a Majorana mass $M_N \sim \widetilde{\langle\mathcal{S}\rangle}\left(f_{\mathcal{S}}(0) + f_{\mathcal{S}}(\pi R)\right)$ to the right-handed neutrino, through the superpotential couplings

$$W \supset \mathcal{F}^c\mathcal{F}^c\mathcal{S} \ , \tag{3.38}$$

allowed on both branes. The usual see-saw mechanism can then occur.

To summarize, the $U(1)'$ breaking, triggered by a brane FI term, permits to generate the $y_{\mathcal{F}}$ Yukawa coupling and achieve the see-saw mechanism. We now have to control the operators inducing fast proton decay. The leading UV brane operator is $\mathcal{T}\mathcal{T}\mathcal{T}\mathcal{F}\mathcal{S}/M^{*2}$. In comparison to the original matter sector of the HGU model (3.28), this operators feels an additional suppression of $\widetilde{\langle\mathcal{S}\rangle} f_{\mathcal{S}}(0)/M^*$. Given that $\widetilde{\langle\mathcal{S}\rangle}/M^*$ cannot be much smaller than 0.01 to provide a sufficiently large y_b, one has to rely on the suppression of the profile $f_{\mathcal{S}}(0)$. In other words, localizing $\mathcal{S}$ toward the IR brane permits to avoid fast proton decay without the introduction of an additional discrete symmetry.

We do not go further here, but simply mention the subsequent developments. The localization of $\mathcal{S}$ can be eventually forced by choosing an appropriate bulk mass $c_{\mathcal{S}}$. As both the FI term and bulk masses modify the profiles of $\mathcal{S}$, one has to solve properly equations of motions from the beginning. One has also to check if the profiles of other bulk

fields are not modified, such that proper flavour hierarchy is still generated by exponential profiles. This is ensured if the bulk masses, proportional to the curvature k, are dominant over the FI term effects.

Note that if the FI term is localized on the UV brane, this means in the 4D picture that it is contained in the elementary sector. It can be in particular generated if the $U(1)'$ gauge symmetry is anomalous. On the other hand, if the FI term is localized on the IR brane, this means that the strong dynamics of the G group generates it, and it spontaneously breaks the CFT global $U(1)'$.

3.2.4 Supersymmetry breaking

We now consider supersymmetry breaking in this framework. This time, there is no reason to forbid one of the sources F^Z, $F^T/2R$ and F^φ. We will assume that $F^T/2R \gg F^\varphi/8\pi^2$, such that anomaly mediated contributions are negligible.

In this framework, the Higgses are localized on the IR brane, and matter fields have appropriate exponential profiles in the bulk to generate a realistic flavour hierarchy. In order to alleviate the SUSY flavour problem, the crucial assumption made is that the source of SUSY breaking is also localized on the IR brane, i.e. SUSY breaking $F^Z \neq 0$ is triggered by the CFT strong dynamics. The brane scalar soft terms will then follow roughly the same hierarchical pattern as the Yukawa couplings.

Generic supersymmetry breaking can be parameterized by F- and D-type spurions in the Kähler potential, which we generally denote by $\widetilde{\mathbf{\Phi}}$ and $\widetilde{\mathbf{\Delta}}$, and by F-type spurions in the superpotential denoted by $\widetilde{\mathbf{\Lambda}}$. Omitting the neutrinos from now on, the 4D Lagrangian of matter fields can be brought into the form

$$\begin{aligned}
\mathcal{L} = \int d^4\theta \Bigg[& \left(\mathbf{Y}_{H_u} + \left(\widetilde{\mathbf{\Phi}}_{H_u} \theta^2 + \text{h.c.} \right) + \widetilde{\mathbf{\Delta}}_{H_u} \theta^4 \right) H_u^\dagger H_u + (H_u \leftrightarrow H_d) \\
& + \left(\mathbf{Y}^u_{ij} + \left(\widetilde{\mathbf{\Phi}}^u_{ij} \theta^2 + \text{h.c.} \right) + \widetilde{\mathbf{\Delta}}^u_{ij} \theta^4 \right) U_i^\dagger U_j + (U \leftrightarrow \{D,\, Q,\, L,\, E,\, N\}) \Bigg] \\
+ \int d^2\theta \Bigg[& \left(\tilde{y}^u_{ij} + \widetilde{\mathbf{\Lambda}}^u_{ij} \theta^2 \right) H_u U_i Q_j + \left(\tilde{y}^d_{ij} + \widetilde{\mathbf{\Lambda}}^d_{ij} \theta^2 \right) H_d D_i Q_j \\
& + \left(\tilde{y}^e_{ij} + \widetilde{\mathbf{\Lambda}}^e_{ij} \theta^2 \right) H_d E_i L_j + \tilde{\mu} H_u H_d \Bigg] \\
& + \text{h.c.}
\end{aligned} \tag{3.39}$$

Here the $\mathbf{Y}$, $\widetilde{\mathbf{\Delta}}$, $\widetilde{\mathbf{\Phi}}$ and $\widetilde{\mathbf{\Lambda}}$ are functions of the radius and of the SUSY breaking sources. Assuming the absence of brane kinetic terms, which are generically subdominant at large

volume, the wave-function coefficient $\mathbf{Y}$ for the bulk fields are :

$$\begin{aligned} \mathbf{Y}_{H_{u,d}} &= e^{-2\pi kR}\,, \\ \mathbf{Y}^x_{ij} &= \delta_{ij}\frac{e^{(\frac{1}{2}-c_i^x)2\pi kR}-1}{(\frac{1}{2}-c_i^x)2\pi kR}\,. \end{aligned} \tag{3.40}$$

where $x = u,\ d,\ q,\ l,\ e$.

Again for $x =$ any matter field, we define rescaled quantities by

$$\begin{aligned} &\mathbf{\Phi}^x_{ij} = \frac{\widetilde{\mathbf{\Phi}}^x_{ij}}{\left(\mathbf{Y}^x_{ii}\mathbf{Y}^x_{jj}\right)^{1/2}}, \quad \mathbf{\Phi}_{H_{u,d}} = \frac{\widetilde{\mathbf{\Phi}}_{H_{u,d}}}{\mathbf{Y}_{H_{u,d}}}, \quad \mathbf{\Delta}^x_{ij} = \frac{\widetilde{\mathbf{\Delta}}^x_{ij}}{\left(\mathbf{Y}^x_{ii}\mathbf{Y}^x_{jj}\right)^{1/2}}, \\ &\mathbf{\Lambda}^{u,d}_{ij} = \frac{\widetilde{\mathbf{\Lambda}}^{u,d}_{ij}}{\left(\mathbf{Y}^{u,d}_{ii}\mathbf{Y}^q_{jj}\mathbf{Y}_{H_{u,d}}\right)^{1/2}}, \quad \mathbf{\Lambda}^e_{ij} = \frac{\widetilde{\mathbf{\Lambda}}^e_{ij}}{\left(\mathbf{Y}^e_{ii}\mathbf{Y}^l_{jj}\mathbf{Y}_{H_d}\right)^{1/2}}\,. \end{aligned} \tag{3.41}$$

The Yukawa matrices for canonically normalized fields are then

$$y^u_{ij} = \frac{\tilde{y}^u_{ij}}{\left(\mathbf{Y}^u_{ii}\mathbf{Y}^q_{jj}\mathbf{Y}_{H_u}\right)^{1/2}}, \quad y^d_{ij} = \frac{\tilde{y}^d_{ij}}{\left(\mathbf{Y}^d_{ii}\mathbf{Y}^q_{jj}\mathbf{Y}_{H_d}\right)^{1/2}}, \quad y^e_{ij} = \frac{\tilde{y}^e_{ij}}{\left(\mathbf{Y}^e_{ii}\mathbf{Y}^l_{jj}\mathbf{Y}_{H_d}\right)^{1/2}}\,. \tag{3.42}$$

The scalar soft masses for matter fields are

$$m^2_x = \left(\mathbf{\Phi}^x\right)^\dagger \mathbf{\Phi}^x - \mathbf{\Delta}^x\,, \tag{3.43}$$

and the trilinear terms are given by

$$\begin{aligned} a^u &= (\mathbf{\Phi}^q)^T y^u + y^u(\mathbf{\Phi}^u)^T + \mathbf{\Phi}_{H_u}\, y^u - \mathbf{\Lambda}^u\,, \\ a^d &= (\mathbf{\Phi}^q)^T y^d + y^d(\mathbf{\Phi}^d)^T + \mathbf{\Phi}_{H_d}\, y^d - \mathbf{\Lambda}^d\,, \\ a^e &= (\mathbf{\Phi}^l)^T y^e + y^e(\mathbf{\Phi}^e)^T + \mathbf{\Phi}_{H_d}\, y^e - \mathbf{\Lambda}^e\,. \end{aligned} \tag{3.44}$$

The convention for these soft terms are defined by Eq. (1.17).

We thus have the generic expressions of supersymmetry breaking terms, as a function of the spurions $\widetilde{\mathbf{\Phi}}$, $\widetilde{\mathbf{\Delta}}$ and $\widetilde{\mathbf{\Lambda}}$, and of the wave function normalization coefficients $\mathbf{Y}^x$. We now have to give the content of these generic parameters, as a function of SUSY breaking and geometric parameters.

With the profile functions of Eq. (2.53), and with the dependence on the radion mul-

tiplet restored, the 4D Lagrangian is

$$\begin{aligned}
\mathcal{L} = & \int d^4\theta\, \varphi\overline{\varphi} \sum_i \frac{e^{(\frac{1}{2}-c_i^u)k\pi(T+\overline{T})}-1}{(\frac{1}{2}-c_i^u)2\pi kR}\, U_i^\dagger U_i \\
& \quad + (U \leftrightarrow \{D,\, Q,\, L,\, E,\, N\}) \\
& + \int d^4\theta\, \varphi\overline{\varphi}\, e^{-k\pi(T+\overline{T})} \left(1 + \left(\widehat{\mathbf{\Phi}}_{H_u}\theta^2 + \text{h.c.}\right) + \widehat{\mathbf{\Delta}}_{H_u}\theta^4\right) H_u^\dagger H_u \\
& \quad + (H_u \leftrightarrow H_d) \\
& + \int d^4\theta\, \varphi\overline{\varphi} \sum_{ij} \frac{e^{\frac{1}{2}(1-c_i-c_j)k\pi(T+\overline{T})}}{\pi R} \left(\widehat{\mathbf{\Phi}}_{ij}^u\theta^2 + \text{h.c.} + \widehat{\mathbf{\Delta}}_{ij}^u\theta^4\right) U_i^\dagger U_j \\
& \quad + (U \leftrightarrow \{D,\, Q,\, L,\, E,\, N\}) \\
& + \int d^2\theta\, \varphi^3\, W_{\text{brane}} + \text{h.c.}
\end{aligned} \tag{3.45}$$

where

$$\begin{aligned}
W_{\text{brane}} = \sum_{ij} \Big[& \left(h_{ij}^u + \widehat{\mathbf{\Lambda}}_{ij}^u\theta^2\right) \frac{e^{-(c_i^u+c_j^q)\pi kT}}{\pi R}\, H_u U_i Q_j \\
& + \left(h_{ij}^d + \widehat{\mathbf{\Lambda}}_{ij}^d\theta^2\right) \frac{e^{-(c_i^d+c_j^q)\pi kT}}{\pi R}\, H_d D_i Q_j \\
& + \left(h_{ij}^e + \widehat{\mathbf{\Lambda}}_{ij}^e\theta^2\right) \frac{e^{-(c_i^e+c_j^l)\pi kT}}{\pi R}\, H_d E_i L_j \Big] + e^{-3\pi kT}\hat{\mu} H_u H_d\,.
\end{aligned} \tag{3.46}$$

The spurions $\widehat{\mathbf{\Phi}}$, $\widehat{\mathbf{\Delta}}$ and $\widehat{\mathbf{\Lambda}}$ capture the effect of the brane Goldstino Z.

For the spurionic coefficients one obtains, using profile factors f_i^x defined in Eq. (3.30),

$$\begin{aligned}
\widetilde{\mathbf{\Phi}}_{H_{u,d}} &= \left(F^\varphi - \pi k F^T + \widehat{\mathbf{\Phi}}_{H_{u,d}}\right) e^{-2\pi kR}\,, \\
\widetilde{\mathbf{\Phi}}_{ij}^x &= \delta_{ij} F^\varphi \frac{e^{(\frac{1}{2}-c_i^x)2\pi kR}-1}{(\frac{1}{2}-c_i^x)2\pi kR} + \delta_{ij} F^T \frac{e^{(\frac{1}{2}-c_i^x)2\pi kR}}{2R} + \widehat{\mathbf{\Phi}}_{ij}^x\, f_i^x\, f_j^x\,, \\
\widetilde{\mathbf{\Delta}}_{ij}^x &= \delta_{ij}\, \frac{e^{(\frac{1}{2}-c_i^x)2\pi kR}}{(\frac{1}{2}-c_i^x)2\pi kR} \left|F^\varphi + k\pi\left(\frac{1}{2}-c_i^x\right)F^T\right|^2 - \delta_{ij}|F^\varphi|^2 \frac{1}{(\frac{1}{2}-c_i^x)2\pi kR} \\
&\quad + \left(\left(\frac{1}{2}(1-c_i^x-c_j^x)k\pi\, \overline{F}^{\overline{T}} + \overline{F}^{\bar{\varphi}}\right)\widehat{\mathbf{\Phi}}_{ij}^x + \text{h.c.} + \widehat{\mathbf{\Delta}}_{ij}^x\right) f_i^x\, f_j^x\,, \\
\widetilde{\mathbf{\Lambda}}_{ij}^u &= \left(\left(3F^\varphi - (c_i^u+c_j^q)k\pi F^T\right) h_{ij}^u + \widehat{\mathbf{\Lambda}}_{ij}^u\right) e^{-k\pi R}\, f_i^u\, f_j^q\,, \\
\widetilde{\mathbf{\Lambda}}_{ij}^d &= \left(\left(3F^\varphi - (c_i^d+c_j^q)k\pi F^T\right) h_{ij}^d + \widehat{\mathbf{\Lambda}}_{ij}^d\right) e^{-k\pi R}\, f_i^d\, f_j^q\,, \\
\widetilde{\mathbf{\Lambda}}_{ij}^e &= \left(\left(3F^\varphi - (c_i^e+c_j^l)k\pi F^T\right) h_{ij}^e + \widehat{\mathbf{\Lambda}}_{ij}^e\right) e^{-k\pi R}\, f_i^e\, f_j^l\,.
\end{aligned} \tag{3.47}$$

The non-canonical Yukawa couplings $\tilde{y}_{ij}$ can be read off to be

$$\begin{aligned}
\tilde{y}_{ij}^u &= h_{ij}^u\, e^{-\pi kR}\, f_i^u\, f_j^q\,, \\
\tilde{y}_{ij}^d &= h_{ij}^d\, e^{-\pi kR}\, f_i^d\, f_j^q\,, \\
\tilde{y}_{ij}^e &= h_{ij}^e\, e^{-\pi kR}\, f_i^e\, f_j^l\,.
\end{aligned} \tag{3.48}$$

Using Eq. (3.42) and the wave function normalizations from Eq. (3.40), this gives canonical Yukawa couplings (note that the Higgs wave function normalization cancels the explicit warp factor).

After scalar soft terms, let us finally discuss gaugino masses. The 4D gauge field Lagrangian is

$$\mathcal{L} \supset \frac{1}{4}\sum_a \int d^2\theta \left(\frac{1}{g_{\rm UV}^2} + \frac{\pi T}{g_5^2} + \frac{1}{g_{{\rm IR}\,a}^2} + \widehat{\mathbf{\Omega}}^a\theta^2\right) W^{a\alpha}W^a_\alpha + \text{ h.c.} + \ldots \tag{3.49}$$

We have omitted terms irrelevant for gaugino masses, and neglected possible effects from bulk Chern-Simons terms [92,99]. In this expression, $a = 1, 2, 3$ labels the Standard Model gauge factors, g_5 is the bulk gauge coupling, and $1/g_{\rm UV}^2$, $1/g_{{\rm IR}\,a}^2$ originates from gauge kinetic terms on the UV and IR brane. Note that the UV term is universal with respect to the Standard Model gauge fields, as the UV brane preserves SU(5). The gaugino masses are then given by

$$M_a = \frac{1}{2}g_4^2\left(\widehat{\mathbf{\Omega}}^a + \frac{\pi F^T}{g_5^2}\right), \tag{3.50}$$

with $1/g_4^2 = 1/g_{\rm UV}^2 + \pi R/g_5^2 + 1/g_{{\rm IR}\,a}^2$. We have to assume that the SU(5) violating IR brane contributions are small to not spoil coupling unification. This is in particular the case in the large volume regime. Universal gaugino masses are induced by the leading contributions in the HGU model, since in this model the GUT group is broken only by expectation values on the IR brane. Higher-dimensional operators involving powers of the GUT Higgs Φ can lead to gaugino mass splittings, but we assume that they are sufficiently suppressed. In a more general setup where the gauge symmetry is broken by boundary conditions on the SUSY breaking brane, the universality condition could be relaxed.

In the following, we will assume exact gaugino mass universality :

$$M_1 = M_2 = M_3 \equiv M_{1/2}\,. \tag{3.51}$$

SUSY breaking dominated by brane fields

In the case that the dominant source for the soft terms is the brane field Z, there is a large number of unknown coupling parameters. Their magnitudes can be estimated by naive dimensional analysis. Indeed, in accordance with the holographic interpretation, the theory is taken to be strongly coupled on the IR brane and in the bulk. We use loop factors $\ell_5 = 24\pi^3$ for 5D superfields (of dimension 3/2) and $\ell_4 = 16\pi^2$ for 4D superfields (of dimension 1) [100]. Up to $\mathcal{O}(1)$ uncertainty, the coefficient for a superpotential term composed of n bulk zero modes and m brane fields is

$$\frac{M_*^3}{16\pi^2}\left(\frac{\sqrt{\ell_5}}{M_*^{3/2}}\right)^n\left(\frac{\sqrt{\ell_4}}{M_*}\right)^m, \tag{3.52}$$

while for a Kähler potential term it is

$$\frac{M_*^2}{16\pi^2}\left(\frac{\sqrt{\ell_5}}{M_*^{3/2}}\right)^n\left(\frac{\sqrt{\ell_4}}{M_*}\right)^m . \tag{3.53}$$

Here M_* is again the cutoff scale, taken to be close to the reduced Planck scale in 4D. The 5D Yukawa couplings are thus estimated to be

$$h_{ij} \approx \frac{6\pi^2}{M_*} . \tag{3.54}$$

We obtain

$$\begin{aligned}
\widehat{\mathbf{\Phi}}_{H_{u,d}} &\approx 4\pi\frac{F^Z}{M_*}, \\
\widehat{\mathbf{\Phi}}^x_{ij} &\approx \frac{6\pi^2}{M_*}\frac{F^Z}{M_*}, \\
\widehat{\mathbf{\Delta}}^x_{ij} &\approx \frac{24\pi^3}{M_*}\left|\frac{F^Z}{M_*}\right|^2 , \\
\widehat{\mathbf{\Lambda}}^{u,d,e}_{ij} &\approx \frac{24\pi^3}{M_*}\frac{F^Z}{M_*}.
\end{aligned} \tag{3.55}$$

It is now convenient to define matrices

$$\kappa^x_{ij} = \frac{6\pi^2}{M_*}\frac{f^x_i\, f^x_j}{\left(\mathbf{Y}^x_i\, \mathbf{Y}^x_j\right)^{1/2}} . \tag{3.56}$$

The κ^x_{ij} are dimensionless and hierarchical, with their largest entries at most of order of the top Yukawa coupling (as their structure is determined by the same profile factors as the Yukawa matrices). With Eqns. (3.56), (3.55), (3.47) and (3.41) one obtains, up to $\mathcal{O}(1)$ uncertainty,

$$\mathbf{\Phi}^x_{ij} \approx \kappa^x_{ij}\frac{F^Z}{M_*} , \qquad \mathbf{\Delta}^x_{ij} \approx 4\pi\kappa^x_{ij}\left|\frac{F^Z}{M_*}\right|^2 . \tag{3.57}$$

Hence the soft masses $m_x^2 = \mathbf{\Phi}^{x\dagger}\mathbf{\Phi}^x - \mathbf{\Delta}^x$ are dominated by $\mathbf{\Delta}^x$.

For the trilinear soft terms of Eq. (3.44) we find

$$a^u_{ij} \approx (\kappa^q y^u)_{ij}\frac{F^Z}{M_*} + (y^u\kappa^u)_{ij}\frac{F^Z}{M_*} + 4\pi\, y^u_{ij}\frac{F^Z}{M_*} - \mathbf{\Lambda}^u_{ij} , \tag{3.58}$$

where

$$\mathbf{\Lambda}^u_{ij} \approx 4\pi y^u_{ij}\frac{F^Z}{M_*} . \tag{3.59}$$

It turns out a^u_{ij} is dominated by the last two terms in Eq. (3.58). Provided that there are no accidental cancellations taking place between them, it is of the order

$$a^u_{ij} \approx 4\pi y^u_{ij}\frac{F^Z}{M_*} . \tag{3.60}$$

Analogous statements hold for the other a-terms. Comparing Eqns. (3.57) and (3.60), the largest a-terms will be around a factor of $\approx \sqrt{4\pi}$ larger than the largest scalar soft masses.

The NDA estimate for $\widehat{\mathbf{\Omega}}^a$ in Eq. (3.49) is [101]

$$\widehat{\mathbf{\Omega}}^a \approx \frac{6\pi^2}{\sqrt{C}\, g_5^2} \frac{F^Z}{M_*^2}\,, \tag{3.61}$$

with C a group-theoretical factor, taken to be $C = C_2\,(\mathrm{SU}(6)) = 6$. The canonically normalized gaugino masses of Eq. (3.50) are thus

$$M_a \approx \frac{3\pi^2}{\sqrt{6}} \frac{g_4^2}{g_5^2}\, \frac{F^Z}{M_*^2}\,. \tag{3.62}$$

The four-dimensional gauge coupling gets contributions from both the 5D bulk gauge coupling and a UV brane-localized kinetic term (cf. Eq. (3.49)):

$$\frac{1}{g_4^2} = \frac{1}{g_{\mathrm{UV}}^2} + \frac{\pi R}{g_5^2}\,. \tag{3.63}$$

The bulk gauge coupling can also be estimated from naive dimensional analysis; this gives

$$\frac{1}{g_5^2} \approx \frac{C}{24\pi^3} M_*\,. \tag{3.64}$$

The UV brane, in the holographic picture, can be weakly coupled and thus g_{UV} can be smaller than its NDA value. In fact, unless R is rather large, g_{UV} must be small in order to obtain the proper unified gauge coupling $g_4^2 \approx 0.5$ from Eq. (3.63).

Eqns. (3.64) and (3.62) lead to suppressed gaugino masses:

$$M_a \approx \frac{\sqrt{6}}{8\pi} g_4^2 \frac{F^Z}{M_*} \approx 0.05 \frac{F^Z}{M_*}\,. \tag{3.65}$$

It appears that IR brane terms cannot be the only source of SUSY breaking , to have gaugino masses which are comparable with the other soft terms. Alternatively one could consider models which are weakly coupled also in the bulk and where, consequently, there is no large NDA suppression as in Eq. (3.64).

Finally, the Higgs mass matrix is degenerate at the GUT scale [102]:

$$m_{H_u}^2 + |\mu|^2 = m_{H_d}^2 + |\mu|^2 = |B_\mu|\,. \tag{3.66}$$

This is necessarily the case because the Higgs fields there arise as pseudo-Nambu-Goldstone bosons in the HGU framework. The relation Eq. (3.66) has the advantage of constraining our free parameters somewhat more, but could easily be relaxed in a more general model.

The NDA estimate for the Higgs mass parameters is[2]

$$\begin{aligned} \mu &\approx 4\pi \frac{F^Z}{M_*}\,, \\ m^2_{H_{u,d}} &\approx 16\pi^2 \left|\frac{F^Z}{M_*}\right|^2\,, \\ m^2_{H_{u,d}} + |\mu|^2 = |B_\mu| &\approx 16\pi^2 \left|\frac{F^Z}{M_*}\right|^2\,. \end{aligned} \tag{3.67}$$

SUSY breaking dominated by radion mediation

Let us consider now the opposite limit case, where brane contributions to soft masses are negligible and the dominant source is radion mediation. The soft terms in this case are well known (see, for example, [57, 103]): bulk field soft masses become

$$m^2_{xij} = \delta_{ij} \left|\frac{F^T}{2R}\right|^2 \left(\frac{(\frac{1}{2} - c^x_i)\pi kR}{\sinh\left((\frac{1}{2} - c^x_i)\pi kR\right)}\right)^2\,, \tag{3.68}$$

and the trilinear terms are

$$\begin{aligned} a^u_{ij} &= \frac{F^T}{2R}\left(\frac{(\frac{1}{2} - c^u_i)2\pi kR}{e^{(\frac{1}{2}-c^u_i)2\pi kR} - 1} + \frac{(\frac{1}{2} - c^q_j)2\pi kR}{e^{(\frac{1}{2}-c^q_j)2\pi kR} - 1}\right) y^u_{ij}\,, \\ a^d_{ij} &= \frac{F^T}{2R}\left(\frac{(\frac{1}{2} - c^d_i)2\pi kR}{e^{(\frac{1}{2}-c^d_i)2\pi kR} - 1} + \frac{(\frac{1}{2} - c^q_j)2\pi kR}{e^{(\frac{1}{2}-c^q_j)2\pi kR} - 1}\right) y^d_{ij}\,, \\ a^e_{ij} &= \frac{F^T}{2R}\left(\frac{(\frac{1}{2} - c^e_i)2\pi kR}{e^{(\frac{1}{2}-c^e_i)2\pi kR} - 1} + \frac{(\frac{1}{2} - c^l_j)2\pi kR}{e^{(\frac{1}{2}-c^l_j)2\pi kR} - 1}\right) y^e_{ij}\,. \end{aligned} \tag{3.69}$$

The Higgs mass parameters cannot depend on F^T since the Higgs fields are brane-localized. In addition, it is well-known that soft scalar masses cannot be induced by F^φ at tree-level. Together with the Higgs mass degeneracy condition which holds in the HGU framework, as discussed earlier, the Higgs mass parameters are then [85,102], up to anomaly mediated contributions

$$m^2_{H_u} = m^2_{H_d} = 0, \qquad \mu = F^T k\pi - F^\varphi, \qquad |B_\mu| = |F^T k\pi - F^\varphi|^2\,. \tag{3.70}$$

We will see in Section 5 that it is difficult to obtain realistic spectra with this condition.

Finally, the gaugino mass is

$$M_{1/2} = \frac{\pi}{2}\frac{g_4^2}{g_5^2} F^T\,. \tag{3.71}$$

As discussed in the previous Section, the gauge fields could be predominantly UV brane fields. In that case the radion-mediated gaugino mass will be suppressed, and since the

[2]One may notice that, given the NDA estimates of μ and $m^2_{H_{u,d}}$, B_μ should have a factor $32\pi^2$ instead of $16\pi^2$. This is part of the uncertainty inherent to the NDA approach.

brane contribution to $M_{1/2}$ is also small, no realistic phenomenology can be expected. We are thus led to focus on the other case where R is large enough to overcome the NDA suppression of Eq. (3.64), $RM_* \sim \mathcal{O}(100)$. The second term on the RHS of Eq. (3.63) contributes then sizeably to $1/g_4^2$, and in the limit case where the UV brane term can be neglected, we obtain

$$M_{1/2} = \frac{F^T}{2R} \,, \tag{3.72}$$

comparable with the largest other radion-mediated soft masses.

3.3 The degenerate Higgs mass matrix

In both frameworks presented, the Higgs sector mass terms follow the peculiar relation

$$m_{H_u}^2 + |\mu|^2 = m_{H_d}^2 + |\mu|^2 = \pm B_\mu \,, \tag{3.73}$$

that we call degenerate Higgs mass matrix (DHMM). We will now discuss in more details some aspects of this equality: sign ambiguities, and two different origins for this relation.

3.3.1 Sign ambiguities

On one hand, even if the phase of the supersymmetric μ term is neglected, a freedom on sign$\mu = \pm 1$ still remains. This sign ambiguity is well known. On the other hand, there is also an ambiguity on the corresponding soft term B_μ. Indeed, changing simultaneously the sign of μ, B_μ and one of the Higgs fields leaves invariant the Lagrangian. We parametrize this second degree of freedom by a coefficient ε_H, which appears in front of both μ and B_μ.s

There are therefore 4 branches of solutions. By convention, B_μ is taken positive at the weak scale. So, for a given parameter space point of the high energy model, only one value of ε_H can trigger electroweak breaking at the weak scale. But one cannot know by advance which branch will be the good one. This question will be studied in details in Chapter 3.1. Note that this freedom does not appear in the usual, CMSSM-like configurations, where B_μ is automatically fixed at the electroweak breaking scale.

It is clear that the DHMM at GUT scale does not fulfill the necessary conditions for electroweak breaking (1.19) and (1.20). However, one has to take into account the radiative corrections, through the renormalization group equations, to make the link with the electroweak scale. We thus implemented the DHMM condition in `Suspect 2` [104], `SoftSUSY` [105] and `SPheno 3` [106]. We found a simple way to bypass deep modifications of the typical algorithm of computation, by setting the GUT scale condition

$$m_{H_{u,d}}^2 \equiv \varepsilon_H B_\mu - |\mu|^2 \,, \tag{3.74}$$

at each iterations in the code. These spectrum calculators were used to carry out quantitative analysis in Chapters 4 and 5, and 6.

3.3.2 Higgses as gauge bosons

Let us now explain in detail why a DHMM appear in the gauge-Higgs unification framework. As we already mentioned, the 5D gauge multiplet decomposes, in terms of 4d superfields, into a 4d gauge superfield $V = -A_\mu \sigma^\mu \theta\bar{\theta} + \dots$ ($\mu = 0, \dots, 3$) and a chiral adjoint $\Phi = \Sigma + iA_5 + \dots$ (where we have only written the leading terms in the θ-expansion, and V is in Wess-Zumino gauge as usual). By construction, Φ contains the MSSM Higgs fields, $\Phi \supset H_1 \oplus H_2$. We can now choose a Kähler-Weyl frame such that the superpotential is independent of Φ when setting the MSSM matter fields to zero. By 5D gauge invariance, the Kähler potential can then only depend on the combination $\Phi^\dagger + \Phi$ on the quadratic level. The orthogonal combination $\Phi^\dagger - \Phi \sim A_5$, being a 5D gauge field, is protected from getting a mass term.

This can be seen explicitly as follows : suppose for the moment that the gauge symmetry were just $U(1)$. The action is invariant under 5D gauge transformations

$$V \;\to\; V + \Lambda + \bar{\Lambda}, \qquad \Phi \;\to\; \Phi + \partial_5 \Lambda. \tag{3.75}$$

Here Λ is an x^5-dependent chiral superfield. The inhomogeneous transformation behaviour of Φ shows that Φ cannot appear in the superpotential if W is to be 5D gauge-invariant, when setting the MSSM matter fields to zero. That is to say, it is always possible to shift harmonic terms from the Kähler potential into the superpotential, and any terms from W into K, but a particularly natural formulation is one where W and K are separately 5D gauge invariant. Consequently Φ cannot appear in W (except in combination with other charged fields such as matter fields, which only give rise to Yukawa terms irrelevant to the Higgs potential).

The crucial observation is now [99] that in this manifestly 5D gauge-invariant formulation, the Φ-dependent part of K must be a function of the unique gauge-invariant combination

$$\Phi + \overline{\Phi} - \partial_5 V. \tag{3.76}$$

This combination reduces to $\Phi + \overline{\Phi}$ on the zero-mode level. In other words, if there is no linear term in Φ, the low-energy effective Kähler potential for the zero modes has the structure

$$K = \mathcal{K}\left(Z^i, \overline{Z}^{\bar{\jmath}}\right) + \tilde{\mathcal{Y}}\left(Z^i, \overline{Z}^{\bar{\jmath}}\right)\left(\Phi + \overline{\Phi}\right)^2 + \dots \tag{3.77}$$

Here the Z^i denote collectively the compactification moduli and general hidden sector fields. K cannot depend on the orthogonal combination $A_5 = \operatorname{Im}\Phi = (\Phi - \overline{\Phi})/2$ essentially because the transformation law for $\operatorname{Im}\Phi$ involves $\operatorname{Im}\Lambda$, whereas the transformation law for V only involves $\operatorname{Re}\Lambda$, and therefore the gauge variation of $\operatorname{Im}\Phi$ cannot be canceled.

The similar structure is encountered in realistic models. The gauge symmetry should of course contain the Standard Model gauge group, and Φ should contain the MSSM Higgs superfields, so the abelian example is too simple. In a non-abelian model, the 5D gauge transformations read

$$e^V \;\to\; e^{\Lambda^\dagger}\, e^V\, e^{\Lambda}, \qquad \Phi \;\to\; e^{-\Lambda}(\partial_5 + \Phi)e^{\Lambda}. \tag{3.78}$$

Gauge-invariant operators involving Φ can be constructed from the covariant derivative $\nabla_5 = \partial_5 + \Phi$ [107]. In particular the operator

$$-e^{-V}\nabla_5 e^V = \Phi + \Phi^\dagger - \partial_5 V + (\text{commutators}) \tag{3.79}$$

(where ∇_5 acts on e^V as $\nabla_5 e^V = \partial_5 e^V - \Phi^\dagger e^V - e^V\Phi$) is the appropriate non-abelian generalization of (3.76). Note that it is not gauge invariant by itself but transforms analogously to a field strength superfield:

$$e^{-V}\nabla_5 e^V \;\to\; e^{-\Lambda}\, e^{-V}\nabla_5 e^V\, e^{\Lambda}. \tag{3.80}$$

The lowest-order gauge invariant operator one can construct is in fact [107]

$$\mathrm{tr}\left(e^{-V}\nabla_5 e^V\right)^2 = \mathrm{tr}\left(\Phi + \Phi^\dagger\right)^2 + (\text{terms involving } V) \tag{3.81}$$

since $\mathrm{tr}\,(e^{-V}\nabla_5 e^V)$ vanishes identically, as can be seen from Eq. (3.79).

As in the abelian case, any V-independent terms cannot depend on the orthogonal combination $\Phi - \Phi^\dagger$ since it transforms as

$$\Phi - \Phi^\dagger \;\to\; e^{-\Lambda}\Phi e^{\Lambda} - \text{h.c.} + \partial_5\left(\Lambda - \Lambda^\dagger\right), \tag{3.82}$$

while the gauge field transforms as

$$V \;\to\; V + \Lambda + \Lambda^\dagger + (\text{terms involving } V). \tag{3.83}$$

Therefore there is no function of V whose gauge variation can cancel the inhomogeneous piece in Eq. (3.82).

We conclude that again W is Φ-independent, and that K has the structure

$$K = \mathcal{K}\left(Z^i, \overline{Z}^{\bar{\jmath}}\right) + \tilde{\mathcal{Y}}\left(Z^i, \overline{Z}^{\bar{\jmath}}\right)\mathrm{tr}\left(\Phi + \Phi^\dagger\right)^2 + \ldots \tag{3.84}$$

The resulting quadratic Lagrangian for the zero modes of Φ can then be written as

$$\mathcal{L}_{\text{quad}} = \int d^4\theta\, \overline{\varphi}\varphi\, \mathcal{Y}\left(Z^i, \overline{Z}^{\bar{\jmath}}\right)(\overline{H}_1 + H_2)(H_1 + \overline{H_2}) \;, \tag{3.85}$$

where $\varphi = 1 + F^\varphi\theta^2$ is the conformal compensator of 4d supergravity. A non-vanishing F^φ or non-vanishing F^i will give rise to an effective Higgs mass matrix satisfying the relations

Eq. (3.66), with mass parameters

$$
\begin{aligned}
m_{H_1}^2 = m_{H_2}^2 &= -F^i \overline{F}^{\bar{\jmath}} \frac{\partial^2}{\partial Z^i \partial \overline{Z}^{\bar{\jmath}}} \log \mathcal{Y}, \\
\pm\mu &= \overline{F}^{\bar{\varphi}} + \overline{F}^{\bar{\imath}} \frac{\partial}{\partial \overline{Z}^{\bar{\imath}}} \log \mathcal{Y}, \\
\pm B_\mu &= \left| F^\varphi + F^i \frac{\partial}{\partial Z^i} \log \mathcal{Y} \right|^2 - F^i \overline{F}^{\bar{\jmath}} \frac{\partial^2}{\partial Z^i \partial Z^{\bar{\jmath}}} \log \mathcal{Y}.
\end{aligned}
\tag{3.86}
$$

The relations Eq. (3.66) are a direct consequence of 5D gauge symmetry, which is however not a symmetry of the 4d effective theory (but instead mixes the KK modes). Eq. (3.66) is therefore valid at the compactification scale, but it will be modified by radiative corrections below this scale. This will be necessary in order for the conditions Eq. (1.19) (1.20). to be satisfied as strict inequalities, after renormalization group running to the electroweak scale.

By similar arguments as above, the relations (3.66) also apply in a large class of heterotic string orbifold models [108–111] with gauge-Higgs unification, if their moduli space admits a corresponding 5D orbifold GUT limit [99]. For more recent realizations see [112, 113], and [78] for a review.

3.3.3 Higgses as pseudo-Goldstone bosons

A degenerate Higgs mass matrix also arises in the holographic GUT framework. The basic idea is to identify the Higgses as the pseudo Goldstone bosons of a spontaneously broken approximate global symmetry. This idea was proposed without supersymmetry in [27, 29]. In fact, while the Goldstone bosons are protected from getting a mass at any loop order by a non linear symmetry, pseudo Goldstone bosons can get a mass from radiative effects. If the Goldstone bosons are embedded in a supermultiplet, the whole supermultiplet is then protected from getting a mass. Once supersymmetry is broken , the partners of the Goldstone bosons can get a mass of order of the SUSY breaking scale.

In the HGU framework, regarding SU(6) as a spontaneously broken global symmetry of the 4D theory, the Higgs fields are massless in the absence of SUSY breaking because their imaginary parts are Goldstone bosons associated with the breaking to SU(4) $\times$ SU(2) $\times$ U(1), and their real parts are then protected by SUSY. The fact that the imaginary parts contain the Goldstone bosons can be checked explicitely. SU(6) is also broken explicitly by boundary conditions on the Planck brane (or on the level of the 4d theory by gauging only its SU(5) $\times$ U(1) subgroup), and therefore the Higgs fields are merely pseudo-Goldstone bosons. However, this explicit breaking gives tree-level masses to only 12 out of the 16 Goldstone modes. In other words, if SU(5) $\times$ U(1) $\subset$ SU(6) is gauged, only 12 of the Goldstone bosons will be eaten by the Higgs mechanism, corresponding to the 12 broken generators in SU(5) $\times$ U(1) $\rightarrow$ SU(3) $\times$ SU(2) $\times$ U(1) $\times$ U(1). The remaining four Goldstone

modes and their complex partners form two massless weak doublets which are identified with the MSSM Higgs fields. (For some earlier work along these lines, see [27, 114].)

Provided that the SUSY breaking mechanism respects this symmetry breaking pattern, it will lead to Eq. (3.66) because once more the fields from the combination $\Phi^\dagger + \Phi$ can pick up a tree-level mass term, while the (pseudo-) Goldstone bosons in $\Phi^\dagger - \Phi$ remain massless. Since the SU(6) symmetry is explicitly broken, radiative corrections can again lift the relations of Eq. (3.66) below the SUSY breaking scale, as required for phenomenology.

Résumé de la section

Dans cette Section, nous avons introduit de façon détaillée les deux modèles de Théorie de Grande Unification supersymmétrique sur un orbifold $S^1/(\mathbf{Z} \times \mathbf{Z}')$ sur lesquels nous nous sommes basés. Nous avons, chaque fois, présenté le modèle original , puis les modifications et développements que nous lui avons apporté. Le premier de ces modèles a la particularité de faire apparaître les champs de Higgs du MSSM dans le supermultiplet vecteur $\mathcal{N} = 2$, c'est donc une unification jauge-Higgs. Le second de ces modèles fait apparaître les champs de Higgs du MSSM comme des bosons de Goldstone d'une symmétrie globale à la fois brisée spontanément et partiellement jaugée. Ce modèle admet une description holographique, dans lequel les Higgs sont des objets composites, issus de la dynamique d'une théorie de jauge fortement couplée. Un point crucial commun à ces deux modèles est la condition de matrice de Higgs dégénérée.

Chapter 4

Phenomenology of gauge-Higgs unification

After having discussed the two frameworks of orbifold SUSY GUTs, we can now present the different phenomenology works that have been carried out for this thesis. In this chapter, we present our study of the low energy implications of the gauge-Higgs unification framework 3.1. This chapter is largely based on our publication [99].

A crucial step is to evolve the model from GUT scale to the electroweak scale, using the MSSM renormalization group equations (RGE). We will first present a qualitative study of the RGE running expected features in Section 4.1. Then, the numerical setup permitting to carry out a quantitative, precise study will be presented in Section 4.2, and the results for different GUT scale boundary conditions will then be discussed in Section 4.3, 4.4, 4.5. The study and the results are summarized in Section 4.6.

4.1 Qualitative renormalization group study

Before we present the numerical results, let us briefly discuss what general features we expect. Needless to say, the complete system of two-loop renormalization group equations (RGEs), which will be solved numerically in the following sections, is far too complicated to permit an analytical treatment. Some aspects can nevertheless be qualitatively understood by inspection of the dominant contributions to the one-loop RGEs.

The scale of electroweak symmetry breaking (EWSB) is defined as usual as the geometric mean of the stop masses, $M_{\rm EWSB} = \sqrt{m_{\tilde{t}_1} m_{\tilde{t}_2}}$. At this scale the conditions (1.19,1.20) have to hold. Once EWSB occurs, one finds the well-known relations between μ, B_μ, M_Z,

the Higgs soft masses $m^2_{H_i}$ and the ratio $\tan\beta$ of Higgs expectation values:

$$\begin{aligned}\mu^2 &= \frac{1}{2}\left[\tan 2\beta\,(m^2_{H_2}\tan\beta - m^2_{H_1}\cot\beta) - M_Z^2\right],\\ B_\mu &= \frac{1}{2}\sin 2\beta\left[m^2_{H_1} + m^2_{H_2} + 2\mu^2\right].\end{aligned} \tag{4.1}$$

We also recall the definitions $m_1^2 = m^2_{H_d} + |\mu|^2$, $m_2^2 = m^2_{H_u} + |\mu|^2$, $m_3^2 = B_\mu$.

We focus on the region of moderately large $\tan\beta$, roughly $\tan\beta \gtrsim 5$, to ensure that the tree-level bound on the lightest Higgs mass, $m_h \leq M_Z$, is approximately saturated. The Higgs mass can then be lifted above the direct search limit by radiative corrections, mainly due to stop loops.

The latter involves a significant fine-tuning (the notorious MSSM "little hierarchy problem"), because the soft mass scale must be large compared to M_Z instead of being of the same order of magnitude, which would be the natural situation. For sizeable $\tan\beta$ one has

$$\frac{M_Z^2}{2} \approx -m_2^2, \tag{4.2}$$

so m_2^2 must be negative and small compared to typical soft masses. We will not discuss this fine-tuning any further (see however [115–118]), but accept it and focus on the implications for models with GHU boundary conditions. One immediate consequence is that $m_2^2 > 0$ at the GUT scale, because the soft mass $m^2_{H_2}$ and hence also m_2^2 runs down towards lower energies (the running of μ is insignificant). While this also fixes the GUT-scale sign of m_1^2 to be positive, either sign for B_μ is possible (cf. Eq. 3.86). In other words, we can have $\epsilon_H = +1$ or $\epsilon_H = -1$ in the GHU relations

$$m^2_{H_1} = m^2_{H_2} = \epsilon_H B_\mu - |\mu|^2\,. \tag{4.3}$$

However, as we will now argue, ϵ_H is always determined by the sign of μ: Out of the four sign choices $\mu > 0$ or $\mu < 0$ and $\epsilon_H = \pm 1$, only two can generically lead to realistic spectra. To establish this observe first that m_1^2 will typically not evolve by more than a factor of $2-3$, and therefore remains of the order of magnitude of the typical soft mass scale during RG running. Furthermore, we just stated that m_2^2 at M_{EWSB} should be small compared to the typical soft mass scale, and that $\tan\beta$ should at least be moderately large. From all this it follows that B_μ at the EWSB scale should be small compared to the typical soft mass-squared scale as well, as can be read off from

$$\tan\beta + \cot\beta = \frac{m_1^2 + m_2^2}{2B_\mu} \tag{4.4}$$

(which is equivalent to the second line of Eqs. (4.1)). We will now show that requiring small EWSB-scale B_μ generically fixes ϵ_H in terms of $\text{sign}(\mu)$.

The RG evolution of B_μ is primarily governed by the terms involving the top trilinear coupling and the weak gaugino mass:

$$16\pi^2\frac{d}{dt}B_\mu = \mu(6A_t|y_t|^2 + 6g_2^2M_2) + \ldots \tag{4.5}$$

We can choose positive gaugino masses without loss of generality. Let us now discuss the relevance of the two dominant terms on the r.h. side of Eq. (4.5):

The gluino contribution to the A_t-RGE

$$16\pi^2 \frac{d}{dt} A_t = 12\,|y_t|^2\, A_t + \frac{32}{3} g_3^2\, M_3 + \dots \tag{4.6}$$

forces A_t to run negative towards low scales. This is fairly universal, i.e. more or less independent of the values of the other parameters. The value of A_t at any given scale is thus to a good approximation dictated only by its GUT-scale boundary value and $M_{1/2}$. The running of gaugino masses is also approximately universal: at one-loop, they simply evolve according to the respective gauge coupling beta functions. In the RG evolution of B_μ, A_t will therefore always dominate at low energies, when it has become large and negative and when also y_t has grown large. Correspondingly, the M_2 term on the r.h. side of Eq. (4.5) can dominate only at energies near $M_{\rm GUT}$, before it is overwhelmed by A_t.

For negative μ, B_μ initially increases from its GUT-scale value and then runs down; for positive μ, it evolves in the opposite way. The relative importance of the A_t and the M_2 contributions is set by their GUT-scale initial values: the larger A_t at $M_{\rm GUT}$, the longer it will take to run negative and to finally dominate the B_μ RG evolution. For small or negative GUT-scale A_t, the B_μ running at low energies is more important than the initial, M_2-dominated phase near $M_{\rm GUT}$.

The direction and slope of the running of B_μ are set by the sign and magnitude of μ, which itself does not run significantly as mentioned. We observed before that B_μ should be small at the EWSB scale — for the sake of the argument, let us try to construct a situation where it is exactly zero. It should in particular change significantly with respect to its initial GUT-scale value, so $|\mu|$ should be sizeable. Furthermore, changing the sign of μ will lead to B_μ evolving in the opposite way (at least as far as the evolution is governed by the terms in Eq. (4.5)). If there is a solution with, e.g., $\epsilon_H = -1$ and $\mathrm{sign}(\mu) = -1$, we therefore expect a nearby mirror solution for the opposite sign choice. On the other hand, changing only one of the signs will generically not lead to a solution due to the approximately universal behaviour of A_t and M_2. We have sketched this behaviour in Fig. 4.1 for large GUT-scale A_t, and in Fig. 4.2 for small or negative GUT-scale A_t.

Thus, while one might naively have expected four branches of solutions of the RGEs to give realistic spectra (corresponding to the two choices of each $\mathrm{sign}(\mu)$ and of ϵ_H), by the above discussion there should in fact appear only two. Furthermore, we expect sizeable $|\mu|$ in all cases.

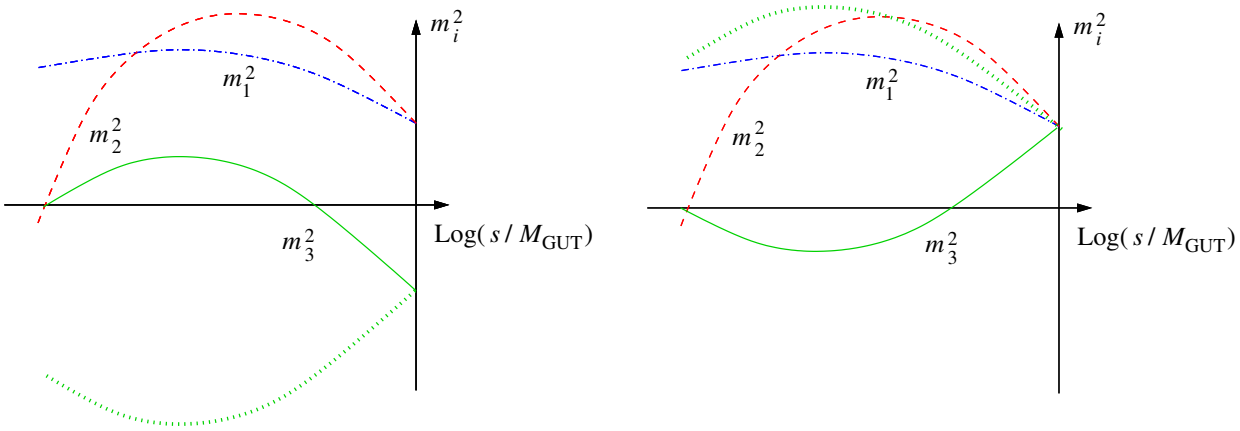

Figure 4.1: Qualitative RG evolution of m_1^2 (blue dot-dashed curve), m_2^2 (red dashed curve), and m_3^2 (green solid curve) as a function of the scale s, between $s = M_{\rm EWSB}$ and $s = M_{\rm GUT}$. A_t at the GUT scale is sizeable and positive. The green dotted curve is m_3^2 for the wrong sign(μ), which does not lead to realistic EWSB. Left panel: $\epsilon_H = -1$ requires sign(μ) $= -1$. Right panel: $\epsilon_H = +1$ requires sign(μ) $= +1$.

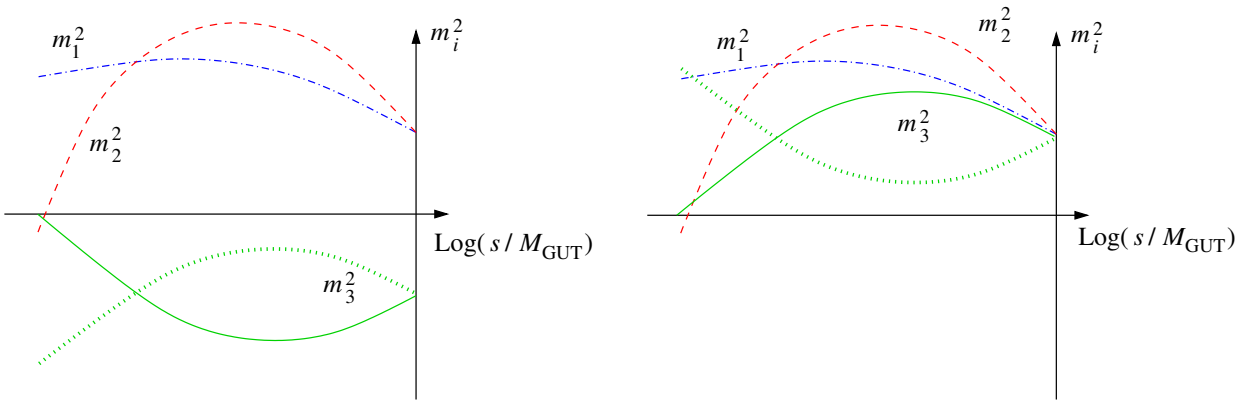

Figure 4.2: Same as Fig. 4.1 for small or negative GUT-scale A_t. Left panel: $\epsilon_H = -1$ requires sign(μ) $= +1$. Right panel: $\epsilon_H = +1$ requires sign(μ) $= -1$.

4.2 Setup

For the numerical analysis, we make use of the public state-of-the-art SUSY spectrum code `Suspect 2.41` [104], appropriately modified to be applied to our SUSY GHU model. The usual procedure in `Suspect` and in other SUSY spectrum codes is to use $\tan\beta$ and M_Z as inputs and to compute μ and B_μ from the EWSB condition Eqs. (4.1). In our model, however, the Higgs soft masses and μ and B_μ are not independent, since they are related by the GHU conditions (4.3) at the GUT scale.

The free parameters in the gauge–Higgs sector of the model are actually $F^T/2R$, F^φ and c', from which the GUT-scale values for $M_{1/2}$, μ, B_μ and $m^2_{H_{1,2}}$ are determined according to Eqs. (3.15), (3.16) and (3.18). Together with the GUT-scale values for the sfermion mass parameters and trilinear couplings, they furnish a set of GUT-scale boundary conditions

for the MSSM renormalization group equations.

It is in principle possible to change the usual procedure of spectrum computation such that μ and B_μ become high-scale inputs, while $\tan\beta$ as well as M_Z are output determined by Eq. (4.1). We have implemented this scheme in `Suspect 2.41`; the requirement to find the correct experimental value of M_Z, however, makes parameter scans very inefficient.

For the present analysis we have therefore chosen a different approach: We work with the conventional SUGRA scheme of `Suspect 2.41`, which takes $\tan\beta(M_Z)$ together with the GUT-scale values of all soft-breaking parameters except B_μ as input. We only modify this scheme by not specifying fixed GUT-scale values for the Higgs soft masses $m^2_{H_1}$ and $m^2_{H_2}$, but instead determining them from the GHU boundary conditions Eq. (4.3).

Our input parameters are thus $M_{1/2}(M_{\rm GUT})$ and $\tan\beta(M_Z)$, the two sign coefficients $\mathrm{sign}(\mu)$ and ϵ_H, plus the sfermion mass parameters and A-terms at $M_{\rm GUT}$. The values of μ, B_μ, $m^2_{H_1}$, $m^2_{H_2}$ are computed iteratively applying Eqs. (4.1) at the EWSB scale and Eq. (4.3) and the GUT scale. When a stable solution is found, the model parameters $F^T/2R$, F^φ and c' are inferred from $M_{1/2}$, μ and B_μ at $M_{\rm GUT}$ by inverting Eqs. (3.15), (3.16) and (3.18).

A complication arises, however, from the sfermion sector. As discussed in Section 3.1.2, we assume no-scale boundary conditions, i.e. a common scalar mass $m_0 \equiv 0$ and a common trilinear coupling $A_0 \equiv 0$, for squarks and sleptons of the first two generations. The soft terms of the third generation, on the other hand, can be non-zero. To be more precise, they will depend on $F^T/2R$ and c' (and possibly also on other model parameters) according to their kinetic functions. This requires an extra level of iteration in the spectrum computation.

It turns out to be convenient to let this iteration act on c'. We thus start the procedure described above with an initial guess of c', which is kept constant until a first convergence of the spectrum is reached. This has the virtue that the GUT-scale sfermion soft masses are unambiguously fixed in terms of c', $M_{1/2}$, and other input parameters (as will become clear once we describe how we are modelling the matter sector) so the EWSB scale does not change too much in each iteration step, which could lead to numerical instabilities. When convergence is reached, an updated value of c' as computed from $M_{1/2}$, μ and B_μ is taken as the new input c', and the whole procedure is iterated until c' converges as well.

Let us finally list the Standard Model (SM) input values and experimental constraints. For the SM input values, we take $\alpha^{-1}(M_Z) = 127.934$, $\alpha_s(M_Z) = 0.1172$ and $m_b(m_b) = 4.25$ GeV in the $\overline{MS}$ scheme, and an onshell top mass of $m_t = 172.4$ GeV [20]. Moreover, $M_Z = 91.187$ and $m_\tau = 1.777$ GeV, and $G_F = 1.16639 \cdot 10^{-5}$ GeV^{-2}.

To take into account the limits from direct SUSY searches at LEP [119], we require $m_{\tilde\chi_1^\pm} > 103.5$ GeV and $m_{\tilde e,\tilde\mu} > 100$ GeV. The limit on $m_{\tilde\tau_1}$ is parametrized as a function of $m_{\tilde\chi_1}$ as given by [119]; in case of a stau LSP, we take $m_{\tilde\tau_1} > 94$ GeV. For the light

scalar Higgs, we apply the limits from LEP for the m_h^{max} scenario given in [120], taking into account a ~ 2 GeV theoretical error [121]. [1]

We also take into account additional constraints from B-physics. For the branching ratio of inclusive radiative B decay, we use the experimental result $\mathrm{BR}(b \to s\gamma) = (3.52 \pm 0.23 \pm 0.09) \times 10^{-4}$ from HFAG [122], together with the SM theoretical prediction of $\mathrm{BR}(b \to s\gamma)^{\mathrm{SM}} = (3.15 \pm 0.23) \times 10^{-4}$ of [123]. Combining experimental and theoretical errors in quadrature, we require $2.85 \leq \mathrm{BR}(b \to s\gamma) \times 10^4 \leq 4.19$ at 2σ. Another important constraint comes from the B_s decay into a pair of muons. Here we apply the 95% CL upper limit $\mathrm{BR}(B_s \to \mu^+\mu^-) < 5.8 \times 10^{-8}$ from CDF [124]. Regarding the anomalous magnetic moment of the muon, we do not impose any limits but simply note that $(g-2)_\mu$ favours $\mu > 0$.

Last but not least, if the lightest neutralino is the LSP, we compare its relic density to the results from the 5-year WMAP data on the dark matter relic density, $\Omega h^2 = 0.1099 \pm 0.0062$ [125], although we do not impose this as a strict constraint [2]. The values of $\mathrm{BR}(b \to s\gamma)$, $\mathrm{BR}(B_s \to \mu^+\mu^-)$ and Ωh^2 are computed using the `micrOMEGAs2.2` package [126].

4.3 Results for simplified boundary conditions

Here we perform a first exploration of the parameter space using simplified boundary conditions in the matter sector according to [90]. More precisely, we assume that not only the first two generations but also the third-generation leptons and r.h. bottom are brane-localized. The top and l.h. bottom have a flat profile in the fifth dimension. The relevant kinetic functions then are[3]

$$Y_{Q_3} \approx Y_{U_3} \approx \frac{\pi}{2}(T + \overline{T}), \tag{4.7}$$

which leads to

$$m_{Q_3}^2 \approx m_{U_3}^2 \approx \left|\frac{F^T}{2R}\right|^2 \tag{4.8}$$

and

$$A_t \approx \frac{F^T}{2R}\frac{1}{1+c'}. \tag{4.9}$$

The setup for the first parameter scan is therefore as follows:

- We vary $M_{1/2}$ from 100 and 1000 GeV and $\tan\beta$ from 2 and 20. (For higher values of $\tan\beta$, the bottom Yukawa coupling would be no longer negligible.)

[1] Moreover, the limits from direct squark and gluino searches at the Tevatron for $m_{\tilde{q}} \simeq m_{\tilde{g}}$ apply, in particular $m_{\tilde{g}} > 392$ GeV, but these are automatically fulfilled here.

[2] These constraints have slightly evolved since the publication of the paper in 2009, but this hardly influences the results presented here.

[3] In this approximation $y_t = g_4$ is the only non-vanishing Yukawa coupling. We will however not enforce this in the numerical analysis.

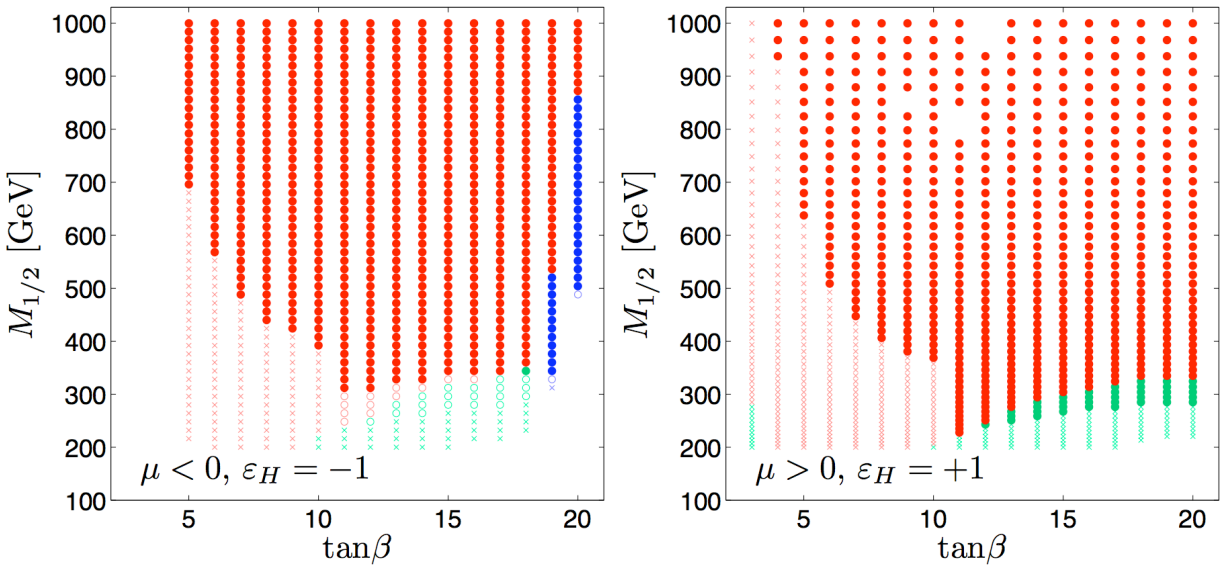

Figure 4.3: Parameter points giving correct EWSB from a scan over $M_{1/2}$ and $\tan\beta$ with simplified boundary conditions. The red, green and blue points have a neutralino, stau and selectron LSP, respectively. Small crosses denote points excluded by LEP, while open circles denote points excluded by B-physics constraints. The big full dots pass these constraints.

- We set $m_{U_3}^2 = m_{Q_3}^2 = M_{1/2}^2(1+c')^2$ and $A_t = M_{1/2}$; this requires the additional iteration on c' as detailed in Section 4.2. All other sfermion soft terms are assumed to be zero at the GUT scale.
- We allow for all four sign combinations of sign$(\mu) = \pm 1$ and $\epsilon_H = \pm 1$.
- μ and B_μ are determined from Eq. (4.1) at the EWSB scale, while $m_{H_1}^2$ and $m_{H_2}^2$ are determined from Eq. (4.3) at $M_{\rm GUT}$.
- For each point that gives correct EWSB, we check the mass limits from LEP as well as the constraints from BR$(b \to s\gamma)$ and BR$(B_s \to \mu^+\mu^-)$ given in Section 4.2

Figure 4.3 shows the result of this scan in the $\tan\beta$ versus $M_{1/2}$ plane. As expected, correct EWSB is obtained only for two of the four possible combinations of sign(μ) and ϵ_H. In particular, it turns out that the two signs need to be equal. This is a consequence of the relation $A_t = M_{1/2}$, in accord with the discussion in Section 4.1. Phenomenological bounds further constrain the parameter space. Points marked as small crosses in Fig. 4.3 are excluded by the mass bounds from LEP, while points shown as open circles are excluded by BR$(b \to s\gamma)$; the constraint from BR$(B_s \to \mu^+\mu^-)$ has no effect. The remaining big full points are phenomenologically viable. The different colours denote the nature of the LSP: red for a neutralino, blue for a selectron [4], and green for a stau LSP. As one can see, most of

[4]Selectrons and smuons are taken to be mass-degenerate. Here and in the following we only refer to selectrons for simplicity, implicitly meaning "selectrons and smuons".

the parameter space features a neutralino LSP, which is interesting in point of view of dark matter.[5] As anticipated in Section 4.1, $|\mu|$ turns out to be large throughout the parameter space. Numerically we find $|\mu| \sim (2.5-3.5)M_{1/2}$ for $\mu > 0$ and $|\mu| \sim (2.5-4)M_{1/2}$ for $\mu < 0$; in both cases the values at the high end are obtained for larger $\tan\beta$. The $\tilde{\chi}_1^0$ is hence almost a pure bino, and the $\tilde{\chi}_2^0$ and $\tilde{\chi}_1^\pm$ almost pure winos.

The projections onto the space of fundamental model parameters $F^T/2R$, F^φ and c' are shown in Fig. 4.4. We observe that for both, $\mu < 0$ and $\mu > 0$, there is a strong correlation between F^φ and $F^T/2R$, with roughly $F^\varphi \sim 3 \times F^T/2R$. This comes from setting $A_t = M_{1/2}$, which enforces $\epsilon_H = \text{sign}(\mu)$. It translates into a large value of F^φ, because $F^\varphi = \epsilon_H \mu + F^T/2R\,\frac{1+2c'}{1+c'}$ from Eq. (3.15). Nevertheless F^φ is small enough so that contributions from anomaly mediation, being $\mathcal{O}(F^\varphi/8\pi^2)$, can safely be neglected.

It is particularly interesting to note that we find no valid spectra for which $c' = 0$. This also holds when considering points excluded by LEP constraints. In this sense our analysis confirms the result of [90], who did not include the effects of a Chern–Simons term and consequently did not find any viable parameter regions, except for extremely unnatural values for the gaugino masses far above our scan limits. At the same time it is important that c', which is an $\mathcal{O}(1)$ parameter, never becomes large.

Implications for collider phenomenology can be deduced from Fig. 4.5, which shows the neutralino and slepton mass spectrum in the neutralino LSP region. We see that the second-lightest neutralino $\tilde{\chi}_2^0$ and the lighter chargino $\tilde{\chi}_1^\pm$, which are mainly winos ($m_{\tilde{\chi}_1^\pm} \simeq m_{\tilde{\chi}_2^0}$), are always heavier than $\tilde{e}_{R,L}$ and $\tilde{\tau}_1$ (with the exception of a few points at $\mu < 0$ which have $m_{\tilde{e}_R} > m_{\tilde{\chi}_2^0} > m_{\tilde{e}_L}$). Note the clear separation of the selectron masses with $m_{\tilde{e}_L} < m_{\tilde{e}_R}$ for $\mu < 0$, while for $\mu > 0$ we have $m_{\tilde{e}_L} \sim m_{\tilde{e}_R}$. The squark and gluino masses are not shown, but they are roughly $m_{\tilde{q}} \sim m_{\tilde{g}} \sim (2-3)M_{1/2}$. At the LHC, squarks and gluinos will hence be produced both as $\tilde{q}\tilde{q}$ or $\tilde{g}\tilde{g}$ pairs, and in $\tilde{q}\tilde{g}$ associated production. Their decays are $\tilde{g} \to q\tilde{q}_{R,L}$, $\tilde{q}_R \to q\tilde{\chi}_1^0$, $\tilde{q}_L \to q'\tilde{\chi}_1^\pm$ or $q\tilde{\chi}_2^0$, as in the mSUGRA scheme with large $|\mu|$ [127]. Moreover, the decays $\tilde{\chi}_2^0 \to e^\pm\tilde{e}_L^\mp \to e^+e^-\tilde{\chi}_1^0$ and $\tilde{\chi}_2^0 \to \tau^\pm\tilde{\tau}_1^\mp \to \tau^+\tau^-\tilde{\chi}_1^0$ are always open and together have about 50% branching ratio; the other 50% go into neutrinos. This leads to the gold-plated same-flavour opposite-sign (SFOS) dilepton signature at the LHC [128], which allows to reconstruct sparticle masses. Furthermore, the decay of the lighter chargino always leads to a charged lepton, $\tilde{\chi}_1^\pm \to (\ell^\pm\tilde{\nu}_\ell \text{ or } \nu_\ell\tilde{\ell}_L^\pm) \to \ell^\pm\nu_\ell\tilde{\chi}_1^0$, giving rise to a large number of events with jets plus 1 hard lepton plus missing transverse energy, E_T^{miss}. If combined with $\tilde{\chi}_2^0 \to ... \to l^+l^-\tilde{\chi}_1^0$, this leads to the rather clean trilepton signature (plus jets plus E_T^{miss}).

[5] Alternative dark matter candidates would be gravitino or axino. A rough estimate for a no-scale radion Kähler potential $K = -3\log(T+\overline{T})$ gives $m_{3/2} > |F^T/2R|$, while $m_{\tilde{\chi}_1^0} \simeq 0.4\,M_{1/2}$. In this case a gravitino LSP is only possible for $c' < -0.6$, which does not occur in our analysis. Moreover, we expect other contributions from hidden sectors to further increase $m_{3/2}$. An axino LSP is a valid option, but leads to a very different phenomenology, beyond the scope of this paper.

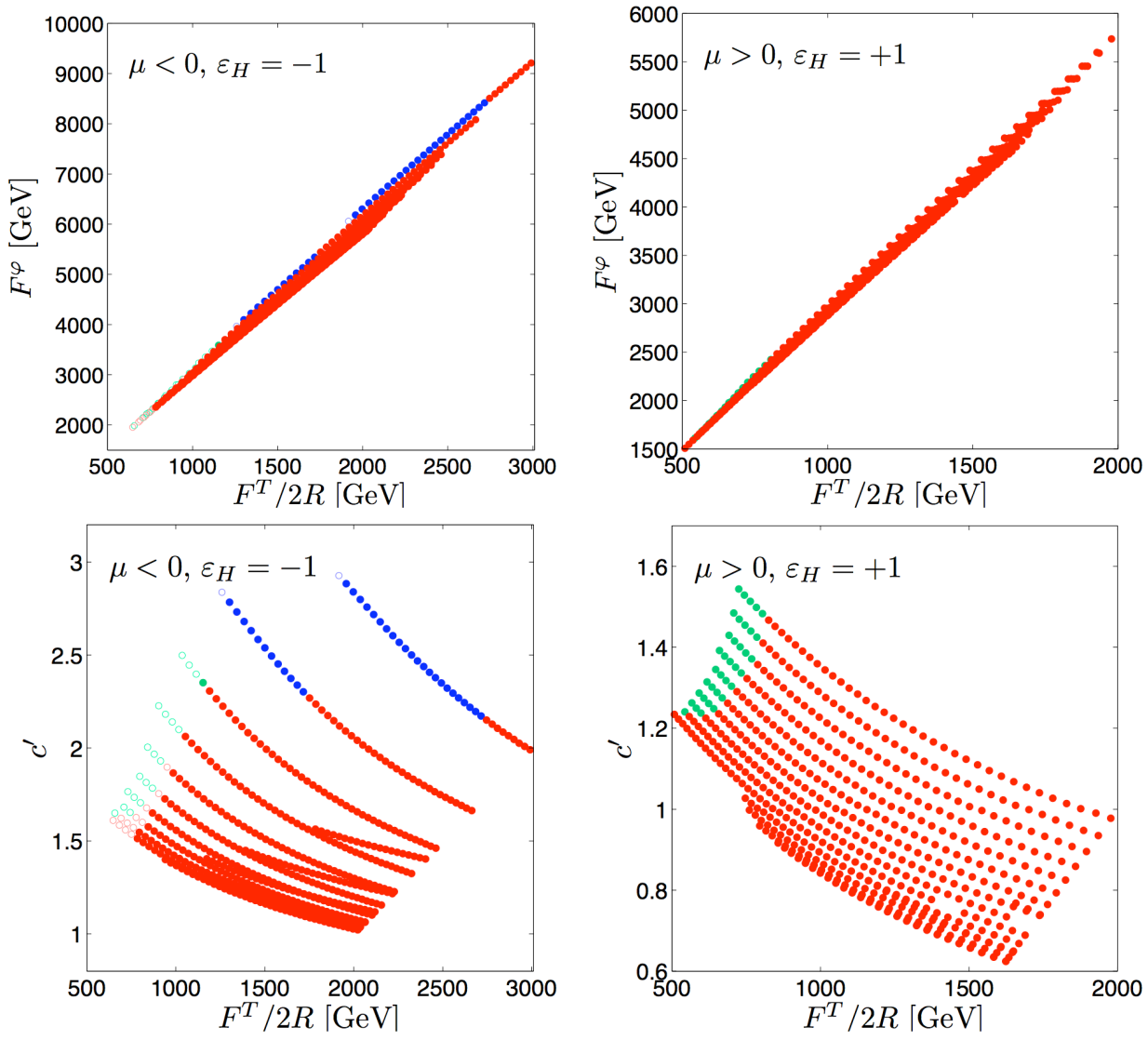

Figure 4.4: Scatter plot of points which give a valid spectrum solution in the $F^T/2R$ vs. F^{φ} plane (top row) and in the $F^T/2R$ vs. c' plane (bottom row). The red, green and blue points have a neutralino, stau and selectron LSP, respectively. Open circles denote points excluded by B-physics constraints. Points excluded by LEP are not shown.

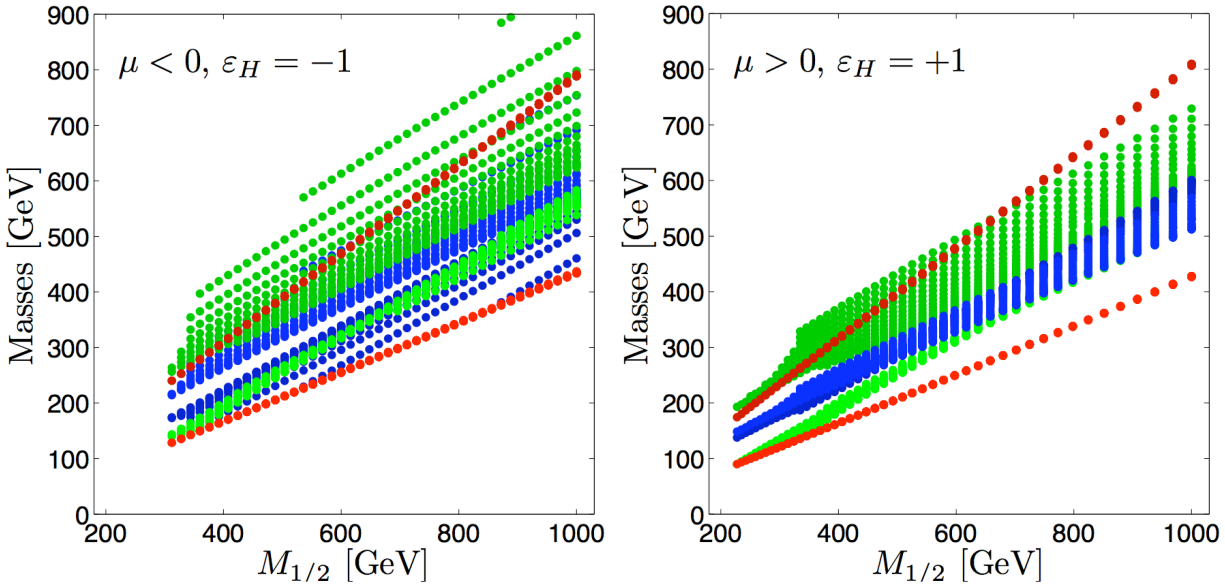

Figure 4.5: Mass spectrum in the neutralino LSP region, passing LEP and B-physics constraints, as a function of $M_{1/2}$. The colour convention is as follows: red: $\tilde{\chi}_1^0$, green: $\tilde{\tau}_1$, blue: $\tilde{e}_R$, dark blue: $\tilde{e}_L$, , dark green: $\tilde{\tau}_2$, dark red: $\tilde{\chi}_2^0$.

The scenario becomes even more predictive if we require that the neutralino LSP have a relic density in agreement with cosmological observations (assuming standard cosmology). Imposing the 3σ upper bound from WMAP5, $\Omega h^2 < 0.1285$, constrains $M_{1/2} \lesssim 390$ GeV with $\tan\beta \gtrsim 11$ for $\mu > 0$. For $\mu < 0$, it gives an upper limit on $M_{1/2}$ which increases with $\tan\beta$, from $M_{1/2} \lesssim 312$ GeV at $\tan\beta = 12$ to $M_{1/2} \lesssim 920$ GeV at $\tan\beta = 20$. The reason is that the LSP is almost a pure bino and has a small pair-annihilation cross section (s-channel Higgs exchange is not efficient in this scenario); in order to have a small enough relic density, the LSP needs to co-annihilate with another sparticle which is close in mass, typically the next-to-lightest SUSY particle (NLSP). This constrains the scenario to the region of small NLSP–LSP mass differences near the boundary to the slepton LSP region, which is realized for $\mu < 0$ up to large $M_{1/2}$ (depending on $\tan\beta$), but for $\mu > 0$ only at small $M_{1/2}$, cf. Figs. 4.3 and 4.5. Note, however, that this is a direct consequence of the simplified assumptions for the matter sector.

4.4 Realistic sfermion soft terms

In this section we explain how improved sfermion soft terms can be obtained if we model the matter sector as in the Burdman–Nomura model [84]. The third generation matter fields arise from the mixing of brane and bulk fields. Bulk fields with flat profile have Yukawa couplings determined by the 5D gauge coupling. Non-trivial bulk profiles cause a reduced overlap with the Higgs wave function and hence smaller Yukawa couplings. Thus,

using both bulk masses and mixing angles we can obtain realistic values for y_t, y_b and y_τ.

For the third generation quarks in particular, we introduce a 5D bulk hypermultiplet $\{\mathcal{U},\mathcal{U}^c\}$ in the **20** of SU(6) containing as 4d zero modes the right-handed top quark superfield and a weak doublet, and another bulk hypermultiplet $\{\mathcal{D},\mathcal{D}^c\}$ in the **15** containing the right-handed bottom quark and a second doublet. We give these fields bulk masses M_u and M_d. Furthermore, brane-localized superfields must be introduced to decouple unwanted massless fields. They couple to the doublet components of both the $\mathcal{U}$ and $\mathcal{D}$ fields, leaving a single massless quark doublet instead of the two we were starting with. This effect is parametrized by a mixing angle ϕ_Q.

Similarly, leptons descend from two 5D bulk hypermultiplets, $\{\mathcal{E},\mathcal{E}^c\}$ in the **15** and $\{\mathcal{N},\mathcal{N}^c\}$ in the **6**. In analogy with the quark sector this leads to three more model parameters, two bulk masses M_e and M_n and a mixing angle ϕ_L. For details of the model, in particular for the proper choice of boundary conditions, brane fields and bulk-brane couplings, we refer to [84].

The kinetic functions are computed by integrating the zero-mode profiles over the fifth dimension, replacing its radius R by $(T+\overline{T})/2$. This gives

$$Y_{U_3} = \frac{1}{2|M_u|}\left(1-e^{-\pi(T+\overline{T})|M_u|}\right), \tag{4.10}$$

$$Y_{Q_3} = \frac{1}{2|M_u|}\left(1-e^{-\pi(T+\overline{T})|M_u|}\right)\sin^2(\phi_Q) + \frac{1}{2|M_d|}\left(1-e^{-\pi(T+\overline{T})|M_d|}\right)\cos^2(\phi_Q), \tag{4.11}$$

$$Y_{D_3} = \frac{1}{2|M_d|}\left(1-e^{-\pi(T+\overline{T})|M_d|}\right). \tag{4.12}$$

The kinetic functions for the lepton sector are obtained in the same manner, and are given by the same expressions with the obvious parameter replacements. The soft masses and A-terms are then derived from Eqs. (3.21) – (3.23). We refrain from giving closed-form expressions for them, since these are rather cumbersome and not very illuminating.

The parameters $M_u, M_d, M_n, M_e, \phi_Q$ and ϕ_L cannot be chosen entirely freely, because they also have to account for the proper physical values of the Yukawa and gauge couplings. Since the Higgs wave function normalization is just given by $\langle Y_H\rangle = 1/g_4^2$ and in particular is independent of c', the relations given in [84] apply:[6]

$$y_t = \sin(\phi_Q)\,\frac{\pi R|M_u|}{\sinh \pi R|M_u|}\,g_4,\,, \quad y_b = \cos(\phi_Q)\,\frac{\pi R|M_d|}{\sinh \pi R|M_d|}\,g_4\,, \tag{4.13}$$

$$y_n = \sin(\phi_L)\,\frac{\pi R|M_n|}{\sinh \pi R|M_n|}\,g_4\,, \quad y_\tau = \cos(\phi_L)\,\frac{\pi R|M_e|}{\sinh \pi R|M_e|}\,g_4\,. \tag{4.14}$$

In the numerical analysis, in order to avoid additional model dependence from the unknown neutrino sector, we will assume that M_n is large enough not to contribute to the

[6]Note that our conventions for ϕ_Q and ϕ_L slightly differ from those of [84].

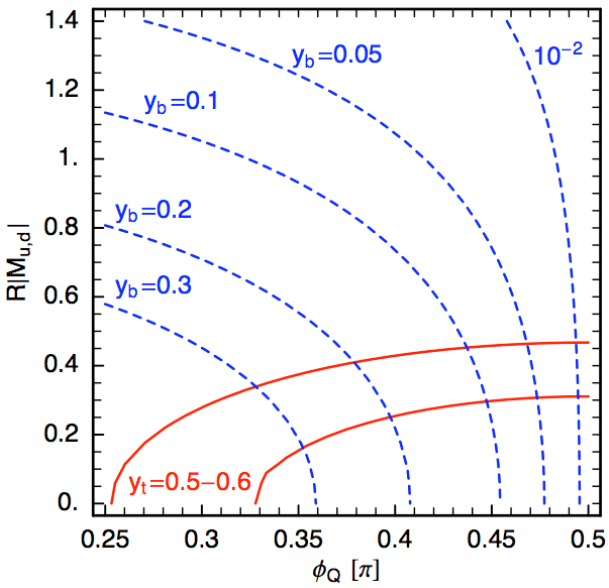

Figure 4.6: Values of $R|M_u|$ and $R|M_d|$ as function of the mixing angle ϕ_Q for various values of y_t (full red lines) and y_b (dashed blue lines). Note that y_t gives the lower and y_b the upper bound of the allowed range of ϕ_Q.

stau soft terms. We also introduce a Majorana mass term for the right-handed neutrinos on the $y = 0$ brane as in [84]. Since M_n is large, the neutrino wave function will be strongly localized towards the $y = \pi R$ brane, resulting in an exponentially suppressed Yukawa coupling and a doubly exponentially suppressed Majorana mass. The suppression factors will cancel out in the see-saw formula for the lighter neutrino mass eigenstate, leading to the same lighter neutrino mass as in the standard see-saw mechanism. The heavier neutrino mass, on the other hand, will be lowered by a factor $\sim e^{-4\pi R|M_n|}$ with respect to the GUT scale. This may be beneficial for leptogenesis [129].

It is instructive to see how Eq. (4.13) constrains the possible ranges of squark soft terms. In the remainder of this section we will therefore give some estimates of the bounds on the squark masses and trilinear couplings.

For $\tan\beta \sim 5-50$, the relevant GUT-scale Yukawa couplings take values $0.5 \lesssim y_t \lesssim 0.6$ and $0.02 \lesssim y_b \lesssim 0.3$. We also know that the gauge couplings unify at $g_4 \approx 0.7$.

To reproduce the top Yukawa coupling, we must have $\tan\phi_Q \gtrsim 1$ by Eq. (4.13). The small ratio y_b/y_t can then be generated either by choosing $\tan\phi_Q$ to be large, or choosing $|M_d| > |M_u|$, or by a combination of these. The relation between M_u, M_d, ϕ_Q and the Yukawa couplings is illustrated in Fig. 4.6. We note that for given y_t and y_b, the allowed range for the mixing angle ϕ_Q is

$$\phi_Q = \big[\arcsin(y_t/g_4),\ \arccos(y_b/g_4)\big]. \tag{4.15}$$

For estimating the size of the squark-mass parameters, let us consider two limiting cases:

- If the difference between y_t and y_b is mainly due to the different bulk masses, then $\tan\phi_Q \approx 1$. This corresponds to the far left region of Fig. 4.6. In that case $\sin\Phi_Q \approx 1/\sqrt{2}$ already accounts for the ratio $y_t/g_4 \approx 0.7$ in Eq. (4.13). The top Yukawa coupling should thus not receive much additional suppression from large bulk masses, hence we need $|M_u| \ll 1/R$. Expanding Eq. (4.10) and retaining only the leading term, we reproduce Y_{U_3} as in Eq. (4.7):

$$Y_{U_3} = \frac{\pi}{2}\left(T + \overline{T}\right), \qquad m_{U_3}^2 = \left|\frac{F^T}{2R}\right|^2 . \tag{4.16}$$

  On the other hand, $R|M_d|$ must be sizeable to obtain an appropriately suppressed y_b, cf. Fig. 4.6. With Eq. (4.12), $m_{D_3}^2$ turns out to be

$$m_{D_3}^2 = \left(\frac{\pi R|M_d|}{\sinh\left(\pi R|M_d|\right)}\right)^2 \left|\frac{F^T}{2R}\right|^2 \approx 4y_b^2 \left|\frac{F^T}{2R}\right|^2 . \tag{4.17}$$

  Finally, the quark doublet soft mass-squared $m_{Q_3}^2$ obtained from Eq. (4.11) is numerically

$$m_{Q_3}^2 \approx (0.7 - 0.8) \times \left|\frac{F^T}{2R}\right|^2 . \tag{4.18}$$

- If $\tan\phi_Q \gg 1$, i.e. $\sin\phi_Q \approx 1$ (which is the case in the far right region of Fig. 4.6), then the ratio $y_t/g_4 \approx 0.7$ is mainly due to a sizeable bulk mass M_u. Numerically, we need $R|M_u| \approx 0.3 - 0.5$. Therefore we should use the full expression for Y_{U_3}, rather than just the leading term:

$$m_{U_3}^2 = \left(\frac{\pi R|M_u|}{\sinh\left(\pi R|M_u|\right)}\right)^2 \left|\frac{F^T}{2R}\right|^2 \approx (0.5 - 0.8) \times \left|\frac{F^T}{2R}\right|^2 . \tag{4.19}$$

  Dropping the $\cos^2\phi_Q$ piece in Y_{Q_3} and setting $\sin\phi_Q = 1$, we obtain the same expression for Y_{Q_3} and eventually $m_{Q_3}^2$:

$$m_{Q_3}^2 = \left(\frac{\pi R|M_u|}{\sinh\left(\pi R|M_u|\right)}\right)^2 \left|\frac{F^T}{2R}\right|^2 \approx (0.5 - 0.8) \times \left|\frac{F^T}{2R}\right|^2 . \tag{4.20}$$

  As is evident from Fig. 4.6, if y_b is to remain finite, $\tan\phi_Q$ cannot become arbitrarily large. In any case, this limit requires very small y_b. The constraints on $|M_d|R$ are rather weak, although smaller $|M_d|R$ is somewhat favoured in order not to get additional y_b suppression. Hence

$$m_{D_3}^2 \lesssim \left|\frac{F^T}{2R}\right|^2 . \tag{4.21}$$

In the end we expect the squark masses-squared to lie somewhere in between these two extremes:

$$0.5 \times \left|\frac{F^T}{2R}\right|^2 \lesssim \left(m_{Q_3}^2,\, m_{U_3}^2\right) \lesssim \left|\frac{F^T}{2R}\right|^2 , \quad 0 \lesssim m_{D_3}^2 \lesssim \left|\frac{F^T}{2R}\right|^2 . \tag{4.22}$$

In order to obtain limits on A_t, we can make the same case distinction:

- for $\tan\phi_Q \approx 1$ and small $|M_u|$, we get

$$A_t \approx \frac{F^T}{2R}\left(-\frac{1+2c'}{1+c'}+1+\frac{2\pi R|M_d|\,\left(1+e^{-2\pi R|M_d|}\right)}{2\pi R|M_d|+1-e^{-2\pi R|M_d|}}\right); \tag{4.23}$$

- for $\sin\phi_Q \approx 1$, we obtain

$$A_t \approx \frac{F^T}{2R}\left(-\frac{1+2c'}{1+c'}+2\frac{2\pi R|M_u|}{\exp\left(2\pi R|M_u|\right)-1}\right). \tag{4.24}$$

Numerically,

$$A_t \approx \frac{F^T}{2R}\left(-\frac{1+2c'}{1+c'}+\alpha\right) \tag{4.25}$$

where $0.3 \lesssim \alpha \lesssim 2$, with $\alpha = 2$ corresponding to the first of the above two cases (with $R|M_d| \approx 1$), and $\alpha = 0.3$ to the second (with $R|M_u| = 0.5$). Evidently A_t can take a wide range of values, significantly departing from the simplified case of Section 4.3. In particular it can become large and negative, which will be of relevance in the next Section. A similar statement turns out to be true for A_b, for which we find an analogous estimate with $0 \lesssim \alpha \lesssim 1.4$.

4.5 Results for realistic sfermion soft terms

Let us finally investigate to what extent the phenomenological features found in Section 4.3 remain valid when invoking realistic stop, sbottom and stau parameters derived from the Burdman–Nomura model. The six new parameters M_u, M_d, M_n, M_e, ϕ_Q, ϕ_L are subject to four constraints, since they are related to the Yukawa couplings according to Eqs. (4.13) and (4.14). As detailed above we assume that M_n is large enough not to affect the stau soft terms. This corresponds to a negligible neutrino Yukawa coupling, and we do not need to worry about lepton flavour violation [130]. The precise value of M_n is irrelevant. (If M_n did contribute to the stau soft terms, its main effect would be to increase m_{L_3}, thus rendering the staus heavier, but leaving the overall picture intact.) We are therefore left with five parameters, $M_{u,d,e}$ and $\phi_{Q,L}$, and three constraints from y_t, y_b and y_τ.

We choose ϕ_Q and ϕ_L as the two independent new parameters and scan the parameter space as in Section 4.3, with the following modifications:

- We vary $M_{1/2}$ from 100 to 1000 GeV, ϕ_Q from $\pi/4$ to $\pi/2$, and ϕ_L from 0 to $\pi/2$. For $\tan\beta$, we consider three distinct values, $\tan\beta = 10$, 20, and 30, in order to avoid excessive computing times.

- For each point, the bulk masses $M_{u,d,e}$ are computed from the GUT-scale gauge and Yukawa couplings g_4, y_t, y_b, y_τ by numerically inverting Eqs. (4.13) and (4.14). They

then serve as input in the kinetic functions Eqs. (4.10)–(4.12), and the analogous expressions for the leptons, from which the sfermion soft masses and A-terms are obtained according to Eqs. (3.21)–(3.23). The soft terms of the first and second generation are again assumed to be zero at the GUT scale.

The result of this scan is shown in Figs. 4.7 and 4.8 for the two signs of μ. For better readability, we only show $M_{1/2}$ in steps of 200 GeV, although the scan had a much finer grid. Contrary to the case of simplified boundary conditions, now μ and ϵ_H need to be of opposite sign. The reason is that now A_t turns out to be negative at the GUT scale (cf. the discussion in Section 4.1).

It is interesting to see how the mixing angles ϕ_Q and ϕ_L influence the nature of the LSP. ϕ_L determines the size of the stau parameters. Since it is constrained by the tau Yukawa coupling it can only vary over a sizable range if $\tan\beta$ is large. The reason is that A_τ is generically large, leading to a charge-breaking minimum if m_{L_3,E_3} are too small. Thus for $\tan\beta \sim 10$, ϕ_L is close to $\pi/2$ and the staus are rather heavy compared to the selectrons. For larger $\tan\beta$ (i.e. larger y_τ), ϕ_L can be small and the $\tilde{\tau}_1$ can become the LSP, corresponding to the green points in Figs. 4.7 and 4.8. Note, however, that the stau LSP region is highly constrained by direct mass bounds and B-physics, and that a stable LSP is excluded by cosmology. ϕ_L also has some effect on the selectron masses through RG evolution, but this is much less pronounced.

The angle ϕ_Q, on the other hand, determines the size of the stop and sbottom parameters. Through RG evolution it also influences the slepton masses, in particular $m_{\tilde{e}_R}$: larger ϕ_Q leads to a larger m_{D_3}, which in turn decreases $m_{\tilde{e}_R}$. In Figs. 4.7 and 4.8 one can see clearly that for increasing ϕ_Q, the $\tilde{e}_R$ eventually becomes the LSP. This behaviour can be understood easily from the $\mathrm{U}(1)_\mathrm{Y}$ D-term contribution to the evolution of the scalar soft masses m_i^2 [35]. At one loop

$$\frac{d}{dt} m_i^2 \sim \frac{6}{5} \frac{g_1^2 Y_i}{16\pi^2} S \,, \tag{4.26}$$

where Y_i is the weak hypercharge and

$$S = \left(m_{H_2}^2 - m_{H_1}^2\right) + \mathrm{Tr}\left(m_Q^2 - 2m_U^2 + m_D^2 + m_R^2 - m_L^2\right) \tag{4.27}$$

with the trace running over generations. Since S is an RG invariant, it simply causes a shift of the low-scale masses by $\Delta m_i^2 \approx -(0.052)\, Y_i\, S_\mathrm{GUT}$ [131] with respect to the values they would have had for $S \equiv 0$. Here S_GUT is the value of S at M_GUT. For simplified boundary conditions, we had $S_\mathrm{GUT} = -m_{U_3}^2$. With $Y_{e_R} = 1$ and $Y_{e_L} = -1/2$, making S_GUT less negative obviously lowers $m_{\tilde{e}_R}$ and increases $m_{\tilde{e}_L}$ (note also that the effect for the left-chiral state is only half the size of that for the right-chiral one). Moreover, comparing $m_{\tilde{e}_R} \approx (0.39\, M_{1/2})^2 - 0.052\, S_\mathrm{GUT}$ to $m_{\tilde{\chi}_1^0} \approx 0.43\, M_{1/2}$, we understand why the $\tilde{e}_R$ eventually becomes the LSP.

The projections onto the underlying model parameters $F^T/2R$, F^φ and c' are shown in Fig. 4.9. Since here we need $\mathrm{sign}(\mu) = -\epsilon_H$ to obtain a valid spectrum, F^φ now turns out to be small and can even be zero. Contributions to the soft terms from anomaly mediation are therefore completely negligible. Moreover, we find a somewhat smaller range for the c' parameter, roughly $0.5 \lesssim c' \lesssim 1.2$, as compared to $0.5 \lesssim c' \lesssim 3$ for simplified boundary conditions. The important point, however, is that c' remains non-zero. We conclude that the Chern–Simons term is indeed essential to achieve correct EWSB.

Let us now turn to the implications for collider phenomenology. We again focus on the neutralino LSP region. The mass spectrum in this region, taking into account the constraints from LEP and from B-physics, is depicted in Fig. 4.10. As one can see, there is a definite mass ordering $m_{\tilde{\chi}_1^\pm} \simeq m_{\tilde{\chi}_2^0} > m_{\tilde{e}_L} > m_{\tilde{e}_R} > m_{\tilde{\chi}_1^0}$. The $\tilde{\tau}_2$ turns out to be heavier than the $\tilde{\chi}_2^0$, while the $\tilde{\tau}_1$ can be lighter than the $\tilde{\chi}_2^0$, and for small ϕ_L also lighter than the selectrons, cf. the above discussion of the mixing-angle dependence. This gives a picture that is qualitatively similar to the simplified case discussed in Section 4.3; the main difference lies in the masses and mass ratios of the sleptons. For the squarks, this effect of non-universality — on the one hand the splitting of the third generation from the first and second generations due to non-zero $m^2_{Q_3,U_3,D_3}$, on the other hand the splitting of left- and right-chiral states due to non-zero S — is much less pronounced, because the running of the squark mass parameters is mainly driven by M_3. The squark and gluino masses are hence again about $m_{\tilde{q}} \approx m_{\tilde{g}} \approx (1.7-2.5)M_{1/2}$. The masses of the higgsino-like neutralinos and chargino are given by $|\mu|$ and lie above $m_{\tilde{g}}$.

It is also remarkable that now the neutralino relic density can vary over a large range, because of the extra parameters ϕ_Q and ϕ_L. This is illustrated in Fig. 4.11 for the example of $M_{1/2} = 500$ GeV and two values of $\tan\beta$ for each sign of μ. For $\mu > 0$, we take $\tan\beta = 10$ and 30; for $\mu < 0$, we take $\tan\beta = 10$ and 20 since higher values are too tightly constrained. The figure compares the neutralino relic density Ωh^2, as a function of ϕ_Q and ϕ_L, with the WMAP5 observation at 3σ. In the orange regions Ωh^2 is too low, which would require other constituents of dark matter in addition to the neutralino. In the brown regions, on the other hand, Ωh^2 is too high (at least within standard cosmology; it could be viable if there was, e.g., additional entropy production after freeze-out). The minimal and maximal values found are $\Omega h^2 \simeq 6 \times 10^{-3}$ and 0.9, respectively. In the red band in between, however, $0.0913 \leq \Omega h^2 \leq 0.1285$ agrees within 3σ with the value measured by WMAP5. The reason is that here the mass difference between the LSP and NLSP (or co-NLSPs) is just right to make co-annihilation processes efficient enough, but not too efficient, to obtain $\Omega h^2 \simeq 0.1$. To be precise, in the red bands of Fig. 4.11 we typically have $\Delta m = m_{\tilde{e}_R} - m_{\tilde{\chi}_1^0} \simeq 7 - 10$ GeV. An exception is $\mu > 0$, $\tan\beta = 30$ and small ϕ_L, where the $\tilde{\tau}_1$ becomes light and also contributes to co-annihilations, such that $\Delta m \approx 20$ GeV is needed; this leads to the red band bending down towards lower ϕ_Q. Sample spectra of five representative points, indicated as points A–E in Fig. 4.11, are given in Tables 4.1 and 4.2.

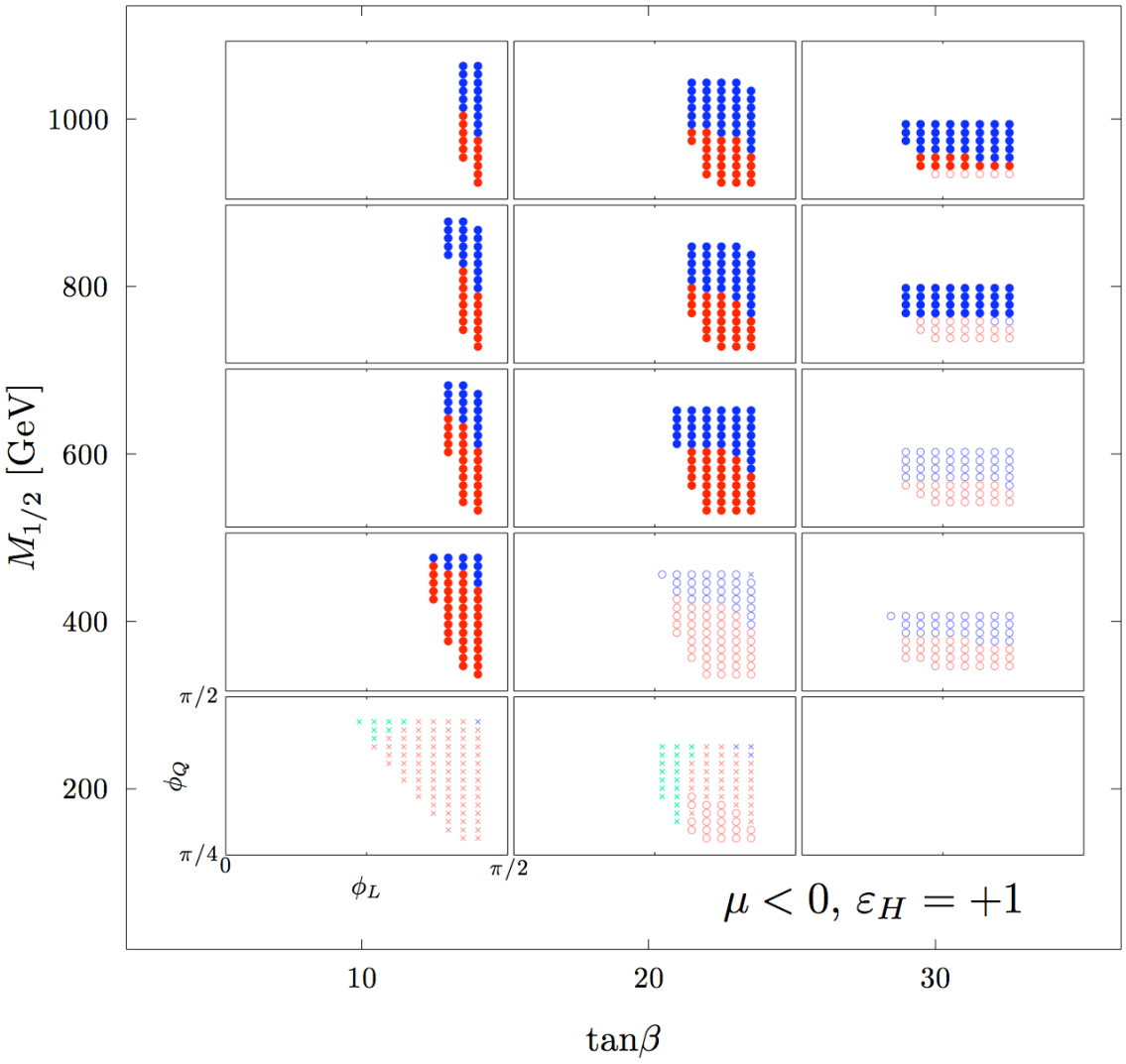

Figure 4.7: Points which lead to correct EWSB from a scan over $M_{1/2}$, $\tan\beta$, ϕ_Q and ϕ_L, for $\mu < 0$, $\epsilon_H = +1$ and sfermion soft terms determined according to the Burdman–Nomura model. Small crosses denote points excluded by LEP, while open circles denote points excluded by B-physics constraints. Points passing these constraints are shown as big full dots. The colours denote the nature of the LSP: red, green and blue points have a neutralino, stau and selectron LSP, respectively.

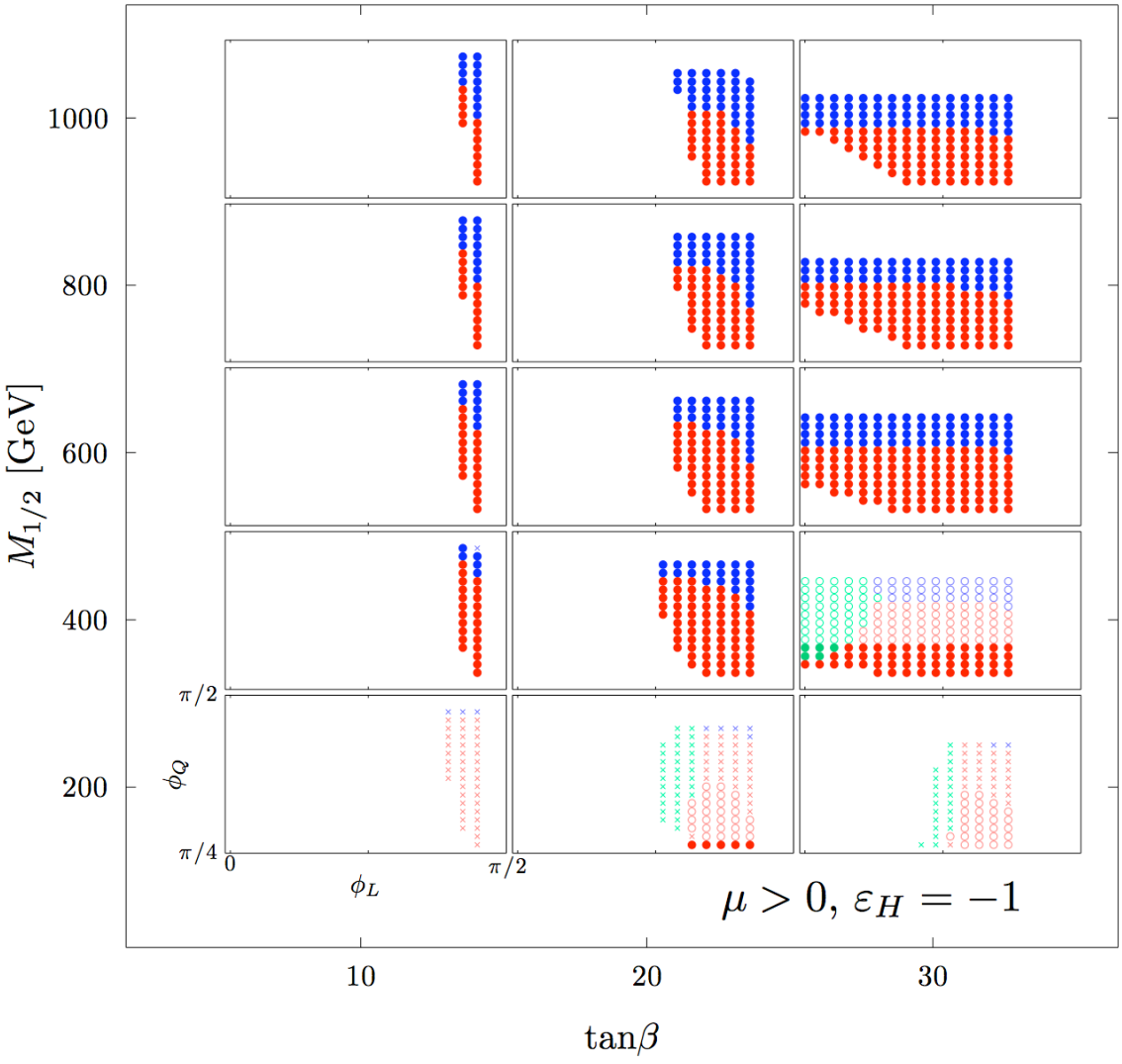

Figure 4.8: Same as Fig. 4.7 but for $\mu > 0$ and $\epsilon_H = -1$.

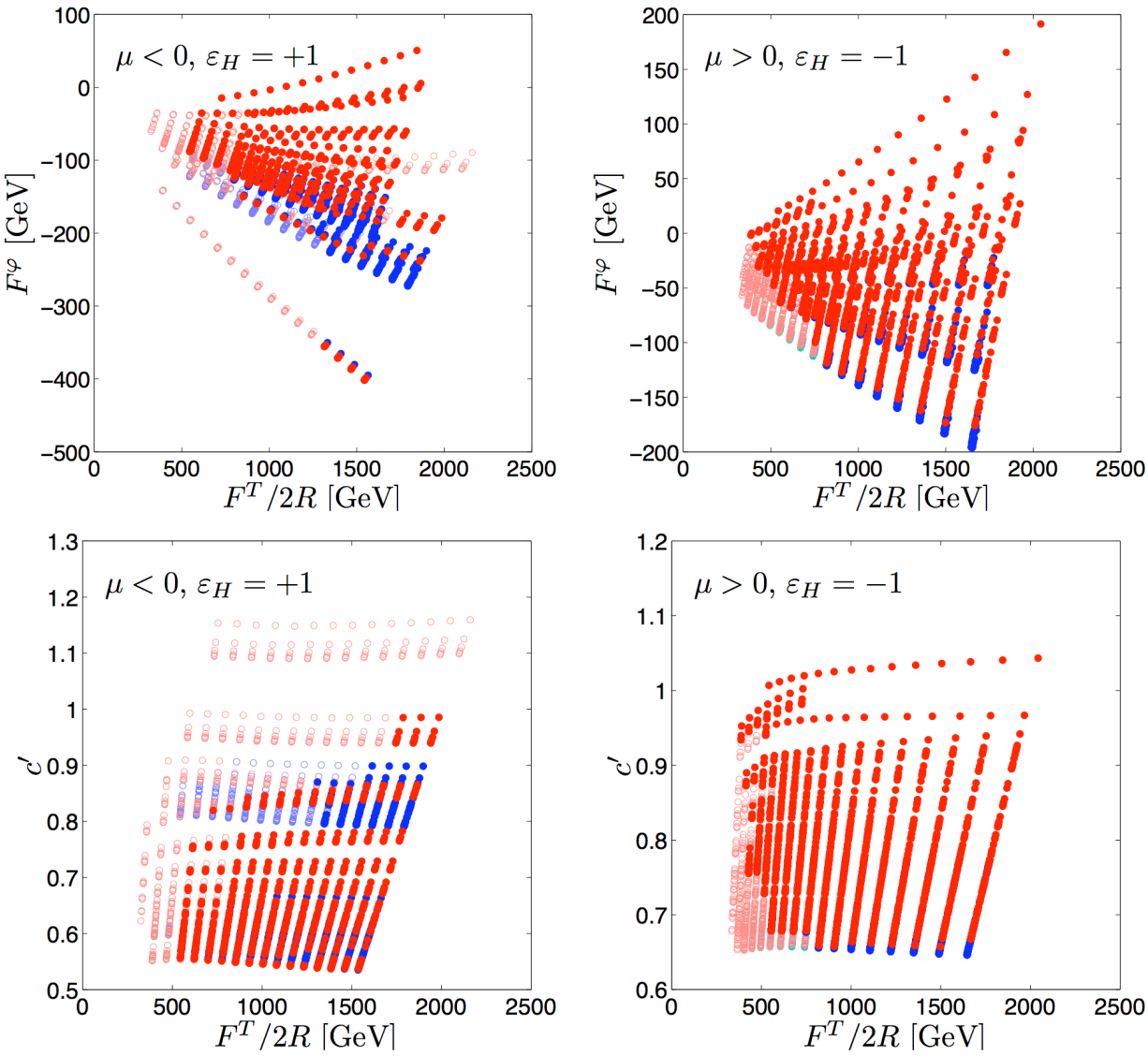

Figure 4.9: Points of Figs. 4.7 and 4.8 in the $F^T/2R$ vs. F^φ plane (top row) and in the $F^T/2R$ vs. c' plane (bottom row). The red, green and blue points have a neutralino, stau and selectron LSP, respectively. Open circles denote points excluded by B-physics constraints. Points excluded by LEP are not shown.

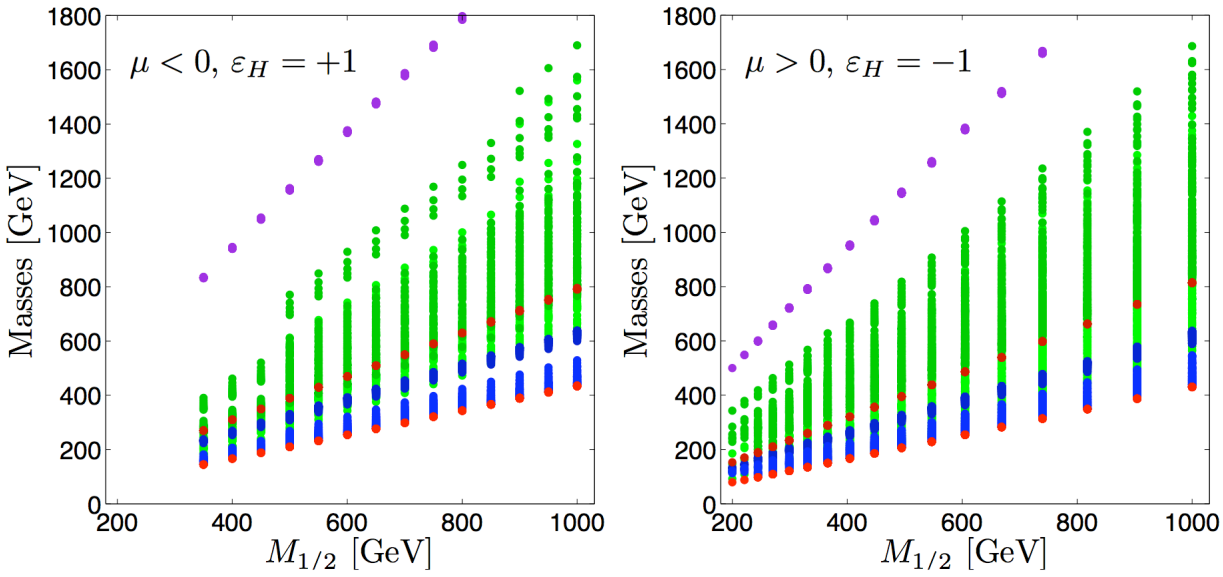

Figure 4.10: Mass spectrum in the neutralino LSP region, passing LEP and B-physics constraints, as a function of $M_{1/2}$. From bottom to top: $\tilde{\chi}_1^0$ (red), $\tilde{e}_R$ (blue), $\tilde{e}_L$ (dark blue), $\tilde{\tau}_1$ (green), $\tilde{\chi}_2^0$ (dark red), $\tilde{\tau}_2$ (dark green) and $\tilde{g}$ (purple).

Table 4.1 gives GUT and EWSB scale parameters, and Table 4.2 lists the resulting masses together with B-physics observables, the neutralino relic density and the neutralino–proton scattering cross section for direct detection. The possibility to tune the NLSP–LSP mass difference by adjusting ϕ_Q and ϕ_L and to obtain the correct relic density persists also for other values of $M_{1/2}$.

To summarize, the expected LHC phenomenology is as follows:

- Squarks and gluinos with masses up to about 2 TeV will be abundantly produced at the LHC, both as $\tilde{q}\tilde{q}$ or $\tilde{g}\tilde{g}$ pairs, and in $\tilde{q}\tilde{g}$ associated production. They decay as $\tilde{g} \to q\tilde{q}_{R,L}$, $\tilde{q}_R \to q\tilde{\chi}_1^0$ ($\sim 100\%$), $\tilde{q}_L \to q'\tilde{\chi}_1^\pm$ ($\sim 65\%$) or $q\tilde{\chi}_2^0$ ($\sim 30\%$).

- The decay $\tilde{\chi}_2^0 \to e^\pm\tilde{e}_L^\mp \to e^+e^-\tilde{\chi}_1^0$ is always open and has a sizable branching ratio ($\sim$45% for points A–D, 35% for point E). This leads to a rather large rate for the gold-plated SFOS dilepton signature. In parts of the parameter space, also $\tilde{\chi}_2^0 \to \tau^\pm\tilde{\tau}_1^\mp \to \tau^-\tau^+\tilde{\chi}_1^0$ can be kinematically allowed; c.f. point E, where it has 22% branching ratio. Decays into Z, h, or $\tilde{e}_R$ are negligible because the $\tilde{\chi}_2^0$ is almost a pure wino.

- The decay of the $\tilde{\chi}_1^\pm$ always leads to a charged lepton, $\tilde{\chi}_1^\pm \to \ell^\pm\tilde{\nu}_\ell/\nu_\ell\tilde{\ell}_L^\pm \to \ell^\pm\nu_\ell\tilde{\chi}_1^0$, giving rise to a large number of events with jets plus one hard lepton plus $E_T^{\rm miss}$. If combined with $\tilde{\chi}_2^0 \to ... \to l^+l^-\tilde{\chi}_1^0$ on the other side of the event, it leads to the rather clean trilepton signature (plus jets plus $E_T^{\rm miss}$).

- The higgsino states $\tilde{\chi}_{3,4}^0$ and $\tilde{\chi}_2^\pm$ have masses around or above the gluino mass and are hence too heavy to be studied at the LHC.

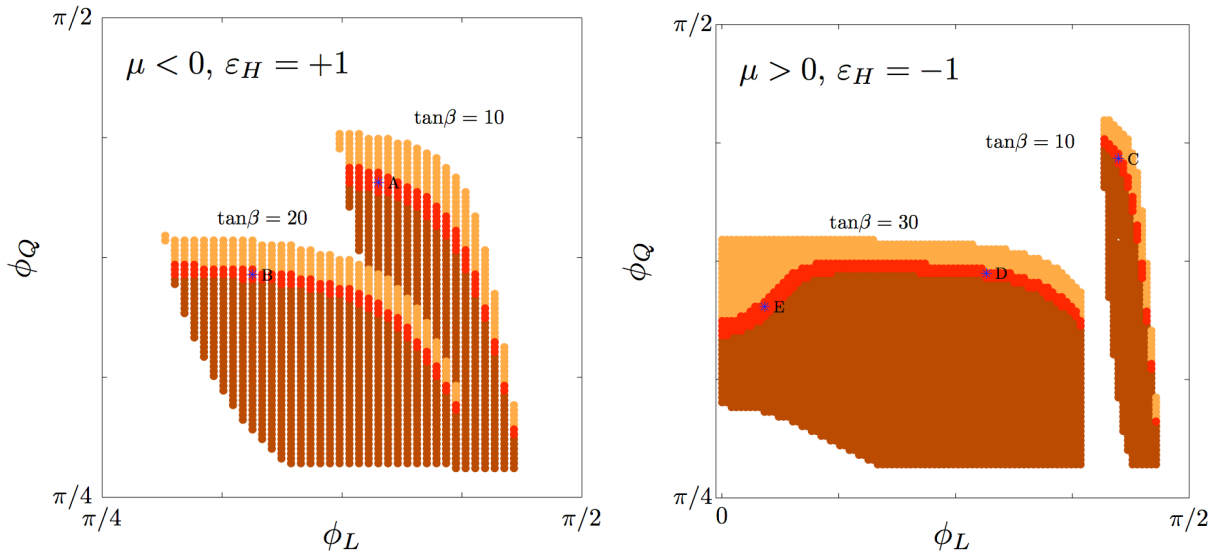

Figure 4.11: Dependence of the neutralino relic density on the mixing angles ϕ_Q and ϕ_L, for $M_{1/2} = 500$ GeV and various values of $\tan\beta$. In the red bands, Ωh^2 lies within 3σ of the WMAP5 observation, $0.0913 < \Omega h^2 < 0.1285$. In the orange regions, $\Omega h^2 < 0.0913$ is too low, while in the brown regions $\Omega h^2 > 0.1285$ is too high. Also indicated are the sample points A–E.

Overall the scenario resembles the mSUGRA/CMSSM case with small m_0, or the case of Higgs boson exempt no-scale supersymmetry (HENS) [131]. An important difference are the sizeable third-generation high-scale soft terms which our construction predicts. Ways to distinguish between the different models include, e.g., the rate of leptonic events, which is expected to be higher in our scenario as compared to the mSUGRA case with the same $M_{1/2}$. Other distinctive features are the ratios of left- and right-chiral slepton masses and the non-universality of the third generation.[7] Note, however, that the $\tilde{e}_R$ does not couple to the wino-like $\tilde{\chi}_2^0$ and $\tilde{\chi}_1^\pm$ and hence does not appear in decay chains at the LHC. The $\tilde{e}_R$ is therefore best studied in e^+e^- collisions, as are the staus if they are too heavy to be produced in $\tilde{\chi}_2^0$ decays.

Last but not least, a decisive test of GHU requires the precise measurement of the complete spectrum, including stops, sbottoms, heavy Higgs bosons and higgsinos, such that the SUSY Lagrangian parameters can be extracted and a bottom-up evolution along the lines of [132] performed. This can only be achieved at a (multi-)TeV e^+e^- linear collider with a very good beam performance.

[7] We leave a detailed study of characteristic mass ratios and model footprints for future work.

Point	A	B	C	D	E
$M_{1/2}$	500	500	500	500	500
$\tan\beta$	10	20	10	30	30
$\mathrm{sign}(\mu)$	-1	-1	$+1$	$+1$	$+1$
ε_H	$+1$	$+1$	-1	-1	-1
ϕ_Q	1.3011	1.1503	1.3486	1.1582	1.1027
ϕ_L	1.2376	1.0314	1.3329	0.8889	0.1437
c'	0.5712	0.6118	0.7577	0.6686	0.6811
$F^T/2R$	785.6	805.9	878.9	834.3	840.9
F^φ	-107.7	-120.6	-38.9	-114.6	-109.9
Parameters at M_{GUT}					
μ	-1178.9	-1232.4	1296.6	1283.2	1291.0
B	-344.0	-381.3	-298.0	-393.2	-390.2
m_{U_3}	564.8	615.2	622.9	634.9	657.3
m_{D_3}	239.5	371.2	279.5	413.9	369.2
m_{Q_3}	555.5	592.4	615.9	613.5	626.3
A_t	-812.6	-793.7	-980.0	-842.2	-823.1
A_b	-932.3	-923.6	-1105.6	-966.3	-978.8
m_{R_3}	226.7	304.9	364.1	432.6	278.8
m_{L_3}	161.8	269.4	225.2	407.9	278.5
A_τ	-1055.8	-1073.7	-1216.8	-1070.4	-1149.6
Parameters at M_{EWSB}					
μ	-1217.6	-1238.8	1342.0	1275.3	1282.9
B	-46.8	-16.7	45.9	11.4	10.6
m_1^2	554195	405781	598972	428198	401063
m_2^2	2022	-2969	2560	-3429	-3467

Table 4.1: Parameters of sample points A–E in Fig. 4.11. Dimensionful quantities are in GeV, $B \equiv B_\mu/\mu$.

Point	A	B	C	D	E
$m_{\tilde{\chi}_1^0}$	210.1	210.3	208.1	208.7	208.7
$m_{\tilde{\chi}_2^0}$	389.3	389.5	399.2	400.4	400.3
$m_{\tilde{\chi}_3^0}$	1219.7	1240.7	1332.0	1265.2	1272.8
$m_{\tilde{\chi}_4^0}$	1220.3	1241.9	1335.1	1267.7	1275.3
$m_{\tilde{\chi}_1^\pm}$	389.3	389.4	399.2	400.4	400.3
$m_{\tilde{\chi}_2^\pm}$	1222.8	1244.1	1335.4	1268.4	1276.0
$m_{\tilde{e}_L}$	327.7	328.1	327.5	326.8	323.1
$m_{\tilde{e}_R}$	218.6	217.0	216.6	217.1	228.3
$m_{\tilde{\tau}_1}$	295.9	322.0	370.4	387.7	225.4
$m_{\tilde{\tau}_2}$	372.6	441.2	438.0	549.5	457.0
$m_{\tilde{\nu}_e}$	318.4	318.3	318.1	317.3	313.4
$m_{\tilde{\nu}_\tau}$	354.3	408.0	386.2	499.0	398.4
$m_{\tilde{u}_L}$	1046.1	1045.8	1042.1	1041.8	1041.9
$m_{\tilde{u}_R}$	1003.5	1003.2	1000.0	999.6	997.6
$m_{\tilde{d}_L}$	1049.0	1048.7	1045.1	1044.8	1044.9
$m_{\tilde{d}_R}$	1005.9	1005.6	1001.9	1001.8	1002.3
$m_{\tilde{t}_1}$	948.0	971.1	955.7	971.4	983.5
$m_{\tilde{t}_2}$	1147.0	1155.0	1187.9	1167.6	1175.2
$m_{\tilde{b}_1}$	1022.3	1016.7	1029.9	1021.7	1007.9
$m_{\tilde{b}_2}$	1108.4	1119.6	1137.6	1130.6	1135.5
$m_{\tilde{g}}$	1155.5	1156.5	1154.2	1154.7	1155.0
m_h	115.0	116.4	117.2	117.3	116.8
m_H	762.4	658.5	770.7	637.4	635.9
m_A	761.6	658.5	770.8	637.6	635.9
$m_{H^\pm}$	766.7	663.9	775.1	642.9	641.0
BR($b \to s\gamma$)	3.70×10^{-4}	4.16×10^{-4}	3.20×10^{-4}	2.89×10^{-4}	2.91×10^{-4}
BR($B_s \to \mu^+\mu^-$)	2.89×10^{-9}	2.10×10^{-9}	3.06×10^{-9}	6.76×10^{-9}	6.68×10^{-9}
Ωh^2	0.110	0.108	0.110	0.108	0.106
$\sigma(\tilde{\chi}p)^{\rm SI}$ [pb]	2.92×10^{-11}	1.39×10^{-10}	1.01×10^{-10}	2.90×10^{-10}	2.89×10^{-10}

Table 4.2: Masses (in GeV), B-physics observables, relic density and spin-independent neutralino–proton scattering cross section for points A–E.

4.6 Conclusions

We have investigated SUSY grand unified models with gauge-Higgs unification (GHU). A particularly interesting class of such models are 5D orbifold GUTs and heterotic string models which admit a 5D orbifold GUT limit. With the natural assumption of radion mediation, GHU models are quite predictive as far as the Higgs sector is concerned. The GUT-scale Higgs mass parameters are subject to the GHU relations, and are also tied to the gaugino mass. Despite these strong constraints, models of this type can be fully realistic, as we have shown. If the effects of a Chern–Simons term (which is generically present in 5D models) are taken into account, one finds regions in the parameter space which lead to proper electroweak symmetry breaking and satisfy the experimental bounds from direct Higgs and superpartner searches, rare decays and cosmology. We demonstrated this by using a variation of a 5D SU(6) orbifold GUT model due to Burdman and Nomura as a concrete example. We gave detailed expressions for the soft SUSY breaking parameters in terms of the fundamental model data, including the Chern–Simons term.

Using the high-scale relations between soft terms and estimates of running effects, we discussed qualitatively which parts of the parameter space might be promising. We then presented a detailed numerical analysis of the corresponding RGEs. This analysis was done in two parts, the first for a simplified model of the sfermion sector, and the second treating the relevant sfermion contributions properly as in the Burdman–Nomura model. The latter part of the analysis, while more realistic, is more involved because it depends on more parameters. In both cases we indeed find viable solutions to the RGEs, satisfying all present experimental constraints. A non-zero Chern–Simons term is essential to get a valid spectrum.

We extracted some characteristic experimental signatures of this class of models, which will be tested at the LHC. In particular, selectrons are generically predicted to be lighter than the $\tilde{\chi}_2^0$, leading to a rather large rate for same-flavour opposite-sign dileptons over the whole parameter space. Higgsinos, on the other hand, are expected to be heavy, presumably beyond the reach of the LHC. Characteristic mass ratios could be tested in detail at a future e^+e^- linear collider.

The LHC will have the potential to narrow down the allowed region in the parameter space of GHU models significantly, or to rule them out. This applies even more to a future linear collider. It would be worthwhile to study in detail how well the scenario discussed here could be reconstructed at the LHC and a linear e^+e^- collider, thereby testing the GHU relation. To this end we proposed a set of benchmark points which may be useful for Monte Carlo simulations.

Résumé de la section

Dans ce modèle d'Unification jauge-Higgs, nous avons montré qu'il était possible d'obtenir la brisure électrofaible une fois que les effets du terme de Chern-Simons 5D sont bien pris en compte. La brisure de supersymmétrie la plus naturelle et la moins problématique pour la physique des saveurs est la brisure sous l'effet du radion. Nous avons ensuite analysé en détail les conséquences phénoménologiques de cette classe de modèle, en prenant en particulier en compte la contrainte de densité de reliques de matière noire et de physique des saveurs, et obtenus des prédictions pour le LHC.

Chapter 5

Phenomenology of models with a degenerate Higgs mass matrix

In the previous chapter, it is shown that the gauge-Higgs framework is phenomenologically viable. We now investigate in a more generic way models with a degenerate Higgs mass matrix (DHMM). This chapter is largely based on our publication [102].

We are at the beginning of a discovery era. If the LHC, and/or a dark matter detector, and/or any of the other experiments probing new physics, find some signal, it will be only the beginning of the adventure. We will then have the task of discriminating among all possible models. These models will be only partially constrained: continuous part of their parameter space will be consistent with avalaible data. Even if the LHC measure some supersymmetric particles masses, the precision and the quantity of observables will be insufficient to allow a bottom-up reconstruction of the GUT scale parameters. In such a situation, the adequate framework is Bayesian statistics. It allows to consider models and parameters as random variables, permitting to apply to them well defined statistics. One can do parameter inference for a given model, or compare the evidence between two models, using a probability ratio called Bayes factor. For a brief introduction to Bayesian statistics, we refer to Appendix B.

The Chapter is organized as follows. We will first present a qualitative analysis of the expected features in Section 5.1. We then carry out a study using Bayesian inference, whose setup and results are presented in Section 5.2. Conclusions are presented in Section 5.3.

5.1 Soft term patterns

In the common public SUSY spectrum generators, μ and B_μ at the GUT scale are computed according to their renormalization group equations from their IR-scale values, which in turn are calculated from m_Z and the given $\tan\beta$. Here we use `SOFTSUSY` [105]. Following what

we explained in Section 4.2, we implement the Higgs mass relation Eq. (3.66) by iteratively adjusting the Higgs soft masses,

$$m_{H_1}^2 = m_{H_2}^2 \;\to\; \epsilon_H B_\mu - |\mu|^2 \tag{5.1}$$

at $M_X = M_{\rm GUT}$. Here $\epsilon_H = \pm 1$ takes care of the sign ambiguity in B_μ which we mentioned in the previous section. Throughout this analysis we assume gaugino mass unification, $M_1 = M_2 = M_3 \equiv M_{1/2}$ at $M_{\rm GUT}$. The free parameters in our study are thus $M_{1/2}(M_{\rm GUT})$, $\tan\beta(M_Z)$, the two signs ϵ_H and $\mathrm{sign}(\mu)$, and the sfermion soft terms at $M_{\rm GUT}$. We take the latter to be flavour-diagonal.

Whether EWSB and a viable phenomenology can be obtained strongly depends on the sfermion soft terms. Two limiting cases are of particular interest:

- assuming a common sfermion mass m_0 and a common trilinear coupling A_0. This makes the DHMM models a subclass of non-universal Higgs mass models (see e.g. [133] and references therein) with $m_{H_1}^2 = m_{H_2}^2$ ("NUHM1" in the terminology of [134]);
- no-scale boundary conditions for the first and second generation, $m_0(1,2) = A_0(1,2) \equiv 0$, but allowing for arbitrary soft terms in the third generation.

The first case may be considered as representative for a generic scenario with all sfermion soft terms of the same order of magnitude, whereas the second case represents models with hierarchical soft terms reflecting the Yukawa hierarchy. As we have seen in Section 3, both these scenarios are well motivated from the model-building point of view. Moreover, it is interesting to investigate whether the stronger condition of Eq. (3.70), $m_{H_{1,2}}^2 \to 0$ and $|\mu|^2 \to |B_\mu|$, can be realized.

It turns out that the following patterns emerge in the soft terms:

1. in almost all of the admissible regions of parameter space, ϵ_H corresponds to the GUT-scale sign of B_μ;
2. for $\mathrm{sign}(\mu) = +1$, B_μ has almost always the same sign as A_t at the GUT scale (and the opposite one if $\mathrm{sign}(\mu) = -1$);
3. for $\mathrm{sign}(\mu) = +1$, the stricter relation

$$m_{H_1}^2 = m_{H_2}^2 = 0, \qquad \epsilon_H\, B_\mu = |\mu|^2 \qquad \text{at } M_{\rm GUT} \tag{5.2}$$

can only be satisfied with $\epsilon_H = +1$.

These observations can be explained by a close inspection of the relevant RGEs. Part of this, in particular regarding **point 1.** and **2.**, has already been discussed in Section 4.1. We repeat and expand on that discussion.

To start with, it is useful to recall the dominant contributions to the one-loop RG evolution of the stop trilinear A_t, Eq. (4.6). As discussed in Section 4.1, the large gluino contribution will drive A_t to a large negative value towards "late times" (i.e. towards the low energy scale), until it is compensated for by the first term in Eq. (4.6).

Now concerning **point 1.**, if sign(B_μ) does not match with ϵ_H at the GUT scale, this implies that the GUT-scale m_1^2 and m_2^2 are negative. The running of m_1^2 and m_2^2 is almost exclusively due to the running of the soft masses $m_{H_1}^2$ and $m_{H_2}^2$, since μ is approximately constant. The dominant terms in the one-loop RGE for the up-type Higgs soft mass-squared are

$$16\pi^2 \frac{d}{dt} m_{H_2}^2 = 6\,|y_t|^2\,\left(|A_t|^2 + m_{H_2}^2 + m_{Q_3}^2 + m_{U_3}^2\right) - 6\,g_2^2\,|M_2|^2 + \dots\,, \tag{5.3}$$

where $m_{U_3}^2$ and $m_{Q_3}^2$ are the soft masses of the third generation up-type squarks and squark doublets respectively. In scenarios like the CMSSM, by scalar mass universality the terms in parentheses are typically positive. Thus m_2^2 is driven to lower values as the RG scale decreases, assisted also by the top Yukawa coupling and $|A_t|$ growing large. Eventually radiative electroweak symmetry breaking is triggered. Most of the DHMM parameter space also has this property. There is only a tiny region with initially small A_t, very large negative $m_{H_{1,2}}^2$, small or negative squark soft masses-squared, and sizeable $M_{1/2}$, in which m_2^2 runs up significantly at first. In that case it can be driven to positive values even if it starts out negative, and electroweak symmetry breaking can be triggered later when the A_t contribution in Eq. (5.3) dominates and when also the squark masses have grown positive.

Concerning **point 2.** above, note that B_μ at the low scale should be somewhat small compared to the typical soft masses. This is in order to satisfy the electroweak symmetry breaking conditions 1.19, 1.20 , and in particular to have at least moderately large $\tan\beta$ ($\tan\beta \gtrsim 5$ say). Let us for now assume positive μ. The one-loop RGE of B_μ, Eq. 4.5, is dominated by the A_t and gaugino contributions. The gaugino contribution tends to dominate the RG evolution of B_μ at scales close to the GUT scale, driving B_μ down. However, eventually A_t itself will run large and negative because of the gluino contribution to Eq. (4.6). Far in the IR it will thus primarily drive the B_μ evolution, causing B_μ to run up instead. For sizeable and positive initial GUT-scale A_t, this latter effect will be less important. But for small or even negative GUT-scale values, A_t will quickly evolve towards large negative values, and thus dominate over the gaugino term in Eq. (4.5).

We conclude that positive starting values for the GUT-scale A_t are preferred if $B_\mu > 0$ (in which case B_μ should mainly run down towards the electroweak scale, to end up small) and small or negative values are preferred if $B_\mu < 0$ (in which case it should mainly run up, to end up positive). For negative μ, the signs are reversed. These correlations are illustrated in Fig. 5.1 with the help of some slices through the parameter space, at fixed sfermion and gaugino masses, fixed $\tan\beta$, and universal trilinears.

Our choice for the soft masses in Fig. 5.1 may seem rather high, but as can be seen

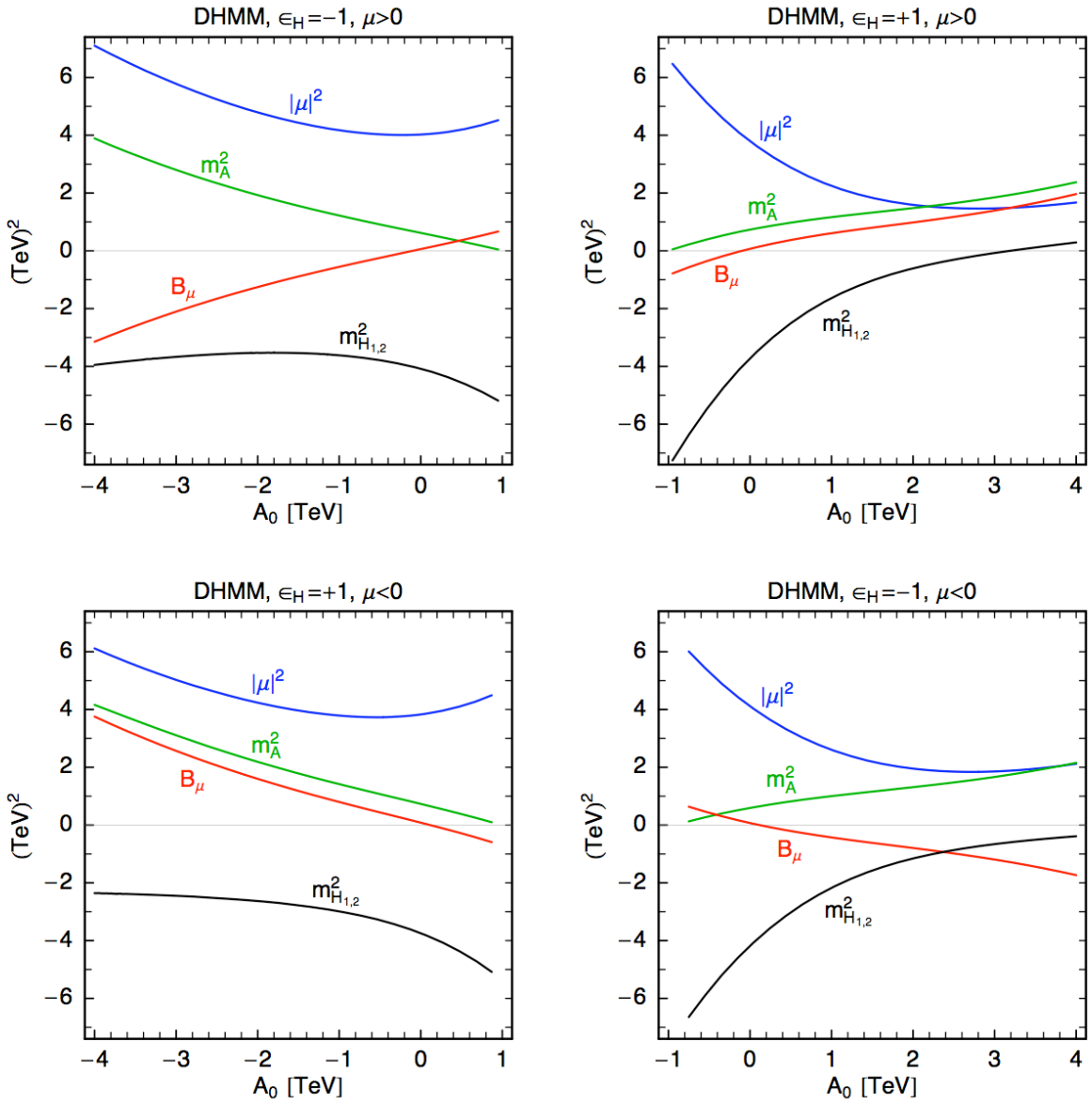

Figure 5.1: A set of slices through the four branches of DHMM parameter space with $M_{1/2} = 1$ TeV, $\tan\beta = 10$, and $m_0 = 500$ GeV. For the panels on the left, regions of larger A_0 do not lead to electroweak symmetry breaking, as can be seen from the pseudoscalar Higgs mass m_A^2 approaching zero. The same is true for regions of smaller A_0 for the panels on the right. The upper panels show, as explained in the text, that for $\mathrm{sign}(\mu) = +1$ the GUT-scale sign of A_t is equal to the GUT-scale sign of B_μ in almost all of the allowed regions. The lower panels show that this correlation is reversed if $\mathrm{sign}(\mu) = -1$. As also explained in the text, $m_{H_{1,2}}^2 = 0$ is only possible if $\epsilon_H = +1$ and $\mathrm{sign}(\mu) = +1$ (top right panel). Finally note that there is a tiny slice of the allowed parameter space where ϵ_H does *not* correspond to $\mathrm{sign}(B_\mu)$ at the GUT scale. In this region $|A_t|$ is small and $m_{H_2}^2$ is large and negative as expected.

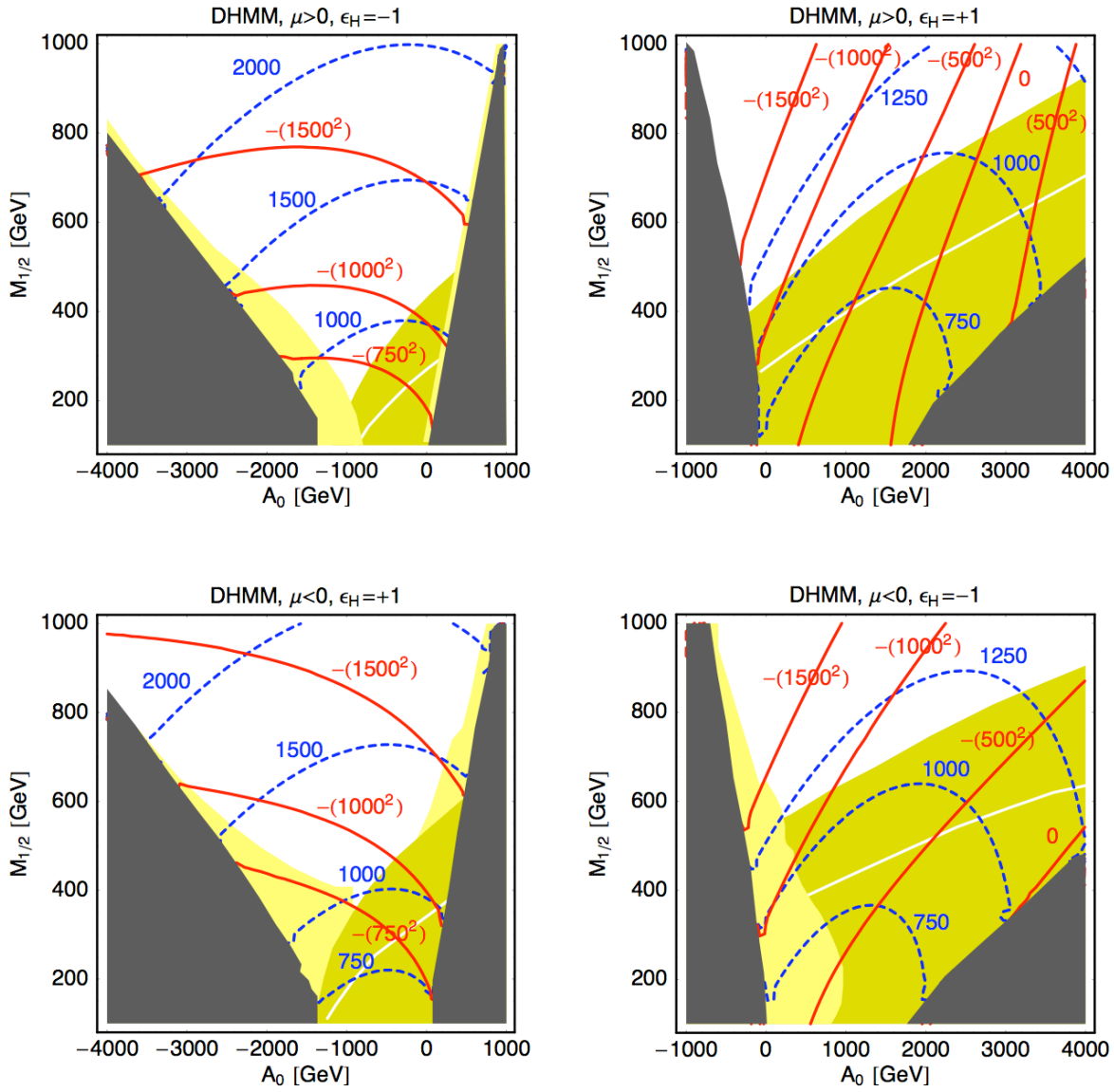

Figure 5.2: Contours of constant $m^2_{H_{1,2}}$ (full red lines) and $|\mu|$ (dashed blue lines) at $M_{\rm GUT}$ in the $M_{1/2}$ versus A_0 plane, for $\tan\beta = 10$ and $m_0 = 500$ GeV. Grey regions do not lead to electroweak symmetry breaking, light yellow regions are excluded by $b \to s\gamma$ (at 2σ), and dark yellow regions have $m_h < 114$ GeV, with the lines indicating $m_h = 111$ GeV.

from Fig. 5.2, satisfying the LEP Higgs bound requires fairly large $M_{1/2}$, the more so the larger A_0 is.

Finally let us come to **point 3.**: The A_t parameter also enters the $m^2_{H_2}$ RGE Eq. (5.3). A large $|A_t|$ will accelerate the decrease of $m^2_{H_2}$ when running down from the GUT scale, which is of course a particularly severe effect if A_t starts out negative, i.e. if $\epsilon_H = -\text{sign}(\mu)$. Then $m^2_{H_2}$ will run negative too quickly, unless there is some other contribution to counterbalance the effect of A_t. Large gaugino masses could provide such a contribution, but they would

again slow down the B_μ evolution, as is evident from Eq. (4.5). If we allow for non-vanishing Higgs soft masses-squared, they can in particular be negative and thus counteract the A_t effect in Eq. (5.3). However, in the case that $m^2_{H_{1,2}}$ is constrained to vanish, A_t should be positive at the GUT scale to minimize its effect on the $m^2_{H_2}$ running. In addition, small (or even negative) GUT-scale squark masses-squared are preferred to slow down the $m^2_{H_2}$ evolution. Indeed, in Figs. 5.1 and 5.2 the case $m^2_{H_{1,2}} \to 0$ occurs only for $\epsilon_H = \mathrm{sign}(\mu)$ and requires large positive A_0 to start with, leading to small negative A_t at the EW scale.

As can also be seen from Fig. 5.2, large positive A_0 leads to a tension with the direct search bound from LEP of $m_h > 114.4$ GeV at 95% C.L. [135], even when taking into account a 2–3 GeV theoretical uncertainty [121] on the calculation of m_h in the MSSM. This can be understood as follows: At lowest order, the light CP-even Higgs boson of the MSSM is at most as heavy as the Z^0 boson, $m_h^2 \leq m_Z^2 \cos^2 2\beta$. Radiative corrections have to lift m_h above the LEP limit. The dominant effect is proportional to the fourth power of the top Yukawa coupling, y_t^4, and comes from an incomplete cancellation of top and stop loops. This increases m_h approximately to

$$m_h^2 \lesssim m_Z^2 + \frac{3g^2 m_t^4}{8\pi^2 m_W^2} \left[\log\left(\frac{M_S^2}{m_t^2}\right) + \frac{X_t^2}{M_S^2}\left(1 - \frac{X_t^2}{12 M_S^2}\right)\right] + \dots \,, \tag{5.4}$$

where

$$M_S^2 \equiv \frac{1}{2}\left(m^2_{\tilde{t}_1} + m^2_{\tilde{t}_2}\right) \,, \quad X_t \equiv A_t - \mu \cot\beta \,. \tag{5.5}$$

For large $\tan\beta$ and large $|\mu|$, also bottom and sbottom loops become important, giving an analogous contribution proportional to y_b^4. For details see, e.g., [136] and references therein. The logarithmic sensitivity to the average stop mass M_S in Eq. (5.4) suggests that heavy stops are preferred in order to render m_h large enough. However, this sensitivity is rather mild, and the dependence on the stop mixing parameter X_t can be at least as important. Indeed, m_h initially increases with $|X_t|$ and reaches maximal values for $X_t = \pm\sqrt{6} M_S$; this is known as the 'maximal mixing' or $m_h^{\max}$ case, see again [136]. Therefore a large low-scale $|A_t|$, together with moderately large $\tan\beta$, is favoured to satisfy the LEP Higgs mass bound. This is exactly what we find in the right-hand side panels of Fig. 5.2: For too large starting values of A_t, the low-scale $|A_t|$ will be too small (recall that A_t generically runs towards negative values) and the Higgs mass bound becomes important.

The DHMM model with universal sfermion soft terms is a special case of a NUHM model. Fig. 5.3 shows for comparison the dependence of m_A^2, μ^2 and B_μ in a general NUHM1 model with $m^2_{H_{1,2}} = 0$. The other parameters are as in Fig. 5.1. The CMSSM limit with $m^2_{H_{1,2}} = m_0^2$ gives almost the same picture, the only difference being a slightly larger m_A^2 and slightly smaller μ^2. Note that there is only one "DHMM point" in Fig. 5.1 (with meeting $|\mu|^2$ and B_μ curves), which occurs for $\mu > 0$. Away from this point where the models coincide, DHMM has a much larger $|\mu|$ and smaller m_A than NUHM1 (or the CMSSM), cf. Fig. 5.1. In particular, in the DHMM case m_A becomes small for small $|A_0|$, and we can have $m_A \approx M_{1/2}$ even for small $\tan\beta$. This will be important later when we

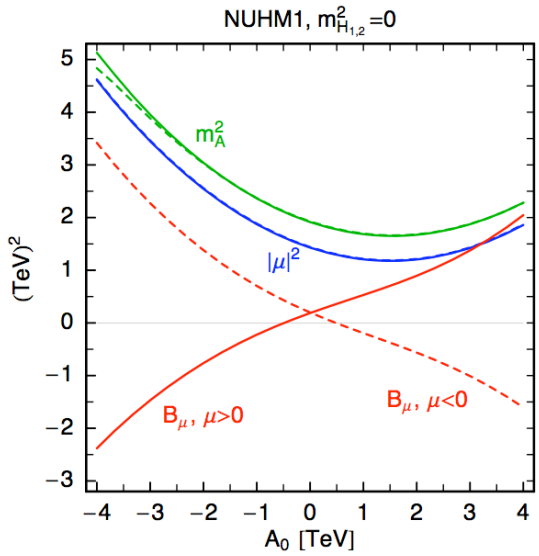

Figure 5.3: Higgs mass parameters in the MSSM with non-universal Higgs masses, for a universal gaugino mass $M_{1/2} = 1$ TeV, a universal sfermion mass $m_0 = 500$ GeV, $\tan\beta = 10$, and vanishing Higgs soft masses. Note that there is only a "DHMM point" (with meeting $|\mu|^2$ and B_μ curves) for $\mu > 0$.

consider the neutralino relic density. At this stage we just remark that in Fig. 5.2 s-channel annihilation through the Higgs funnel occurs for small $|A_0| \lesssim 100 - 300$ GeV.

Let us now explore the consequences of non-universal third generation soft terms. This is interesting in particular for the gauge-Higgs unification models discussed in Section 3.1 and Chapter 4, where we expect vanishing first and second generation soft masses, $m_0(1,2) \approx 0$. In this case we have roughly $m^2_{\tilde{e}_R} \approx (0.39\, M_{1/2})^2 - 0.052\, S_{\rm GUT}$, and $m^2_{\tilde{e}_L} \approx (0.68\, M_{1/2})^2 + 0.026\, S_{\rm GUT}$, which has to be compared to $m_{\tilde{\chi}^0_1} \approx 0.43\, M_{1/2}$. $S_{\rm GUT}$ is the GUT-scale value of the hypercharge S parameter, Eq. (4.27). We see that a non-zero and negative $S_{\rm GUT}$ of about $-(0.8\, M_{1/2})^2$ to $-(3.3\, M_{1/2})^2$ is necessary if one wants the neutralino to be the lightest SUSY particle (LSP). Since we have $m^2_{H_1} = m^2_{H_2}$ in DHMM, the way to ensure a neutralino LSP is non-universality of the third generation, as illustrated in Fig. 5.4.[1] We can see that taking a slice along $m_{U_3} = m_{Q_3} = m_{D_3}$, as we have done in the previous plots, indeed results in qualitatively similar patterns as the more general case in which the squark soft masses are split. On the other hand, negative soft masses-squared can give much smaller $m^2_{H_{1,2}}$ and $|\mu|$. This is of interest in particular for $\epsilon_H = \text{sign}(\mu) = +1$, where one can achieve a mixed bino–higgsino LSP (see the dark matter discussion in the next section). Note moreover that in the RHS plots of Fig. 5.4, $m^2_{H_{1,2}}$ is very sensitive to A_0, while μ does not vary much when passing from $A_0 = M_{1/2}$ to $A_0 = 3M_{1/2}$. This is in accord with Fig. 5.1.

[1] We use the notation $m_{U_3} \equiv m^2_{U_3}/\sqrt{|m^2_{U_3}|}$, so the sign of m_{U_3} is actually that of $m^2_{U_3}$, and analogously for m_{Q_3} etc.

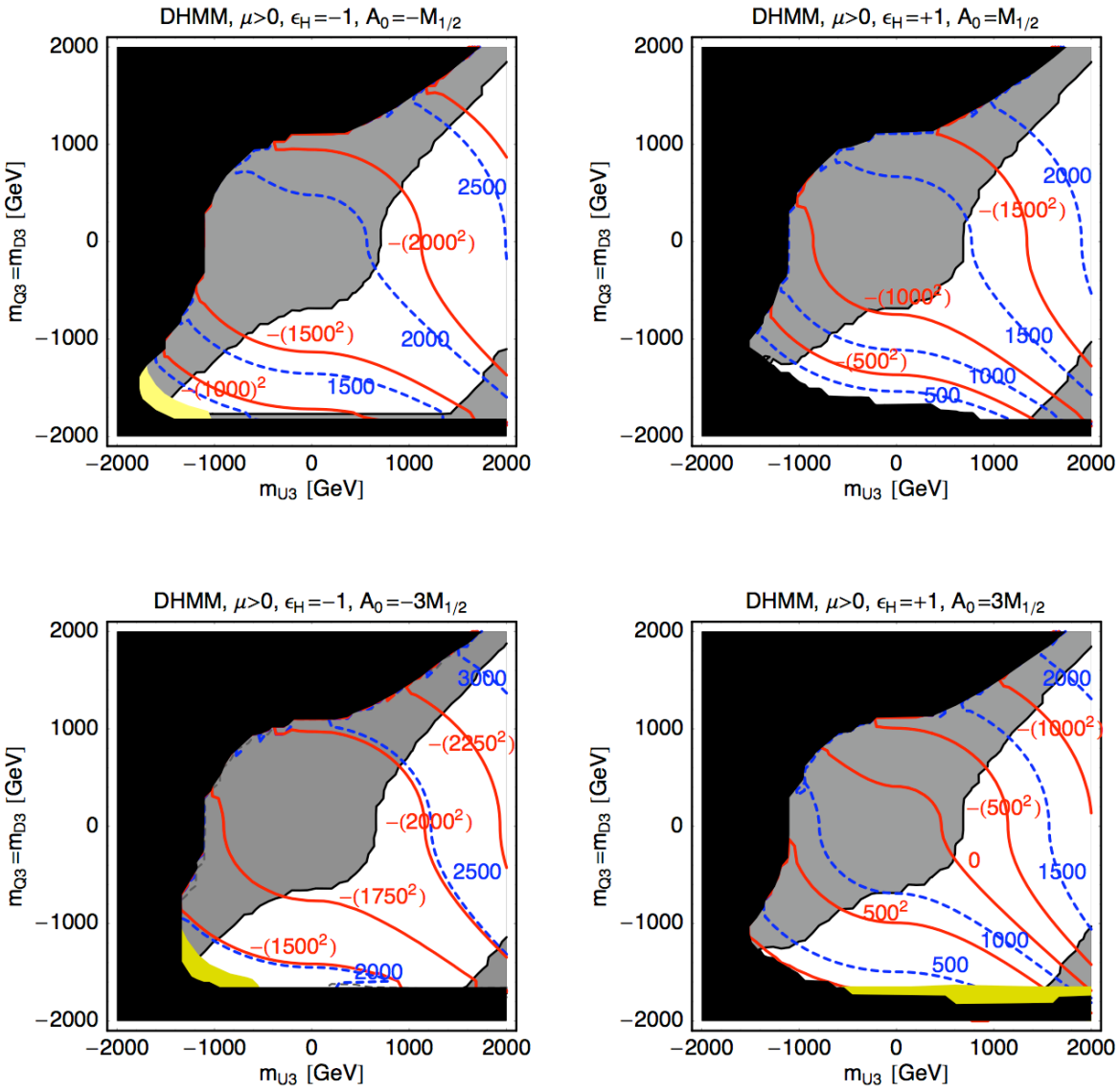

Figure 5.4: Contours of constant $m^2_{H_{1,2}}$ (full red lines) and $|\mu|$ (dashed blue lines) at $M_{\rm GUT}$ in the m_{U_3} versus m_{Q_3} plane, for $M_{1/2} = 1$ TeV, $\tan\beta = 10$ and vanishing 1st/2nd generation soft terms. Moreover, $\mu > 0$, $\epsilon_H = \pm 1$, and $A_0 = \pm M_{1/2}$ (upper row) and $A_0 = \pm 3M_{1/2}$ (lower row). Black regions do not lead to electroweak symmetry breaking, gray regions have a slepton LSP, and white regions a neutralino LSP; the light yellow stripe is excluded by $b \to s\gamma$ at 2σ, while the dark yellow stripes have $m_h < 114$ GeV. $\mu < 0$ gives qualitatively very similar results.

We conclude this section with a few remarks on potentially dangerous tachyonic directions. In our analysis we have permitted tachyonic GUT-scale masses for both the Higgs and the sfermion fields. This is well-known to generally lead to charge- and colour-breaking minima in the potential, as well as to directions in field space which are unbounded from

below (at tree-level and without higher-dimensional operators); see, for instance, [137].

While tachyonic scalar masses appear to rule out a large part of the parameter space at first sight, two points must be considered. First, a careful analysis is required in each case to determine if such dangerous vacua really are present. In particular, calculations using only the RG-improved tree-level potential may give unreliable results if the field VEVs are found to be vastly different from the renormalization scale, because of the presence of large logarithms in the loop corrections. Second, these vacua need not be dangerous even if they are present. If the tunnelling rate from our false vacuum is sufficiently small, our vacuum may well be effectively stable on cosmological timescales. It then depends on early-universe cosmology whether or not it is preferred for our universe. See [138] for a recent analysis of the CMSSM and of NUHM models in that context, and [139] for a recent analysis of the cosmological lifetime of related Higgs-exempt no-scale models.

A detailed investigation of charge- and colour-breaking minima is beyond the scope of this work. We therefore merely stress that we expect them to appear in large regions of parameter space, but depending on their lifetime and on the cosmological scenario, these regions may still be acceptable phenomenologically.

5.2 Bayesian analysis with Markov chains Monte Carlo

So far we have only considered the constraints from m_h and $b \to s\gamma$, and taken one- or two-dimensional slices through the parameter space. In order to take into account more constraints and in particular to find regions of parameter space where the neutralino LSP is a good dark matter candidate, we next perform a Markov Chain Monte Carlo scan of DHMM models. As above, we consider the two cases of (i) universal sfermion soft terms and (ii) vanishing first/second but non-universal third generation soft terms.

MCMC is a method to probe a large-dimensional parameter space, and to gain information about it by using Bayesian statistics. The basic idea is to set up a random walk, starting at some parameter point and proposing a candidate next point at random nearby. This candidate point is then accepted or rejected at random, with an acceptance probability depending on its likelihood compared to the likelihood of the original point. Parameter points which are more likely to reproduce existing experimental data and constraints within errors have a greater probability of being accepted. If accepted, the new point is chosen as the starting point and the procedure is iterated. Otherwise it is repeated with the old starting point. A properly set-up ensemble of Markov chains should eventually fill out all the allowed parameter space, with a high density of points in those regions which are best compatible with existing measurements. In the sense of Bayesian statistics, the distributions of points are interpreted as probability density functions. MCMC provides a

simple means to marginalise these distributions and to evaluate probability regions.

The setup and procedure of our MCMC analysis closely follows [140], and we refer the reader to this paper for technical details (see also [141–144]). Here we just explain the constraints and priors used in our analysis. We apply the limits from direct SUSY [119] and Higgs [120, 135] searches at LEP. The computation of m_h suffers from a theoretical uncertainty which has been estimated to amount to up to 2–3 GeV [121]. This theoretical error is most likely non-Gaussian and can give an underestimation as well an overestimation of m_h. We therefore use the direct experimental search limit for a SM-like Higgs of $m_h > 114.4$ GeV at 95% C.L. without further modification. One should however bear in mind that the favoured regions of parameter space may in fact be somewhat larger (where the Higgs mass is underestimated by the calculation) or smaller (where it is overestimated) than the ones we find.

Regarding the anomalous magnetic moment of the muon, we limit our scans to $\mu > 0$, which gives a positive SUSY contribution, but do not require that SUSY explains the discrepancy between the measurement and SM prediction; instead we only apply an upper limit on $\Delta a_\mu^{\mathrm{SUSY}}$.

The complete set of constraints applied is given in Table 5.1. For observables on which there is merely an experimental upper or lower bound available, we use a Fermi likelihood function L_1. For quantities which have been measured, we use a Gaussian likelihood function L_2. The total likelihood of a parameter point is the product of all individual likelihoods, $L = \prod_n (L_i)_n$. In the notation of Table 5.1, we have

$$L_1(x, x_0, dx) = \frac{1}{1 + \exp[(x - x_0)/dx]}\,, \quad L_2(x, x_0, dx) = \exp\left[-\frac{(x - x_0)^2}{2\,dx^2}\right]. \tag{5.6}$$

The neutralino relic density, the B-decay branching ratios, $\Delta a_\mu^{\mathrm{SUSY}}$, and the SUSY mass limits are evaluated with `micrOMEGAs` [126, 145].[2] [3]

We choose to work with two different prior probability distributions. Our first prior is flat in the GUT-scale soft parameters and in $\tan\beta$. That is, within a certain fixed range, any value for a given parameter is treated as equally probable. As a second prior, for comparison, we use a "naturalness prior" [141]: Since a prior choice ultimately reflects theoretical prejudice as to what parameter choices should be more or less likely, we find it appropriate to use a prior which disfavours the more fine-tuned parameter points. The main source for fine-tuning in the MSSM is caused by the sensitivity of the electroweak

[2] In the likelihood function for Ωh^2, we use the 2008 central value of [146] with a Gaussian width of about 10%. This is to approximately account for uncertainties from the cosmological model, from the data sets used, and from the SUSY spectrum calculation. It is consistent with the most recent determination of Ωh^2 from seven-year WMAP data, published in early 2010 [147, 148].

[3] The current searches at the LHC with 1 1 fb^{-1} are pushing the limits on squarks and gluino masses up to ~ 1 TeV. These are not taken into account in this 2010 publication.

Observable	Limit	Likelihood function	Ref.
m_h	> 114.4	$L_1(x, 114.5, -0.6)$	[120]
m_t	173.1 ± 1.3	$L_2(x, 173.1, 1.3)$	[149]
m_W	80.398 ± 0.025	$L_2(x, 80.398, 0.025)$	[20]
$\mathrm{BR}(b \to s\gamma)$	$(3.52 \pm 0.34) \times 10^{-4}$	$L_2(x, 3.52 \times 10^{-4}, 0.34 \times 10^{-4})$	[122, 123]
$\mathrm{BR}(B_s \to \mu^+\mu^-)$	$\leq 5.8 \times 10^{-8}$	$L_1(x, 5.8 \times 10^{-8}, 5.8 \times 10^{-10})$	[124]
$\mathrm{R}(B_u \to \tau\nu_\tau)$	1.11 ± 0.52	$L_2(x, 1.11, 0.52)$	[122]
$\Delta a_\mu^{\mathrm{SUSY}}$	$\leq 4.48 \times 10^{-9}$	$L_1(x, 4.48 \times 10^{-9}, 4.5 \times 10^{-11})$	[150]
Ωh^2	0.1131 ± 0.0034	$L_2(x, 0.113, 0.011)$	[146]
SUSY mass limits	LEP limits	1 or 10^{-9}	[119]

Table 5.1: Observables used in the likelihood calculation. L_1 and L_2 are defined in Eq. (5.6).

scale to parameter variations. We therefore use a fine-tuning measure c defined as [151]

$$c = \max_i \left| \frac{\partial \log m_Z}{\partial \log a_i} \right| . \tag{5.7}$$

Here $\{a_i\}$ includes all GUT-scale soft masses and trilinear soft terms, as well as μ. With the naturalness prior, every parameter point is then weighted with a measure $1/c$, thus penalizing the more fine-tuned ones.

Before presenting the results, let us comment on the viable dark matter regions. In general in the MSSM there are only a few mechanisms that provide the correct amount of neutralino annihilation consistent with cosmological observations (see e.g. [152] for a review). In the DHMM case we consider here, we expect:

A) Coannihilation with sleptons. This requires small neutralino–slepton mass differences of roughly $10 - 1$ GeV for $m_{\tilde{\chi}_1^0} \sim 100 - 500$ GeV; for heavier LSPs, coannihilation with sleptons alone is not efficient enough. Another possibility is coannihilation with light $\tilde{t}_1$ or $\tilde{b}_1$, which is efficient for larger mass differences, or larger LSP masses.

B) Annihilation through s-channel pseudoscalar Higgs exchange. Here the key quantities are the distance from the A pole, $m_A - 2m_{\tilde{\chi}_1^0}$, and the width of the A resonance. The process is efficient for a bino LSP, although some higgsino admixture is necessary to provide the $\tilde{\chi}_1^0\tilde{\chi}_1^0 A$ coupling.

C) Annihilation of a mixed bino-higgsino LSP through t-channel chargino and neutralino exchange, and through s-channel Z exchange. This requires a sizable LSP higgsino fraction $f_H \gtrsim 0.25\%$. Heavier LSPs need a larger higgsino fraction, so that eventually coannihilation with other neutralinos and charginos also becomes important. Besides, if $2m_{\tilde{\chi}_1^0} \sim m_A$, s-channel A exchange also contributes in this region.

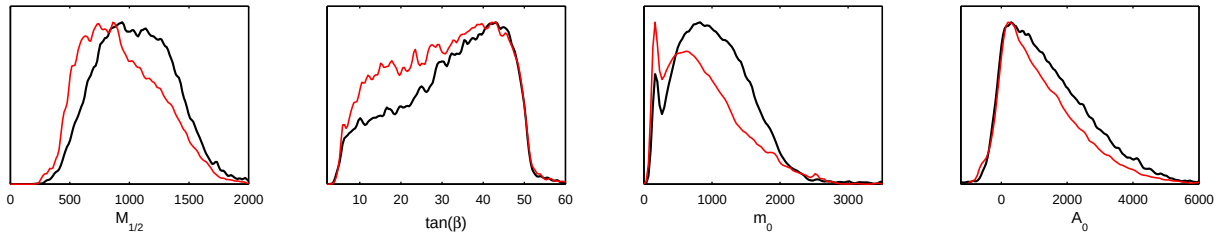

Figure 5.5: Marginalized 1D posterior probability distributions of the input parameters for universal soft terms and $\epsilon_H = +1$. Black lines are for flat prior, red lines for natural prior. Dimensionful quantities are in GeV.

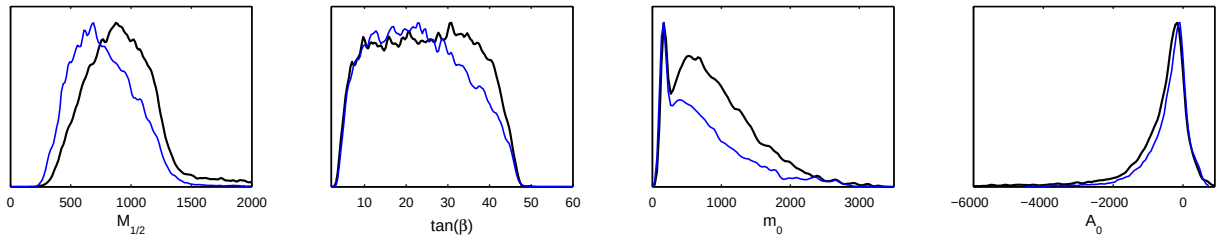

Figure 5.6: Same as Fig. 5.5 but for $\epsilon_H = -1$; black (blue) lines are for flat (natural) prior.

Finally note that throughout this work the squark and slepton mass matrices and A-terms are assumed to be diagonal. The issue of flavour-changing neutral currents due to non-diagonal terms arising in the full flavoured case [65, 103] is left for Section 6.

5.2.1 Results for universal soft terms

Here the model parameters to scan over are universal gaugino and sfermion mass parameters $M_{1/2}$ and m_0, a universal trilinear coupling A_0, and $\tan\beta$. In addition there are the two discrete parameters $\text{sign}(\mu)$ and ϵ_H. We choose $\mu > 0$ as favoured by $\text{BR}(b \to s\gamma)$ and run ten chains with 10^6 iterations each, for both $\epsilon_H = +1$ and -1, allowing $M_{1/2}$ to vary from 0 to 2 TeV, m_0 from 0 to 5 TeV, A_0 within ± 10 TeV and $\tan\beta$ from 2 to 60.

Figure 5.5 shows the marginalized 1D posterior probability distributions of the input parameters comparing flat (in black) to natural (in red) prior. The case of $\epsilon_H = -1$ is shown in Fig. 5.6. As can be seen, in both cases the naturalness prior results in a pull towards smaller masses and smaller $\tan\beta$. The general features, which are detailed below, however remain the same.

$M_{1/2}$ is bounded from below by the Higgs and SUSY mass limits, and from above by the requirement of sufficient neutralino annihilation. The processes that bring the neutralino relic density within the desired range are A) or B) from above: coannihilation with sleptons ($\tilde{e}_R$, $\tilde{\mu}_R$, or $\tilde{\tau}_1$) or annihilation through the Higgs funnel. On the other hand, we do not find

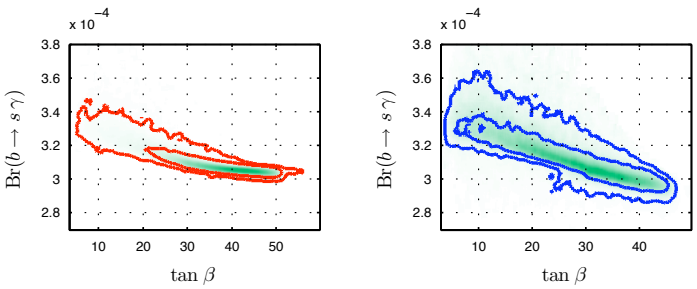

Figure 5.7: Contours of 68% and 95% probability in the BR($b \to s\gamma$) versus $\tan\beta$ plane, on the left for $\epsilon_H = +1$, on the right for $\epsilon_H = -1$. The green shading maps the average likelihood per bin, normalized to the maximum likelihood.

any region where the LSP higgsino fraction is large enough to render processes C) efficient. Coannihilation with stops or sbottoms is also absent. For $\epsilon_H = +1$ it becomes difficult to achieve small enough $|m_A - 2m_{\tilde{\chi}_1^0}|$ and $m_{\tilde{l}} - m_{\tilde{\chi}_1^0}$ when $m_{\tilde{\chi}_1^0} \gtrsim 750 - 800$ GeV. For $\epsilon_H = -1$ this is the case when $m_{\tilde{\chi}_1^0} \gtrsim 600$ GeV.

The relic density constraint also prefers higher $\tan\beta$, for which the Higgs funnel is more efficient. This is the reason for the preference of high $\tan\beta$ in the distribution for $\epsilon_H = +1$ and flat prior (which is still softened by the natural prior). High values around $\tan\beta \sim 50$ are constrained by BR($b \to s\gamma$) becoming too low. For $\epsilon_H = -1$, the $\tan\beta$ distribution is more flat because the BR($b \to s\gamma$) constraint becomes effective earlier as $\tan\beta$ grows. These correlations are illustrated in Fig. 5.7.

Regarding the m_0 probability distribution, the peak at low m_0 is where coannihilation with sleptons takes place. Slepton coannihilation, and with it the low m_0 peak, becomes more relevant when using the natural prior because of its preference for smaller $\tan\beta$ for which the Higgs funnel is less efficient. Overall, however, the annihilation through the pseudoscalar resonance is by far the dominant mechanism: for $\epsilon_H = +1$ and flat (natural) prior, 88% (83%) of the points exhibit predominantly annihilation into $b\bar{b}$, while 10% (15%) predominantly show coannihilation with sleptons. For $\epsilon_H = -1$, the A resonance is more difficult to hit, partly because $\tan\beta$ is smaller, so that for flat (natural) prior 22% (26%) of the points predominantly show slepton coannihilation.

As opposed to the CMSSM there is no "focus point" behaviour in this scenario: The m_0 distribution shows a clear preference for lower values $\lesssim 2$ TeV, and m_0 is significantly correlated with μ. In fact the CMSSM focus point hinges on having a single parameter which governs the scalar soft masses for both Higgs and matter fields. This is clearly not the case in DHMM models.

Finally, the A_0 distribution confirms our discussion of the sign correlations in Section 5.1.

An important issue in our considerations are the values of $m^2_{H_{1,2}}$, μ and B_μ at the

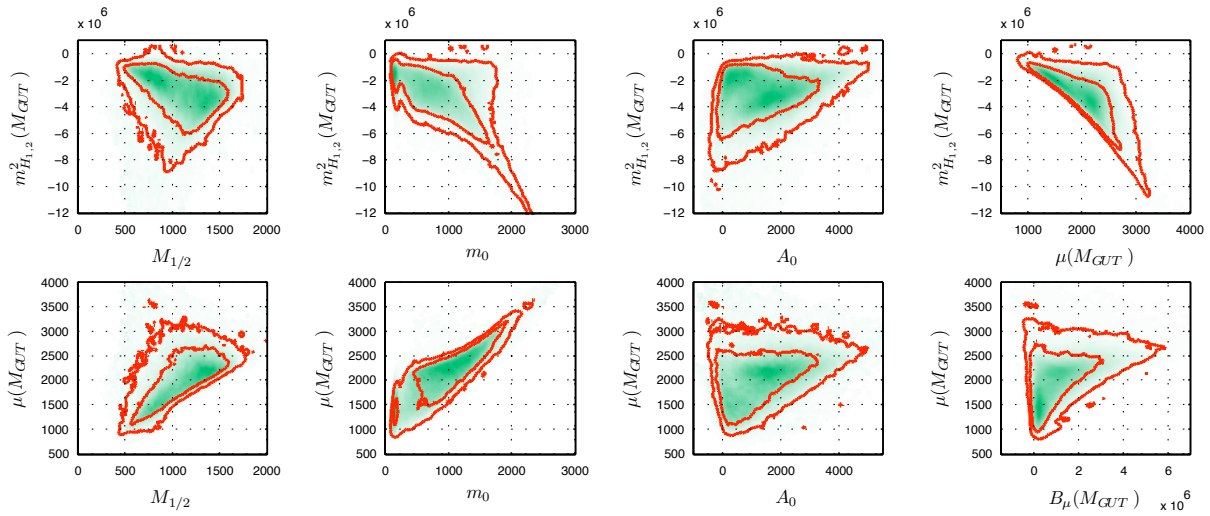

Figure 5.8: Contours of 68% and 95% probability showing correlations between $m^2_{H_{1,2}}$, μ, B_μ and the input parameters for universal soft terms, $\epsilon_H = +1$ and flat prior.

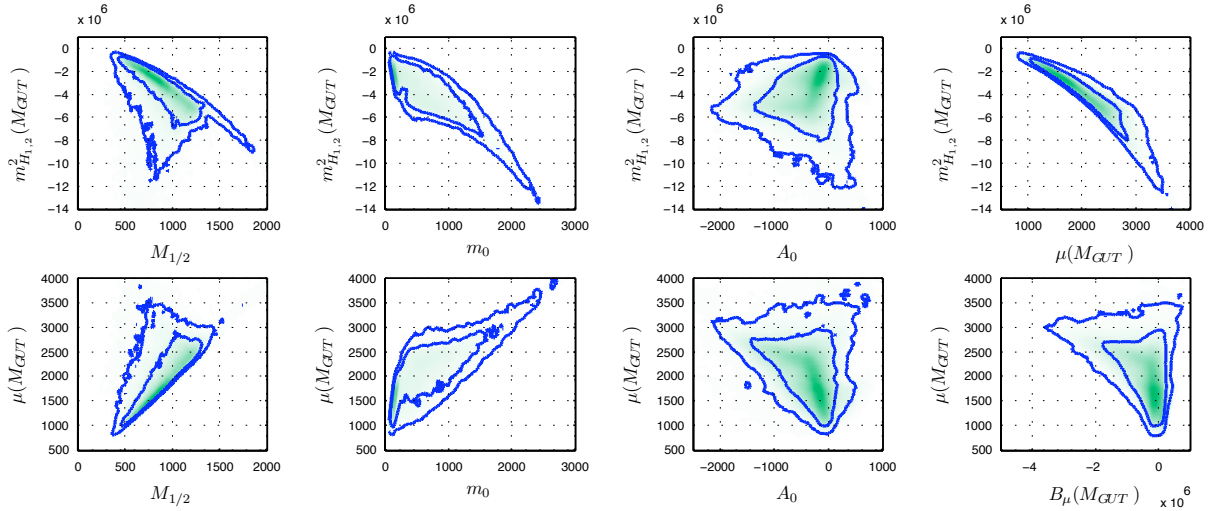

Figure 5.9: Same as Fig. 5.8 but for $\epsilon_H = -1$.

GUT scale resulting from the DHMM condition. In Figs. 5.8 and 5.9 we therefore show 2D posterior probability distributions for these parameters.[4] The tight correlation between $m^2_{H_{1,2}}$ and μ is clearly visible. Moreover, as can be seen, for both $\epsilon_H = \pm 1$ small $|m^2_{H_{1,2}}|$ and $|\mu|$ prefers small values of $M_{1/2}$, m_0 and $\epsilon_H A_0$.

Regarding consequences for experiments, Figs. 5.10 and 5.11 show 1D posterior probability distributions for SUSY and Higgs masses. Also shown are the distributions for the LSP higgsino fraction f_H and the cross section for spin-independent direct detection $\sigma^{\rm SI}_{\chi p}$. The pull of the natural prior towards lighter masses and in particular towards smaller μ is again evident. We also note that most of the parameter space lies within reach of the LHC

[4]To limit the proliferation of figures we only show 2D distributions for flat prior; those for natural prior look very similar.

at 14 TeV centre-of-mass energy. In fact, for $\epsilon_H = +1$ (-1) and flat prior, 82% (97%) of the points have gluino and squark masses below 3 TeV. Moreover, 55% (58%) of these points have sleptons that are lighter than the $\tilde{\chi}_2^0$, so that a same-flavour opposite-sign dilepton signal from $\tilde{\chi}_2^0 \to \tilde{\ell}^{\pm}\ell^{\mp} \to \ell^{\pm}\ell^{\mp}\tilde{\chi}_1^0$ may be visible in SUSY cascade decays (if decays into sleptons are absent or kinematically suppressed, then $\tilde{\chi}_2^0 \to h\tilde{\chi}_1^0$ is the most important decay mode of $\tilde{\chi}_2^0$). For naturalness prior, 88% (99%) of the $\epsilon_H = -1$ points have gluino and squark masses below 3 TeV, with 64% of these featuring $m_{\tilde{e},\tilde{\tau}} < m_{\tilde{\chi}_2^0}$.

If the $\tilde{\chi}_2^0$ decay into sleptons is open, $\tilde{\chi}_2^0 \to \tilde{e}^{\pm}e^{\mp}, \tilde{\mu}^{\pm}\mu^{\mp}$ has up to about 40% branching ratio. It is however important to keep in mind that owing to the universality assumption, the typical mass ordering is $m_{\tilde{\tau}_1} < m_{\tilde{e}_R} < m_{\tilde{e}_L}$. Therefore $\tilde{\chi}_2^0 \to \tilde{\tau}_1^{\pm}\tau^{\mp}$ decays are often dominant.

Concerning direct dark matter detection, we note that because the LSP is always almost a pure bino, the neutralino scattering cross section on proton is typically of the order of $10^{-11} - 10^{-10}$ pb and hence beyond the reach of current experiments.

Finally, we observe that even with the natural prior the fine-tuning tends to be very large, of the level of per-mil, and points with $c < 100$, corresponding to less than 1% fine-tuning are difficult to obtain. Correlations of the finetuning measure c are illustrated in Fig. 5.12 for natural prior. The lowest fine-tuning occurs for small $M_{1/2}$, medium $\tan\beta \sim$ 20–30, $A_0 \sim 0$ and $m_0 \sim 1$ TeV, with μ being around 1.5–2 TeV.

5.2.2 Results for vanishing 1st/2nd generation soft terms

Let us now turn to the pattern of soft terms obtained from models such as the gauge-Higgs unification (GHU) model of Section 3.1. Here the first- and second-generation matter fields were localized on a brane and SUSY breaking was mediated by the radion, leading to vanishing 1st/2nd generation and non-universal 3rd generation soft terms. We will call this "GHU-like boundary conditions" in the following. The free parameters in this case are $M_{1/2}$, $\tan\beta$, and the third-generation soft terms m_{Q_3}, m_{U_3}, m_{D_3}, A_t, A_b, m_{L_3}, m_{E_3}, A_τ. We allow $M_{1/2}$ to vary from 0 to 2 TeV, $\tan\beta$ from 2 to 60, $m^2_{Q_3,U_3,D_3}$ within ± 25 TeV^2, $m^2_{L_3,E_3}$ from 0 to 4 TeV^2, and $A_{t,b,\tau}$ within ± 10 TeV.

The marginalized 1D posterior probability distributions of the input parameters are displayed in Fig. 5.13 for $\epsilon_H = +1$ and in Fig. 5.14 for $\epsilon_H = -1$. Analogously, Figs. 5.15 and 5.16 show the probability distributions of masses, μ parameter, LSP higgsino fraction, and the spin-independent LSP scattering cross section on protons.

Two important differences to the case of universal soft terms are that $M_{1/2}$ can now go to much higher values, and that $\tan\beta$ peaks around 10. The reason is on the one hand that due to the no-scale boundary conditions for the 1st/2nd generation, coannihilation with selectrons and smuons becomes more likely; this is mainly relevant for $m_{\tilde{\chi}_1^0} \lesssim 500$ GeV.

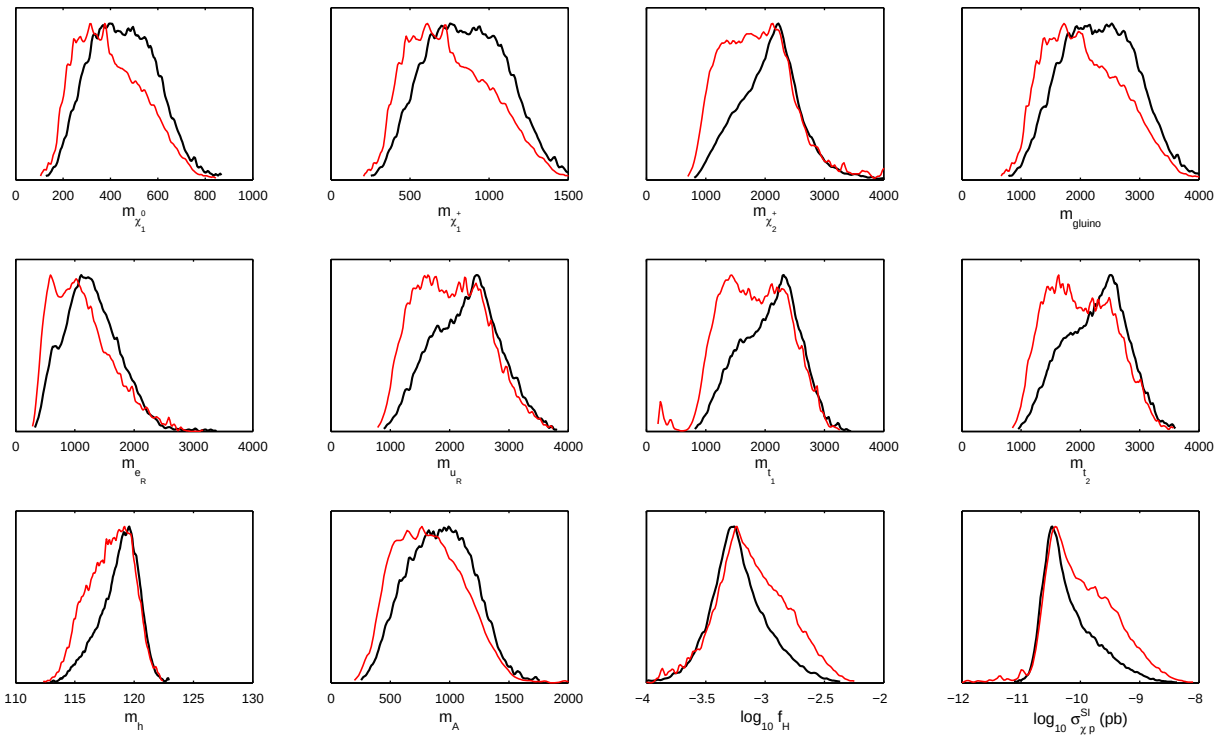

Figure 5.10: Posterior probability distributions of the most relevant masses for universal soft terms and $\epsilon_H = +1$. The bottom-right plots show the LSP higgsino fraction, $f_H := |N_{13}|^2 + |N_{14}|^2$, and the spin-independent scattering cross section on protons. As above, black lines are for flat and red lines for natural prior.

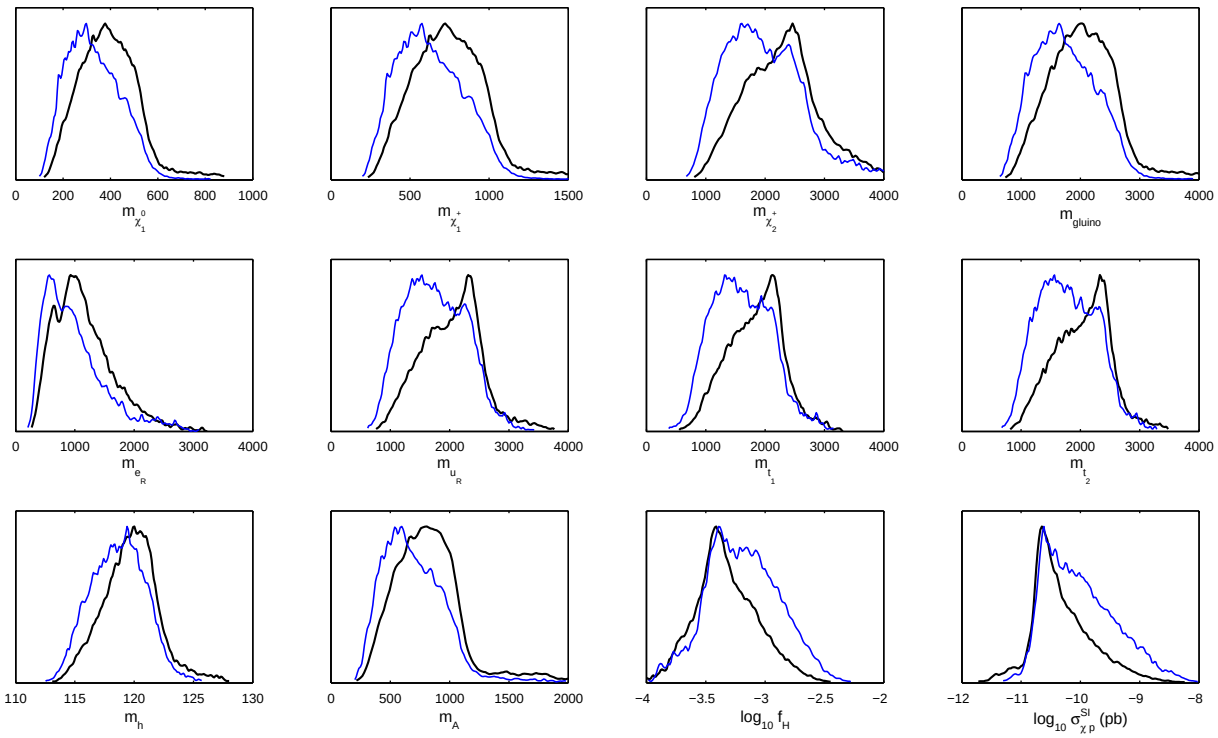

Figure 5.11: Same as Fig. 5.10 but for $\epsilon_H = -1$; black (blue) lines are for flat (natural) prior.

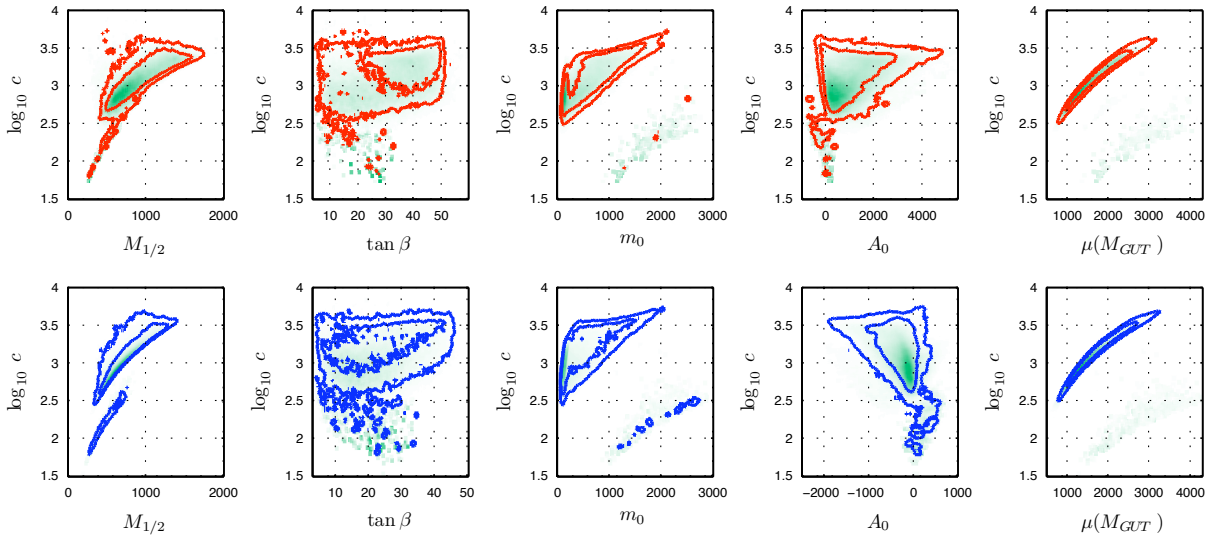

Figure 5.12: 2D posterior probability distributions of the fine-tuning measure c for natural prior. The contours enclose regions of 68% and 95% probability. The top row (red contours) is for $\epsilon_H = +1$, the bottom row (blue contours) for $\epsilon_H = -1$.

Accordingly, there are distinct peaks at $m_{\tilde{\chi}_1^0} \approx 400$ GeV in Figs. 5.15 and 5.16, corresponding to the peaks at $M_{1/2} \approx 900$ GeV in Figs. 5.13 and 5.14. On the other hand, due to the non-universal 3rd generation we can obtain smaller values of μ, and hence processes C) become important. This is mainly relevant for heavy $\tilde{\chi}_1^0$ and leads to the peak at large $M_{1/2}$ for $\epsilon_H = +1$. For $\epsilon_H = -1$, μ tends to be larger (*i.e.* f_H tends to be smaller) and consequently the high $M_{1/2}$ region is less favoured. Besides, for both $\epsilon_H = \pm 1$, we find some coannihilation with $\tilde{b}_1$ and/or $\tilde{t}_1$, though this is diminished by the naturalness prior. (For $\epsilon_H = -1$, this leads to the peak at large negative m_{D_3}, which gives light $\tilde{b}_1 \sim \tilde{b}_R$, c.f. Fig. 5.16. Coannihilation with $\tilde{t}_1$ is less frequent, in particular for $\epsilon_H = +1$, as the Higgs mass bound pushes the stop masses up.)

Concerning collider phenomenology, we first observe that, because of the vanishing 1st/2nd generation soft terms, the $\tilde{\chi}_2^0 \to \tilde{\ell}^\pm \ell^\mp \to \ell^\pm \ell^\mp \tilde{\chi}_1^0$ decay, with $\ell = e$ or μ, is almost always present. Staus are heavier and hence much less important for the $\tilde{\chi}_2^0$ decays. Second, for $\epsilon_H = -1$, squark and gluino masses peak around 2 TeV, which means that the LHC at 14 TeV centre-of-mass energy has again a very good discovery potential over most of the parameter space. More precisely, 88% of the $\epsilon_H = -1$ points have $m_{\tilde{q},\tilde{g}} \leq 3$ TeV. For $\epsilon_H = +1$, on the other hand, we find that a considerable fraction of the parameter space lies beyond the reach of the LHC. In this region the $\tilde{\chi}_1^0$ is heavy and is very likely to have a large higgsino fraction (since we require $\Omega h^2 \sim 0.1$). In turn this leads to a large cross section for direct dark matter detection of up to around 10^{-7} pb, see the bottom right plot in Fig. 5.15: Interestingly, this is just at the edge of current CDMS-II exclusion limit [153] for heavy masses.[5] The 2D probability distributions in the plane $\sigma_{\chi p}^{\rm SI}$ versus $m_{\tilde{\chi}_1^0}$

[5]While we have not used constraints from direct dark matter searches in the MCMC, a posteriori it

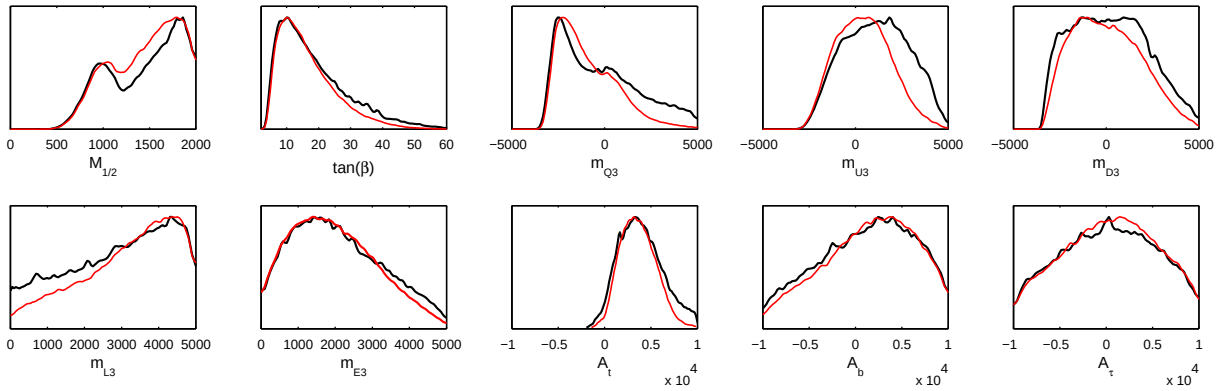

Figure 5.13: Marginalized 1D posterior probability distributions of the input parameters for GHU-like boundary conditions and $\epsilon_H = +1$. Black lines are for flat prior, red lines for natural prior. Dimensionful quantities are in GeV.

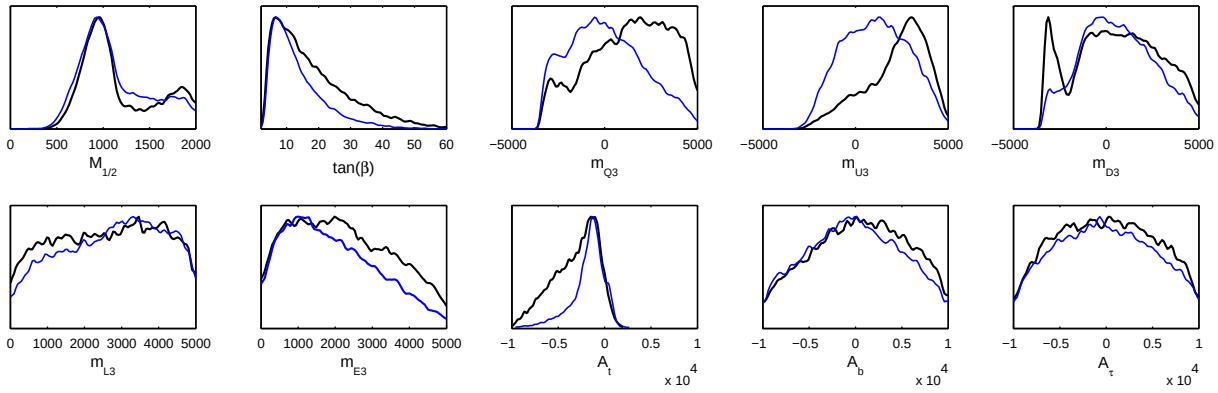

Figure 5.14: Same as Fig. 5.13 but for $\epsilon_H = -1$; black (blue) lines are for flat (natural) prior.

are shown in Fig. 5.17 for the natural prior. It is very gratifying that these models can be experimentally tested with complimentary methods, by both LHC and direct dark matter searches.

For completeness, Figs. 5.18 to 5.21 show various parameter correlations in 2D. It is interesting to see that $m^2_{H_{1,2}}(M_{\rm GUT}) = 0$ is easily obtained for $\epsilon_H = +1$, but does not occur for $\epsilon_H = -1$. Moreover, the sign correlation between ϵ_H, B_μ and A_t discussed in Section 5.1 is evident.

turns out that only about 1% of the points with higgsino LSP violate the current limits.

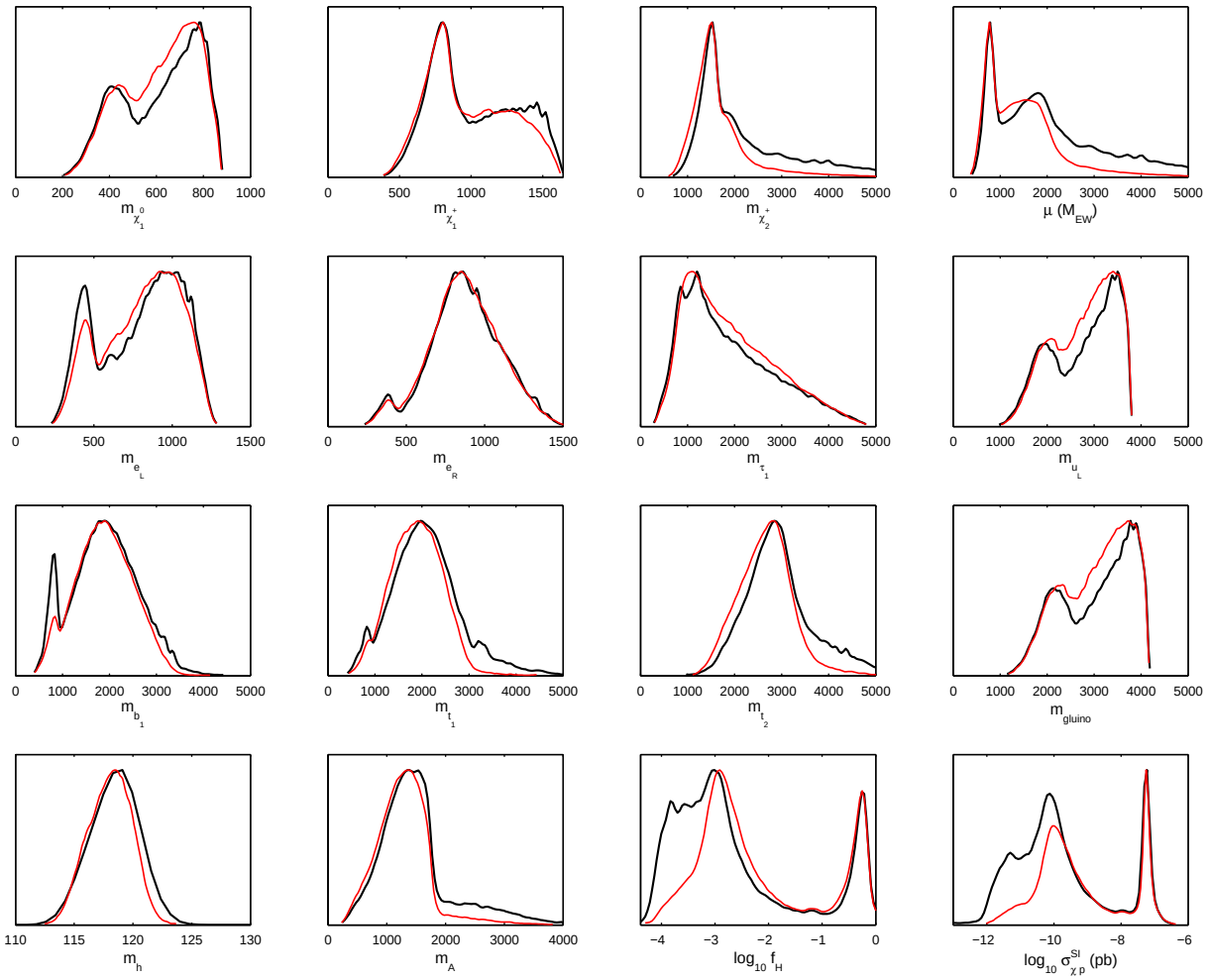

Figure 5.15: Posterior probability distributions of the most relevant masses, $\mu(M_{\rm EW})$, LSP higgsino fraction, and the spin-independent LSP scattering cross section on protons for GHU-like boundary conditions with $\epsilon_H = +1$. As above, black lines are for flat and red lines for natural prior.

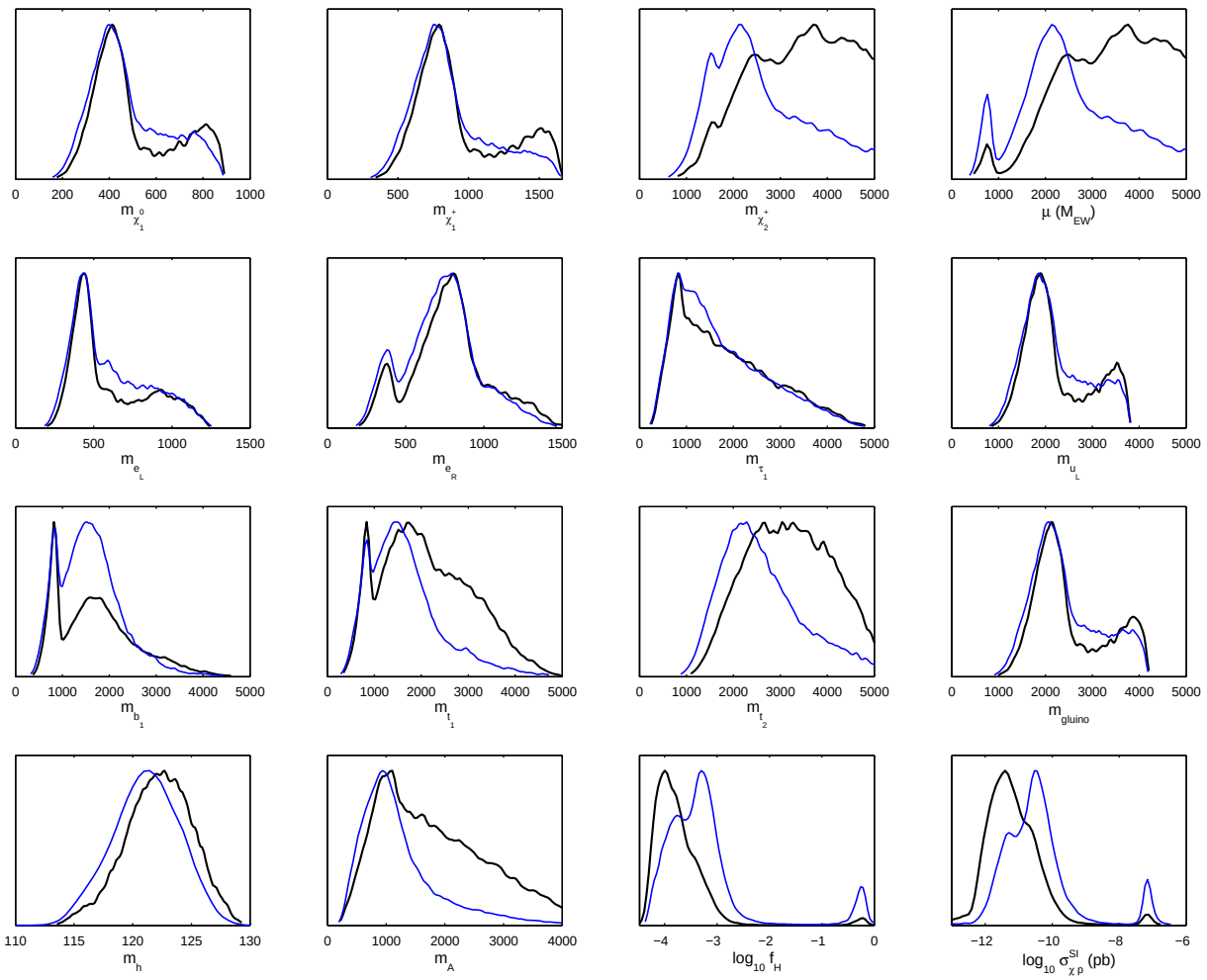

Figure 5.16: Same as Fig. 5.15 but for $\epsilon_H = -1$; black (blue) lines are for flat (natural) prior.

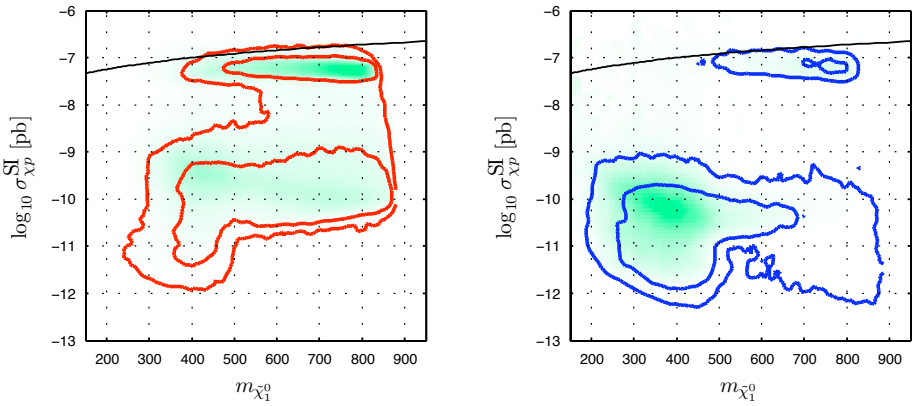

Figure 5.17: Probability distributions in the plane $\sigma^{\rm SI}_{\chi p}$ versus $m_{\tilde{\chi}^0_1}$ for naturalness prior, on the left for $\epsilon_H = +1$, on the right for $\epsilon_H = -1$. The inner (outer) contours enclose regions of 68% (95%) probability, the green shading maps the average likelihood, and the black lines show the limit from CDMS-II, which is currently providing the strongest bound in this mass range.

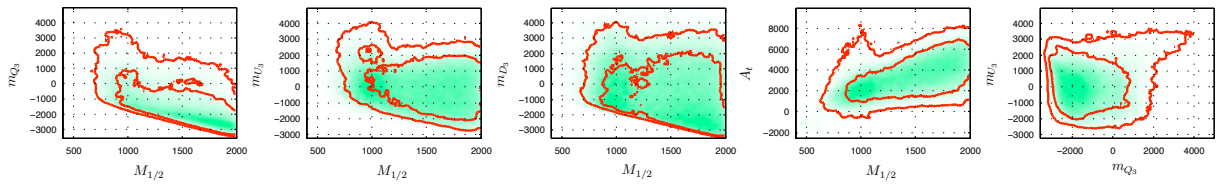

Figure 5.18: Contours of 68% and 95% probability showing correlations between the most relevant input parameters for GHU-like boundary conditions, $\epsilon_H = +1$ and naturalness prior.

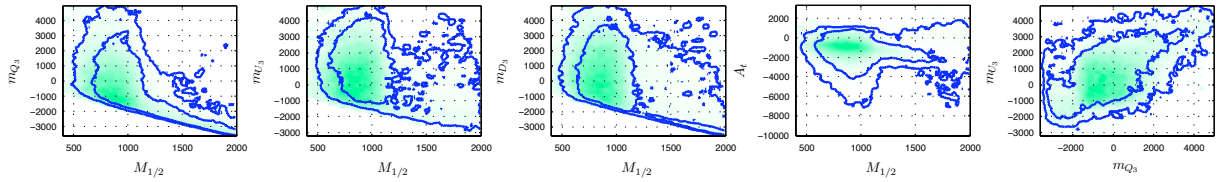

Figure 5.19: Same as Fig. 5.18 but for $\epsilon_H = -1$.

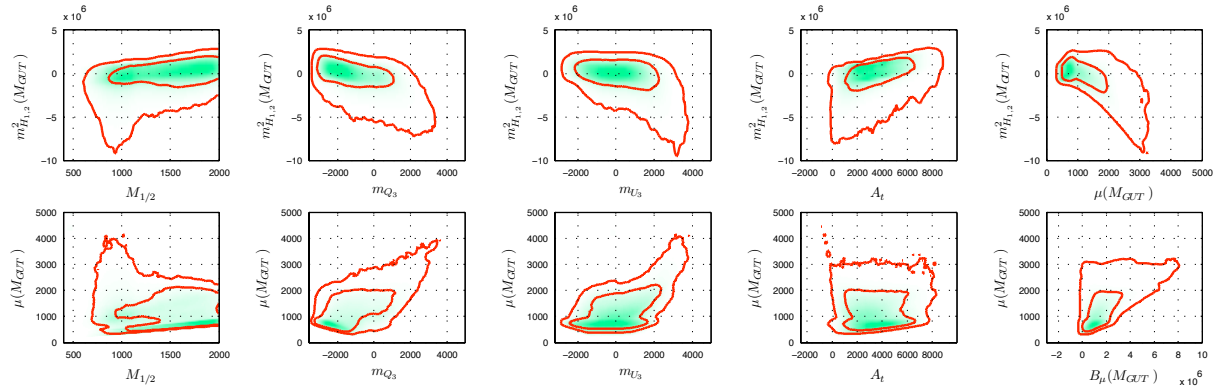

Figure 5.20: Contours of 68% and 95% probability showing correlations between $m^2_{H_{1,2}}$, μ, B_μ and the most relevant input parameters for GHU-like boundary conditions, $\epsilon_H = +1$ and naturalness prior.

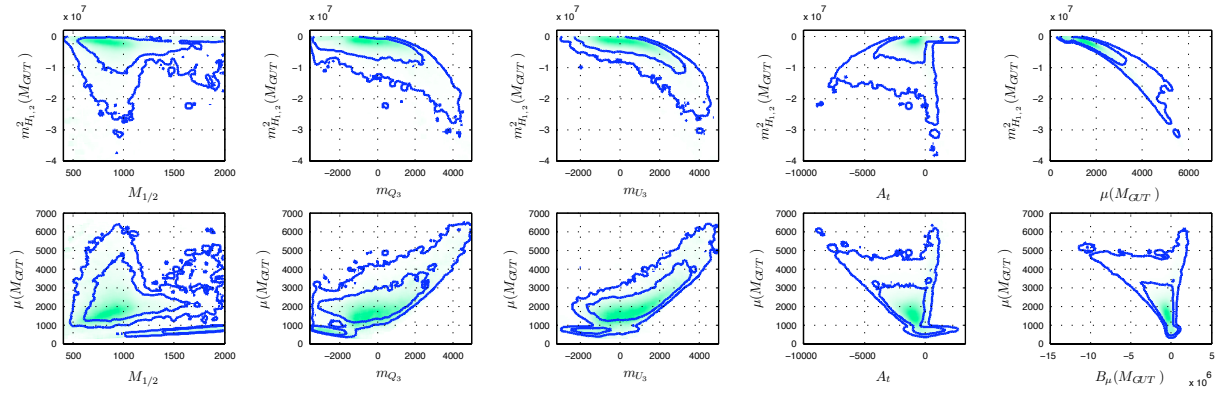

Figure 5.21: Same as Fig. 5.20 but for $\epsilon_H = -1$.

5.3 Conclusions

Among the many possible embeddings of the MSSM into a grand-unified theory, there are some interesting classes of models which predict a degenerate GUT-scale Higgs mass matrix. We have investigated the origin of this prediction in some example high-scale models, as well as its consequences for low-scale mass spectra and phenomenology.

With the additional assumption of universal GUT-scale gaugino masses (which is valid in most simple GUT scenarios) the low-energy spectrum still depends sensitively on the sfermion soft terms. Different high-scale models will give rise to various patterns of sfermion masses and trilinear terms. We have chosen to investigate two representative cases in detail: first, universal sfermion soft terms, and second, vanishing soft terms for the first two generations but non-vanishing and non-universal ones for the third. Both these cases are well motivated from the GUT model building point of view.

We explained how the remaining independent high-scale parameters are constrained by the requirement of realistic electroweak symmetry breaking and a sufficiently large Higgs mass. We also briefly compared with the related CMSSM and NUHM scenarios. Finally we presented a detailed parameter scan using Markov Chain Monte Carlo methods, highlighting the preferred ranges of parameters as well as correlations between them.

Our analysis shows that models with degenerate Higgs mass matrix can be viable UV-completions of the MSSM for large ranges of gaugino and sfermion soft terms. They are, however, already strongly constrained by direct Higgs and SUSY searches, flavour physics, and cosmology (as is the MSSM as a whole). In particular, the need to evade the LEP Higgs mass bound leads to preferred sparticle masses in the TeV range. This implies large fine-tuning in obtaining the correct electroweak scale (see Appendix C for a comment on the interpretation of fine-tuning). Another stringent constraint arises from the dark matter relic density: In the models we considered, the neutralino relic density is generically larger than the observed value, so rather special parameter values are necessary in order to enhance the neutralino annihilation cross section.

Nevertheless, we find $\Omega h^2 \simeq 0.1$ over a large part of the parameter space. This is mainly due to Higgs funnel annihilation, a large $\tilde{\chi}_1^0$ higgsino fraction, or coannihilation with sleptons. In the case of universal sfermion soft terms, the Higgs funnel is clearly the most important process. Here it is worth noting that the shapes of the 1D posterior probability distributions are more or less generated by just demanding correct EWSB, with the other constraints adding little to the shapes. In other words, the EWSB condition already selects the parameters such that most of the low energy observables are of roughly the correct magnitude, with exception of the relic density. It is then mainly the relic density constraint that helps shape the likelihood maps, and this reshaping can be understood in terms of the different (co-)annihilation channel contributions. The global features of the probability distributions are also quite robust against the fine-tuning prior.

Most of the parameter space lies within the reach of LHC at 14 TeV. In the region which is most difficult for the LHC to access, the LSP is higgsino-like and spin-independent direct dark matter detection experiments should soon see a signal. Should the MSSM with degenerate Higgs mass matrix be realized in nature, it will therefore almost certainly be observed within the next few years. This naturally raises the question of model discrimination: Can we look for a piece of experimental evidence pointing more or less uniquely to DHMM models? Unfortunately it seems to us that there is no such "smoking gun" signature for this kind of scenario. LHC may be able to exclude our models, but even if, conversely, an MSSM spectrum compatible with DHMM was found, it would need a future linear collider to accurately measure the sparticle masses and make a bottom-up reconstruction of the GUT-scale structure feasible.

However, even if it is not possible to do a full bottom-up reconstruction, one can still test the DHMM hypothesis against a non-DHMM scenario, using Bayesian model discrimination, taking into account all data available. The Bayes factor, in such a situation of "nested-model comparison", takes a simplified form usually called Savage-Dickey density ratio (see [154] and references therein). Note that this idea enters in a more general "program" of testing GUT hypothesis at the LHC. By combining LHC data with other measurements, it may be possible to get crucial insights on GUT scale physics. This could include testing the hypothesis of gaugino masses universality, or of universal Higgs soft masses for example. A work along that line was initiated in the Les Houches PhysTeV 2009 Workshop, with a contribution published in [155].

Résumé de la section

Dans cette Section, nous analisâmes de façon générique les conséquences phénoménologiques d'un MSSM doté d'une matrice de Higgs dégénérée à l'échelle de Grande Unification. Nous nous concentrâmes sur deux scénarios bien motivés du point de vue de la construction de modèle : un scénario avec termes scalaires de brisures universels, comme dans le CMSSM, et un scénario dans lequel seul les termes scalaires de troisième génération sont importants. Cette analyse fut réalisée en utilisant l'inférence Bayesienne, à l'aide de Chaînes de Markov pour échantilloner et marginaliser les densités de probabilités postérieures. Bien que de nombreuses régions de l'espace des paramètres eusses satisfaite toutes les contraintes expérimentales, il apparut qu'il n'y avait pas de signatures caractérisant de façon unique ces modèles à matrice de Higgs dénénérée. Toutefois, un travail de discrimination est envisageable en combinant les données et en utilisant la comparaison Bayesienne de modèle

Chapter 6

The supersymmetric flavour problem in holographic grand unification

In this Chapter, we investigate the low-energy implications of the HGU framework, with a particular emphasis on flavour physics. Even if we focus on HGU for concreteness, this analysis should be sufficiently broad to cover any 5D models which explains flavour hierarchy by wave-function localization, with the Higgses and SUSY breaking localized on the same brane. The results obtained should generalise, at least qualitatively, to any such model (for example those constructed in [156]). This chapter is largely based on [157].

In Section 6.1, we will first remind what is the SUSY flavour problem, and which solutions are available. Section 6.2 is devoted to our approach of the problem in HGU, including assumptions, parameterization and treatment of matrix anarchy. In Section 6.3, we first discuss constraints on the parameter space, then implications for LHC phenomenology, which are splitted into a radion dominated regime and a mixed brane-radion regime.

6.1 The SUSY flavour problem

The soft breaking part of the MSSM Lagrangian defined in Eq. (1.17) contains SUSY breaking trilinear couplings and masses for all sfermions associated to the SM fermions. These soft masses, as well as trilinear terms once $\mathrm{SU}(2)_L$ is broken, contribute to the sfermion mass matrices denoted $\mathcal{M}^{u,d,l}$. The indexes u, d, l stands respectively for up squark, down squark and charged slepton matrices. Unless these sfermion masses be rather heavy, it turns out that arbitrary entries in these matrices can induce large flavour changing neutral currents (FCNCs), like flavour-violating lepton or meson decays, or neutral meson mixing, in conflict with observations. In fact, in the basis where the up, down and charged lepton yukawa couplings are diagonal (the superCKM basis, see e.g. [158]), any non-diagonal entry in the sfermion mass matrices potentially induces flavour changing processes. The

magnitude of these contributions can be roughly estimated using the dimensionless quantities $\delta^x_{IJ} = \mathcal{M}_{IJ}/\sqrt{\mathcal{M}_{II}\mathcal{M}_{JJ}}$. While flavour violation is often studied at the level of these mass insertions δ^x_{IJ}, we will rely in our study on the exact (one or two-loop) calculation of the flavour violating processes. Indeed, it turns out that the mass insertion approximation itself, as well as the bounds on the δ^x_{IJ} computed in the literature, can be rather crude, particularly in the lepton sector.

There are several way out this SUSY flavour problem, that we will now briefly discuss.

Decoupling An omnipresent solution is to make the scalar superpartners heavier, such that their effects decouple from the Standard Model processes. This solution, however, increases the little hierarchy problem, which is already present due to the tension between the electroweak and TeV scales.

Alignment Another solution to the SUSY flavour problem is to make the soft masses and trilinear coupling proportional to the identity matrix 1_3. This appears in particular if the mediation of SUSY breaking is flavour-blind, for example in the case of gauge mediation. This property is taken as ad-hoc hypothesis in popular models like the CMSSM.

Special structure Finally, one can also give to the scalar soft terms a peculiar structure, generated by an underlying mechanism, such that they do not induce large unobserved FCNCs. In particular, an attractive possibility is to consider that the mechanism giving the hierarchical structure to the SM sector (described in Section 1.7) also structures the scalar soft terms. Such a framework is called "flavourful supersymmetry" in [156, 159, 160].

This is that last possibility which is realized in the HGU framework. In the 5D picture, the mechanism generating flavour hierarchy is wave-function localization, with the Higgses localized on the IR brane. With radion mediation or an IR-brane source of SUSY breaking, the soft SUSY breaking terms will also be sensitive to matter fields localization, and will have roughly the same structure as Yukawa couplings. Note that even if we focus our analysis on the HGU framework, this flavour-oriented study is generalizable, at least qualitatively, to other models with same features of localization and SUSY breaking.

The soft supersymmetry breaking terms are derived in Subsection 3.2.4. Their definition is given in the Lagrangian Eq. (1.17).

6.2 Parameterisation

As we showed in Section 3.2.4, if SUSY breaking is dominated by brane sources alone, then the gaugino masses will be relatively suppressed (to the extent that naive dimensional

analysis is valid). In order to pass the constraints on chargino and gluino searches, the remaining soft terms would then have to be in the multi-TeV range. This scenario is clearly disfavoured on from the naturalness point of view, and would probably be impossible to probe at the LHC. Furthermore, large a-terms and soft masses as predicted NDA tend to lead to tachyonic sfermions in the low-energy spectrum. On these grounds we will dismiss the possibility that soft terms are induced by brane sources alone, and instead focus on the case where radion mediation gives a significant contribution.

However, if the soft terms are exclusively generated by radion mediation and brane sources can be entirely neglected, we do not find realistic electroweak symmetry breaking. In fact previous analyses [90,99] have shown that it is difficult to reconcile minimal radion-mediated scenarios with a GUT-scale degenerate Higgs mass. While more refined scenarios [92, 99] can give realistic TeV-scale physics, in our case the Higgs sector is subject to the even stronger condition Eq. (3.70), which turns out to be too restrictive. This property is due to the fact that brane soft masses cannot be induced by the supergravity background, i.e $F^T/2R$ or F^φ, at tree level, and does not depend on the details of the model.

In short, radion mediation is necessary to provide sizeable gaugino masses, while brane sources are necessary to avoid vanishing Higgs soft masses. We will therefore study the general case where both sources of supersymmetry breaking are present. Their relative importance will evidently depend on the relative size of $F^T/2R$ and F^Z/M_*. It will also depend on $\tan\beta$, since we will determine the c parameters from the Yukawa couplings which are fixed by $\tan\beta$ and the known fermion masses, and the soft masses depend on the c_i.

The phenomenologically most problematic soft terms are the trilinear a-terms originating from brane-localised SUSY breaking. Note that these are enhanced over the other soft terms according to the NDA analysis of Section 3.2.4. Large a-terms lead not only to large flavour violation but also to tachyonic third-generation sfermions; we find that to avoid this, the brane contribution should be subdominant with respect to the radion-mediated contribution,

$$\frac{F^Z}{M_*} \lesssim 0.2\,\frac{F^T}{2R}\,. \tag{6.1}$$

Even with this condition satisfied, anarchic a-terms still tend to induce unacceptably large flavour violation – unless, again, the overall scale of SUSY breaking is unnaturally large. We therefore choose to set the brane trilinear term of Eq. (3.58) to zero, which is justified if the SUSY breaking fields on the brane are charged under some symmetry (for a comprehensive discussion see e.g. [156, 160]).

To now investigate supersymmetric flavour violation, we decompose the brane-induced soft mass matrices into a hierarchical part which depends on the c-parameters and an $\mathcal{O}(1)$

part:

$$m^2_{x\,ij,\text{brane}} = 4\pi \left|\frac{F^Z}{M_*}\right|^2 \kappa^x_{ij}\, \lambda^{m^2_x}_{ij} \qquad (x = U, D, Q, E, L)\,, \tag{6.2}$$

where $\lambda^{m^2_x}_{ij}$ are dimensionless hermitian matrices with $\mathcal{O}(1)$ entries. Recall that κ^x_{ij} was defined as

$$\kappa^x_{ij} = \frac{6\pi^2}{M_*} \frac{f^x_i\, f^x_j}{\left(\mathbf{Y}^x_i\, \mathbf{Y}^x_j\right)^{1/2}} \tag{6.3}$$

with f^x_i and $\mathbf{Y}^x_i$ as in Eqns. (3.30) and (3.40). Similarly, we write the Yukawa matrices y_{ij} as

$$\begin{aligned} y^u_{ij} &= \frac{6\pi^2}{M_*} \frac{f^u_i\, f^q_j}{\left(\mathbf{Y}^u_i\, \mathbf{Y}^q_j\right)^{1/2}}\, \lambda^u_{ij}, \\ y^d_{ij} &= \frac{6\pi^2}{M_*} \frac{f^d_i\, f^q_j}{\left(\mathbf{Y}^d_i\, \mathbf{Y}^q_j\right)^{1/2}}\, \lambda^d_{ij}, \\ y^e_{ij} &= \frac{6\pi^2}{M_*} \frac{f^e_i\, f^l_j}{\left(\mathbf{Y}^e_i\, \mathbf{Y}^l_j\right)^{1/2}}\, \lambda^e_{ij}\,. \end{aligned} \tag{6.4}$$

Here $\lambda^{u,d,e}_{ij}$ are dimensionless $\mathcal{O}(1)$ matrices. Such a parameterisation can be applied to any model which predicts the Yukawa matrices to be hierarchical, with power-suppressed entries, up to a priori unknown anarchical $\mathcal{O}(1)$ coefficients. Examples include, besides our wave function localisation scheme, also Froggatt-Nielsen type models.

Even though the structure of the Yukawa matrices is dominated by the hierarchical part, it is important to take also the anarchical λ-coefficients properly into account. An adequate framework for this is Bayesian statistics. We will treat the λ-parameters as random variables with associated probability density functions (PDFs) $f(\lambda)$. The choice of PDF reflects our theoretical bias (for instance, that all matrix entries should be $\mathcal{O}(1)$), so this PDF represents a "prior", in the usual Bayesian vocabulary. The predictions of the model, such as masses or low-energy observables, will then also be probability density functions. In particular, this approach will enable us to compute Bayesian credibility intervals, the equivalent of confidence intervals in the frequentist approach.

We restrict ourselves to real couplings since the CP problem is not the subject of our study. We also neglect the neutrino sector, because it would induce additional model dependence. We focus on lepton flavour violation in the charged lepton sector, where the constraints are most stringent [20]. The wave-function suppression factors f^X_i, and consequently the hierarchy structure, are determined by the six 5D bulk mass parameters $c_{\mathcal{T}_i}$ and $c_{\mathcal{F}_i}$ as described in Section 3.2. In addition to these, the following unknown $\mathcal{O}(1)$ flavour coefficients enter the analysis: Five symmetric 3×3 matrices $\lambda^{m^2_X}$ for the squark and slepton masses in Eq. (6.2), a symmetric Yukawa coefficient matrix λ^U, and two unconstrained 3×3 Yukawa coefficient matrices $\lambda^{D,E}$ in Eq. (6.4); or a total of 54 additional parameters.

In the Standard Model subsector, we have the six c-parameters and the 24 Yukawa coefficients $\lambda_{ij}^{U,D,E}$. On the other hand, the experimental observables are the nine Standard Model fermion masses and the three CKM angles. Simply setting all $|\lambda_{ij}^{U,D,E}| = 1$ and adjusting the six $c_{\mathcal{T}_1}$, $c_{\mathcal{T}_2}$, $c_{\mathcal{T}_3}$, $c_{\mathcal{F}_1}$, $c_{\mathcal{F}_2}$, $c_{\mathcal{F}_3}$ would not reproduce the Standard Model data with reasonable accuracy, so some deviation of the $\lambda_{ij}^{U,D,E}$ parameters from unity is clearly needed. However, allowing all 24 $\lambda_{ij}^{U,D,E}$ to vary and attempting a full Bayesian analysis would require us to take into account the entire SUSY model, because of SUSY threshold corrections to the Yukawa couplings. This would be computationally very involved, and the results rather unwieldy. Instead we will take a simplified approach, which still allows us to extract the essential information.

To quantify matrix anarchy, we allow the $|\lambda_{ij}|$ to vary independently within the range

$$|\lambda_{ij}| \in [1/\mathscr{L}, \mathscr{L}]\,, \tag{6.5}$$

where $\mathscr{L} \geq 1$ is a constant which is universal for all $|\lambda_{ij}|$. With logarithmic weighting, the prior PDF is

$$f(\log|\lambda_{ij}|) = U(-\log\mathscr{L}, \log\mathscr{L})\,, \tag{6.6}$$

$U(a,b)$ being the uniform distribution on the interval $[a,b]$. We also allow the signs of the λ_{ij} to be independently ± 1 (subject to certain restrictions; see below). As stated above, to satisfy the experimental constraints at some reasonable level of precision (e.g., 1σ–3σ), a minimum $\mathscr{L} > 1$ denoted by $\mathscr{L}_{\min}$ is necessary.

We also need to take experimental uncertainties into account. Each MSSM observable has an associated experimental PDF f_{ex}, characterizing the uncertainty with which it is measured. On the other hand, any MSSM observable can be expressed in terms of our model parameters λ_{ij}, which for any given $\mathscr{L}$ defines its theoretical PDF $f_{\mathscr{L}}$. The combination of these two PDFs gives the total PDF for any given observable.[1]

For each independent experimental constraint (or equivalently, each independent observable), there is now a a characteristic value of $\mathscr{L}$, denoted by $\mathscr{L}^*$, above which the total PDF is dominated by $f_{\mathscr{L}}$. This happens when f_{ex} and $f_{\mathscr{L}}$ have roughly the same width. Taking the f_{ex} to be normal distributions of variance σ_{ex}^2, with GUT-scale propagated errors from [161], we estimate the $\mathscr{L}^*$ associated to each constraint to be $\log\mathscr{L}^* \sim \sigma_{\text{ex}}$. While this is only a rough estimate, it will be sufficient for our purposes.

The constraints with the largest $\mathscr{L}^*$ correspond to those that are the "hardest to fulfill" (i.e. to observables that are the hardest to fit). For a given constraint, once $\mathscr{L} \geq \mathscr{L}^*$, its

[1] In the present situation, the PDFs are combined simply by convolution. For example, the top Yukawa coupling is given by $y_t = |\lambda_{33}^U| e^{-2\pi k R(c_{\mathcal{T}_3} - 1/2)}$ to leading order (cf. Appendix D), hence $-\pi k R(c_{\mathcal{T}_3} - 1/2) = (\log y_t - \log|\lambda_{33}^U|)/2$. The PDF of $\log y_t - \log|\lambda_{33}^U|$ is the convolution of the $\log y_t$ and $\log|\lambda_{33}^U|$ PDFs, in other words, of $f_{\text{ex}}(\log y_t)$ and $f_{\mathscr{L}} = U(-\log\mathscr{L}, \log\mathscr{L})$. The λ_{ij} can be regarded as nuisance parameters, the parameter of interest being $c_{\mathcal{T}_3}$. For the other couplings, the $f_{\mathscr{L}}$ are more complicated because the dependence on the λ_{ij} is more involved (see Appendix D).

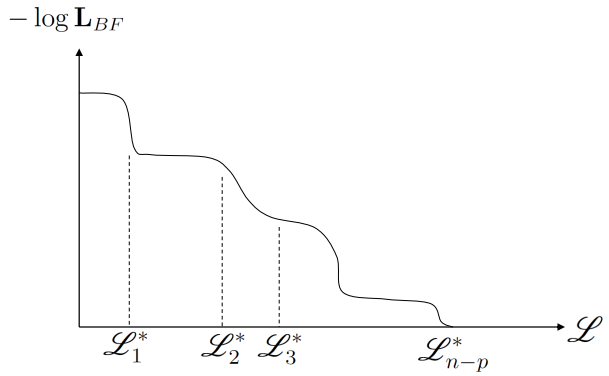

Figure 6.1: Logarithm of the likelihood of the best fit point, $-\log \mathbf{L}_{\rm BF}$ as a function of $\mathscr{L}$, for a fit involving n constraints and p parameters. The constraints weaken and eventually decouple as $\mathscr{L}$ increases. The fit becomes perfect, i.e. $-\log \mathbf{L}_{\rm BF} = 0$, once only p of the n constraints remain.

width (dominated by $f_{\mathscr{L}}$) increases with $\mathscr{L}$, which makes the constraint easier to fulfill, until it effectively decouples from the fit. In a fit involving n constraints and p parameters, whose best-fit point has likelihood $\mathbf{L}_{\rm BF}$, the quantity $-\log \mathbf{L}_{\rm BF}$ will decrease as $\mathscr{L}$ increases. The fit becomes perfect, with $-\log \mathbf{L}_{\rm BF} = 0$, once only p of the n constraints remain. This is illustrated in Figure 6.1.

These observations can be used to determine $\mathscr{L}_{\rm min}$ as follows. We first perform a fit involving the six c-parameters, and the seven constraints with largest $\mathscr{L}^*$. This gives a best-fit point with likelihood $\mathbf{L}_{\rm BF} < 1$. Using the PDF of the seventh constraint, we can then deduce the value of $\mathscr{L}$ necessary to increase $\mathbf{L}_{\rm BF}$ until the required level of precision is reached. This value of $\mathscr{L}$ gives $\mathscr{L}_{\rm min}$, provided that the constraints which were previously not taken into account can also be satisfied with this $\mathscr{L}$. If one of these constraints is not satisfied, we repeat the procedure, including this additional constraint in the fit.

The estimation of $\mathscr{L}_{\rm min}$ depends on the precision required to fulfill the constraints. It also depends on the running of the Yukawa couplings, which in turn depends on $\tan\beta$ and on threshold corrections. Finally, the estimation depends on the efficiency of finding the best fit point. We estimate $\mathscr{L}_{\rm min}$ to be

$$\mathscr{L}_{\rm min} = 1.2 - 1.5\,. \tag{6.7}$$

The value $\mathscr{L}_{\rm min} = 1.2$ is obtained for a fit with 3σ of precision[2], while the value $\mathscr{L}_{\rm min} = 1.5$ corresponds to a more conservative 1σ fit. It is reasonable to also impose an upper bound on $\mathscr{L}$, our starting point being that the λs should all be $\mathcal{O}(1)$, but this bound is of course much less rigorously defined. In the analysis of Section 6.3, $\mathscr{L}$ will be allowed to vary within the range

$$\mathscr{L} \in [1.2,\, 3]\,. \tag{6.8}$$

[2]More precisely, we recquire the normalized χ^2 to be smaller than 9.

Flavour matrix anarchy is an essential ingredient in our framework, so $\mathscr{L}$ can in a sense be regarded as a model parameter which measures the allowed deviation from the superimposed hierarchical structure.

Finally, to determine the c-parameters we use the constraints with largest $\mathscr{L}^*$, which turn out to be the quark Yukawa couplings. The $c_{\mathcal{T}_i}$ are then deduced from the expressions given in Appendix D, subsection D.2. The $c_{\mathcal{F}_i}$, on the other hand, are not hierarchical, $c_{\mathcal{F}_1} \simeq c_{\mathcal{F}_2} \simeq c_{\mathcal{F}_3}$, so they cannot be determined from the analytic expressions for the down-type Yukawa couplings. We therefore set $c_{\mathcal{F}_1} = c_{\mathcal{F}_2} = c_{\mathcal{F}_3} \equiv c_{\mathcal{F}}$, with $c_{\mathcal{F}}$ determined by the bottom Yukawa coupling. We have checked that this choice does not sensitively influence the mass spectrum, the mixings, or the rates of flavour violating processes.

We close this Section with some remarks on the signs of the λ_{ij}. In the limit $\mathscr{L} \to 1$, such that all λ_{ij} are ± 1, some sign combinations give rise to accidental cancellations when rotating to the mass eigenstate basis, by which one or two of the fermion masses vanish exactly. For instance, if all $\lambda_{ij} = +1$ then there is only one mass eigenstate with nonzero mass. When ultimately taking $\mathscr{L} > 1$, the corresponding masses will acquire widespread, $\mathscr{L}$-dependent PDFs. For greater predictivity we thus restrict our analysis to sign combinations which are non-singular in the limit $\mathscr{L} \to 1$.

Furthermore, we expect the y^d and y^e Yukawa matrices to obey GUT relations at the level of signs. This is because all Yukawa couplings originate on the IR brane, where SU(6) is broken only spontaneously. Higher-dimensional operators involving some powers of $\langle \Sigma \rangle$ can lead to violation of the GUT relations, but the leading contributions which determine the signs are given by the SU(6)-symmetric second term in Eq. (3.29), which implies sign $\left(\lambda^d_{ij}\right) =$ sign $\left(\lambda^e_{ji}\right)$. The same argument holds for soft masses in the $\mathcal{T}$ and $\mathcal{F}$ sector, that is sign $\left(m^2_{Q\,ij}\right) =$ sign $\left(m^2_{U\,ij}\right) =$ sign $\left(m^2_{D\,ij}\right)$ and sign $\left(m^2_{L\,ij}\right) =$ sign $\left(m^2_{E\,ij}\right)$.

6.3 Results

We are finally in a position to describe our numerical analysis. The dominant flavour constraint comes from the lepton sector, more precisely from BR($\mu \to e\gamma$), as is the case for many other SUSY GUT models – see for instance [162]. The lepton sector comprises 21 relevant λ-parameters, 9 from the Yukawa matrix and 6 each from the soft mass matrices m^2_E and m^2_L. The soft terms in the quark sector have negligible influence on BR($\mu \to e\gamma$), so these are all the λ-parameters which need to be fixed.

Despite the fact that $\mathscr{L}$ should be larger than $\mathscr{L}_{\min}$ in order to fit the Standard Model, we initially set $\mathscr{L} = 1$, so the only variables are the signs of the $\lambda_{ij} = \pm 1$. There are $3 \cdot 2^{13}$ physically inequivalent relevant sign combinations: By field redefinitions one can choose five of the signs in the Yukawa coefficients λ^E_{ij} to be positive, and of the remaining 16 combinations, only 6 lead to non-vanishing fermion masses for all three generations.

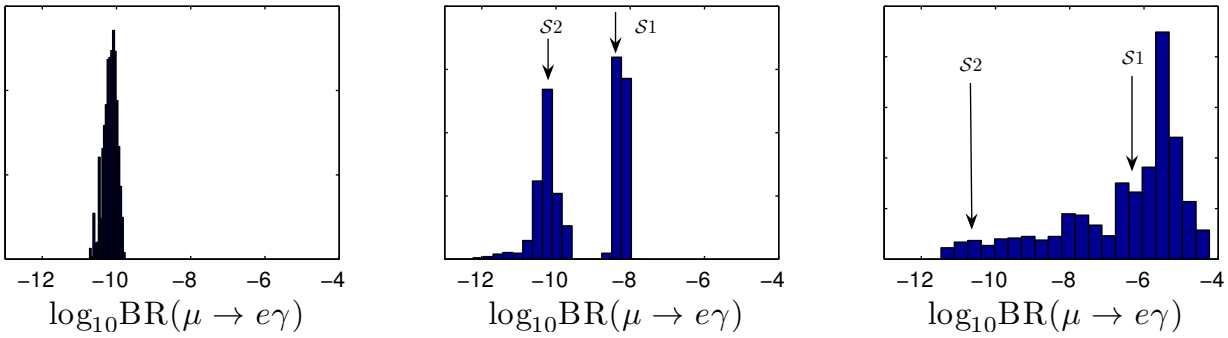

Figure 6.2: Distributions of $\mathrm{BR}(\mu \to e\gamma)$ for all permissible sign combinations in the λ matrices at $\mathscr{L} = 1$. The model parameters are $F^T/2R = F^Z/M^* = 1500$ GeV, and $\tan\beta = 5$, 10, 30 (from left to right). The current experimental bound is $\mathrm{BR}(\mu \to e\gamma) < 1.2 \cdot 10^{-11}$ [163]. The arrows indicate the positions of two benchmark sign combinations S1 and S2 used later in our analysis.

Six independent signs in each $\lambda_{ij}^{m_E^2}$ and $\lambda_{ij}^{m_L^2}$ can be chosen independently, hence we have $6 \cdot 2^6 \cdot 2^6 = 3 \cdot 2^{13} = 24576$ combinations. We first scan over these sign combinations while keeping $\mathscr{L} = 1$, and subsequently allow for $\mathscr{L} > 1$.

For any given $\tan\beta$, the c-parameters are now determined as described in Section 6.2. For any given scale of radion-mediated SUSY breaking $F^T/2R$ and of brane-source mediated SUSY breaking F^Z/M_*, the soft terms at the GUT scale are calculated from Eqns. (3.68)–(3.70), (3.72), and (6.2). The sparticle mass spectrum, mixing matrices, and low-energy flavour observables are computed using `SPheno3` [106], appropriately modified to handle, in particular, the DHMM condition Eq. (3.66).

Figure 6.2 shows some sample distributions for $\mathrm{BR}(\mu \to e\gamma)$ at $\mathscr{L} = 1$ for various $\tan\beta$. At low $\tan\beta$, the dominant contribution to $\mathrm{BR}(\mu \to e\gamma)$ comes from the trilinear term a^E. By assumption, the trilinears are induced only by radion mediation and so do not depend on the λ-parameters. This explains why in the left panel of Fig. 6.2 the value of $\mathrm{BR}(\mu \to e\gamma)$ is hardly sensitive to the sign combination. By contrast, at large $\tan\beta$, a^E and the brane soft masses $m^2_{E\,\mathrm{brane}}$, $m^2_{L\,\mathrm{brane}}$ (defined in Eq. (6.2)) give comparable contributions to $\mathrm{BR}(\mu \to e\gamma)$. Since these depend on the $\lambda_{ij}^{m_E^2}$ and $\lambda_{ij}^{m_L^2}$, the distributions span a much wider range at large $\tan\beta$.

To also allow for $\mathscr{L} > 1$, and hence for a good Standard Model fit, we choose two benchmark sign combinations in the λ matrices, which we denote by S1 and S2 (indicated by arrows in Fig. 6.2). Explicitly, we have

$$\lambda^E = \begin{pmatrix} + & + & + \\ + & + & - \\ + & - & - \end{pmatrix}, \qquad \lambda^{m_E^2} = \begin{pmatrix} + & + & + \\ + & + & + \\ + & + & + \end{pmatrix}, \qquad \lambda^{m_L^2} = \begin{pmatrix} + & + & + \\ + & + & + \\ + & + & + \end{pmatrix} \tag{6.9}$$

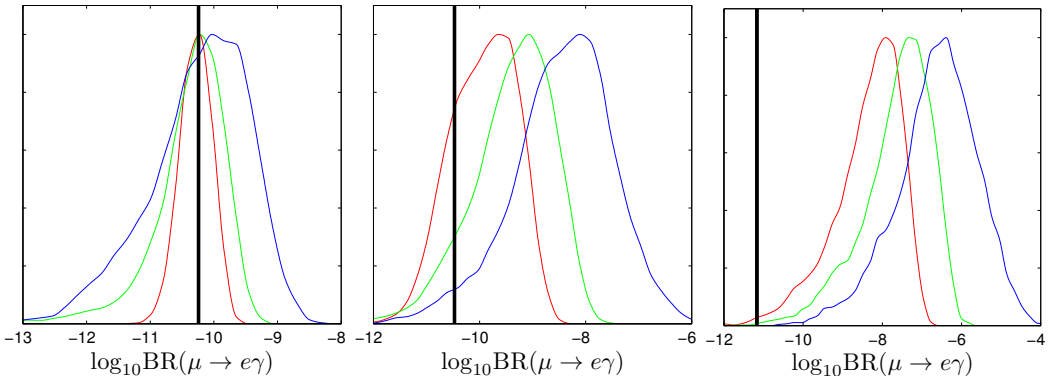

Figure 6.3: Probability density functions of $\mathrm{BR}(\mu \to e\gamma)$ for the sign combination S2, with $F^T/2R = F^Z/M_* = 1500$ GeV, and $\tan\beta = 5$, 10, 30 from left to right. The red, green, blue lines correspond to $\mathscr{L} = 1.2$, 1.5, 3 respectively, with the vertical black lines showing the values at $\mathscr{L} = 1$. Radion mediation dominates at $\tan\beta = 5$, while the brane source dominates at $\tan\beta = 30$. The PDFs are normalized to have the same maximum.

for S1, and

$$\lambda^E = \begin{pmatrix} + & + & + \\ + & + & - \\ + & - & + \end{pmatrix}, \qquad \lambda^{m_E^2} = \begin{pmatrix} + & + & + \\ + & + & + \\ + & + & + \end{pmatrix}, \qquad \lambda^{m_L^2} = \begin{pmatrix} + & + & + \\ + & + & + \\ + & + & + \end{pmatrix}. \quad (6.10)$$

for S2. As is evident from Fig. 6.2, with the sign combination S2 the $\mu \to e\gamma$ decay rate is suppressed even for large $\tan\beta$, whereas the S1 point exhibits increasingly large flavour violation. We then scan several values of $\tan\beta$, $F^T/2R$, and F^Z/M_* for these two sign combinations, and allow the $|\lambda_{ij}|$ to deviate from 1. The values of the $|\lambda_{ij}|$ are drawn from their prior defined by Eq. (6.6).

Figure 6.3 shows a typical example for the sign combination S2 and $F^T/2R = F^Z/M_*$, such that a^E (i.e. radion mediation) dominates at low $\tan\beta$, and brane soft masses dominate at large $\tan\beta$. In this case, $\mathrm{BR}(\mu \to e\gamma)$ is suppressed at large $\tan\beta$. One can also see that the width of the PDF increases with $\mathscr{L}$ as expected. Note, moreover, that at large $\tan\beta$, where the brane contribution dominates, the mean value of the PDF is shifted towards larger values when increasing $\mathscr{L}$. The reason for this $\mathscr{L}$-dependent shift is that certain cancellations occur between the brane contributions for this sign combination in the limit $\mathscr{L} \to 1$. At low $\tan\beta$, where radion mediation dominates, this effect is less important.

Regardless of the chosen sign combination, when radion mediation dominates, the $\mathrm{BR}(\mu \to e\gamma)$ constraint is weakened by at least an order of magnitude, depending on $\mathscr{L}$. By contrast, when the brane-induced soft terms dominate, there are large contributions to $\mathrm{BR}(\mu \to e\gamma)$.

In Figs. 6.4 and 6.5 we show the lower bounds on $\mathrm{BR}(\mu \to e\gamma)$, given by 95% Bayesian credibility intervals (BCIs), for various $\mathscr{L} \geq \mathscr{L}_{\min}$. Figure 6.4 is for combination S1, while Fig. 6.5 is for combination S2. For any given value of $\mathscr{L}$, the red regions to the right of the

corresponding $\mathscr{L}$-line pass the experimental constraints.[3] In the left panel, where radion mediation dominates, the bound on $F^T/2R$ is weakened by a factor 2–3 when increasing $\mathscr{L}$. Since we have $M_{1/2} \sim F^T/2R$, the gluino mass is typically $m_{\tilde{g}} \sim 2\,(F^T/2R)$ due to RG running. Moreover, squark masses are dominated by the gluino contribution to their RGEs, so we have $m_{\tilde{q}} \approx m_{\tilde{g}}$. Therefore, the weakening of the BR($\mu \to e\gamma$) bound opens a part of the parameter space which is relevant for the production of SUSY particles at the LHC.

We conclude from Figs. 6.4 and 6.5 that there are regions of the parameter space which pass the flavour constraints, and where SUSY particles are within discovery reach [164] at the LHC. ATLAS and CMS searches with about 1 fb^{-1} of data at 7 TeV already put lower limits on gluino and squark masses of roughly $m_{\tilde{g},\tilde{q}} \gtrsim 1$ TeV for $m_{\tilde{q}} \simeq m_{\tilde{g}}$ [165, 166]. It is worthwhile noting that in our case the BR($\mu \to e\gamma$) constraint [4] forces the SUSY spectrum to be heavy, generically beyond the current LHC limits. In that sense the most severe constraints on our class of models still originate from flavour precision experiments, rather than from direct superpartner searches.

At this point a comment is in order concerning the effects of subdominant flavour constraints. The next-to-dominant constraint turns out to be BR($\mu \to 3e$), which is strongly correlated to BR($\mu \to e\gamma$), such that a weakening of the latter weakens also the former. We do not show this or other subdominant constraints here, since little would be gained by taking them into account.

Production cross sections at the LHC are very similar to those of the mSUGRA case with $m_{\tilde{q}} \approx m_{\tilde{g}}$, and can be characterized by the gluino–squark mass scale, see e.g. [168]. At $m_{\tilde{g},\tilde{q}} \approx 1$, 2 and 3 TeV, the overall SUSY cross section is of the order of 1 pb, 10 fb and 1 fb, respectively. For $m_{\tilde{g},\tilde{q}} \approx 1$ TeV, the cross section is dominated by gluino–gluino, squark–squark and gluino–squark production. For heavier masses, $m_{\tilde{g},\tilde{q}} \approx$ 2–3 TeV, squark–squark and electroweak ino-ino (mainly $\tilde{\chi}_1^\pm \tilde{\chi}_2^0$) production dominate, while gluino production becomes negligible. However, interesting LHC signatures arise from the slepton mass patterns and mixings, leading to chargino/neutralino and slepton decays that are specific to the setup studied here.

Let us therefore next discuss details of the spectrum, of mixings, and of LHC phenomenology. Two cases will be distinguished. First, we will treat the case where the effects of F^Z/M_* in the scalar soft masses are negligible compared to those of $F^T/2R$. In this scenario, which we call radion dominated, the only effect of brane-localized SUSY breaking is to provide nonzero Higgs soft masses. Since our model has a GUT-scale degenerate Higgs mass matrix, Eq. (3.66), it is convenient to fix the Higgs soft masses by this condition, and

[3] We consider $m_h > 114$ GeV and $m_h > 111$ GeV to account for the ~ 3 GeV theoretical uncertainty on the light Higgs mass.

[4] When submitting the paper [157], a new bound from the MEG experiment BR($\mu \to e\gamma$) $< 2.4 \cdot 10^{-12}$ was announced [167].

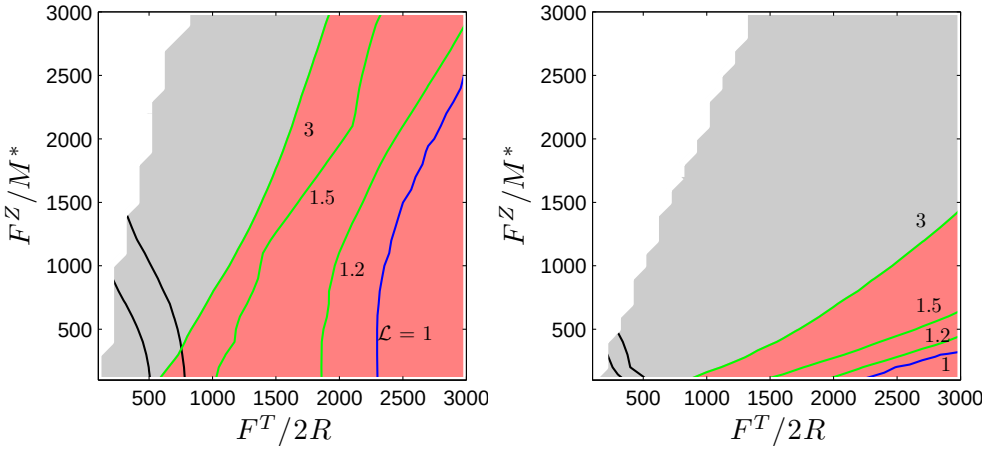

Figure 6.4: The dominant constraints in the $(F^T/2R,\ F^Z/M_*)$ plane for the sign combination S1, $\tan\beta = 5$ (left) and $\tan\beta = 30$ (right). $F^T/2R$ and F^Z/M_* are in GeV units. The black lines on the bottom left are $m_h = 111$ GeV and $m_h = 114$ GeV isolines. The blue lines show the BR$(\mu \to e\gamma)$ constraint for $\mathscr{L} = 1$, while green lines show 95% BCIs of the same constraint for $\mathscr{L} = 1.2$, 1.5, 3. The red regions, towards large $F^T/2R$, satisfy $m_h > 111$ GeV and BR$(\mu \to e\gamma) < 1.2 \cdot 10^{-11}$ for at least one value of $\mathscr{L}$. In the white regions, a too large F^Z/M_* leads to tachyonic sleptons.

to set F^Z/M_* to zero for the purposes of calculating sfermion soft terms. We have checked that a small F^Z/M_*, of the order of $\sim 0.02\,(F^T/2R)$, is sufficient to generate the necessary Higgs soft masses but has negligible effect in the sfermion sector.

Second, we will discuss the situation where the scalar soft masses receive contributions both from F^Z/M_* and from $F^T/2R$, which we call mixed brane–radion scenario. F^Z/M_* should be bounded from above, because it can induce tachyonic sleptons through RG running if it is too large, and because it can enhance BR$(\mu \to e\gamma)$ depending on the signs of the λ-parameters. This can also be seen in Figs. 6.4 and 6.5.

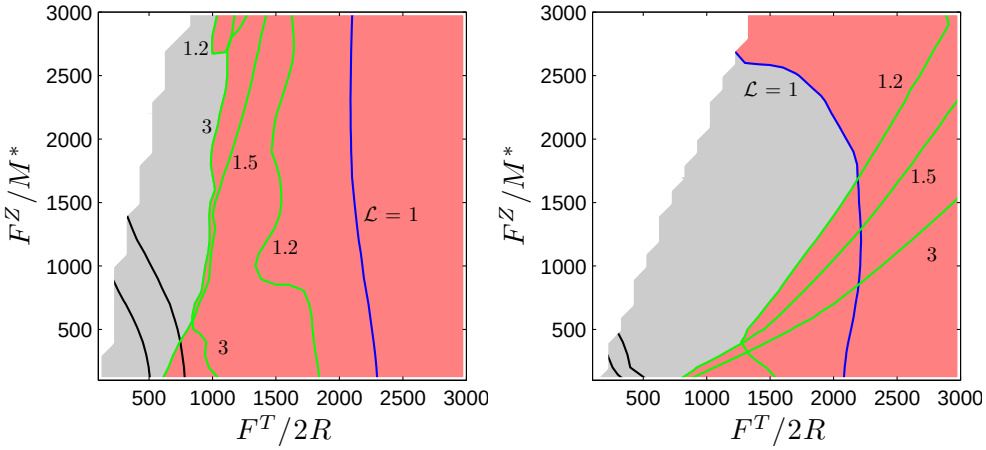

Figure 6.5: Same as Fig. 6.4 but for the sign combination S2.

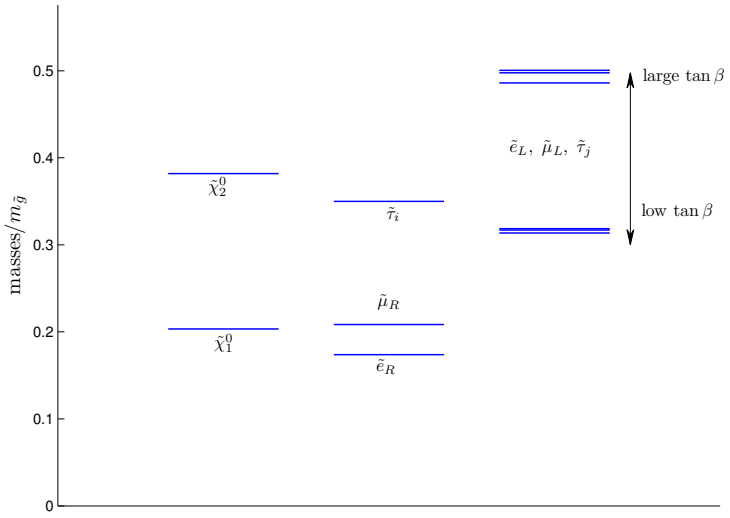

Figure 6.6: Spectrum of SUSY particles, normalized to the gluino mass, when radion mediation dominates. The lightest state is almost completely a right selectron $\tilde{e}_R$. The left-handed slepton masses increase with $\tan\beta$, due to the y^e enhancement (see text). For large $\tan\beta$ and large $\mathscr{L}$, the RGE effects of flavour anarchy cause the slepton mass PDFs to grow wider, except the one for $m_{\tilde{e}_R}$.

6.3.1 Radion dominated scenario

In the case where scalar soft terms are dominated by radion mediation, the effects of flavour matrix anarchy appear only in Yukawa couplings, not in the soft terms. In other words, the soft terms do not directly depend on the λ-parameters. They will be sensitive to flavour matrix anarchy, i.e to $\mathscr{L}$, only through RGE effects. The mass ordering depends mainly on $\tan\beta$, and is charted in Fig. 6.6. Here we denote the six slepton mass eigenstates $\tilde{l}_{1\ldots6}$ by their dominant components, for example $\tilde{l}_1 \sim \tilde{e}_R$, $\tilde{l}_2 \sim \tilde{\mu}_R$, and so forth. The $\tilde{l}_1 \sim \tilde{e}_R$ turns out to be the lightest state of the spectrum, followed by the lightest neutralino $\tilde{\chi}_1^0$ and the $\tilde{l}_2 \sim \tilde{\mu}_R$. The masses of left-handed sleptons and sneutrinos increase with $\tan\beta$. This is because, as $\tan\beta$ grows, the charged lepton Yukawa couplings y^e increase, so the c-parameters shrink and the corresponding soft terms are enhanced.

At small $\tan\beta$, the PDFs are strongly peaked at the values shown in Fig. 6.6. At large $\tan\beta$ and large $\mathscr{L}$ (about $1.5 \lesssim \mathscr{L} \lesssim 3$), the RGE effects of flavour anarchy widen the slepton mass PDFs, again due to the y^e enhancement at large $\tan\beta$. This effect is hierarchical: For the $m_{\tilde{\tau}}$ PDF it is larger than for the $m_{\tilde{\mu}_R}$ PDF, while $m_{\tilde{e}_R}$ shows almost no sensitivity. Typically, for $\tan\beta \geq 30$ and $\mathscr{L} \geq 1.5$, this uncertainty is large enough to flip the mass ordering of $\tilde{\mu}_R$ and $\tilde{\chi}_1^0$, and of $\tilde{\tau}_1$ and $\tilde{\chi}_2^0$. Other mass orderings are conserved.

A stable charged slepton as the lightest SUSY particle (LSP) is obviously excluded by cosmology. In particular it is not a suitable dark matter candidate. Dark matter could instead be composed of gravitinos $\widetilde{G}$, which are the LSP in many models of warped su-

persymmetry (such as the one in Appendix A), or of axinos $\tilde{a}$. In that case the $\tilde{e}_R$ decays as $\tilde{e}_R^\pm \to e^\pm + \text{LSP}$ (LSP $= \widetilde{G}$ or $\tilde{a}$). If this decay occurs at the epoch of Big Bang Nucleosynthesis (BBN) [169], $\tau(\tilde{e}_R) \gtrsim 1\,\text{sec}$, it can alter the yield of light elements. This poses important constraints in particular on the gravitino LSP case. In case of an axino LSP, the $\tilde{e}_R$ decay is much faster [170], so that BBN constraints can be evaded easily. A detailed discussion of this issue is beyond the scope of this paper; in the following we simply assume that $\tilde{e}_R$ is in fact the next-to-LSP and that its abundance and lifetime are small enough to evade cosmological constraints. Note, however, that even in the axino LSP case with $\tau(\tilde{e}_R) \ll 1\,\text{sec}$, the $\tilde{e}_R$ appears as a heavy stable charged particle [171] in collider experiments. For definiteness, we will refer to the $\tilde{e}_R$ as the "lightest massive particle" (LMP) in the following.

Let us now turn to LHC cascade decays. Gluinos and squarks, if produced, decay as $\tilde{g} \to q\tilde{q}_{R,L}$, $\tilde{q}_R \to q\tilde{\chi}_1^0$ ($\sim 100\%$), and $\tilde{q}_L \to q'\tilde{\chi}_1^\pm$ ($\sim 65\%$) or $q\tilde{\chi}_2^0$ ($\sim 30\%$). The $\tilde{\chi}_{1,2}^0$ and $\tilde{\chi}_1^\pm$ decay further, and the decay chains end with the $\tilde{e}_R$ LMP and an electron. If $m_{\tilde{\mu}_R} < m_{\tilde{\chi}_1^0}$, the $\tilde{\chi}_1^0$ can decay both as $\tilde{\chi}_1^0 \to \tilde{e}_R^\pm e^\mp$ and $\tilde{\chi}_1^0 \to \tilde{\mu}_R^\pm \mu^\mp$. The relative rate between the two decays is dictated by the ratio of mass splittings:

$$\frac{\text{BR}(\tilde{\chi}_1^0 \to \tilde{e}_R^\pm e^\mp)}{\text{BR}(\tilde{\chi}_1^0 \to \tilde{\mu}_R^\pm \mu^\mp)} \approx \left(\frac{m_{\tilde{\chi}_1^0}^2 - m_{\tilde{e}_R}^2}{m_{\tilde{\chi}_1^0}^2 - m_{\tilde{\mu}_R}^2} \right)^2 . \tag{6.11}$$

The $\tilde{\mu}_R$ decays dominantly through the three-body mode $\tilde{\mu}_R \to \tilde{e}_R e\mu$ via a virtual $\tilde{\chi}_1^0$. The decay width is typically of $\mathcal{O}(\text{keV})$, so there is no displaced vertex. (In principle the $\tilde{\mu}_R$ may also decay through the LFV mode $\tilde{\mu}_R \to \tilde{e}_R + Z$ if kinematically allowed, but this is suppressed by a very small coupling.) This contrasts with universal scalar mass scenarios, where the lightest slepton is typically the $\tilde{\tau}_1$. Observing an electron or a muon associated to the LMP instead of a τ at the end of the decay chains would therefore be a hint for non-universality in scalar lepton masses.

As mentioned, the $\tilde{e}_R$ LMP is stable inside the detector and behaves like a heavy muon. This can be triggered on in the muon chambers of the ATLAS and CMS experiments. The muon chambers also allow excellent track reconstruction and time of flight measurements with an accuracy of around 1 ns, which should allow to reconstruct the mass of the LMP with good precision [172]. Moreover, the rate of energy loss through ionization (dE/dx) may be used to identify the LMP and measure its properties [173]. Given this striking signature, Drell-Yan production of $\tilde{e}_R$, even with a low cross section, may be exploited. See [172] and references therein for more details.

A further, ambitious idea is to use a stopper detector to observe the LMP late decay [174]. With a sufficient number of events, flavour violating decays could be observed, and eventually used to gain some information on m_E^2. Since m_E^2 is hierarchical, it induces a hierarchical mixing between the right-handed sleptons. LFV processes are thus suppressed

by powers of the typical hierarchy factor $e^{-\pi kR} \equiv \epsilon$. In particular, one has roughly

$$\mathrm{BR}(\tilde{e}_R \to \mu \text{ LSP}) \,/\, \mathrm{BR}(\tilde{e}_R \to e \text{ LSP}) \sim \epsilon^2 \ .$$

Given that ϵ should be $\mathcal{O}(10^{-1})$ to reproduce the SM flavour hierarchy, if the branching ratio can be measured to 1% or better, this would provide a rough test for our scenario.

The features discussed above are generic for our class of models. Other aspects of LHC phenomenology depend on the precise mass ordering, which in turn depend on $\tan\beta$. In the following discussion we will therefore distinguish the cases of small and large $\tan\beta$. For concreteness we will use three representative scenarios, one with low $\tan\beta$, and two different configurations with large $\tan\beta$ (one featurimg $m_{\tilde{\chi}_1^0} < m_{\tilde{\mu}_R}$, the other $m_{\tilde{\chi}_1^0} > m_{\tilde{\mu}_R}$). The spectra for our canonical choice of $F^T/2R = 1.5$ TeV are given in Table 6.1. Since these points lie at the edge of the LHC discovery reach (total cross sections $\lesssim 1$ fb), we also provide in Table 6.2 an analogous set of points for $F^T/2R = 1$ TeV, which is more interesting for LHC studies. The complete SLHA files, including mass matrices and branching ratios, can be obtained from [175].

In these points, the GUT-scale soft mass m_L^2 has been set to a universal value for simplicity, see end of Section 6.2, whereas generically the left-handed lepton soft masses may differ by $\mathcal{O}(1)$ factors (they will, however, not be hierarchical since $c_{\mathcal{F}_1} \approx c_{\mathcal{F}_2} \approx c_{\mathcal{F}_3}$). A universal GUT-scale m_L^2 leads to small, RG-induced mass splittings between $\tilde{\mu}_L$ and $\tilde{e}_L$ of typically $\mathcal{O}(0.1\%)$, and somewhat larger mass splittings between $\tilde{e}_L/\tilde{\mu}_L$ and $\tilde{\tau}_1$ of $\mathcal{O}(5\%)$. This is relevant because, at low $\tan\beta$, the $\tilde{\chi}_2^0$ and $\tilde{\chi}_1^\pm$ are mostly wino and thus decay mostly into the left-handed sleptons $\tilde{e}_L$, $\tilde{\mu}_L$, $\tilde{\tau}_L$. The branching ratios of LFV decays are at most $\sim 10^{-3}$ in that case, and therefore irrelevant for LHC phenomenology.

The main features can be summarized as follows:

- The $\tilde{\chi}_2^0$ decays as $\tilde{\chi}_2^0 \to \tilde{\tau}_1^\pm \tau^\mp$ ($\sim$ 20–30%) or $\tilde{\chi}_2^0 \to \tilde{\mu}_L^\pm \mu^\mp / \tilde{e}_L^\pm e^\mp$ ($\sim$ 10–15% each); the rest goes into $\tilde{\nu}_i \nu_i$. The sleptons subsequently decay into $\tilde{\chi}_1^0 + e/\mu/\tau$, followed by the $\tilde{\chi}_1^0$ decay to the LMP, $\tilde{\chi}_1^0 \to \tilde{e}_R^\pm e^\mp$. The resulting signature is $\tilde{\chi}_2^0 \to l_i^\pm l_i^\mp e \tilde{e}_R$, i.e. same flavour opposite sign (SFOS) dileptons, plus an electron, plus the LMP which behaves like a heavy muon. There is no E_T^{miss}.

- The $\tilde{\chi}_1^\pm$ cascade decays via a charged slepton $\tilde{l}_L$ or sneutrino $\tilde{\nu}$ into $\tilde{\chi}_1^0 \tau^\pm \nu_\tau$ ($\sim$ 50–60%) or into $\tilde{\chi}_1^0 e^\pm \nu_e / \mu^\pm \nu_\mu$($\sim$ 20–25% each). The decay chain gives rise to dilepton signatures of $e + (e/\mu/\tau)$ with uncorrelated charges, plus the LMP, plus E_T^{miss} from the νs. This decay can be combined with the $\tilde{\chi}_2^0$ decay on the other branch.

- The masses of the sparticles appearing in the decay chains may be determined from kinematic distributions. The simplest observable is the endpoint of the SFOS dilepton invariant-mass distribution, $M_{ll}^{\max} = m_{\tilde{\chi}_2^0}(1 - m_{\tilde{l}}^2/m_{\tilde{\chi}_2^0}^2)^{1/2}(1 - m_{\tilde{\chi}_1^0}^2/m_{\tilde{l}}^2)^{1/2}$ from the $\tilde{\chi}_2^0$ decay.[5] For example, for point A', the M_{ll} endpoints are $M_{ee}^{\max} = 308.28$ GeV, $M_{\mu_\mu}^{\max} =$

[5] Note however the ambiguity in the channel with electrons, $\tilde{\chi}_2^0 \to \tilde{e}_L^\pm e^\mp \to \tilde{e}_R + 3e$.

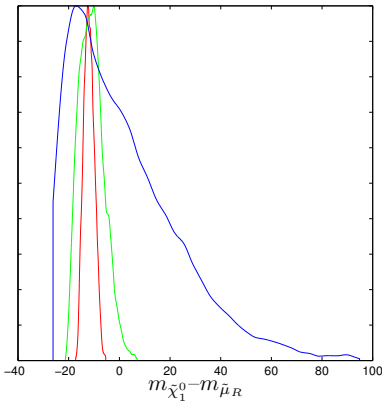

Figure 6.7: PDFs of $\tilde{\chi}_1^0$–$\tilde{\mu}_R$ mass difference, for $F^T/2R = 1500$ GeV and $\tan\beta = 30$. The red, green and blue lines are for $\mathscr{L} = 1.2$, 1.5 and 3, respectively.

308.61 GeV and $M_{\tau\tau}^{\max} = 373.28$ GeV. This may be used to obtain information on the masses of the three left-handed sleptons.

At the LHC, it will most likely be not possible to reconstruct the GUT scale parameters through a bottom-up evolution. However, neglecting muon and electron Yukawa couplings, at the one-loop level, $m_{\tilde{\mu}_L} - m_{\tilde{e}_L}$ is RG invariant, and the running of $m_{\tilde{\tau}_L} - m_{\tilde{e}_L}$ depends on only a single parameter combination $X_\tau = 2|y_\tau|^2(m_{H_d}^2 + m_{\tilde{\tau}_L}^2 + m_{\tilde{\tau}_R}^2) + 2|a_\tau|^2$ (cf. [24]). By combining the measurement of left-handed slepton masses with other information, such as the mass of coloured particles and the limits on (SUSY) LFV processes, one could at least carry out a hypothesis test on the structure of $m_{\tilde{L}}^2$.

At large $\tan\beta$, the situation is quite different. The left-handed sleptons and the sneutrinos are heavier, and the charged lepton Yukawa couplings are enhanced. The latter induces two effects through the RGEs. On the one hand, as explained above, the mass PDFs become much wider and either ordering, $m_{\tilde{\chi}_1^0} > m_{\tilde{\mu}_R}$ or $m_{\tilde{\chi}_1^0} < m_{\tilde{\mu}_R}$, can now occur. On the other hand, LFV processes in the $\mu - \tau$ sector may be sufficiently large to be observed. Since $m_{\tilde{l}_L} > m_{\tilde{\chi}_2^0}$, the sleptons relevant for LHC phenomenology are now the $\tilde{\mu}_R$, $\tilde{e}_R$ and $\tilde{\tau}_1$. The $\tilde{\chi}_2^0$ and $\tilde{\chi}_1^\pm$ decay predominantly into the h^0 and, if kinematically allowed, into the $\tilde{\tau}_1$, because it contains left-handed components induced by left-right mixing. The points B and C (B' and C') in Table 6.1 (6.2) are representative examples.

We will first discuss the leading decays, and then study LFV processes. Those features which are unrelated to LFV can be summarized as follows.

- The $\tilde{\chi}_1^0$ decays into $\tilde{e}_R^\pm e^\mp$ or, if kinematically allowed, also into $\tilde{\mu}_R^\pm \mu^\mp$. If the muonic channel is open, its branching ratio strongly depends on the mass splittings, cf. Eq. (6.11). In this case the $\tilde{\mu}_R$ decays predominantly through a three-body mode $\tilde{\mu}_R \to \tilde{e}_R e\mu$ as before. The signs of e and μ are a priori not correlated, but they are

related to the sign of $\tilde{e}_R$, which may be measured, and the sign of the parent $\tilde{\mu}_R$. (If $m_{\tilde{\mu}_R} > m_{\tilde{\chi}_1^0}$, $\tilde{\mu}_R^\pm \to \tilde{\chi}_1^0 \mu^\pm$ followed by $\tilde{\chi}_1^0 \tilde{e}_R^\pm e^\mp$, giving the same final state.) The PDFs of $m_{\tilde{\chi}_1^0} - m_{\tilde{\mu}_R}$ are shown in Fig. 6.7 for different values of $\mathscr{L}$.

- The $\tilde{\chi}_2^0$ decays predominantly to a Higgs from $\tilde{\chi}_2^0 \to \tilde{\chi}_1^0 h^0$ ($\sim 70\%$), if $m_{\tilde{\tau}_1} > m_{\tilde{\chi}_2^0}$. This is the case for points B, B' and C'. If $m_{\tilde{\tau}_1} < m_{\tilde{\chi}_2^0}$ (point C), the leading $\tilde{\chi}_2^0$ decays give a $\tau^+\tau^-$ pair from $\tilde{\chi}_2^0 \to \tilde{\tau}_1^\pm \tau^\mp$, $\tilde{\tau}_1^\pm \to \tau^\pm \tilde{\chi}_1^0$ ($\sim 85\%$), while $\tilde{\chi}_2^0 \to \tilde{\chi}_1^0 h^0$ has $\sim 10\%$ BR. With the $\tilde{\chi}_1^0$ decay, the whole chain produces an OS ditau or a h^0, plus the LMP, plus e or $e + \mu^\pm + \mu^\mp$, depending on the $\tilde{\mu}_R/\tilde{\chi}_1^0$ mass ordering and splitting. The final e or $e + \mu^\pm + \mu^\mp$ should be rather soft compared to the taus.

- Analogously, the $\tilde{\chi}_1^\pm$ decays mainly either through $\tilde{\chi}_1^\pm \to \tilde{\chi}_1^0 W^\pm$ ($\sim$ 65–70%), or through $\tilde{\chi}_1^\pm \to \tilde{\tau}_1^\pm \nu_\tau \to \tilde{\chi}_1^0 \tau^\pm \nu_\tau$ ($\sim 85\%$) if kinematically allowed. The latter chain gives one hard τ plus E_T^{miss}, plus the LMP, plus e or $e + \mu^\pm + \mu^\mp$ depending on the $\tilde{\mu}_R/\tilde{\chi}_1^0$ mass ordering and splitting. The subleading decay $\tilde{\chi}_1^\pm \to \tilde{\mu}_R^\pm \nu_\mu$ can have 10–20% branching ratio and gives one hard μ plus E_T^{miss}, plus e and the LMP if $m_{\tilde{\mu}_R} > m_{\tilde{\chi}_1^0}$, or one hard μ plus E_T^{miss}, plus the LMP and $e + \mu$ from the $\tilde{\mu}_R$ three-body decay if $m_{\tilde{\mu}_R} < m_{\tilde{\chi}_1^0}$.

- The invariant-mass distribution of the SFOS ditau can be used to determine the mass of the $\tilde{\tau}_1$. For measuring the $\tilde{\mu}_R$ mass, one needs to rely on the analysis of chargino decays, or on LFV processes, in which $\tilde{\mu}_R$ appears as an intermediate decay product (see below). Knowledge of the masses, or mass splittings, of the $\tilde{\tau}_1$, $\tilde{\mu}_R$ and $\tilde{e}_R$ would now permit to obtain information on $m_{\tilde{E}}^2$. As before, this information combined with other measurements would permit to carry out a hypothesis test, this time on the structure of $m_{\tilde{E}}^2$. In particular, one can check wether the hierarchical factors ϵ can be in agreement with values $\mathcal{O}(10^{-1})$ necessary to reproduce the SM flavour hierarchy.

Let us now turn to lepton flavour violation. As mentioned, LFV can be sizeable in the $\mu - \tau$ sector. The most interesting decays are those involving $\tilde{l}_3 \simeq \tilde{\tau}_1$ and $\tilde{l}_2 \simeq \tilde{\mu}_R$. Figure 6.8 shows, in the top row, the PDFs for $\text{BR}(\tilde{\tau}_1 \to \tilde{\chi}_1^0 \mu)$ and $\text{BR}(\tilde{\chi}_2^0 \to \tilde{\mu}_R \tau)$, and for comparison also for $\text{BR}(\tilde{\chi}_2^0 \to \tilde{\mu}_R \mu)$. The bottom row shows the correlation of these branching ratios with $\text{BR}(\tau \to \mu\gamma)$. At the chosen scale, $F^T/2R = 1500$ GeV, the current experimental bound of $\text{BR}(\tau \to \mu\gamma) < 6.8 \times 10^{-8}$ is always satisfied. We observe that $\text{BR}(\tau \to \mu\gamma)$ scales roughly as $\left(F^T/2R\right)^{(-5)\div(-4)}$. Given the strong correlation, if LFV is observed in slepton or neutralino decays, this leads to a prediction for $\tau \to \mu\gamma$. Our main observations regarding LFV processes at the LHC are:

- While the $\tilde{\tau}_1$ decays mainly to $\tilde{\chi}_1^0 \tau$, it can also have a LFV decay $\tilde{\tau}_1 \to \tilde{\chi}_1^0 \mu$. The rate of the LFV decay peaks around 1% but can go up to 10% or more for $\mathscr{L} = 3$, see the top-left plot in Fig. 6.8. In the $\tilde{\chi}_2^0$ decay chain, the ditau is then replaced by a $\mu^\pm \tau^\mp$ pair, potentially giving rise to an interesting flavour structure in kinematic

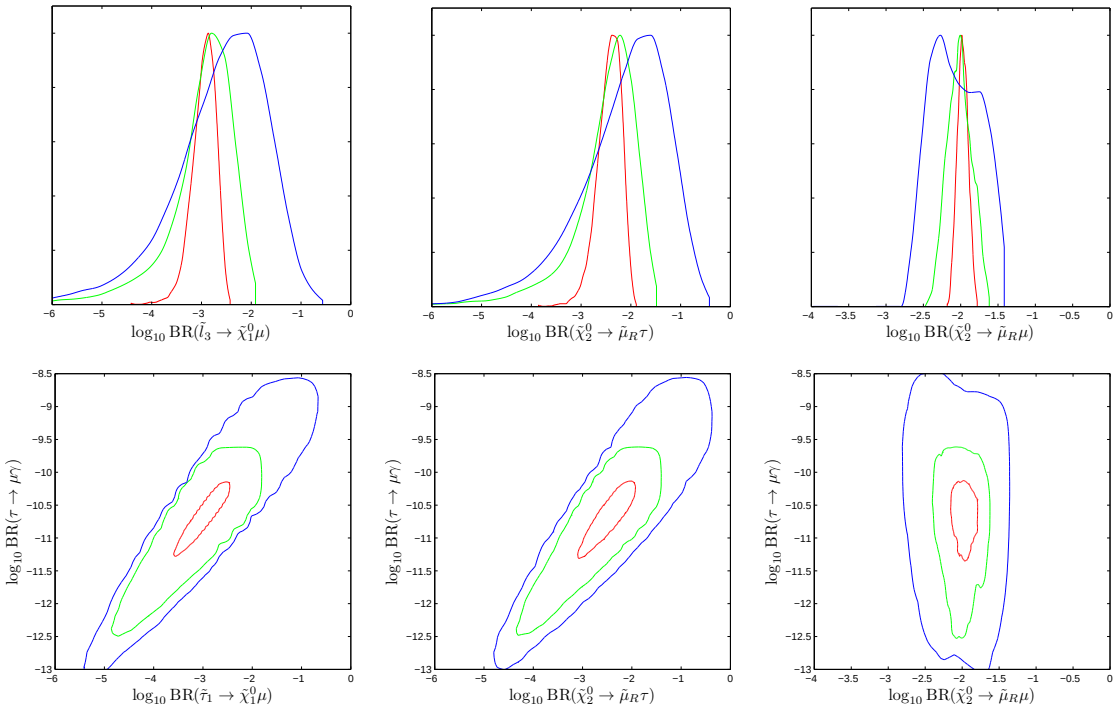

Figure 6.8: PDFs of branching ratios relevant for LFV in the $\mu - \tau$ sector. The parameters are $F^T/2R = 1500$ GeV and $\tan\beta = 30$. The upper row shows 1D PDFs for $\mathrm{BR}(\tilde{\tau}_1 \to \tilde{\chi}_1^0\mu)$, $\mathrm{BR}(\tilde{\chi}_2^0 \to \tilde{\mu}_R\tau)$ and $\mathrm{BR}(\tilde{\chi}_2^0 \to \tilde{\mu}_R\mu)$. The lower row shows 95% BC contours of the joint 2D PDFs of the these branching ratios with $\mathrm{BR}(\tau \to \mu\gamma)$. In all plots, the red, green and blue lines correspond to $\mathscr{L} = 1.2$, 1.5 and 3, respectively.

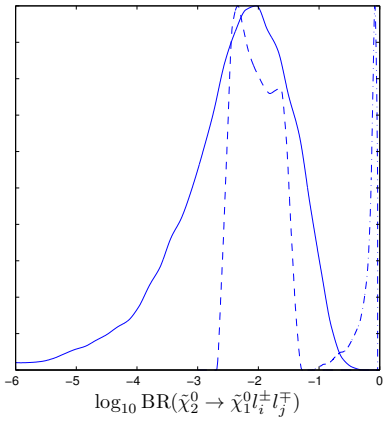

Figure 6.9: PDFs for $\tilde{\chi}_2^0$ cascade decays at $F^T/2R = 1500$ GeV, $\tan\beta = 30$ and $\mathscr{L} = 3$; dash-dotted line: $\mathrm{BR}(\tilde{\chi}_2^0 \to \tilde{\chi}_1^0 \tau^\pm \tau^\mp)$, dashed line: $\mathrm{BR}(\tilde{\chi}_2^0 \to \tilde{\chi}_1^0 \mu^\pm \mu^\mp)$, solid line: $\mathrm{BR}(\tilde{\chi}_2^0 \to \tilde{\chi}_1^0 \tau^\pm \mu^\mp)$.

distributions. Kinematic edges with flavour splitting and mixing have very recently been studied in [176] (see also [177]). In the $\tilde{\chi}_1^\pm$ decay chain, the single τ is replaced by a single μ, which must be separated from the non-LFV $\tilde{\chi}_1^\pm \to \tilde{\mu}_R \nu_\mu$ by kinematics. For example, one may exploit subsystem transverse-mass distributions [178] of, e.g., a lepton associated to the 'upstream' jet originating from $\tilde{q}_L$ cascade decays. This may permit to disentangle decay chains involving different slepton mass-eigenstates.

- LFV can also occur directly in the $\tilde{\chi}_2^0$ decays. Indeed the decay $\tilde{\chi}_2^0 \to \tilde{\mu}_R \tau$ can have a branching ratio of up to $\mathcal{O}(10\%)$ for $\mathscr{L} = 3$, larger than the $\tilde{\chi}_2^0 \to \tilde{\mu}_R \mu$ rate, cf. the middle and top-right plots in Fig. 6.8. The decay chain then is $\tilde{\chi}_2^0 \to \tilde{\mu}_R \tau\,(\to \tilde{\chi}_1^0 \mu\tau) \to \tilde{e}_R e\mu\tau$ with the $\tilde{\chi}_1^0$ being on- or off-shell depending on the $\tilde{\mu}_R/\tilde{\chi}_1^0$ mass ordering.

  The PDFs of the branching ratios of $\tilde{\chi}_2^0 \to \tilde{\chi}_1^0 \tau^\pm \tau^\mp$, $\tilde{\chi}_2^0 \to \tilde{\chi}_1^0 \tau^\pm \mu^\mp$ and $\tilde{\chi}_2^0 \to \tilde{\chi}_1^0 \mu^\pm \mu^\mp$ are shown in Fig. 6.9, to illustrate the global rate of LFV expected in $\tilde{\chi}_2^0$ cascade decays.

6.3.2 Mixed brane-radion scenario

In the previous subsection we investigated the case $F^Z/M_* \ll F^T/2R$, such that the scalar soft terms were dominated by radion mediation. We now consider the case where scalar soft terms receive non-negligible contributions from the brane source. The brane source contributions introduce a large uncertainty directly in the GUT-scale scalar soft terms. In addition to the $\lambda_{ij}^{U,D,E}$, the $\lambda_{ij}^{m_X^2}$ also become relevant. The phenomenology will eventually depend on the signs and magnitudes of all these λ-parameters. Nevertheless we can still identify some generic features.

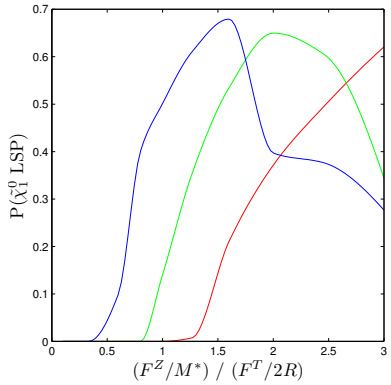

Figure 6.10: Probability of having a $\tilde{\chi}_1^0$ LSP as a function of $(F^Z/M_*)/(F^T/2R)$. The red, green, blue lines correspond to $\mathscr{L} = 1.2$, 1.5, 3, respectively. The other parameters are $\tan\beta = 5$, $F^T/2R = 1.5$ TeV.

Since the case of sizeable F^Z/M_* is much more constrained by BR($\mu \to e\gamma$) at large $\tan\beta$ (see Figs. 6.2, 6.4 and 6.5), we will focus on the small $\tan\beta$ scenario. In this case, the left-right mixing is negligible, because the a-terms are not large. It turns out that the right-right mixing is hierarchical, as in the radion-dominated case. We therefore call the right-handed sleptons $\tilde{e}_R$, $\tilde{\mu}_R$, and $\tilde{\tau}_R$. On the other hand, the left-left mixing can now be very large, so we denote the left-handed sleptons by $\tilde{l}_{L\,1}$, $\tilde{l}_{L\,2}$, and $\tilde{l}_{L\,3}$.

The masses of the right-handed sleptons can now span a wide range. All possible mass orderings with respect to the lightest neutralino can appear: $m_{\tilde{e}_R} < m_{\tilde{\chi}_1^0} < m_{\tilde{\mu}_R}$, $m_{\tilde{e}_R,\tilde{\mu}_R} < m_{\tilde{\chi}_1^0}$, or $m_{\tilde{\chi}_1^0} < m_{\tilde{e}_R,\tilde{\mu}_R}$. This last possibility is particularly interesting since, unlike the radion-dominated case, it features a $\tilde{\chi}_1^0$ LSP which is a viable dark matter candidate. Matrix anarchy again plays a crucial role in realizing this possibility: With $\mathscr{L} = 1$, the RG invariant

$$S \equiv m_{H_u}^2 - m_{H_d}^2 + \mathrm{Tr}(m_Q^2 - m_L^2 - 2\,m_U^2 + m_D^2 + m_E^2) \tag{6.12}$$

would vanish due to exact SU(5) relations, and the LMP would then be the $\tilde{e}_R$ as in the radion-dominated case. However, with $\mathscr{L} > 1$, the $\lambda_{ij}^{m_X^2}$ can be different from one another and induce a non-zero S. If S is sufficiently large and negative, the lightest slepton mass can be lifted above the neutralino mass. The probability of finding a neutralino LSP thus depends on $\mathscr{L}$, as well as on the ratio $(F^Z/M_*)/(F^T/2R)$. This is illustrated in Figure 6.10, which shows the probability of finding a $\tilde{\chi}_1^0$ LSP as a function of $\mathscr{L}$ and $(F^Z/M_*)/(F^T/2R)$ for a favourable sign combination of $\lambda_{ij}^{m_L^2}$. This plot is for $\tan\beta = 5$ and $F^T/2R = 1500$ GeV, but the result is fairly insensitive to the SUSY scale.

We proceed to discuss the left-handed slepton masses. At small $\tan\beta$, the soft masses m_L^2 are suppressed with respect to the gaugino masses (as explained in subsection 6.3.1). The RG running of the masses of the left-handed sleptons is therefore dominated by the gaugino masses and the S parameter. For $(F^Z/M_*)/(F^T/2R) \lesssim 1.5$, we obtain the mass

ordering

$$m_{\tilde{\chi}_1^0} < m_{\tilde{l}_L} < m_{\tilde{\chi}_2^0} \ . \tag{6.13}$$

This property is particularly interesting for LHC phenomenology.[6]

For the remaining discussion, we fix $\tan\beta = 5$, $F^T/2R = 1500$ GeV (i.e. $m_{\tilde{g}} \sim 3$ TeV). It turns out that, even for small F^Z/M_*, the LFV effects in the SUSY decays can be large, particularly in the $e-\mu$ sector, while still satisfying the current BR($\mu \to e\gamma$) bound. The details depend on the signs in both λ^E_{ij} and $\lambda^{m^2_L}_{ij}$. We will focus on the $\tilde{\chi}_2^0 \to \tilde{\chi}_1^0 l_i l_j$ decays. Following [179], we define the observable K_{ij} as

$$K_{ij} = \frac{\mathrm{BR}(\tilde{\chi}_2^0 \to l_i^\pm l_{j\neq i}^\mp \tilde{\chi}_1^0)}{\mathrm{BR}(\tilde{\chi}_2^0 \to l_i^\pm l_i^\mp \tilde{\chi}_1^0) + \mathrm{BR}(\tilde{\chi}_2^0 \to l_j^\pm l_j^\mp \tilde{\chi}_1^0)} \, . \tag{6.14}$$

to quantify the rate of LFV in the $\tilde{\chi}_2^0 \to l_i^\pm l_j^\mp \tilde{\chi}_1^0$ decays. Figures 6.11 and 6.12 show the PDFs of $\tilde{\chi}_2^0 \to \tilde{\chi}_1^0 l_i l_j$ decay branching ratios, with $F^Z/M_* = 50$ GeV and $F^Z/M_* = 1500$ GeV, respectively. For $F^Z/M_* = 50$ GeV, it is in particular LFV in the $e-\mu$ sector that can be large enough to give observable effects at the LHC, while at $F^Z/M_* = 1500$ GeV, LFV in all three sectors can be sizeable (though LFV still tends to be largest in the $e-\mu$ sector). The distributions shown in Fig. 6.11 and 6.12 represent the typical behaviour as far as BRs of SUSY particles are concerned, but the sign combination is chosen such that it slightly favours small BR($\mu \to e\gamma$). Note that, as opposed to Figure 6.8, there is no strong correlation between BR($\tilde{\chi}_2^0 \to e^\pm \mu^\mp \tilde{\chi}_1^0$) and BR($\mu \to e\gamma$).

Let us now discuss possible LHC signatures. Collider signatures will again depend on the various possible mass orderings of the $\tilde{\chi}_1^0$ with respect to the $\tilde{e}_R$ and $\tilde{\mu}_R$. There are the following possibilities:

- If $m_{\tilde{\chi}_1^0} < m_{\tilde{e}_R, \tilde{\mu}_R}$, then the $\tilde{\chi}_1^0$ is stable and a dark matter candidate (barring the $\widetilde{G}$ and $\tilde{a}$ LSP options). In the detector, the decay of $\tilde{\chi}_2^0$ produces OS dileptons plus E_T^{miss}.

- If $m_{\tilde{e}_R} < m_{\tilde{\chi}_1^0} < m_{\tilde{\mu}_R}$, or if $m_{\tilde{\chi}_1^0} - m_{\tilde{\mu}_R}$ is sufficiently small, the $\tilde{\chi}_1^0$ decays mainly to $e\tilde{e}_R$. The $\tilde{\chi}_2^0$ therefore decays as $\tilde{\chi}_2^0 \to l_i^\pm l_j^\mp e \tilde{e}_R$. The signature will be OS dileptons plus an electron, and the track of $\tilde{e}_R$, without E_T^{miss}.

- If $m_{\tilde{e}_R, \tilde{\mu}_R} < m_{\tilde{\chi}_1^0}$ and $|m_{\tilde{\mu}_R} - m_{\tilde{e}_R}|$ is not too small, the $\tilde{\chi}_1^0$ has a sizeable branching fraction to $e\tilde{e}_R$ and $\mu\tilde{\mu}_R$, and the next-to-lightest slepton decays to the lightest slepton within the detector. We will assume in the following that the lightest slepton is the $\tilde{e}_R$.

[6] For $(F^Z/M_*)/(F^T/2R) \gtrsim 1.5$ with $\mathscr{L} = 3$, the S parameter of Eq. (6.12) can be sufficiently large to make the left-handed sleptons lighter than the right-handed ones. This is why, in Figure 6.10, $P(\tilde{\chi}_1^0\ LSP)$ decreases above a value of $(F^Z/M_*)/(F^T/2R) \gtrsim 1.5$. Due to D-term splitting between sneutrino and charged slepton masses, a sneutrino becomes the lightest SUSY particle of the spectrum. Left-handed sneutrino dark matter is strongly constrained by direct detection and cosmology, so one would again have to assume that the actual LSP is the gravitino or an axino. We will not pursue this case any further.

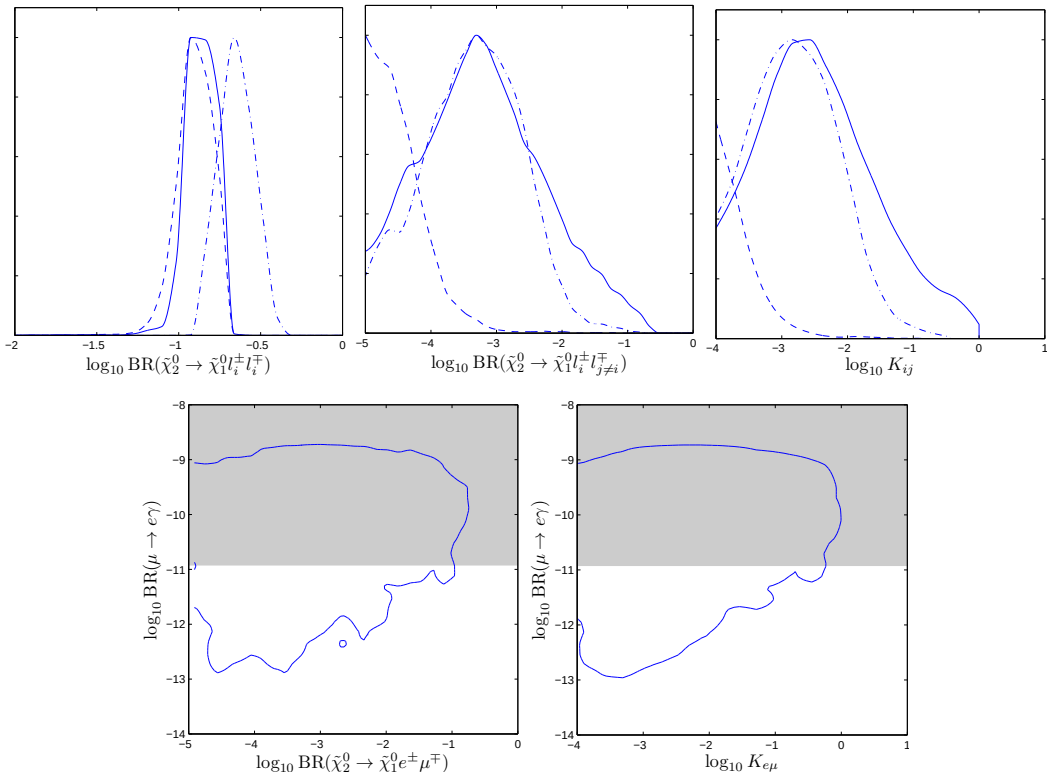

Figure 6.11: *Top left:* PDF of $\mathrm{BR}(\tilde{\chi}_2^0 \to l_i l_i \tilde{\chi}_1^0)$. Plain, dashed and dash-dotted lines correspond to $l_i l_i = ee$, $\mu\mu$, $\tau\tau$ respectively. *Top center:* PDF of $\mathrm{BR}(\tilde{\chi}_2^0 \to l_i l_j \tilde{\chi}_1^0)$. Plain, dashed and dash-dotted lines correspond to $l_i l_j = e\mu$, $e\tau$, $\mu\tau$ respectively. *Top right:* Plain, dashed and dash-dotted lines correspond to $K_{e\mu}$, $K_{e\tau}$, $K_{\mu\tau}$ respectively. *Bottom:* 95% BC region of the joint PDF of $\mathrm{BR}(\mu \to e\gamma)$ with $\mathrm{BR}(\tilde{\chi}_2^0 \to e\mu\tilde{\chi}_1^0)$ *(left)* and $K_{e\mu}$ *(right)*.
All of these distributions are for a fixed sign combination at $F^T/2R = 1500$ GeV, $F^Z/M_* = 50$ GeV and $\tan\beta = 5$. The chosen sign combination represents the typical behaviour of SUSY BRs, while it is somewhat favourable regarding the $\mathrm{BR}(\mu \to e\gamma)$ constraint.

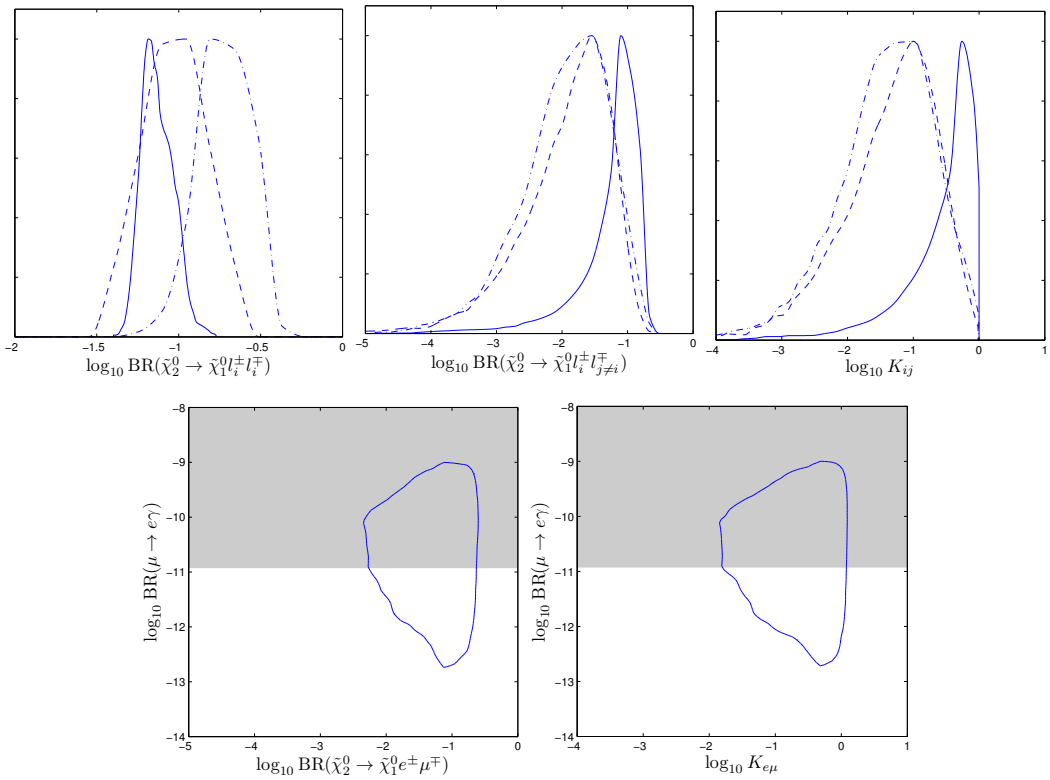

Figure 6.12: As Fig. 6.11, but for $F^Z/M_* = 1500$ GeV.

The $\tilde{\mu}_R$ decays through the three-body decay $\tilde{\mu}_R \to e\mu\tilde{e}_R$. The complete $\tilde{\chi}_2^0$ decay chains are thus $\tilde{\chi}_2^0 \to l_i^\pm l_j^\mp \tilde{\chi}_1^0 \to l_i^\pm l_j^\mp e\tilde{e}_R$ or $\tilde{\chi}_2^0 \to l_i^\pm l_j^\mp \tilde{\chi}_1^0 \to l_i^\pm l_j^\mp [\mu^\pm\mu^\mp] e\tilde{e}_R$. The signature of the $\tilde{\chi}_2^0$ decay will be OS dileptons plus e, and the track of $\tilde{e}_R$, without E_T^{miss} and possibly with additional OS dimuons.

If the $\tilde{\mu}_R$ is guaranteed to decay within the detector, there is no ambiguity in the observation of LFV. One can detect LFV by simply counting leptons: These events will have an odd number of leptons (3 or 5). Flavour conserving events will have an odd number of e and an even number of μ and τ, while LFV processes will have either an even number of e and an odd number of μ or τ, or an odd number of e and an odd number of μ and τ. The observable K_{ij}, defined in Eq. (6.14) to quantify LFV, can be directly measured by lepton counting :

$$\begin{aligned} K_{ij} &= \frac{\mathrm{BR}(\tilde{\chi}_2^0 \to l_i^\pm l_{j\neq i}^\mp [\mu^\pm\mu^\mp] e\tilde{e}_R)}{\mathrm{BR}(\tilde{\chi}_2^0 \to l_i^\pm l_i^\mp [\mu^\pm\mu^\mp] e\tilde{e}_R) + \mathrm{BR}(\tilde{\chi}_2^0 \to l_j^\pm l_j^\mp [\mu^\pm\mu^\mp] e\tilde{e}_R)} \\ &= \frac{N(l_i^\pm l_{j\neq i}^\mp [\mu^\pm\mu^\mp] e)}{N(l_i^\pm l_i^\mp [\mu^\pm\mu^\mp] e) + N(l_j^\pm l_j^\mp [\mu^\pm\mu^\mp] e)} \ . \end{aligned} \tag{6.15}$$

- Finally, if $|m_{\tilde{\mu}_R} - m_{\tilde{e}_R}|$ is sufficiently small, both sleptons are stable within the detector. The $\tilde{\chi}_2^0$ decays are therefore either $\tilde{\chi}_2^0 \to l_i^\pm l_j^\mp \tilde{\chi}_1^0 \to l_i^\pm l_j^\mp e\tilde{e}_R$ or $\tilde{\chi}_2^0 \to l_i^\pm l_j^\mp \tilde{\chi}_1^0 \to l_i^\pm l_j^\mp \mu\tilde{\mu}_R$. The signature of the $\tilde{\chi}_2^0$ decay will be OS dileptons plus e or μ, and the track of $\tilde{e}_R$ or $\tilde{\mu}_R$, without E_T^{miss}. LFV in the $e-\tau$ or $\mu-\tau$ sectors may be observed

by detecting a single τ in these decays. The observables $K_{e\tau}$ and $K_{\mu\tau}$ can be inferred without ambiguity using

$$\begin{aligned} K_{e\tau} &= \frac{\mathrm{BR}(\tilde{\chi}_2^0 \to \tau^\pm e^\mp e \tilde{e}_R)}{\mathrm{BR}(\tilde{\chi}_2^0 \to \tau^\pm \tau^\mp e \tilde{e}_R) + \mathrm{BR}(\tilde{\chi}_2^0 \to e^\pm e^\mp e \tilde{e}_R)} \\ &= \frac{N(\tau^\pm e^\mp e)}{N(\tau^\pm \tau^\mp e) + N(e^\pm e^\mp e)} \ , \end{aligned} \tag{6.16}$$

$$\begin{aligned} K_{\mu\tau} &= \frac{\mathrm{BR}(\tilde{\chi}_2^0 \to \tau^\pm \mu^\mp \mu \tilde{\mu}_R)}{\mathrm{BR}(\tilde{\chi}_2^0 \to \tau^\pm \tau^\mp \mu \tilde{\mu}_R) + \mathrm{BR}(\tilde{\chi}_2^0 \to \mu^\pm \mu^\mp \mu \tilde{\mu}_R)} \\ &= \frac{N(\tau^\pm \mu^\mp \mu)}{N(\tau^\pm \tau^\mp \mu) + N(\mu^\pm \mu^\mp \mu)} \ . \end{aligned} \tag{6.17}$$

On the other hand, in the $e-\mu$ sector, one cannot detect LFV by simple lepton counting since $ee\mu$ or $e\mu\mu$ combinations can be produced both in flavour conserving and in flavour violating channels. However, the flavour-conserving channels give same-flavour dileptons with opposite signs (SFOS), while in the flavour-violating channels all sign combinations of the SF dileptons appear with equal probability. To disentangle the two contributions, one should look out for same-sign dileptons, which can only appear through the flavour violating channels. Neglecting the flavour violating effects of the right-handed slepton sector, which are $\mathcal{O}(10^{-2})$ (more precisely $\mathcal{O}(\epsilon^2)$) because of the hierarchical mixing, $K_{e\mu}$ is given by

$$\begin{aligned} K_{e\mu} &= \frac{2 \times \mathrm{BR}(\tilde{\chi}_2^0 \to e^\pm e^\pm \mu \tilde{e}_R)}{\mathrm{BR}(\tilde{\chi}_2^0 \to e^\pm e^\mp e \tilde{e}_R) + \mathrm{BR}(\tilde{\chi}_2^0 \to \mu^\pm \mu^\mp e \tilde{e}_R) - \mathrm{BR}(\tilde{\chi}_2^0 \to \mu^\pm \mu^\pm e \tilde{e}_R)} \\ &= \frac{2 \times N(e^\pm e^\pm \mu)}{N(e^\pm e^\mp e) + N(\mu^\pm \mu^\mp e) - N(\mu^\pm \mu^\pm e)} \end{aligned} \tag{6.18}$$

or

$$\begin{aligned} K_{e\mu} &= \frac{2 \times \mathrm{BR}(\tilde{\chi}_2^0 \to \mu^\pm \mu^\pm e \tilde{\mu}_R)}{\mathrm{BR}(\tilde{\chi}_2^0 \to \mu^\pm \mu^\mp \mu \tilde{\mu}_R) + \mathrm{BR}(\tilde{\chi}_2^0 \to e^\pm e^\mp \mu \tilde{\mu}_R) - \mathrm{BR}(\tilde{\chi}_2^0 \to e^\pm e^\pm \mu \tilde{\mu}_R)} \\ &= \frac{2 \times N(\mu^\pm \mu^\pm e)}{N(\mu^\pm \mu^\mp \mu) + N(e^\pm e^\mp \mu) - N(e^\pm e^\pm \mu)} \ . \end{aligned} \tag{6.19}$$

The additional term in the denominator supresses the contributions to $\mathrm{BR}(\tilde{\chi}_2^0 \to e^\pm e^\mp \mu \tilde{\mu}_R)$ [$\mathrm{BR}(\tilde{\chi}_2^0 \to \mu^\pm \mu^\mp e \tilde{e}_R)$] coming from flavour violation. This ensures that the denominator contains only flavour conserving contributions.

6.4 Conclusions

We have studied flavour violation in supersymmetric models with a GUT-scale warped extra dimension. With matter fields located in the bulk, and the Higgs fields as well as the SUSY breaking hidden sector localized on the infrared brane, exponential wave function profiles can at the same time generate hierarchical fermion masses and mixings and somewhat suppress flavour changing neutral currents.

However, we find that the constraints on FCNCs (in particular those on lepton flavour violation) are stringent enough to still rule out most generic models. For the concrete example of the holographic GUT model of NPT, several additional assumptions on the hidden sector are necessary in order to obtain a realistic spectrum and evade the experimental bounds. More specifically, there should be contributions to the SUSY breaking soft terms both from the radion superfield and from the brane-localized hidden sector fields; and the brane-induced trilinear soft terms should be small or zero (which could be enforced by symmetry). With these assumptions, substantial regions of the parameter space can give rise to realistic sparticle mass spectra while avoiding unacceptably large lepton flavour violation.

In these surviving regions of parameter space, the LHC phenomenology depends on whether the soft terms are predominantly induced by the radion, or whether the contributions from the radion and from the brane-localized hidden sector fields are comparable. We have given an account of the expected mass spectra and LHC signatures in both cases.

Generically, the bounds on lepton flavour violation, in particular BR($e \to \mu\gamma$), force the spectrum to be heavy, with squark and gluino masses well above 1 TeV. One the one hand this might explain why no signal of SUSY has yet been observed at the LHC operating at $\sqrt{s} = 7$ TeV. On the other hand it means that, should the setup studied here be realized in Nature, it will require the high-luminosity run at 14 TeV to explore it. Moreover, a detailed experimental study of this scenario will most likely require precision measurements at even higher energy and/or luminosity (LHC upgrade), or at a multi-TeV e^+e^- collider.

Point	A	B	C	D
$m_{\tilde{\chi}_1^0}$	652	655	655	670
$m_{\tilde{\chi}_2^0}$	1224	1235	1235	1258
$m_{\tilde{\chi}_3^0}$	2870	3116	3124	5096
$m_{\tilde{\chi}_4^0}$	2872	3117	3125	5097
$m_{\tilde{\chi}_1^\pm}$	1224	1235	1235	1259
$m_{\tilde{\chi}_2^\pm}$	2873	3118	3126	5097
$m_{\tilde{l}_1}$	$555 (\sim \tilde{e}_R)$	$555 (\sim \tilde{e}_R)$	$556 (\sim \tilde{e}_R)$	$772 (\sim \tilde{e}_R)$
$m_{\tilde{l}_2}$	$679 (\sim \tilde{\mu}_R)$	$672 (\sim \tilde{\mu}_R)$	$619 (\sim \tilde{\mu}_R)$	$904 (\sim \tilde{l}_{L\,1})$
$m_{\tilde{l}_3}$	$993 (\sim \tilde{\tau}_1)$	$1267 (\sim \tilde{\tau}_1)$	$1096 (\sim \tilde{\tau}_1)$	$914 (\sim \tilde{\mu}_R)$
$m_{\tilde{l}_4}$	$1057 (\sim \tilde{\mu}_L)$	$1580 (\sim \tilde{\tau}_2)$	$1543 (\sim \tilde{\tau}_2)$	$1012 (\sim \tilde{l}_{L\,2})$
$m_{\tilde{l}_5}$	$1057 (\sim \tilde{e}_L)$	$1582 (\sim \tilde{\mu}_L)$	$1573 (\sim \tilde{\mu}_L)$	$1037 (\sim \tilde{l}_{L\,3})$
$m_{\tilde{l}_6}$	$1069 (\sim \tilde{\tau}_2)$	$1615 (\sim \tilde{e}_L)$	$1581 (\sim \tilde{e}_L)$	$2402 (\sim \tilde{\tau}_R)$
$m_{\tilde{\nu}_1}$	990	1577	1534	901
$m_{\tilde{\nu}_2}$	1053	1579	1569	1009
$m_{\tilde{\nu}_3}$	1054	1604	1579	1034
$m_{\tilde{d}_1}$	2721	2867	2867	2785
$m_{\tilde{d}_2}$	2752	2888	2888	2796
$m_{\tilde{d}_3}$	2753	2911	2912	2797
$m_{\tilde{d}_4}$	2873	2985	2985	2915
$m_{\tilde{d}_5}$	2897	2990	2991	2939
$m_{\tilde{d}_6}$	2943	2992	2992	4358
$m_{\tilde{u}_1}$	2694	2737	2737	2739
$m_{\tilde{u}_2}$	2744	2744	2744	2762
$m_{\tilde{u}_3}$	2776	2818	2819	2914
$m_{\tilde{u}_4}$	2872	2867	2866	2938
$m_{\tilde{u}_5}$	2897	2888	2888	4104
$m_{\tilde{u}_6}$	2967	2998	2999	4373
$m_{\tilde{g}}$	3201	3210	3210	3303
m_{h^0}	118.0	122.0	122.0	118.9
m_{H^0}	1366	864	710	1863
m_{A^0}	1368	865	716	1866
$m_{H^\pm}$	1366	869	710	1837

Table 6.1: Sample spectra for $F^T/2R = 1.5$ TeV. Points A–C are representative for the radion-dominated scenario with low and high $\tan\beta$: point A has $\tan\beta = 5$, while points B and C have $\tan\beta = 30$ with respectively $m_{\tilde{\chi}_1^0} < m_{\tilde{\mu}_R}$ and $m_{\tilde{\chi}_1^0} > m_{\tilde{\mu}_R}$. Point D is an example of a mixed brane-radion scenario with a neutralino LSP.

Point	A'	B'	C'	D'
$m_{\tilde{\chi}_1^0}$	427	429	429	439
$m_{\tilde{\chi}_2^0}$	808	816	816	832
$m_{\tilde{\chi}_3^0}$	1994	2155	2156	3430
$m_{\tilde{\chi}_4^0}$	1997	2157	2157	3431
$m_{\tilde{\chi}_1^\pm}$	809	816	816	832
$m_{\tilde{\chi}_2^\pm}$	1997	2157	2158	3432
$m_{\tilde{l}_1}$	$372 (\sim \tilde{e}_R)$	$373 (\sim \tilde{e}_R)$	$373 (\sim \tilde{e}_R)$	$518 (\sim \tilde{e}_R)$
$m_{\tilde{l}_2}$	$453 (\sim \tilde{\mu}_R)$	$441 (\sim \tilde{\mu}_R)$	$418 (\sim \tilde{\mu}_R)$	$597 (\sim \tilde{\mu}_R)$
$m_{\tilde{l}_3}$	$629 (\sim \tilde{\tau}_1)$	$862 (\sim \tilde{\tau}_1)$	$856 (\sim \tilde{\tau}_1)$	$611 (\sim \tilde{l}_{L\,1})$
$m_{\tilde{l}_4}$	$646 (\sim \tilde{\tau}_2)$	$1051 (\sim \tilde{\mu}_L)$	$1046 (\sim \tilde{\mu}_L)$	$683 (\sim \tilde{l}_{L\,2})$
$m_{\tilde{l}_5}$	$710 (\sim \tilde{\mu}_L)$	$1054 (\sim \tilde{e}_L)$	$1054 (\sim \tilde{e}_L)$	$701 (\sim \tilde{l}_{L\,3})$
$m_{\tilde{l}_6}$	$711 (\sim \tilde{e}_L)$	$1093 (\sim \tilde{\tau}_2)$	$1091 (\sim \tilde{\tau}_2)$	$1604 (\sim \tilde{\tau}_R)$
$m_{\tilde{\nu}_1}$	625	1047	1042	606
$m_{\tilde{\nu}_2}$	706	1050	1050	679
$m_{\tilde{\nu}_3}$	706	1076	1073	697
$m_{\tilde{d}_1}$	1879	1976	1976	1922
$m_{\tilde{d}_2}$	1899	1988	1988	1930
$m_{\tilde{d}_3}$	1900	1993	1993	1930
$m_{\tilde{d}_4}$	1980	2048	2048	2009
$m_{\tilde{d}_5}$	1995	2052	2052	2024
$m_{\tilde{d}_6}$	2024	2063	2064	2939
$m_{\tilde{u}_1}$	1846	1888	1888	1892
$m_{\tilde{u}_2}$	1894	1891	1891	1907
$m_{\tilde{u}_3}$	1914	1933	1933	2007
$m_{\tilde{u}_4}$	1979	1975	1975	2022
$m_{\tilde{u}_5}$	1994	1989	1989	2760
$m_{\tilde{u}_6}$	2060	2079	2079	2962
$m_{\tilde{g}}$	2198	2202	2202	2265
m_{h^0}	115.5	119.7	119.7	116.5
m_{H^0}	890	599	585	1259
m_{A^0}	893	599	586	1260
$m_{H^\pm}$	892	604	591	1244
$\sigma(pp \to \tilde{q}\tilde{q})$	9.53	8.97	8.98	8.65
$\sigma(pp \to \tilde{g}\tilde{g}, \tilde{g}\tilde{q})$	2.39	2.29	2.29	1.91
$\sigma(pp \to \tilde{\chi}\tilde{\chi})$	4.56	4.19	4.19	3.81
$\sigma(pp \to \tilde{q}\tilde{\chi}, \tilde{g}\tilde{\chi})$	1.64	1.63	1.64	1.44
$\sigma(pp \to \tilde{l}_i\tilde{l}_j, \tilde{l}_i\tilde{\nu}_j, \tilde{\nu}_i\tilde{\nu}_j)$	4.01	1.05	1.33	3.23

Table 6.2: Same selection of points as in Table 6.1, with $F^T/2R = 1$ TeV. Production cross sections (in fb) at the LHC with $\sqrt{s} = 14$ TeV, computed with `MadGraph` [**?**], are also given.

Résumé de la section

Dans cette Section, nous nous sommes interessés plus particulièrement à la physique des saveurs dans le modèle holographique avec brisure par radion et sur la brane IR. Prendre en compte les saveurs dans un modèle SUSY augmente fortement le degré de complexité. Il faut dans ce cas, soit avoir recours soit à des approximations souvent très grossières, soit passer par des calculs numériques. Dans un soucis de'exactitude, nous avons choisis la deuxième option. De plus, une incertitude théorique liée aux mécanismes de saveur est toujours présente. Elle est habituellement négligée dans les études de ce type, en particulier parce qu'il est particulièrement ardue de la traiter rigoureusement. Nous avons franchi le pas en effectuant ce traitement rigoureux par une approche Bayesienne. Les conséquences de cette incertitude sont cruciaux pour la phénoménologie. Entre autre, cette incertitude relaxe la contrainte dominante dans le scénario dominé par le radion, et permet d'obtenir un neutralino LSP dans le scénario avec brisure mixte radion-brane.

Conclusion

Among the many possibilities for physics beyond the Standard Model, the paradigm of extradimensional supersymmetric grand unified theories is rather well motivated. We studied, developed and extended certain aspects of two interesting frameworks of this type: a framework with gauge-Higgs unification (GHU), and the framework of holographic grand unification (HGU). We covered the range from these models to experiments, by investigating several aspects of the low-energy implications, including mass spectra, flavor constraints, dark matter and LHC phenomenology. From a more applied point of view, a substantial part of the technical work consisted in elaborating strategies for numerical computations, including the specific SUSY models in spectrum calculation codes `Suspect 2` [104] and `SPheno 3` [106], and using these tools for precise phenomenology studies.

We studied a complete realization of the GHU framework, showing that it is possible to obtain electroweak symmetry breaking if one takes into account the effect of a Chern-Simons term. We then showed that this model can pass the existing experimental constraints, and extracted some characteristic experimental signatures, which will be tested at the LHC. We then carried out a more general study, considering two representative cases of scalar soft terms, well motivated from the model-building point of view: universal sfermion soft terms, and vanishing soft terms for the first two generations, with non-universal ones for the third.

On the whole, we found a good discovery potential for these models, with almost generic dilepton signatures at the LHC, and a complementarity with dark matter direct detection. Note that we adopted the hypothesis of universal GUT-scale gaugino masses (which is valid in most simple GUT scenarios). We also assumed that dark matter was made of the neutralino, which can be a rather constraining assumption.

The remaining question is whether the property of GUT scale degenerate Higgs mass matrix (DHMM) could be detected during the LHC era. Indeed, there is apparently no piece of experimental evidence pointing more or less uniquely to DHMM models. However, even if it is not possible to do a full bottom-up reconstruction, one can still test the DHMM hypothesis against a non-DHMM scenario, using Bayesian model discrimination, taking into account all data available. Note that this idea enters in a more general "program" of testing GUT hypothesis at the LHC. By combining LHC data with other measurements, it

may be possible to get crucial insights on GUT scale physics. This could include testing the hypothesis of gaugino masses universality, or of universal Higgs soft masses for example.

We then investigated low-energy implications of the HGU framework, with particular emphasis on lepton flavour violation. This study is in fact sufficiently broad to cover any 5D models which explains flavour hierarchy by wave-function localization, with the Higgses and SUSY breaking localized on the same brane. The results obtained should generalise, at least qualitatively, to any such model. In our analysis, flavour observables were computed exactly, and the effects of flavour matrix anarchy were properly taken into account by adopting a Bayesian approach. We found that sizeable parts of the parameter space evading the dominant constraint BR($\mu \to e\gamma$) appears to be accessible at the 14 TeV LHC. Depending on the source of SUSY breaking, large LFV in SUSY decay chains may occur in different sectors, and would be observable at the LHC by simple lepton counting in multilepton signatures.

The first LHC analysis, based on ~ 1 fb^{-1} of data, are currently seeing nothing new (see the recent results [180]), except the first signals of the Higgs boson. In particular, squarks and gluino below $\sim$ 1 TeV are now roughly excluded through searches in multilepton channels. However, this is only the beginning of the adventure. It seems that we will have to be patient, and wait for more data to discover which kind of particles are populating the TeV scale and get eventually insights on the Physics beyond.

Conclusion en français

Parmi les différentes spéculations sur la Physique au delà du Modèle Standard, le paradigme de la théorie de Grande Unification supersymmétrique en dimension supplémentaire est particulièrement bien motivé. Nous avons étudié, développé et modifié certains aspects de deux classes de modèles : une classe avec unification jauge-Higgs, et une classe de Grande Unification holographique. Nous nous sommes efforcés de faire le lien entre ces modèles et l'expérience, en explorant les implications basse-énergie de ces modèles, avec en particulier les spectres de masse, les contraintes de physique des saveurs, la matière noire, et la phénoménologie au LHC. D'un point de vue plus appliqué, une part conséquente du travail a consisté en l'élaboration de stratégies de calcul numérique, avec en particulier la modification des codes `Suspect 2` [104], `SPheno 3` [106], puis leur application pour les études phénoménologiques.

A ce jour, une rumeur persistante affirme qu'un excès consistant avec le Higgs aurait été mesuré à 125 GeV au LHC. Cependant, ce n'est que le début de l'aventure, et il va falloir faire preuve de beaucoup de patience pour découvrir quelles particules se cachent à l'échelle du TeV, et obtenir peut-être des réponses profondes sur la Physique au-delà.

Appendix A

Radius stabilization and SUSY breaking

In this Appendix we sketch a warped 5D model (following [181, 182]) in which the radion is stabilized, and in which both the radion superfield and some additional IR brane fields have non-vanishing F-term expectation values. It therefore provides a dynamical origin for the SUSY breaking field background on which we based our analysis.

Consider first a warped extra dimension with two separate sectors: A super-Yang-Mills theory in the bulk and a super-Yang-Mills theory on the IR brane. In the infrared the degrees of freedom are a radion superfield T and two non-abelian gauge superfields which will undergo gaugino condensation. The strong-coupling scales of the SYM theories are taken parametrically smaller than the KK scale. Later we will add an "uplifting" sector, consisting of a dynamical SUSY-breaking sector on the IR brane.

In units of the 4D reduced Planck mass $M_4 = 2.4 \cdot 10^{18}$ GeV, the effective Lagrangian after gaugino condensation can be written as

$$\mathcal{L} = \int d^4\theta\, \overline{\phi}\phi \left(-3\, e^{-K/3}\right) + \int d^2\theta\, \phi^3 \left(a e^{-bT} + c\right) + \text{h.c.} \tag{A.1}$$

Here the radion Kähler potential is

$$K = -3 \log \left[\frac{M_5^3}{k}\left(e^{k\pi(T+\overline{T})} - 1\right)\right], \tag{A.2}$$

and a, b, c are constants. While a and b come from bulk gaugino condensation, and are of order unity (or somewhat large since the theory is weakly coupled at the compactification scale), c comes from the IR brane gaugino condensate and is exponentially small. Note that our conventions differ from those of [182] by the sign of k and by a factor π in the definition of the radion field.

Eqns. (A.1) and (A.2) are written in a frame where the warp factor is unity in the IR and exponentially large on the UV brane. For consistency with our conventions in the

main text, we perform a Weyl rescaling, which is a redefinition of the chiral compensator:

$$\varphi = e^{\pi k T}\phi\,. \tag{A.3}$$

This gives

$$\mathcal{L} = \int d^4\theta\,\overline{\varphi}\varphi\left(-3\,e^{-K/3}\right) + \int d^2\theta\,\varphi^3\left(ae^{-bT}+c\right)e^{-3k\pi T} + \text{ h.c.} \tag{A.4}$$

with

$$K = -3\,\log\left[\frac{M_5^3}{k}\left(1-e^{-k\pi(T+\overline{T})}\right)\right]\,. \tag{A.5}$$

It is convenient to define the warp factor superfield ω by the holomorphic field redefinition

$$\omega = \varphi e^{-k\pi T} \tag{A.6}$$

(note that this does not just amount to undoing the Weyl rescaling of Eq. (A.3); the chiral compensator is always normalized such that $\langle\varphi\rangle = 1 + F^\varphi\theta^2$, while here we are choosing a different way of parameterizing the radion). The Lagrangian becomes

$$\mathcal{L} = -\frac{3M_5^3}{k}\int d^4\theta\,\left(\overline{\varphi}\varphi - \overline{\omega}\omega\right) + \int d^2\theta\,\left(a\,\omega^{3+\nu}\varphi^{-\nu} + c\,\omega^3\right) + \text{ h.c.}\,, \tag{A.7}$$

where $\nu = b/k\pi$. This yields the F-terms

$$\begin{aligned}\overline{F}^{\bar{\omega}} &= -\frac{k}{3M_5^3}\left((3+\nu)a\,\omega^{2+\nu} + 3c\,\omega^2\right)\,,\\ \overline{F}^{\bar{\varphi}} &= -\frac{k}{3M_5^3}\,a\nu\,\omega^{3+\nu}\,,\end{aligned} \tag{A.8}$$

and the scalar potential

$$V = \frac{3M_5^3}{k}\left(|F^\omega|^2 - |F^\varphi|^2\right)\,. \tag{A.9}$$

At large warp factors, i.e. small $|\omega|$, the $|F^\varphi|^2$ term in V is subdominant, and the potential is minimized at a finite value of ω,

$$|\omega| = \left|\frac{3c}{(3+\nu)a}\right|^{1/\nu}\,. \tag{A.10}$$

This ansatz is self-consistent because c is exponentially small. There is also a decompactification solution at $\omega \to 0$, which is however of no interest for us.

For the gravitino mass we find

$$m_{3/2}^2 = e^K|W|^2 \approx \frac{k^3}{M_5^9}\left(\frac{\nu}{3+\nu}\right)^2|c|^2\,|\omega|^6 \sim |F^\varphi|^2\,. \tag{A.11}$$

Returning to the old variables, the radion F-term is

$$\frac{F^T}{2R} = \frac{1}{2\pi kR}\left(F^\varphi - \frac{F^\omega}{\omega}\right)\,. \tag{A.12}$$

F^ω/ω vanishes to leading order, but the subleading terms turn out to be finite and are parametrically of the order $\mathcal{O}(\omega^{\nu+3}) \sim \mathcal{O}(F^\varphi)$.

So far the vacuum energy density is negative, and the vacuum is a non-supersymmetric AdS minimum. This can be remedied by adding an additional sector which breaks supersymmetry dynamically on its own, in the rigid limit, thus providing a positive contribution to the cosmological constant. The details of such an "F-term uplift" have been worked out mainly in the context of effective field theories from type IIB flux compactifications (see e.g. [183]). Our main interest here is the relative importance of the contributions to soft terms from the uplifting sector compared to the radion contributions. In our normalization, including SUSY breaking IR brane fields Z_I in this background as

$$\Delta\mathcal{L}_{\text{brane}} = \int d^4\theta\, e^{-2\pi kR} \sum_I |Z_I|^2 + \int d^2\theta\, e^{-3\pi kR} W\left(Z_I\right) \tag{A.13}$$

will give an additional contribution to the scalar potential,

$$\Delta V = e^{-2\pi kR} \sum_I \left|F^{Z_I}\right|^2 . \tag{A.14}$$

To fine-tune the cosmological constant to zero, we thus need

$$e^{-\pi kR} F^{Z_I} \sim F^\varphi . \tag{A.15}$$

Therefore, in this particular model, the brane-localized contributions to the soft terms dominate over the contributions from the gravitational sector, i.e. the radion and compensator contributions. Since the warp factor is only moderately large in the scenarios we are considering in the main text, this model could still serve as an example for mixed brane-radion mediation. The gravitino is naturally the LSP, as is common in models of warped supersymmetry.

Appendix B

Bayesian statistics

We briefly review the subject of Bayesian statistics, following largely the comprehensive review [154].

In the so-called frequentist approach of probability, the notion of probability is defined as *the number of times the event occurs over the total number of trials, in the limit of an infinite series of equiprobable repetitions.* From a pure logic point of view, this definition of probability in terms of relative frequency of outcomes is circular: it assumes that repeated trials have the same probability of outcomes. However, this uses the notion of probability, that we were precisely trying to define! Even if one tries to formulate a bit differently, the circularity appears as soon as one has to make a statement on randomness. In addition, such a definition does not rigorously allow to treat unrepeatable events, as well as events with a finite number of repetitions.

These problems are solved within the framework of Bayesian statistics, in which the notion of probability is defined as *a measure of the degree of belief about a proposition.* Whatever the definition of probability p is, the axioms of probability theory implies Bayes' law:

$$p(A|B) = p(B|A)\frac{p(A)}{p(B)} \ , \tag{B.1}$$

which, with any additional true information I, takes the form

$$p(A|B,I) = p(B|A,I)\frac{p(A|I)}{p(B|I)} \ . \tag{B.2}$$

This well known result, derived about 250 years ago, gets a crucial meaning when applied to probability as a degree of belief. Indeed, replacing A by any hypothesis H, and B by the known information available (called d for "data"), the previous equality becomes

$$p(H|d,I) = p(d|H,I)\frac{p(H|I)}{p(d|I)} \ . \tag{B.3}$$

On the left-hand side, $p(H|d,I)$ is the posterior probability of the hypothesis once the data is taken into account. On the right-handed side, $p(d|H,I)$ is the probability of

obtaining the data assuming the hypothesis is true, called the likelihood function, and often denoted $\mathcal{L}(H)$. $p(H|I)$ is the probability (i.e. the degree of belief) given to the hypothesis without taking the data into account. It is thus called prior probability, or just "prior". The Bayes formula, applied to d and H (i.e. to known and unknown information), tells in fact how our degree of belief in the hypothesis H should be updated in the light of knowledge d.

Ideally the likelihood function should be built from the probability functions associated to the different pieces of data. However, usually, only a central value with some standard deviation is provided by experiments. There are currently projects in development to improve the interface with experimental analysis, see for example [184].

Two main applications follow from Eq. (B.3): parameter inference and model discrimination. We will now briefly describe these two applications.

If one wants to infer parameters within a given model $\mathcal{M}$, the proposition I in (B.3) is now "model $\mathcal{M}$ is true", simply denoted $\mathcal{M}$,while hypothesis H is "parameters of the model takes the value θ", simply noted θ. Equation (B.3) becomes

$$p(\theta|d,\mathcal{M}) = p(d|\theta,\mathcal{M})\frac{p(\theta|\mathcal{M})}{p(d|\mathcal{M})} \ . \tag{B.4}$$

The overall factor $p(d|\mathcal{M})$ is irrelevant in this application. Indeed, the object of interest it the map within the parameter space of the model, given by $p(d|\theta,\mathcal{M})p(\theta|\mathcal{M})$. In practice, one is often only interested in a partition ψ of the parameters $\theta = (\psi,\xi)$. In that situation, one has to integrate the posterior pdf over the ξ parameters:

$$p(\psi|d,\mathcal{M}) \propto \int p(d|\theta,\mathcal{M})p(\theta|\mathcal{M})d\xi \ . \tag{B.5}$$

This provides, in particular, a rigorous way to deal with unwanted nuisance parameters. In practice, this (possibly very high dimensional) integration recquires techniques like Monte Carlo Markov Chains or Nested Sampling Algorithms.

The second application of Eq. (B.3) is model discrimination. This time, hypothesis H is "model $\mathcal{M}$ is true" and there is no additional proposition I. The equation becomes

$$p(\mathcal{M}|d) = p(d|\mathcal{M})\frac{p(\mathcal{M})}{p(d)} \ . \tag{B.6}$$

Applying it to two models[1] $\mathcal{M}_1, \mathcal{M}_2$ to eliminate the unknown probability $p(d)$, one obtains the equation

$$\frac{p(\mathcal{M}_1|d)}{p(\mathcal{M}_2|d)} = \frac{p(d|\mathcal{M}_1)}{p(d|\mathcal{M}_2)}\frac{p(\mathcal{M}_1)}{p(\mathcal{M}_2)} \ . \tag{B.7}$$

The quantity $\frac{p(\mathcal{M}_1)}{p(\mathcal{M}_2)}$ is called prior odds, while $\frac{p(\mathcal{M}_1|d)}{p(\mathcal{M}_2|d)}$ is called posterior odds. The central quantity is $\frac{p(d|\mathcal{M}_1)}{p(d|\mathcal{M}_2)}$, denoted $\mathcal{B}_{12}$, and called Bayes factor. It tells how the relative degree of

[1]Note that that the two models can be the same model with two different priors.

$\lvert\log \mathcal{B}_{12}\rvert$	Odds	Probability	Strength of evidence
< 1.0	$\lesssim 3:1$	< 0.750	Inconclusive
1.0	$\sim 3:1$	0.750	Weak evidence
2.5	$\sim 12:1$	0.923	Moderate evidence
5.0	$\sim 150:1$	0.993	Strong evidence

Table B.1: The empirical Jeffrey's scale calibrating the odds between model $\mathcal{M}_1$ and model $\mathcal{M}_2$.

belief between two models is updated in the light of information d. A Bayes factor smaller larger [smaller] than 1 favorizes $\mathcal{M}_1$ [$\mathcal{M}_2$].

Bayes factors are usually interpreted with respect to the Jeffreys' scale [185], given in Table B. This is an empirically calibrated scale, with thresholds at values of the odds of $3:1$, $12:1$ and $150:1$, representing respectively weak, moderate and strong evidence.

Bayesian model comparison provides thus a formal way of evaluating relative probabilities of two models in light of the data and any prior information available. There are two effects in balance in that approach: quality of fit and predictivity. It implements in fact naturally the old idea of Occam's razor, by providing a formal way to evaluate whether the extra complexity of a model is required by the data. Another important feature is that an alternative model must be specified against which the comparison is made. A corollary is that, contrary to frequentist goodness-of-fit tests, the Bayesian approach maintains that it is pointless to reject a theory unless an alternative explanation that fits better the observations is available.

Appendix C

On a Bayesian approach to the fine-tuning concept

It is interesting to examine the issue of fine-tuning in the light of Bayesian statistics. Indeed, the Bayes factor can be a global fine-tuning measure, and provides a general definition to "naturalness priors" (priors incorporating information on fine-tuning) [141]. We find that in case of logarithmic priors, a modified definition of the usual sensitivity measure c (Eq. (5.7)) arises. This Bayesian definition provides a quantitative control on the magnitude of the c measure, thanks to Jeffrey's scale (Table B). It allows a better understanding of this measure, and permits interesting applications.

C.1 Sensitivity and Bayesian approach

Consider a given model $\mathcal{M}$, with set of dimensionful parameters $\theta \in \mathcal{D}$, of dimension n, and an observable $\mathcal{O} = f(\theta)$, taking the measured value $\mathcal{O}_{ex}$ on the subset of the parameter space $\mathcal{D}_{ex}$ of dimension $n-1$. Data other than the $\mathcal{O}$ measurement are collectively called d. The likelihood function $p(d|\theta)$ is called $\mathcal{L}(\theta)$. Let's also recall the property of homogeneity for $f(\theta)$ of dimension $d_{\mathcal{O}}$, with parameter θ_i of dimension d_i:

$$f(\theta_i) = f(\hat{\theta}_i \mu^{d_i}) = \mu^{d_{\mathcal{O}}} f(\hat{\theta}_i) \tag{C.1}$$

Fine-tuning can be seen as the propension of a model to give "naturally" the value $\mathcal{O}_{ex}$ to the observable $\mathcal{O}$. In the usual definition, this naturalness is considered as :

- Definition 1 : *"Sensitivity of $\mathcal{O}$ with respect to θ, in the vicinity of a point θ_{ex} belonging to $\mathcal{D}_{ex}$."*

But a second definition, arguably as intuitive as the first, can be :

- Definition 2 : *"Probability of having $\mathcal{O} = \mathcal{O}_{ex}$ in the model."*

This second one is of course Bayesian. One can suspect that these two definitions are somehow related, and this will indeed appear. One can already notice that Definition 1 is local, while Definition 2 is global.

In this discussion, we will consider only dimensionful parameters. Indeed, for dimensionless parameters, the idea of fine-tuning, even if it still exists, is less problematic due to the freedom of redefinition.

Following the idea of Definition 1 (sensitivity with respect to parameters), an intuitive mathematical definition is often given as

$$c = \max\left(\left|\frac{\partial \log f}{\partial \log \theta_i}\right|_{\mathcal{O}=\mathcal{O}_{ex}}\right) \tag{C.2}$$

which can accommodate dimensionful parameters thanks to the logarithms.

Note that the interpretation of the magnitude of c in this definition is of course subjective. Indeed, one has no idea of the meaning of this number, although people sometimes consider that $c > 10 - 1000$ means unacceptably large fine-tuning.[1] Moreover one doesn't know how to compare different c, and one does not have a quantitative interpretation of the relative magnitude between two different c.

A widely known example of such a fine-tuning measure appears in supersymmetric models, where the hierarchy problem is globally solved, but slightly remains because SUSY parameters are constrained to be at the TeV-scale, due to constraints provided by experiments. In that case, Eq. (C.2) is applied to the quantity m_Z, providing a measure of the "electroweak fine-tuning". This tension between electroweak and TeV scales, known as the "little hierarchy problem", is in fact an issue common to a lot of (all?) models of new physics.

Definition 2 provides a different kind of definition. Indeed, one can build a Bayes factor telling how the degree of belief in the model $\mathcal{M}$ is updated once the piece of information $\mathcal{O} = \mathcal{O}_{ex}$ is taken into account. We will call $\mathcal{M}_0$ the model $\mathcal{M}$ constrained by the condition $\mathcal{O} = \mathcal{O}_{ex}$. [2] One therefore defines the Bayes factor $\mathcal{B}$ such that

$$\frac{p(d|\mathcal{M}_0)}{p(d|\mathcal{M})} = \mathcal{B}\,. \tag{C.3}$$

[1] In fact, it is clear that a complete absence of fine-tuning should give $c = 0$ (i.e. the model predicts exactly the observed value, without any parameter dependence). But on which basis should we compare, say $c = 1$, to $c = 0$? On a linear scale, it looks close, but on a log scale, it is infinitely far.

[2] Technically $\mathcal{O} = \mathcal{O}_{ex}$ comes from experiment, so it should appear in the likelihood function. However, one can as well consider it as a different prior (more constraining) for the model, leaving the likelihood unchanged. It just depends whether one considers that $\delta(\mathcal{O}(\theta)/\mathcal{O}_{ex} - 1)$ belongs to the likelihood or to the prior.

Note that if the expression of $\mathcal{O}$ with respect to the parameters θ is bijective, it is still possible to do a variable change, to get $\mathcal{O}$ as an input parameter. In that case $\mathcal{M}_0$ and $\mathcal{M}$ are "nested models", and the Bayes factor simplifies to the Savage dickey density ratio, if one gives a factorisable prior to the input parameter $\mathcal{O}$. In the case of supersymmetric spectrum, this can be applied to the measurement of m_Z. In fact SUSY spectrum calculators are already designed to have m_Z as an input, so the variable change is already done in that case.

This Bayesian definition Definition 2 is quite different from Definition 1. In particular, it gives a global measure of the fine-tuning in a model, while Def 1 gives a local one, at a given point.

A probability involving a model can be written as an integral over the model parameter space, like in Eq. (B.5). Doing so, one has to specify the prior of parameters $p(\theta)$, "inside" the model. The piece of information $\mathcal{O} = \mathcal{O}_{ex}$ has then to appear as a Dirac delta function $\delta(\mathcal{O}(\theta)/\mathcal{O}_{ex} - 1)$. It is interesting to study $p(d|\mathcal{M}_0)$ with this integral form. Indeed, it becomes

$$p(d|\mathcal{M}_0) = \int_{\mathcal{D}} \delta(\mathcal{O}(\theta)/\mathcal{O}_{ex} - 1)\mathcal{L}(\theta)p(\theta)d\theta\,. \tag{C.4}$$

The integration of the Dirac delta function $\delta(\mathcal{O}(\theta)/\mathcal{O}_{ex} - 1)$, defining a level set $\mathcal{D}_{ex}$ inside the parameter space $\mathcal{D}$, will make appear an interesting quantity. We find instructive to write the following steps of the calculation.

The parameter θ_i will have the dimension d_i, and the observable will have the dimension $d_{\mathcal{O}}$. Starting from Eq. C.4 , we will make a variable change to come back to dimensionless parameters $\hat{\theta}_i$, then integrate the delta function. Eq. C.4 becomes:

$$p(d|\mathcal{M}_0) = \int_{\mathcal{D}_{ex}} \mathcal{L}(\theta)p(\theta)\mu^{\sum d_i} d\sigma(\hat{\theta})/\frac{1}{\mathcal{O}_{ex}}\left(\sum_i \left(\frac{\partial f(\hat{\theta}_i\mu^{d_i})}{\partial\hat{\theta}_i}\right)^2\right) \tag{C.5}$$

where $d\sigma(\hat{\theta})$ is the measure on the subspace $\mathcal{D}_{ex}$. This integration makes appear the norm of the f gradient, $\|\nabla f\|$ [186]. Using the homogeneity relations $f(\hat{\theta}_i\mu^{d_i}) = \mu^{d_{\mathcal{O}}} f(\hat{\theta})$ and $\mathcal{O}_{ex} = f(\theta_{ex}) = \mu^{d_{\mathcal{O}}} f(\hat{\theta}_{ex})$, one gets

$$p(d|\mathcal{M}_0) = \int_{\mathcal{D}_{ex}} \mathcal{L}(\theta)p(\theta)\mu^{\sum d_i} d\sigma(\hat{\theta})/\left(\sum_i \left(\frac{\partial \log f(\hat{\theta})}{\partial\hat{\theta}_i}\right)^2\right)\,. \tag{C.6}$$

Coming back to dimensionful parameters, one gets

$$p(d|\mathcal{M}_0) = \int_{\mathcal{D}_{ex}} \mathcal{L}(\theta)p(\theta)d\sigma(\theta)/\left(\sum_i \left(\mu^{d_i}\frac{\partial \log f(\theta)}{\partial\theta_i}\right)^2\right)\,. \tag{C.7}$$

The quantity which appears (the inverse of the f gradient norm) looks a bit like Eq. (C.2), as it measures the sensitivity around the points where $\mathcal{O} = \mathcal{O}_{ex}$. It gives a formal origin

to the naturalness prior. However it is scale dependent: it depends on μ, the unity chosen for parameters. So, taken outside of the integral, it does not constitute a good fine-tuning measure.

This issue is cured by assuming logarithmic priors for dimensionful parameters, $p(\theta) = C/\prod_i \theta_i$. Doing this, Eq. C.4 becomes

$$p(d|\mathcal{M}_0) = \int_{\mathcal{D}} \delta(f(\theta)/\mathcal{O}_{ex} - 1)\mathcal{L}(\theta) C \, d\log\theta \,. \tag{C.8}$$

which integrates to

$$p(d|\mathcal{M}_0) = \int_{\mathcal{D}_{ex}} 1/\left(\sum_i \left(\frac{\partial \log f(\theta)}{\partial \log \theta_i}\right)^2\right)^{1/2}_{\mathcal{O}=\mathcal{O}_{ex}} \mathcal{L}(\theta) C \, d\sigma(\log\theta) \,. \tag{C.9}$$

This time the quantity which appear is very similar to Definition 1. It makes appear the quadratic sum of the derivatives, this is in fact the definition introduced intuitively in [187]. In a limit where the sensitivity with respect to one parameter is dominant, taking only the dominant term is a good approximation and corresponds exactly to Definition 1. A consequence for the use of naturalness priors (defined by $1/c$) is that one should use these prior associated not with flat priors, but with log priors to stay consistent. It is interesting to compare this result to what is done in [188].

Moreover, if one wants to consider only a single point θ_{ex} of the parameter space $\mathcal{D}_{ex}$ (thus satisfying $\mathcal{O} = \mathcal{O}_{ex}$), this corresponds to choose the prior as a $n-1$ dimensional delta function $\delta(\log\theta - \log\theta_{ex})$. Eq. (C.9) corresponds then to $1/\tilde{c}$ with

$$\tilde{c} = \left(\sum_i \left(\frac{\partial \log f(\theta_{ex})}{\partial \log \theta_i}\right)^2\right)^{1/2}_{\mathcal{O}=\mathcal{O}_{ex}} = \|\nabla \log f\|_{\mathcal{O}=\mathcal{O}_{ex}} \,. \tag{C.10}$$

We can see that Definition 1 is in fact contained in Definition 2. Definition 2 reduces to Definition 1 if one choose logarithmic priors for dimensionful parameters, and select a particular point of the parameter space. This correspondence will now permit to have a better conceptual understanding of Definition 1 and of its consequences.

C.2 Consequences on the use of the sensitivity definition

So far we just considered $p(d|\mathcal{M}_0)$. Let us consider now the Bayes factor $\mathcal{B}$ given by Eq. (C.3), restricted to a point in the parameter space using the logarithmic prior $C\delta(\theta - \theta_{ex})/\prod_i \theta_i$. The denominator $p(d|\mathcal{M})$ will provide a factor representing the volume K of the

one-dimensional space complementary of $\mathcal{D}_{ex}$: [3]

$$\mathcal{B} = \frac{K}{\tilde{c}} \tag{C.11}$$

This volume factor K represents the other values that $\mathcal{O}$ can take. It depends on the choice of prior. For example, if one chooses a different interval for the parameters (which is a change of prior), this may change the value of K. This makes finally the link between the subjectivity of Definition 1 and the subjectivity of Definition 2. We see that the measure $\tilde{c}$ is in fact in balance with the volume factor K. This Bayes factor (C.11) tells us formally what is the price for setting to $\mathcal{O}_{ex}$ the value of the observable $\mathcal{O}$, within a given model $\mathcal{M}$.

In contrast with Definition 1, the interest of Definition 2 is that the subjectivity is calibrated by the Jeffreys' scale. The volume factor K can be evaluated if the observable is natural bounded in the model. However, it remains prior dependent, such that it is delicate to give a meaning to the absolute scale of $\tilde{c}$. This contrasts with what is usually done in the literature.

Instead, one can build a Bayes factor comparing two different points in the parameter space of the same model $\mathcal{M}$, using two punctual log priors :

$$\mathcal{B}_{01} = \frac{p(d|\mathcal{M},\, \theta^0_{ex})}{p(d|\mathcal{M},\, \theta^1_{ex})} = \frac{\tilde{c}_1}{\tilde{c}_0}\ . \tag{C.12}$$

Jeffreys' scale is now calibrating the relative values of the $\tilde{c}$'s. Based on that scale, it is now possible to state that the values $\tilde{c}_1/\tilde{c}_0 \sim 3\,(12)\,(150)$ corresponds to weak (moderate) (strong) evidence for point 1 with respect to point 0.

It is interesting to look carefully at what is usually done in CMSSM studies. Indeed, in such studies, typically $\tilde{c} \sim 10 - 20$ is considered as moderate and $\tilde{c} \sim 100$ is considered as strong degree of belief against such points. As these considerations are on the absolute magnitude, they look a bit meaningless. But if one assumes that they are a comparison with a reference point $\tilde{c}_{ref} \sim 1$, this is in fact no so far from Jeffrey's scale. What one could do is to look for the point with minimal fine-tuning within the model, then compare other points to this one. For example, in the CMSSM, the point with lowest fine-tuning, taken as reference, has roughly $\tilde{c}_{ref} \sim 10$. With respect to this point, the values of $\tilde{c}$ corresponding to moderate and strong evidence for the reference point are 120 and 1500. This contrasts with what is usually believed.

Besides these considerations on subjectivity, it is also possible to evaluate the common fine-tuning induced by several observables together. If two observables are uncorrelated in the model, they do not depend on the same set of parameters, and one can simply write two δ functions. The two simple layer integrals will make multiply the gradient norms :

$$\mathcal{B} = \frac{K}{\tilde{c}_a \tilde{c}_b}\ . \tag{C.13}$$

[3] i.e, the space such that $\theta = \theta_{ex}$, letting the observable $\mathcal{O}$ unconstrained

This is interesting because in the intuitive approach, one does not know at all how to deal with such a common fine-tuning. Sometimes the maximum of both is chosen, which is very different from taking the product. In MSSM studies, these observables could be m_Z and Ωh^2 for example.

The situation where observables are correlated is more subtle. Indeed, in the limit of maximal correlation (i.e proportionality), one can guess that the correct result should be

$$\mathcal{B} = \frac{K}{\tilde{c}}\,. \tag{C.14}$$

with $\tilde{c} \sim \tilde{c}_a = \tilde{c}_b$. In the case of two observables $\mathcal{O}_a$, $\mathcal{O}_b$ constraining a two-dimensional model, it is not difficult to check that

$$\mathcal{B} = \frac{K}{\tilde{c}_{ab}}\,. \tag{C.15}$$

with

$$\tilde{c}_{ab} = \left|\det\left(\nabla \log \mathcal{O}_a, \nabla \log \mathcal{O}_b\right)\right| = \left(\left|\nabla \log \mathcal{O}_a\right|^2 \left|\nabla \log \mathcal{O}_b\right|^2 - \left(\nabla \log \mathcal{O}_a . \nabla \log \mathcal{O}_b\right)^2\right)^{1/2}$$

If the two observables are decorrelated, the scalar product of the gradients is null and one finds Eq. C.13 as expected. If the correlation increases, $\tilde{c}_{ab}$ decreases. This can be interpreted as the fact that it is more economical for a model to predict correlated data. One has also to remember that only the relative value of $\tilde{c}_{ab}$ has a meaning, so that one cannot compare the value of $\tilde{c}_{ab}$ with $\tilde{c}_a$, for example. In the limit of maximal correlation, the observables are linearly dependent and the determinant vanishes, which is worrying. This is in fact equivalent to the apparition of a $\delta(0)$ in the integral. It is once again a matter of normalization. Indeed, when one considers a ratio, the $\delta(0)$ in both integral cancel, and one comes back to Eq. C.12.

Additional work needs to be done to generalize this result to n observables constraining a m-dimensional parameter space with $n \leq m$. It is temptating to suppose that in the general case, the coefficient $\tilde{c}$ is given by the norm of the alternate n-linear form of the gradients.

7 Summary

To summarize, we propose a Bayesian definition of a global fine-tuning measure. This definition is interesting in itself to evaluate globally the fine-tuning of a model. The computation can be particularly simple if the observable can be transformed as an input, as it is the case for the electroweak fine-tuning.

By choosing logarithmic priors for dimensionful parameters and selecting a single point, it turns out that this definition reduces to a modified version of the classical sensitivity definition. The need of logarithmic priors is related to the need of a scale-free quantity.

This link provides a better calibration to the subjectivity of the classical sensitivity definition, thanks to the Jeffrey's scale. Moreover, it allows to treat properly the case of several observables, which is impossible to guess in an intuitive approach.

Appendix D

Matching parameters to fermion masses and mixings

In this Appendix, we derive analytical expressions for quark eigenvalues and mixings coming from the Yukawa textures Eq. (3.31), using an expansion in ϵ^2.

D.1 Preliminaries

The superpotential of the MSSM contains the quark Yukawa terms

$$W = y^u_{ij}\, H_u Q^i U^j + y^d_{ij}\, H_d Q^i D^j \,. \tag{D.1}$$

Both Yukawa matrices y^u and y^d may be diagonalized by bi-unitary transformations,

$$y^u_{\rm diag} = \mathcal{U}_{uL}\; y^u\; \mathcal{U}^\dagger_{uR}, \quad y^d_{\rm diag} = \mathcal{U}_{dL}\; y^d\; \mathcal{U}^\dagger_{dR} \,. \tag{D.2}$$

Here $\mathcal{U}_{uL}$ is a unitary matrix which diagonalizes the Hermitian matrix $y^u y^{u\dagger}$,

$$\mathcal{U}_{uL}\left(y^u y^{u\dagger}\right)\mathcal{U}^\dagger_{uL} = y^u_{\rm diag} y^{u\dagger}_{\rm diag} \,, \tag{D.3}$$

and $\mathcal{U}_{dL}$ is a unitary matrix which diagonalizes the Hermitian matrix $y^d y^{d\dagger}$,

$$\mathcal{U}_{dL}\left(y^d y^{d\dagger}\right)\mathcal{U}^\dagger_{dL} = y^d_{\rm diag} y^{d\dagger}_{\rm diag} \,. \tag{D.4}$$

The CKM matrix $\mathcal{V}_{\rm CKM}$ of quark mixings is given by

$$\mathcal{V}_{\rm CKM} = \mathcal{U}_{uL}\mathcal{U}^\dagger_{dL} \,, \tag{D.5}$$

and the physical quark masses are given by the matrix entries of $y^u_{\rm diag}$ and $y^d_{\rm diag}$ multiplied by the appropriate Higgs expectation value. Three mixing angles, one phase, and six mass eigenvalues constitute the physical observables in the quark sector.

We are interested in situations where the Yukawa matrices are given by

$$y^u = \begin{pmatrix} \lambda^u_{11}\epsilon^4 & \lambda^u_{12}\epsilon^3 & \lambda^u_{13}\epsilon^2 \\ \lambda^u_{21}\epsilon^3 & \lambda^u_{22}\epsilon^2 & \lambda^u_{23}\epsilon \\ \lambda^u_{31}\epsilon^2 & \lambda^u_{32}\epsilon & \lambda^u_{33} \end{pmatrix}, \qquad y^d = \begin{pmatrix} \lambda^d_{11}\epsilon^3 & \lambda^d_{12}\epsilon^3 & \lambda^d_{13}\epsilon^3 \\ \lambda^d_{21}\epsilon^2 & \lambda^d_{22}\epsilon^2 & \lambda^d_{23}\epsilon^2 \\ \lambda^d_{31}\epsilon & \lambda^d_{32}\epsilon & \lambda^d_{33}\epsilon \end{pmatrix}, \tag{D.6}$$

with $\epsilon \approx 0.1$ a small parameter and the $\lambda^{u,d}_{ij}$ of order unity. Note that to leading order in ϵ, the structure of $y^u y^{u\dagger}$ and $y^d y^{d\dagger}$ is similar, up to an overall ϵ^2 factor:

$$y^u y^{u\dagger} = \begin{pmatrix} r_u\epsilon^4 & s_u\epsilon^3 & t_u\epsilon^2 \\ s_u^*\epsilon^3 & u_u\epsilon^2 & v_u\epsilon \\ t_u^*\epsilon^2 & v_u^*\epsilon & w_u \end{pmatrix}, \qquad y^d y^{d\dagger} = \epsilon^2 \begin{pmatrix} r_d\epsilon^4 & s_d\epsilon^3 & t_d\epsilon^2 \\ s_d^*\epsilon^3 & u_d\epsilon^2 & v_d\epsilon \\ t_d^*\epsilon^2 & v_d^*\epsilon & w_d \end{pmatrix}. \tag{D.7}$$

Here we have defined

$$\begin{aligned} r_u &= |\lambda^u_{13}|^2 + |\lambda^u_{12}|^2\epsilon^2 + |\lambda^u_{11}|^2\epsilon^4, \quad s_u = \lambda^u_{13}\lambda^{u*}_{23} + \lambda^u_{12}\lambda^{u*}_{22}\epsilon^2 + \lambda^u_{11}\lambda^{u*}_{21}\epsilon^4, \\ t_u &= \lambda^u_{13}\lambda^{u*}_{33} + \lambda^u_{12}\lambda^{u*}_{32}\epsilon^2 + \lambda^u_{11}\lambda^{u*}_{31}\epsilon^4, \quad u_u = |\lambda^u_{23}|^2 + |\lambda^u_{22}|^2\epsilon^2 + |\lambda^u_{21}|^2\epsilon^4, \\ v_u &= \lambda^u_{23}\lambda^{u*}_{33} + \lambda^u_{22}\lambda^{u*}_{32}\epsilon^2 + \lambda^u_{21}\lambda^{u*}_{31}\epsilon^4, \quad w_u = |\lambda^u_{33}|^2 + |\lambda^u_{32}|^2\epsilon^2 + |\lambda^u_{31}|^2\epsilon^4, \end{aligned} \tag{D.8}$$

and

$$\begin{aligned} r_d &= |\lambda^d_{11}|^2 + |\lambda^d_{12}|^2 + |\lambda^d_{13}|^2, \quad s_d = \lambda^d_{11}\lambda^{d*}_{21} + \lambda^d_{12}\lambda^{d*}_{22} + \lambda^d_{13}\lambda^{d*}_{23}, \\ t_d &= \lambda^d_{11}\lambda^{d*}_{31} + \lambda^d_{12}\lambda^{d*}_{32} + \lambda^d_{13}\lambda^{d*}_{33}, \quad u_d = |\lambda^d_{21}|^2 + |\lambda^d_{22}|^2 + |\lambda^d_{23}|^2, \\ v_d &= \lambda^d_{21}\lambda^{d*}_{31} + \lambda^d_{22}\lambda^{d*}_{32} + \lambda^d_{23}\lambda^{d*}_{33}, \quad w_d = |\lambda^d_{31}|^2 + |\lambda^d_{32}|^2 + |\lambda^d_{33}|^2 . \end{aligned} \tag{D.9}$$

D.2 Fermion masses

A hermitian matrix of the form

$$M = \begin{pmatrix} r\epsilon^4 & s\epsilon^3 & t\epsilon^2 \\ s^*\epsilon^3 & u\epsilon^2 & v\epsilon \\ t^*\epsilon^2 & v^*\epsilon & w \end{pmatrix} \tag{D.10}$$

has the eigenvalues

$$\begin{aligned} \mu_1 &= w + \frac{|v|^2}{w}\epsilon^2 + \frac{1}{w}\left(\frac{|v|^2}{w^2}(uw - |v|^2) + |t|^2\right)\epsilon^4 + \mathcal{O}(\epsilon^6), \\ \mu_2 &= \frac{uw - |v|^2}{w}\epsilon^2 + \frac{1}{w}\left(\frac{|sw - tv^*|^2}{uw - |v|^2} - \frac{|v|^2}{w^2}(uw - |v|^2)\right)\epsilon^4 + \mathcal{O}(\epsilon^6), \\ \mu_3 &= \frac{1}{u}\left((ru - |s|^2) - \frac{|sv - tu|^2}{uw - |v|^2}\right)\epsilon^4 + \mathcal{O}(\epsilon^6) . \end{aligned} \tag{D.11}$$

Note that in the case of $M = y^u y^{u\dagger}$, all of the "minors" $(ru - |s|^2)$, $(sw - tv^*)$, $(sv - tu)$ and $(uw - |v|^2)$ are $\mathcal{O}(\epsilon^2)$ (unless there is some fine-tuned cancellation between the λ^u_{ij}). Their ratios are therefore $\mathcal{O}(1)$, and expressions such as $(sw - tv^*)^2/(uw - |v|^2)$ or $(sv -$

$tu)^2/(uw-|v|^2)$ are $\mathcal{O}(\epsilon^2)$. In particular, the smallest eigenvalue $\mu_3 = y_u^2$ is only generated at higher order, namely at $\mathcal{O}(\epsilon^8)$.

For the case of real λ, we thus find the Yukawa couplings

$$\begin{aligned}
y_t &= |\lambda^u_{33}| + \frac{(\lambda^u_{23})^2 + (\lambda^u_{32})^2}{2\,|\lambda^u_{33}|}\epsilon^2 + \mathcal{O}(\epsilon^4),\\
y_c &= \frac{|\lambda^u_{33}\lambda^u_{22} - \lambda^u_{32}\lambda^u_{23}|}{|\lambda^u_{33}|}\epsilon^2 + \mathcal{O}(\epsilon^4),\\
y_u &= \mathcal{O}(\epsilon^4),\\
y_b &= \sqrt{w_d}\,\epsilon + \mathcal{O}(\epsilon^3),\\
y_s &= \sqrt{u_d - \frac{v_d^2}{w_d}}\,\epsilon^2 + \mathcal{O}(\epsilon^4),\\
y_d &= \mathcal{O}(\epsilon^3)\,.
\end{aligned} \tag{D.12}$$

We can also parameterize the wave function suppression in a more general way, by allowing for several distinct suppression factors in the up-type sector. Define

$$\epsilon_i \equiv e^{-\pi k R(|c_{\mathcal{T}i}|-1/2)}, \tag{D.13}$$

the up-type Yukawa matrices have the structure

$$y_u \sim (\epsilon_3)^2 \begin{pmatrix} \left(\frac{\epsilon_1}{\epsilon_3}\right)^2 & \frac{\epsilon_1\,\epsilon_2}{(\epsilon_3)^2} & \frac{\epsilon_1}{\epsilon_3} \\ \frac{\epsilon_1\,\epsilon_2}{(\epsilon_3)^2} & \left(\frac{\epsilon_2}{\epsilon_3}\right)^2 & \frac{\epsilon_2}{\epsilon_3} \\ \frac{\epsilon_1}{\epsilon_3} & \frac{\epsilon_2}{\epsilon_3} & 1 \end{pmatrix} \tag{D.14}$$

where we didn't explicitly write the λ factors. Assuming that $\epsilon_3 \gg \epsilon_2 \gg \epsilon_1$, the Yukawa couplings of the first two generations are, to leading order,

$$\begin{aligned}
y_t &= |\lambda^u_{33}|(\epsilon_3)^2 + \frac{(\lambda^u_{23})^2 + (\lambda^u_{32})^2}{2\,|\lambda^u_{33}|}(\epsilon_2)^2 + \ldots,\\
y_c &= \frac{|\lambda^u_{33}\lambda^u_{22} - \lambda^u_{32}\lambda^u_{23}|}{|\lambda^u_{33}|}(\epsilon_2)^2 + \ldots
\end{aligned} \tag{D.15}$$

In the down-type sector, with the assumption $c_{\mathcal{F}1} \approx c_{\mathcal{F}2} \approx c_{\mathcal{F}3}$, all that needs to be done is to set

$$\epsilon = e^{-\pi k R(|c_{\mathcal{F}i}|-1/2)} \tag{D.16}$$

in the last three of Eqns. (D.12).

D.3 CKM matrix

M is diagonalized by

$$\mathcal{U}_L = \begin{pmatrix} 1 - \frac{1}{2}|\zeta|^2\,\epsilon^2 & -\zeta\,\epsilon & \frac{sv-tu}{uw-|v|^2}\epsilon^2 \\ \zeta^*\epsilon & 1 - \frac{1}{2}(|\gamma|^2 + |\zeta|^2)\,\epsilon^2 & -\gamma\,\epsilon \\ \frac{t^*}{w}\,\epsilon^2 & \gamma^*\,\epsilon & 1 - \frac{1}{2}|\gamma|^2\,\epsilon^2 \end{pmatrix} + \mathcal{O}(\epsilon^3)\,, \tag{D.17}$$

where

$$\gamma = \frac{v}{w}, \qquad \zeta = \frac{sw - tv^*}{uw - v^2}. \tag{D.18}$$

Applying this to calculate $\mathcal{U}_{uL}$ and $\mathcal{U}_{dL}$, we find for the CKM matrix

$$\mathcal{V}_{\rm CKM} = \mathcal{U}_{uL}\mathcal{U}_{dL}^\dagger = \begin{pmatrix} 1 - \frac{1}{2}\left(|\zeta_d|^2 + |\zeta_u|^2 - 2\zeta_u\zeta_d^*\right)\epsilon^2 & (\zeta_d - \zeta_u)\epsilon & \left(\frac{t_d}{w_d} - \gamma_d\zeta_u + \frac{s_u v_u - t_u u_u}{u_u w_u - |v_u|^2}\right)\epsilon^2 \\ -(\zeta_d^* - \zeta_u^*)\epsilon & 1 - \frac{1}{2}\Big(|\gamma_d|^2 + |\gamma_u|^2 - 2\gamma_u^*\gamma_d \\ & \quad + |\zeta_d|^2 + |\zeta_u|^2 - 2\zeta_u^*\zeta_d\Big)\epsilon^2 & (\gamma_d - \gamma_u)\epsilon \\ \left(\frac{t_u^*}{w_u} - \gamma_u^*\zeta_d^* + \frac{s_d^* v_d^* - t_d^* u_d}{u_d w_d - |v_d|^2}\right)\epsilon^2 & -(\gamma_d^* - \gamma_u^*)\epsilon & 1 - \frac{1}{2}\left(|\gamma_d|^2 + |\gamma_u|^2 - 2\gamma_u\gamma_d^*\right)\epsilon^2 \end{pmatrix} + \mathcal{O}(\epsilon^3)\,. \tag{D.19}$$

Note that the leading terms in γ_u and ζ_u have a rather simple form,

$$\gamma_u = \frac{\lambda^u_{23}}{\lambda^u_{33}} + \mathcal{O}(\epsilon^2), \quad \zeta_u = \frac{\lambda^u_{12}\lambda^u_{33} - \lambda^u_{13}\lambda^u_{32}}{\lambda^u_{22}\lambda^u_{33} - \lambda^u_{23}\lambda^u_{32}} + \mathcal{O}(\epsilon^2)\,, \tag{D.20}$$

while γ_d and ζ_d are fairly complicated when expressed in terms of the λ^d_{ij}.

In terms of our parameters, for all λ real, the CKM mixing angles θ_{12} and θ_{23} are then approximately given by

$$\sin\theta_{12} = (\zeta_d - \zeta_u)\epsilon, \qquad \sin\theta_{23} = (\gamma_d - \gamma_u)\epsilon\,. \tag{D.21}$$

D.4 Mass insertions

To calculate the off-diagonal sfermion masses coming from A-terms, we also need the matrices $\mathcal{U}_{uR}$ and $\mathcal{U}_{dR}$ in Eq. (D.2).

$\mathcal{U}_{uR}$ is obtained by taking $\mathcal{U}_{uL}$ and replacing $\lambda_{ij} \to \lambda^*_{ji}$. From Eq. (D.17) we obtain

$$\mathcal{U}_{uR} = \begin{pmatrix} 1 - \frac{1}{2}|\tilde\zeta_u|^2\,\epsilon^2 & -\tilde\zeta_u\,\epsilon & \left(\tilde\gamma_u\tilde\zeta_u - \tilde\tau_u\right)\epsilon^2 \\ \tilde\zeta_u^*\epsilon & 1 - \frac{1}{2}(|\tilde\gamma_u|^2 + |\tilde\zeta_u|^2)\,\epsilon^2 & -\tilde\gamma_u\,\epsilon \\ \tilde\tau_u^*\,\epsilon^2 & \tilde\gamma_u^*\,\epsilon & 1 - \frac{1}{2}|\tilde\gamma_u|^2\,\epsilon^2 \end{pmatrix} + \mathcal{O}(\epsilon^3)\,, \tag{D.22}$$

where

$$\tilde\gamma_u = \frac{\lambda^{u*}_{32}}{\lambda^{u*}_{33}}, \quad \tilde\zeta_u = \frac{\lambda^{u*}_{21}\lambda^{u*}_{33} - \lambda^{u*}_{31}\lambda^{u*}_{23}}{\lambda^{u*}_{22}\lambda^{u*}_{33} - \lambda^{u*}_{23}\lambda^{u*}_{32}}, \quad \tilde\tau_u = \frac{\lambda^{u*}_{31}}{\lambda^{u*}_{33}}\,. \tag{D.23}$$

Using the standard notation for A-terms (a_{ij} are the parameters in the Lagrangian, while A_{ij} are normalized to the Yukawa couplings) we have, in the RMSB case with general profiles,

$$a^u_{ij} = y^u_{ij}A^u_{ij} \qquad \text{(no summation)}, \tag{D.24}$$

where

$$A^u_{ij} = \frac{F_T}{R}\left(\frac{1}{\epsilon_i^2-1}\log\epsilon_i + \frac{1}{\epsilon_j^2-1}\log\epsilon_j\right), \tag{D.25}$$

again using the shorthand $\epsilon_i = e^{-\pi kR(|c_{T^i}|-1/2)}$. In the case that $\epsilon_3 = 1$, $\epsilon_2 = \epsilon$, and $\epsilon_1 = \epsilon^2$, this becomes

$$a^u_{ij} \approx \frac{F_T}{R}\begin{pmatrix} -4\lambda^u_{11}\,\epsilon^4\log\epsilon & -3\lambda^u_{12}\,\epsilon^3\log\epsilon & \lambda^u_{13}\,\epsilon^2(1/2-2\log\epsilon) \\ -3\lambda^u_{21}\,\epsilon^3\log\epsilon & -2\lambda^u_{22}\,\epsilon^2\log\epsilon & \lambda^u_{23}\,\epsilon(1/2-\log\epsilon) \\ \lambda^u_{31}\,\epsilon^2(1/2-2\log\epsilon) & \lambda^u_{32}(1/2-\log\epsilon)\,\epsilon & \lambda^u_{33} \end{pmatrix}. \tag{D.26}$$

We finally obtain, in the fermion mass eigenstate basis, for real λ,

$$a^{u(\mathrm{CKM})}_{ij} = \left(\mathcal{U}_{uL}\,a^u\,\mathcal{U}^\dagger_{uR}\right)_{ij} \tag{D.27}$$

with matrix elements

$$\begin{aligned}
a^{u(\mathrm{CKM})}_{11} &= -4\,\frac{F_T}{R}\left(\lambda^u_{11} + \lambda^u_{13}\frac{\lambda^u_{22}\lambda^u_{31}-\lambda^u_{21}\lambda^u_{32}}{\lambda^u_{23}\lambda^u_{32}-\lambda^u_{22}\lambda^u_{33}} + \lambda^u_{12}\frac{\lambda^u_{21}\lambda^u_{33}-\lambda^u_{23}\lambda^u_{31}}{\lambda^u_{23}\lambda^u_{32}-\lambda^u_{22}\lambda^u_{33}}\right)\,\epsilon^4\log\epsilon + \ldots \\
a^{u(\mathrm{CKM})}_{12} &= -\frac{F_T}{R}\frac{\lambda^u_{12}\lambda^u_{33}-\lambda^u_{13}\lambda^u_{32}}{\lambda^u_{33}}\,\epsilon^3\log\epsilon + \ldots \\
a^{u(\mathrm{CKM})}_{21} &= -\frac{F_T}{R}\frac{\lambda^u_{21}\lambda^u_{33}-\lambda^u_{23}\lambda^u_{31}}{\lambda^u_{33}}\,\epsilon^3\log\epsilon + \ldots \\
a^{u(\mathrm{CKM})}_{22} &= 2\,\frac{F_T}{R}\frac{\lambda^u_{23}\lambda^u_{32}-\lambda^u_{22}\lambda^u_{33}}{\lambda^u_{33}}\,\epsilon^2\log\epsilon + \ldots
\end{aligned} \tag{D.28}$$

$$\begin{aligned}
a^{u(\mathrm{CKM})}_{13} &= -\frac{F_T}{R}\left(\lambda^u_{13}\,\epsilon^2\log\epsilon + \lambda^u_{33}\frac{\lambda^u_{12}\lambda^u_{23}-\lambda^u_{13}\lambda^u_{22}}{\lambda^u_{23}\lambda^u_{32}-\lambda^u_{22}\lambda^u_{33}}\,\epsilon^2\left(\frac{1}{2}+\log\epsilon\right)\right) + \ldots \\
a^{u(\mathrm{CKM})}_{31} &= -\frac{F_T}{R}\left(\lambda^u_{31}\,\epsilon^2\log\epsilon + \lambda^u_{33}\frac{\lambda^u_{21}\lambda^u_{32}-\lambda^u_{31}\lambda^u_{22}}{\lambda^u_{23}\lambda^u_{32}-\lambda^u_{22}\lambda^u_{33}}\,\epsilon^2\left(\frac{1}{2}+\log\epsilon\right)\right) + \ldots \\
a^{u(\mathrm{CKM})}_{23} &= -\frac{F_T}{R}\lambda^u_{23}\,\epsilon\left(\frac{1}{2}+\log\epsilon\right)\ldots \\
a^{u(\mathrm{CKM})}_{32} &= -\frac{F_T}{R}\lambda^u_{32}\,\epsilon\left(\frac{1}{2}+\log\epsilon\right)\ldots \\
a^{u(\mathrm{CKM})}_{33} &= \frac{F_T}{R}\lambda^u_{33} + \ldots
\end{aligned} \tag{D.29}$$

The radion-mediated soft mass squared is (there appears to be a square missing in the `HGUT_soft_terms` note in Section 3.3!)

$$m^2_{ij} = \delta_{ij}\left(\frac{F_T}{R}\frac{\epsilon_i\log\epsilon_i}{\epsilon_i^2-1}\right)^2 \quad \text{(no summation)}, \tag{D.30}$$

which becomes, for the up-type quarks and with the above simplification where everything is written in terms of a single ϵ,

$$m^2_{u\,ij} = m^2_{q\,ij} = \left(\frac{F_T}{2R}\right)^2\begin{pmatrix} 16\epsilon^4(\log\epsilon)^2 & 0 & 0 \\ 0 & 4\epsilon^2(\log\epsilon)^2 & 0 \\ 0 & 0 & 1 \end{pmatrix}. \tag{D.31}$$

In the CKM basis we obtain

$$
\begin{aligned}
{m_u^{(R)}}^2_{ij} &= \left(\mathcal{U}_{uR}\, m_u^2\, \mathcal{U}_{uR}^\dagger\right)_{ij} \\
&= \left(\frac{F_T}{2R}\right)^2 \begin{pmatrix} 0 & 0 & \frac{\lambda^u_{13}\lambda^u_{22}-\lambda^u_{12}\lambda^u_{23}}{\lambda^u_{23}\lambda^u_{32}-\lambda^u_{22}\lambda^u_{33}}\epsilon^2 \\ 0 & \left(\frac{(\lambda^u_{23})^2}{(\lambda^{33}_u)^2}+4(\log\epsilon)^2\right)\epsilon^2 & -\frac{\lambda^u_{23}}{\lambda^u_{33}}\epsilon \\ \frac{\lambda^u_{13}\lambda^u_{22}-\lambda^u_{12}\lambda^u_{23}}{\lambda^u_{23}\lambda^u_{32}-\lambda^u_{22}\lambda^u_{33}}\epsilon^2 & -\frac{\lambda^u_{23}}{\lambda^u_{33}}\epsilon & 1-\frac{(\lambda^u_{23})^2}{(\lambda^{33}_u)^2}\epsilon^2 \end{pmatrix} + \mathcal{O}(\epsilon^3)\,.
\end{aligned}
\tag{D.32}
$$

and

$$
\begin{aligned}
{m_u^{(L)}}^2_{ij} &= \left(\mathcal{U}_{uL}^\dagger\, m_q^2\, \mathcal{U}_{uL}\right)_{ij} \\
&= \left(\frac{F_T}{2R}\right)^2 \begin{pmatrix} 0 & 0 & \frac{\lambda^u_{21}\lambda^u_{32}-\lambda^u_{22}\lambda^u_{31}}{\lambda^u_{23}\lambda^u_{32}-\lambda^u_{22}\lambda^u_{33}}\epsilon^2 \\ 0 & \left(\frac{(\lambda^u_{32})^2}{(\lambda^{33}_u)^2}+4(\log\epsilon)^2\right)\epsilon^2 & \frac{\lambda^u_{32}}{\lambda^u_{33}}\epsilon \\ \frac{\lambda^u_{21}\lambda^u_{32}-\lambda^u_{22}\lambda^u_{31}}{\lambda^u_{23}\lambda^u_{32}-\lambda^u_{22}\lambda^u_{33}}\epsilon^2 & \frac{\lambda^u_{32}}{\lambda^u_{33}}\epsilon & 1-\frac{(\lambda^u_{32})^2}{(\lambda^{33}_u)^2}\epsilon^2 \end{pmatrix} + \mathcal{O}(\epsilon^3)\,.
\end{aligned}
\tag{D.33}
$$

The down-type rotation matrix $\mathcal{U}_{dR}$ is much less straightforward to compute in any kind of systematic expansion. This is mainly because $y^{d\dagger}y^d$ does not have the structure of Eq. (D.10), as opposed to $y^d y^{d\dagger}$, $y^u y^{u\dagger}$, and $y^{u\dagger}y^u$. For real λ^d_{ij} the matrix $\mathcal{U}_{dR}$ is, to leading order, best expressed in terms of 3-vectors: Define

$$
\boldsymbol{\lambda}_3 = \begin{pmatrix} \lambda^d_{31} \\ \lambda^d_{32} \\ \lambda^d_{33} \end{pmatrix}, \quad \boldsymbol{\lambda}_2 = \begin{pmatrix} \lambda^d_{21} \\ \lambda^d_{22} \\ \lambda^d_{23} \end{pmatrix}
\tag{D.34}
$$

(so in particular $w_d = |\boldsymbol{\lambda}_3|^2$, $u_d = |\boldsymbol{\lambda}_2|^2$, and $v_d = \boldsymbol{\lambda}_2 \cdot \boldsymbol{\lambda}_3$). Then the normalized eigenvectors of $y^{d\dagger}y^d$ are, to leading order,

$$
\boldsymbol{x}_1 = \frac{\boldsymbol{\lambda}_3 \times \boldsymbol{\lambda}_2}{\sqrt{|\boldsymbol{\lambda}_3|^2\,|\boldsymbol{\lambda}_2|^2 - (\boldsymbol{\lambda}_3\cdot\boldsymbol{\lambda}_2)^2}}, \quad \boldsymbol{x}_2 = \frac{\boldsymbol{\lambda}_2\,|\boldsymbol{\lambda}_3|^2 - \boldsymbol{\lambda}_3(\boldsymbol{\lambda}_3\cdot\boldsymbol{\lambda}_2)}{|\boldsymbol{\lambda}_3|\sqrt{|\boldsymbol{\lambda}_3|^2\,|\boldsymbol{\lambda}_2|^2 - (\boldsymbol{\lambda}_3\cdot\boldsymbol{\lambda}_2)^2}}, \quad \boldsymbol{x}_3 = \frac{\boldsymbol{\lambda}_3}{|\boldsymbol{\lambda}_3|},
\tag{D.35}
$$

so that

$$
(\mathcal{U}_{dR})^j_i = x^j_i + \mathcal{O}(\epsilon^2)\,.
\tag{D.36}
$$

The resulting a matrix in the CKM basis is

$$
\begin{aligned}
a^{d(\mathrm{CKM})}_{ij} &= \left(\mathcal{U}_{dL}\, a^d\, \mathcal{U}_{dR}^\dagger\right)_{ij} \\
&= \frac{F_T}{R} \begin{pmatrix} 0 & 0 & 0 \\ 0 & -2(\log\epsilon)\, y_s & -\frac{\lambda^d_{21}\lambda^d_{31}+\lambda^d_{22}\lambda^d_{32}+\lambda^d_{23}\lambda^d_{33}}{\sqrt{(\lambda^d_{31})^2+(\lambda^d_{32})^2+(\lambda^d_{33})^2}}\left(\frac{1}{2}+\log\epsilon\right)\epsilon^2 \\ 0 & 0 & \left(\frac{1}{2}-\log\epsilon\right) y_b \end{pmatrix} + \mathcal{O}(\epsilon^3)\,.
\end{aligned}
\tag{D.37}
$$

Here y_s and y_b are as in Eq. (D.12). It can be checked that this expression is exact including the ϵ^2 terms, even though Eq. (D.36) is only exact to first order in ϵ.

The down-type soft mass matrix is proportional to unity (provided that the $c_{\mathcal{F}_i}$ are degenerate); therefore ${m^{(R)}_{d\,ij}}^2$ remains proportional to unity in the CKM basis. On the other hand, we have

$$
\begin{aligned}
{m^{(L)}_{d\,ij}}^2 &= \left(\mathcal{U}^\dagger_{dL}\, m_q^2\, \mathcal{U}_{dL}\right)_{ij} \\
&= \left(\frac{F_T}{2R}\right)^2 \begin{pmatrix} 0 & 0 & \frac{\lambda^d_{11}\lambda^d_{31}+\lambda^d_{12}\lambda^d_{32}+\lambda^d_{13}\lambda^d_{33}}{(\lambda^d_{31})^2+(\lambda^d_{32})^2+(\lambda^d_{33})^2}\epsilon^2 \\ 0 & \left(\frac{\lambda^d_{21}\lambda^d_{31}+\lambda^d_{22}\lambda^d_{32}+\lambda^d_{23}\lambda^d_{33}}{((\lambda^d_{31})^2+(\lambda^d_{32})^2+(\lambda^d_{33})^2)^2} +4(\log\epsilon)^2\right)\epsilon^2 & \frac{\lambda^d_{21}\lambda^d_{31}+\lambda^d_{22}\lambda^d_{32}+\lambda^d_{23}\lambda^d_{33}}{(\lambda^d_{31})^2+(\lambda^d_{32})^2+(\lambda^d_{33})^2}\epsilon \\ \frac{\lambda^d_{11}\lambda^d_{31}+\lambda^d_{12}\lambda^d_{32}+\lambda^d_{13}\lambda^d_{33}}{(\lambda^d_{31})^2+(\lambda^d_{32})^2+(\lambda^d_{33})^2}\epsilon^2 & \frac{\lambda^d_{21}\lambda^d_{31}+\lambda^d_{22}\lambda^d_{32}+\lambda^d_{23}\lambda^d_{33}}{(\lambda^d_{31})^2+(\lambda^d_{32})^2+(\lambda^d_{33})^2}\epsilon & 1-\frac{\lambda^d_{21}\lambda^d_{31}+\lambda^d_{22}\lambda^d_{32}+\lambda^d_{23}\lambda^d_{33}}{((\lambda^d_{31})^2+(\lambda^d_{32})^2+(\lambda^d_{33})^2)^2}\epsilon^2 \end{pmatrix} \\
&\quad + \mathcal{O}(\epsilon^3)\,.
\end{aligned}
\tag{D.38}
$$

Bibliography

[1] M. Nakahara. *Geometry, topology and physics*. Inst. of Physics Publ., 2002.

[2] Bertrand Delamotte. A hint of renormalization. *Am. J. Phys.*, 72:170–184, 2004.

[3] Matthew J. Strassler. An unorthodox introduction to supersymmetric gauge theory. 2003.

[4] Michael E. Peskin and Daniel V. Schroeder. *An Introduction to Quantum Field Theory*. Perseus Books, Cambridge, Massachusetts, 1995.

[5] C. H. Llewellyn Smith. High-Energy Behavior and Gauge Symmetry. *Phys. Lett.*, B46:233–236, 1973.

[6] J. S. Bell. High-Energy Behavior of Tree Diagrams in Gauge Theories . *Nucl. Phys.*, B60:427–436, 1973.

[7] John M. Cornwall, David N. Levin, and George Tiktopoulos. Uniqueness of spontaneously broken gauge theories. *Phys. Rev. Lett.*, 30:1268–1270, 1973.

[8] John M. Cornwall, David N. Levin, and George Tiktopoulos. Derivation of Gauge Invariance from High-Energy Unitarity Bounds on the s Matrix. *Phys. Rev.*, D10:1145, 1974.

[9] Michael S. Chanowitz. Strong W W scattering at the end of the 90's: Theory and experimental prospects. 1998.

[10] Yoichiro Nambu. Axial vector current conservation in weak interactions. *Phys. Rev. Lett.*, 4:380–382, 1960.

[11] J. Goldstone. Field Theories with Superconductor Solutions. *Nuovo Cim.*, 19:154–164, 1961.

[12] F. Englert and R. Brout. Broken symmetry and the mass of gauge vector mesons. *Phys. Rev. Lett.*, 13:321–322, 1964.

[13] Peter W. Higgs. Broken symmetries and the masses of gauge bosons. *Phys. Rev. Lett.*, 13:508–509, 1964.

[14] Csaba Csaki, Christophe Grojean, and Hitoshi Murayama. Standard Model Higgs from Higher Dimensional Gauge Fields. *Phys. Rev.*, D67:085012, 2003.

[15] Csaba Csaki, Christophe Grojean, Hitoshi Murayama, Luigi Pilo, and John Terning. Gauge theories on an interval: Unitarity without a Higgs. *Phys. Rev.*, D69:055006, 2004.

[16] Robert Shrock. Some recent results on models of dynamical electroweak symmetry breaking. 2007.

[17] M. Baak et al. Updated Status of the Global Electroweak Fit and Constraints on New Physics. 2011.

[18] Paul Langacker. Introduction to the Standard Model and Electroweak Physics. 2009.

[19] Oscar Cata and Jernej F. Kamenik. ElectroWeak Precision Observables at One-Loop in Higgsless models. *Phys. Rev.*, D83:053010, 2011.

[20] Claude Amsler et al. Review of particle physics. *Phys. Lett.*, B667:1–1340, 2008.

[21] https://twiki.cern.ch/twiki/bin/view/AtlasPublic/HiggsPublicResults.

[22] https://twiki.cern.ch/twiki/bin/view/CMSPublic/PhysicsResults.

[23] Abdelhak Djouadi. The Anatomy of electro-weak symmetry breaking. I: The Higgs boson in the standard model. *Phys. Rept.*, 457:1–216, 2008.

[24] Stephen P. Martin. A Supersymmetry Primer. 1997.

[25] Thibault Damour and John F. Donoghue. Constraints on the variability of quark masses from nuclear binding. *Phys. Rev.*, D78:014014, 2008.

[26] Lisa Randall and Raman Sundrum. A large mass hierarchy from a small extra dimension. *Phys. Rev. Lett.*, 83:3370–3373, 1999.

[27] Kenzo Inoue, Akira Kakuto, and Hiroshi Takano. Higgs as (Pseudo)Goldstone Particles. *Prog. Theor. Phys.*, 75:664, 1986.

[28] N. Arkani-Hamed et al. The Minimal Moose for a Little Higgs. *JHEP*, 08:021, 2002.

[29] Roberto Contino, Yasunori Nomura, and Alex Pomarol. Higgs as a holographic pseudo-Goldstone boson. *Nucl. Phys.*, B671:148–174, 2003.

[30] D. B. Fairlie. Higgs' Fields and the Determination of the Weinberg Angle. *Phys. Lett.*, B82:97, 1979.

[31] N. S. Manton. A New Six-Dimensional Approach to the Weinberg-Salam Model. *Nucl. Phys.*, B158:141, 1979.

[32] Yutaka Hosotani. Dynamical Mass Generation by Compact Extra Dimensions. *Phys. Lett.*, B126:309, 1983.

[33] Marco Serone. Holographic Methods and Gauge-Higgs Unification in Flat Extra Dimensions. *New J. Phys.*, 12:075013, 2010.

[34] Adrian Signer. Abc of SUSY. *J. Phys.*, G36:073002, 2009.

[35] Stephen P. Martin and Michael T. Vaughn. Two loop renormalization group equations for soft supersymmetry breaking couplings. *Phys. Rev.*, D50:2282, 1994.

[36] H. Georgi and S. L. Glashow. Unity of All Elementary Particle Forces. *Phys. Rev. Lett.*, 32:438–441, 1974.

[37] H. Georgi, Helen R. Quinn, and Steven Weinberg. Hierarchy of Interactions in Unified Gauge Theories. *Phys. Rev. Lett.*, 33:451–454, 1974.

[38] S. Dimopoulos, S. Raby, and Frank Wilczek. Supersymmetry and the Scale of Unification. *Phys. Rev.*, D24:1681–1683, 1981.

[39] Pran Nath and Pavel Fileviez Perez. Proton stability in grand unified theories, in strings, and in branes. *Phys. Rept.*, 441:191–317, 2007.

[40] Stuart Raby. Searching for the Standard Model in the String Landscape : SUSY GUTs. *Rept. Prog. Phys.*, 74:036901, 2011.

[41] Wolfgang Altmannshofer, Andrzej J. Buras, Stefania Gori, Paride Paradisi, and David M. Straub. Anatomy and Phenomenology of FCNC and CPV Effects in SUSY Theories. *Nucl. Phys.*, B830:17–94, 2010.

[42] Jonathan J. Heckman and Cumrun Vafa. Flavor Hierarchy From F-theory. *Nucl. Phys.*, B837:137–151, 2010.

[43] Keith R. Dienes, Emilian Dudas, and Tony Gherghetta. Grand unification at intermediate mass scales through extra dimensions. *Nucl. Phys.*, B537:47–108, 1999.

[44] Ann E. Nelson and Matthew J. Strassler. Suppressing flavor anarchy. *JHEP*, 09:030, 2000.

[45] Tony Gherghetta. TASI Lectures on a Holographic View of Beyond the Standard Model Physics. 2010.

[46] M. Libanov and F. S. Ling. Flavour puzzle or Why neutrinos are different? 2011.

[47] M. V. Libanov and Sergey V. Troitsky. Three fermionic generations on a topological defect in extra dimensions. *Nucl. Phys.*, B599:319–333, 2001.

[48] Markus A. Luty. 2004 TASI lectures on supersymmetry breaking. 2005.

[49] Adel Bilal. Introduction to supersymmetry. 2001.

[50] Bernard de Wit. Supergravity. 2002.

[51] Csaba Csaki. TASI lectures on extra dimensions and branes. 2004.

[52] Csaba Csaki, Jay Hubisz, and Patrick Meade. Electroweak symmetry breaking from extra dimensions. 2005.

[53] M. Quiros. New ideas in symmetry breaking. 2003.

[54] Steven Weinberg. *The quantum theory of fields. Vol. 3: Supersymmetry*. 2000. Cambridge, UK: Univ. Pr. (2000) 419 p.

[55] J. Polchinski. *String theory. Vol. 2: Superstring Theory and Beyond*. 1998.

[56] Nima Arkani-Hamed, Thomas Gregoire, and Jay G. Wacker. Higher dimensional supersymmetry in 4D superspace. *JHEP*, 03:055, 2002.

[57] Daniel Marti and Alex Pomarol. Supersymmetric theories with compact extra dimensions in N = 1 superfields. *Phys. Rev.*, D64:105025, 2001.

[58] Kenneth A. Intriligator, Nathan Seiberg, and David Shih. Supersymmetry Breaking, R-Symmetry Breaking and Metastable Vacua. *JHEP*, 07:017, 2007.

[59] Kenneth A. Intriligator, Nathan Seiberg, and David Shih. Dynamical SUSY breaking in meta-stable vacua. *JHEP*, 04:021, 2006.

[60] Vadim Kaplunovsky and Jan Louis. Field dependent gauge couplings in locally supersymmetric effective quantum field theories. *Nucl. Phys.*, B422:57–124, 1994.

[61] Lisa Randall and Raman Sundrum. Out of this world supersymmetry breaking. *Nucl. Phys.*, B557:79–118, 1999.

[62] Theodor Kaluza. On the Problem of Unity in Physics. *Sitzungsber. Preuss. Akad. Wiss. Berlin (Math. Phys.)*, 1921:966–972, 1921.

[63] O. Klein. Quantum theory and five-dimensional theory of relativity. *Z. Phys.*, 37:895–906, 1926.

[64] Yuval Grossman and Matthias Neubert. Neutrino masses and mixings in non-factorizable geometry. *Phys. Lett.*, B474:361–371, 2000.

[65] Ki-woon Choi, Do Young Kim, Ian-Woo Kim, and Tatsuo Kobayashi. Supersymmetry breaking in warped geometry. *Eur. Phys. J.*, C35:267–275, 2004.

[66] Juan Martin Maldacena. The large N limit of superconformal field theories and supergravity. *Adv. Theor. Math. Phys.*, 2:231–252, 1998.

[67] Nima Arkani-Hamed, Massimo Porrati, and Lisa Randall. Holography and phenomenology. *JHEP*, 08:017, 2001.

[68] R. Rattazzi and A. Zaffaroni. Comments on the holographic picture of the Randall-Sundrum model. *JHEP*, 04:021, 2001.

[69] Joel Scherk and John H. Schwarz. Spontaneous Breaking of Supersymmetry Through Dimensional Reduction. *Phys. Lett.*, B82:60, 1979.

[70] Joel Scherk and John H. Schwarz. How to Get Masses from Extra Dimensions. *Nucl. Phys.*, B153:61–88, 1979.

[71] Tony Gherghetta and Alex Pomarol. The standard model partly supersymmetric. *Phys. Rev.*, D67:085018, 2003.

[72] Riccardo Barbieri, Lawrence J. Hall, and Yasunori Nomura. Models of Scherk-Schwarz symmetry breaking in 5D: Classification and calculability. *Nucl. Phys.*, B624:63–80, 2002.

[73] Tatsuo Kobayashi and Koichi Yoshioka. Kaluza-Klein mediated supersymmetry breaking. *Phys. Rev. Lett.*, 85:5527–5530, 2000.

[74] Z. Chacko and Markus A. Luty. Radion mediated supersymmetry breaking. *JHEP*, 05:067, 2001.

[75] Yoshiharu Kawamura. Triplet-doublet splitting, proton stability and extra dimension. *Prog. Theor. Phys.*, 105:999–1006, 2001.

[76] Arthur Hebecker and John March-Russell. The structure of GUT breaking by orbifolding. *Nucl. Phys.*, B625:128–150, 2002.

[77] Wilfried Buchmuller, Koichi Hamaguchi, Oleg Lebedev, and Michael Ratz. Supersymmetric standard model from the heterotic string. *Phys. Rev. Lett.*, 96:121602, 2006.

[78] Hans Peter Nilles, Saul Ramos-Sanchez, Michael Ratz, and Patrick K. S. Vaudrevange. From strings to the MSSM. *Eur. Phys. J.*, C59:249–267, 2009.

[79] Vadim S. Kaplunovsky. Mass Scales of the String Unification. *Phys. Rev. Lett.*, 55:1036, 1985.

[80] Luis E. Ibanez and Dieter Lust. Duality anomaly cancellation, minimal string unification and the effective low-energy Lagrangian of 4-D strings. *Nucl. Phys.*, B382:305–364, 1992.

[81] Edward Witten. Strong Coupling Expansion Of Calabi-Yau Compactification. *Nucl. Phys.*, B471:135–158, 1996.

[82] Arthur Hebecker and M. Trapletti. Gauge unification in highly anisotropic string compactifications. *Nucl. Phys.*, B713:173–203, 2005.

[83] Ben Dundee, Stuart Raby, and Akin Wingerter. Reconciling Grand Unification with Strings by Anisotropic Compactifications. *Phys. Rev.*, D78:066006, 2008.

[84] Gustavo Burdman and Yasunori Nomura. Unification of Higgs and Gauge Fields in Five Dimensions. *Nucl. Phys.*, B656:3–22, 2003.

[85] Yasunori Nomura, David Poland, and Brock Tweedie. Holographic Grand Unification. *JHEP*, 12:002, 2006.

[86] Hyun Min Lee, Hans Peter Nilles, and Max Zucker. Spontaneous localization of bulk fields: The six- dimensional case. *Nucl. Phys.*, B680:177–198, 2004.

[87] W. Buchmuller, C. Ludeling, and Jonas Schmidt. Local SU(5) Unification from the Heterotic String. *JHEP*, 09:113, 2007.

[88] Pierre Hosteins, Rolf Kappl, Michael Ratz, and Kai Schmidt-Hoberg. Gauge-top unification. *JHEP*, 07:029, 2009.

[89] Naoyuki Haba and Yasuhiro Shimizu. Gauge-Higgs unification in the 5 dimensional E(6), E(7), and E(8) GUTs on orbifold. *Phys. Rev.*, D67:095001, 2003.

[90] Ki-woon Choi et al. Electroweak symmetry breaking in supersymmetric gauge - Higgs unification models. *JHEP*, 02:037, 2004.

[91] G. F. Giudice and A. Masiero. A Natural Solution to the mu Problem in Supergravity Theories. *Phys. Lett.*, B206:480–484, 1988.

[92] Arthur Hebecker, John March-Russell, and Robert Ziegler. Inducing the μ and the $B\mu$ Term by the Radion and the 5d Chern-Simons Term. *JHEP*, 08:064, 2009.

[93] Nima Arkani-Hamed, Andrew G. Cohen, and Howard Georgi. Anomalies on orbifolds. *Phys. Lett.*, B516:395–402, 2001.

[94] C. A. Scrucca, M. Serone, L. Silvestrini, and F. Zwirner. Anomalies in orbifold field theories. *Phys. Lett.*, B525:169–174, 2002.

[95] R. Barbieri, R. Contino, P. Creminelli, R. Rattazzi, and C. A. Scrucca. Anomalies, Fayet-Iliopoulos terms and the consistency of orbifold field theories. *Phys. Rev.*, D66:024025, 2002.

[96] Claudio A. Scrucca and Marco Serone. Anomalies in field theories with extra dimensions. *Int. J. Mod. Phys.*, A19:2579–2642, 2004.

[97] David Elazzar Kaplan and Timothy M. P. Tait. New tools for fermion masses from extra dimensions. *JHEP*, 11:051, 2001.

[98] Hiroyuki Abe, Tetsutaro Higaki, and Tatsuo Kobayashi. Wave-function profile and SUSY breaking in 5D model with Fayet-Iliopoulos term. *Prog. Theor. Phys.*, 109:809–830, 2003.

[99] Felix Brummer, Sylvain Fichet, Arthur Hebecker, and Sabine Kraml. Phenomenology of Supersymmetric Gauge-Higgs Unification. *JHEP*, 08:011, 2009.

[100] Z. Chacko, Markus A. Luty, and Eduardo Ponton. Massive higher-dimensional gauge fields as messengers of supersymmetry breaking. *JHEP*, 07:036, 2000.

[101] Wilfried Buchmuller, Koichi Hamaguchi, and Joern Kersten. The gravitino in gaugino mediation. *Phys. Lett.*, B632:366–370, 2006.

[102] Felix Brummer, Sylvain Fichet, Sabine Kraml, and Ritesh K. Singh. On SUSY GUTs with a degenerate Higgs mass matrix. *JHEP*, 08:096, 2010.

[103] Ki-woon Choi, Do Young Kim, Ian-Woo Kim, and Tatsuo Kobayashi. SUSY flavor problem and warped geometry. 2003.

[104] Abdelhak Djouadi, Jean-Loic Kneur, and Gilbert Moultaka. SuSpect: A Fortran code for the supersymmetric and Higgs particle spectrum in the MSSM. *Comput. Phys. Commun.*, 176:426–455, 2007.

[105] B. C. Allanach. SOFTSUSY: a program for calculating supersymmetric spectra. *Comput. Phys. Commun.*, 143:305–331, 2002.

[106] Werner Porod. SPheno, a program for calculating supersymmetric spectra, SUSY particle decays and SUSY particle production at e+ e- colliders. *Comput. Phys. Commun.*, 153:275–315, 2003.

[107] Arthur Hebecker. 5D super Yang-Mills theory in 4-D superspace, superfield brane operators, and applications to orbifold GUTs. *Nucl. Phys.*, B632:101–113, 2002.

[108] Ignatios Antoniadis, E. Gava, K. S. Narain, and T. R. Taylor. Effective mu term in superstring theory. *Nucl. Phys.*, B432:187–204, 1994.

[109] A. Brignole, Luis E. Ibanez, C. Munoz, and C. Scheich. Some issues in soft SUSY breaking terms from dilaton / moduli sectors. *Z. Phys.*, C74:157–170, 1997.

[110] A. Brignole, Luis E. Ibanez, and C. Munoz. Orbifold-induced mu term and electroweak symmetry breaking. *Phys. Lett.*, B387:769–774, 1996.

[111] A. Brignole, Luis E. Ibanez, and C. Munoz. Soft supersymmetry-breaking terms from supergravity and superstring models. 1997.

[112] Wilfried Buchmuller, Koichi Hamaguchi, Oleg Lebedev, and Michael Ratz. Supersymmetric standard model from the heterotic string. II. *Nucl. Phys.*, B785:149–209, 2007.

[113] Oleg Lebedev et al. A mini-landscape of exact MSSM spectra in heterotic orbifolds. *Phys. Lett.*, B645:88–94, 2007.

[114] A. A. Anselm and A. A. Johansen. SUSY GUT with Automatic Doublet - Triplet Hierarchy. *Phys. Lett.*, B200:331–334, 1988.

[115] Riccardo Barbieri and Alessandro Strumia. The 'LEP paradox'. 2000.

[116] J. A. Casas, J. R. Espinosa, and I. Hidalgo. The MSSM fine tuning problem: A Way out. *JHEP*, 01:008, 2004.

[117] Ryuichiro Kitano and Yasunori Nomura. A solution to the supersymmetric fine-tuning problem within the MSSM. *Phys. Lett.*, B631:58–67, 2005.

[118] G. F. Giudice and R. Rattazzi. Living dangerously with low-energy supersymmetry. *Nucl. Phys.*, B757:19–46, 2006.

[119] LEP2 SUSY Working Group [ALEPH, DELPHI, L3 and OPAL experiments]. `http://lepsusy.web.cern.ch/lepsusy/`.

[120] S. Schael et al. Search for neutral MSSM Higgs bosons at LEP. *Eur. Phys. J.*, C47:547–587, 2006.

[121] G. Degrassi, S. Heinemeyer, W. Hollik, P. Slavich, and G. Weiglein. Towards high-precision predictions for the MSSM Higgs sector. *Eur. Phys. J.*, C28:133–143, 2003.

[122] E. Barberio et al. Averages of b-hadron and c-hadron Properties at the End of 2007. 2008.

[123] M. Misiak et al. The first estimate of $B\bar{B} \to X_s\gamma$ at $O(\alpha_s^2)$. *Phys. Rev. Lett.*, 98:022002, 2007.

[124] T. Aaltonen et al. Search for $B_0(s) \to \mu^+\mu^-$ and $B_0(d) \to \mu^+\mu^-$ decays with $2\,fb^{-1}$ of p anti-p collisions. *Phys. Rev. Lett.*, 100:101802, 2008.

[125] J. Dunkley et al. Five-Year Wilkinson Microwave Anisotropy Probe (WMAP) Observations: Likelihoods and Parameters from the WMAP data. *Astrophys. J. Suppl.*, 180:306–329, 2009.

[126] G. Belanger, F. Boudjema, A. Pukhov, and A. Semenov. micrOMEGAs2.0: A program to calculate the relic density of dark matter in a generic model. *Comput. Phys. Commun.*, 176:367–382, 2007.

[127] Howard Baer, Chih-hao Chen, Frank Paige, and Xerxes Tata. Signals for minimal supergravity at the CERN large hadron collider: Multi - jet plus missing energy channel. *Phys. Rev.*, D52:2746–2759, 1995.

[128] Howard Baer, Chih-hao Chen, Frank Paige, and Xerxes Tata. Signals for Minimal Supergravity at the CERN Large Hadron Collider II: Multilepton Channels. *Phys. Rev.*, D53:6241–6264, 1996.

[129] Arthur Hebecker, J. March-Russell, and T. Yanagida. Higher-dimensional origin of heavy sneutrino domination and low-scale leptogenesis. *Phys. Lett.*, B552:229–236, 2003.

[130] Francesca Borzumati and Antonio Masiero. Large Muon and electron Number Violations in Supergravity Theories. *Phys. Rev. Lett.*, 57:961, 1986.

[131] Jason L. Evans, David E. Morrissey, and James D. Wells. Higgs boson exempt no-scale supersymmetry and its collider and cosmology implications. *Phys. Rev.*, D75:055017, 2007.

[132] G. A. Blair, W. Porod, and P. M. Zerwas. Reconstructing supersymmetric theories at high energy scales. *Phys. Rev.*, D63:017703, 2001.

[133] John R. Ellis, Toby Falk, Keith A. Olive, and Yudi Santoso. Exploration of the MSSM with Non-Universal Higgs Masses. *Nucl. Phys.*, B652:259–347, 2003.

[134] Howard Baer, Azar Mustafayev, Stefano Profumo, Alexander Belyaev, and Xerxes Tata. Direct, indirect and collider detection of neutralino dark matter in SUSY models with non-universal Higgs masses. *JHEP*, 07:065, 2005.

[135] R. Barate et al. Search for the standard model Higgs boson at LEP. *Phys. Lett.*, B565:61–75, 2003.

[136] Marcela S. Carena and Howard E. Haber. Higgs boson theory and phenomenology. *Prog. Part. Nucl. Phys.*, 50:63–152, 2003.

[137] J. A. Casas, A. Lleyda, and C. Munoz. Strong constraints on the parameter space of the MSSM from charge and color breaking minima. *Nucl. Phys.*, B471:3–58, 1996.

[138] John R. Ellis, Joel Giedt, Oleg Lebedev, Keith Olive, and Mark Srednicki. Against Tachyophobia. *Phys. Rev.*, D78:075006, 2008.

[139] Jason L. Evans, David E. Morrissey, and James D. Wells. Vacuum Stability with Tachyonic Boundary Higgs Masses in No-Scale Supersymmetry or Gaugino Mediation. *Phys. Rev.*, D80:095011, 2009.

[140] G. Belanger, F. Boudjema, A. Pukhov, and R. K. Singh. Constraining the MSSM with universal gaugino masses and implication for searches at the LHC. *JHEP*, 11:026, 2009.

[141] B. C. Allanach. Naturalness priors and fits to the constrained minimal supersymmetric standard model. *Phys. Lett.*, B635:123–130, 2006.

[142] Roberto Ruiz de Austri, Roberto Trotta, and Leszek Roszkowski. A Markov chain Monte Carlo analysis of the CMSSM. *JHEP*, 05:002, 2006.

[143] Ben C. Allanach, Kyle Cranmer, Christopher G. Lester, and Arne M. Weber. Natural Priors, CMSSM Fits and LHC Weather Forecasts. *JHEP*, 08:023, 2007.

[144] Roberto Trotta, Farhan Feroz, Mike P. Hobson, Leszek Roszkowski, and Roberto Ruiz de Austri. The Impact of priors and observables on parameter inferences in the Constrained MSSM. *JHEP*, 12:024, 2008.

[145] G. Belanger, F. Boudjema, A. Pukhov, and A. Semenov. Dark matter direct detection rate in a generic model with micrOMEGAs2.1. *Comput. Phys. Commun.*, 180:747–767, 2009.

[146] E. Komatsu et al. Five-Year Wilkinson Microwave Anisotropy Probe (WMAP 1) Observations:Cosmological Interpretation. *Astrophys. J. Suppl.*, 180:330–376, 2009.

[147] N. Jarosik et al. Seven-Year Wilkinson Microwave Anisotropy Probe (WMAP) Observations: Sky Maps, Systematic Errors, and Basic Results. *Astrophys. J. Suppl.*, 192:14, 2011.

[148] E. Komatsu et al. Seven-Year Wilkinson Microwave Anisotropy Probe (WMAP) Observations: Cosmological Interpretation. *Astrophys. J. Suppl.*, 192:18, 2011.

[149] Combination of CDF and D0 Results on the Mass of the Top Quark. 2009.

[150] Zhiqing Zhang. Muon g-2: a mini review. 2008.

[151] Riccardo Barbieri and G. F. Giudice. Upper Bounds on Supersymmetric Particle Masses. *Nucl. Phys.*, B306:63, 1988.

[152] Gerard Jungman, Marc Kamionkowski, and Kim Griest. Supersymmetric dark matter. *Phys. Rept.*, 267:195–373, 1996.

[153] Z. Ahmed et al. Dark Matter Search Results from the CDMS II Experiment. *Science*, 327:1619–1621, 2010.

[154] Roberto Trotta. Bayes in the sky: Bayesian inference and model selection in cosmology. *Contemp. Phys.*, 49:71–104, 2008.

[155] G. Brooijmans et al. New Physics at the LHC. A Les Houches Report: Physics at TeV Colliders 2009 - New Physics Working Group. 2010.

[156] Yasunori Nomura, Michele Papucci, and Daniel Stolarski. Flavorful Supersymmetry from Higher Dimensions. *JHEP*, 07:055, 2008.

[157] Felix Brummer, Sylvain Fichet, and Sabine Kraml. The supersymmetric flavour problem in 5D GUTs and its consequences for LHC phenomenology. 2011.

[158] B. C. Allanach et al. SUSY Les Houches Accord 2. *Comp. Phys. Commun.*, 180:8–25, 2009.

[159] Yasunori Nomura, Michele Papucci, and Daniel Stolarski. Flavorful Supersymmetry. *Phys. Rev.*, D77:075006, 2008.

[160] Yasunori Nomura and Daniel Stolarski. Naturally Flavorful Supersymmetry at the LHC. *Phys. Rev.*, D78:095011, 2008.

[161] Graham Ross and Mario Serna. Unification and Fermion Mass Structure. *Phys. Lett.*, B664:97–102, 2008.

[162] Andrzej J. Buras. Minimal flavour violation and beyond: Towards a flavour code for short distance dynamics. *Acta Phys. Polon.*, B41:2487–2561, 2010.

[163] M. L. Brooks et al. New Limit for the Family-Number Non-conserving Decay μ^+ to $e^+\gamma$. *Phys. Rev. Lett.*, 83:1521–1524, 1999.

[164] G. L. Bayatian et al. CMS technical design report, volume II: Physics performance. *J. Phys.*, G34:995–1579, 2007.

[165] `https://twiki.cern.ch/twiki/bin/view/AtlasPublic/SupersymmetryPublicResults`.
D. Charlton, "Highlights and Searches in ATLAS", talk at EPS-HEP, 20–27 July 2011, Grenoble, France.

[166] `https://twiki.cern.ch/twiki/bin/view/CMSPublic/PhysicsResults`.
G. Tonelli, "Highlights and Searches in CMS", talk at EPS-HEP, 20–27 July 2011, Grenoble, France.

[167] J. Adam et al. A limit for the mu -¿ e gamma decay from the MEG experiment. *Nucl. Phys.*, B834:1–12, 2010.

[168] H. Baer and X. Tata. Weak scale supersymmetry: From superfields to scattering events. Cambridge, UK: Univ. Pr. (2006) 537 p.

[169] Fabio Iocco, Gianpiero Mangano, Gennaro Miele, Ofelia Pisanti, and Pasquale D. Serpico. Primordial Nucleosynthesis: from precision cosmology to fundamental physics. *Phys. Rept.*, 472:1–76, 2009.

[170] A. Brandenburg, L. Covi, K. Hamaguchi, L. Roszkowski, and F. D. Steffen. Signatures of axinos and gravitinos at colliders. *Phys. Lett.*, B617:99–111, 2005.

[171] Jie Chen and Todd Adams. Searching for high speed long-lived charged massive particles at the LHC. *Eur. Phys. J.*, C67:335–342, 2010.

[172] M. Fairbairn et al. Stable massive particles at colliders. *Phys. Rept.*, 438:1–63, 2007.

[173] Vardan Khachatryan et al. Search for Heavy Stable Charged Particles in pp collisions at sqrt(s)=7 TeV. *JHEP*, 03:024, 2011.

[174] Koichi Hamaguchi, Yoshitaka Kuno, Tsuyoshi Nakaya, and Mihoko M. Nojiri. A study of late decaying charged particles at future colliders. *Phys. Rev.*, D70:115007, 2004.

[175] `http://cern.ch/kraml/data/hgut/`.

[176] Iftah Galon and Yael Shadmi. Kinematic Edges with Flavor Splitting and Mixing. 2011.

[177] A. Bartl et al. Test of lepton flavour violation at LHC. *Eur. Phys. J.*, C46:783–789, 2006.

[178] A. J. Barr et al. Guide to transverse projections and mass-constraining variables. 2011.

[179] Yu. M. Andreev, S. I. Bityukov, N. V. Krasnikov, and A. N. Toropin. Using the $e^{\pm}\mu^{\mp} + E_T^{miss}$ signature in the search for supersymmetry and lepton flavour violation in neutralino decays. *Phys. Atom. Nucl.*, 70:1717–1724, 2007.

[180] See results presented at the EPS-HEP 2011 conference `http://eps-hep2011.eu/`.

[181] Markus A. Luty and Raman Sundrum. Radius stabilization and anomaly-mediated supersymmetry breaking. *Phys. Rev.*, D62:035008, 2000.

[182] Markus A. Luty and Raman Sundrum. Hierarchy Stabilization in Warped Supersymmetry. *Phys. Rev.*, D64:065012, 2001.

[183] Marta Gomez-Reino and Claudio A. Scrucca. Locally stable non-supersymmetric Minkowski vacua in supergravity. *JHEP*, 05:015, 2006.

[184] The RooStats Project. arXiv:1009.1003.

[185] H. Jeffreys. *Theory of probability*. International series of monographs on physics. The Clarendon press, 1939.

[186] L. Hormander. *The Analysis of Linear Partial Differential Operators: Differential operators with constant coefficients*. Classics in mathematics. Springer, 2004.

[187] J. Alberto Casas, Jose Ramon Espinosa, and Irene Hidalgo. Implications for new physics from fine-tuning arguments. II: Little Higgs models. *JHEP*, 03:038, 2005.

[188] M. E. Cabrera, J. A. Casas, and R. Ruiz de Austri. Bayesian approach and Naturalness in MSSM analyses for the LHC. *JHEP*, 03:075, 2009.